



ENHANCEMENT OF HEAT TRANSFER FOR GROUND SOURCE HEAT PUMP SYSTEMS

Hiromi Mori, BSc, MEng and MSc

Thesis submitted to the University of Nottingham
for the degree of Doctor of Philosophy

OCTOBER 2010

“Though the bamboo forest is dense, water flows through it freely.”

Zen Proverb

Abstract

Uptake of geothermal heat pump (GSHP) systems has been slow in some parts of the world due to the unpredictable operational performance, large installation space requirement and high installation costs. Therefore, design modification was searched in order to improve the feasibility. With regard to relatively small impact of the construction costs, efficient thermal energy collection was targeted in horizontal ground-loop systems with shallow underground construction.

The research started with a sensitivity analysis of the underground heat collection system using computational fluid dynamics (CFD). The results indicated essential design parameters to enhance the performance. Strategies to improve one of the parameters, thermal conductivity of soil surrounding the heat exchanger, were investigated through lab experiments. Subsequently, further design optimisation with the CFD intended to select the most competitive modified design against the existing design.

It was discovered that an indication to achieve economic and practical modifications for efficient heat collection was to increase the moisture content of sub-soil up to the optimum moisture content (OMC). Annual operation analysis with the CFD disclosed that additional costs for even simple design modifications could easily worsen the payback period. Consequently, solutions to improve the performance of the GSHP within reasonable payback period were proposed.

Acknowledgement

The author wishes to thank Professor Saffa Riffat and Dr. Guohui Gan for supervising with their abundant experiences to enrich this research. Special thanks must go to Dr. Matthew Hall and Dr. David Allinson for their generous offers to guide with their considerable expertise. The experimental investigations would never have been as productive and educational as they had been without their regular help. It is a pleasure to acknowledge the effective assistance of the technicians and the staff in the School of the Built Environment, which led to the smooth completion of this project.

The author would like to express special gratitude to Mitsubishi Chemical Engineering Corporation for the generous grant to accomplish this three year research project. Their continuous trust to allow this international project has been greatly appreciated.

The loving care and deep understanding toward education from family were inevitable to finally achieve the highest academic degree. It should be also mentioned that sharing experiences with friends and their pleasant company created great encouragement.

Table of Contents

Abstract	
Acknowledgement	
Table of Contents	
List of Figures	i
List of Tables	viii
Chapter 1 Introduction	1
1.1 Background	1
1.2 Objectives in the Use of Heat Pumps	3
1.2.1 Objectives in the use of renewables	3
1.2.2 Objectives in the use of geothermal energy	5
1.3 Design Example	7
1.3.1 Considered system	8
1.3.2 Strategies to reduce cooling demand	11
1.3.3 Strategies to enhance the underground heat extraction	13
1.4 Purpose and Approaches of Project	14
Chapter 2 Literature Review	19
2.1 Heat Pumps	20
2.1.1. Advantages of heat pumps	20
2.1.2 Types of heat pumps	25
2.1.3 Conditions for efficient operation	29
2.1.4 Ground source heat pump (GSHP)	32

2.2 Rainwater Collection Systems	37
2.2.1 Usage of rainwater	38
2.2.2 System design	39
2.2.3 Potentials of rainwater for the efficient heat collection in the GSHP	40
2.3 Evaporative Cooling Systems	45
2.3.1 Mechanisms of evaporative cooling	46
2.3.2 Integration into building systems	47
2.3.3. Evaporative cooling on building surface	48
2.4 Highly Conductive Materials	51
2.4.1 Comparison in thermal properties	51
2.4.2 Environmental issues	52
2.4.3 Graphite	54
2.5 Methodologies to Obtain Thermal Properties of Soil Samples	57
2.5.1 Heat flow meter (HFM)	58
2.5.2 Dual-probe heat-pulse method (DPHP)	60
2.5.3 Method for the analysis with the DPHP	63
2.5.4 Comparison between the HFM and the DPHP	70
2.5.5 Theories to predict thermal conductivity of sub-soil	72
2.6 Conclusions	77
Chapter 3 Building a Model for Case Studies	80
3.1 Characteristics of Building	80
3.1.1 Background of the model	80

Table of Contents

3.1.2 Plan and building components	81
3.1.3 Estimation of design demands	83
3.1.4 Selection of heat pump	94
3.1.5 Building example to meet the approved document L2B	96
3.2 Environment Data	99
3.2.1 Weather data in Nottingham	99
3.2.2 Estimation of soil temperature	102
3.3 Conclusions	105
Chapter 4 Design Optimisation of Rainwater Collection Tank for the GSHP Application	106
4.1 Investigation of Meshing	107
4.1.1 Indications for accurate meshing	107
4.1.2 Case study	109
4.1.3 Calculation results	110
4.1.4 Conclusion	114
4.2 Verification of Simulation Models	115
4.2.1 Method	115
4.2.2 Results	117
4.3 Preparation for Design Optimisation	119
4.3.1 Simulation model	119
4.3.2 Standard conditions	126
4.4 Variations for Sensitivity Analysis	131
4.4.1 Effects of tank shape	131
4.4.2 Effects of thermal conductivity of concrete bed	133

Table of Contents

4.4.3 Effects of thermal conductivity of the surrounding soil	135
4.4.4 Effects of thickness of concrete bed	136
4.4.5 Effects of thickness of the surrounding soil	137
4.4.6 Effects of thermal conductivity of tank	138
4.5 Simulation Results	139
4.5.1 Comparison in different tank shape	139
4.5.2 Comparison in different thermal conductivity of concrete bed	143
4.5.3 Comparison in different thermal conductivity of the surrounding soil	145
4.5.4 Comparison in different thickness of concrete bed	145
4.5.5 Comparison in different thickness of modified soil	146
4.5.6 Comparison in different thermal conductivity of tank	147
4.5.7 Summary of design analysis	148
4.6 Conclusions	150
Chapter 5 Optimisation of Soil Thermal Properties for the GSHP	152
5.1 Methodology	153
5.1.1 Setup of the DPHP	153
5.1.2 The DPHP calibration with agar	155
5.1.3 Error analysis	159
5.2 Preparation of Experiments	162
5.2.1 Conditions of experiments	162
5.2.2 Fundamental characteristics	163
5.2.3 Sample making	167

5.3 Experimental Results – Effects of Water Content	170
5.3.1 Results of fundamental tests	171
5.3.2 Results with the HFM	174
5.3.3 Results with the DPHP	177
5.3.4 Comparison between two methods	181
5.3.5 Comparison with Campbell's theory	183
5.4 Investigations for Higher Thermal Conductivity	185
5.4.1 Introduction of samples for the comparison	185
5.4.2 Measurement of pore size distribution	186
5.4.3 Comparison in thermal conductivity	191
5.5 Defining the Status of Natural Soil	192
5.6 Investigation of Contributing Design Elements	193
5.6.1 Effects of high dry density attained by compaction	194
5.6.2 Effects of high dry density attained by packing ratio	195
5.6.3 Effects of water content added by suction	198
5.7 Results of Sensitive Analysis	200
5.7.1 Enhancement of dry density attained by compaction	200
5.7.2 Effects of dry density attained by packing ratio	205
5.7.3 Contribution of additional water content	207
5.8 Evaluation in Heat Transfer Efficiency	210
5.9 Conclusions	211
Chapter 6 Design Optimisation of Underground Structure with Modified Soil	214
6.1 Design Potentials with Convective Heat Transfer	215

6.2 Simulation Models	217
6.2.1 Standard model	217
6.2.2 Effects of different depth of heat exchanger	219
6.2.3 Effects of solar gain	219
6.2.4 Effects of modified soil	220
6.2.5 Effects of length of thermal pillars	220
6.2.6 Effects of sub-roots added to thermal pillars	222
6.2.7 Effects of thermal conductivity of thermal pillars	224
6.2.8 Effects of diameter of thermal pillars	225
6.2.9 Effects of thermal pillars in three dimensional calculation	225
6.2.10 Effects of modified soil space	226
6.3 Results of Sensitivity Analysis	227
6.3.1 Different depth of heat exchanger	227
6.3.2 Solar gain	227
6.3.3 Thermal conductivity of modified soil space	229
6.3.4 Length of thermal pillars	230
6.3.5 Sub-roots of thermal pillars	231
6.3.6 Thermal conductivity of thermal pillars	232
6.3.7 Diameter of thermal pillars	233
6.3.8 Thermal pillars in three dimensional calculation	233
6.3.9 Modified soil space	234
6.3.10 Summary of underground design analysis	236
6.4 Conclusions	237

Chapter 7 Economic Analysis of Soil Modification for an	239
Insulated Office Building	
7.1 Comparison in a Variety of Underground Design for Heating	240
7.1.1 Study cases	240
7.1.2 Evaluation of underground heat collection system	243
7.2 Estimation of Yearly Demands	247
7.2.1 Methodology	248
7.2.2 Calculation of heating and cooling demand	248
7.3 Conditions for Annual Operation	249
7.3.1 Estimation of soil thermal conductivity	250
7.3.2 Other environmental conditions	251
7.3.3 Calculation for designing	253
7.3.4 Thermal resistance at heat exchanger	254
7.3.5 Backup energy suppliers	258
7.3.6 Consideration of pump electricity consumption	258
7.3.7 Other assumptions for analysis	259
7.4 Estimation of the Annual Operation	260
7.4.1 Monthly heat collection	260
7.4.2 Year-round electricity consumption	261
7.4.3 Economic and ecological feasibility	264
7.5 Conditions for Practical Use of Soil Modification	265
7.5.1 Prospects in electricity prices	265
7.5.2 Prospects in the initial cost	265
7.5.3 Design proposal to retain soil moisture content	269
7.6 Conclusions	272

Chapter 8	Conclusions and Future Works	274
8.1	Conclusions	274
8.2	Suggestions for Future Works	276
References		278
Appendix A	Background Data for Building a Model System for the Simulation Analysis	296
Appendix B	Programme to Control a Data Collection Process of the DPHP	306
Appendix C	Programme to Define Heat Resistance	309
Appendix D	Information in Association with Measurements of Thermal Properties	311
Appendix E	Investigation of Thermal Resistance Caused by Aluminium Plate	312
E.1	Sample Making	312
E.2	Measurement of Thermal Conductivity	312
E.3	Conclusion	313
Appendix F	Processed Field Data between Soil Moisture Content and Rainfall	314
Publications		315

List of Figures

Chapter 1

Figure 1.1	Learning curves for power generation technologies up to 2030	5
Figure 1.2	Historic oil price development (WTI) and forward projections between 1981 and 2029	6
Figure 1.3	Ground source in the USA	8
Figure 1.4	System example: circuit for heat sources	9
Figure 1.5	System example: circulation of rainwater	12
Figure 1.6	Flowchart of the procedure	15

Chapter 2

Figure 2.1	Electricity-powered heat pump	21
Figure 2.2	Energy consumption in the UK, 2002	23
Figure 2.3	Potential reduction of CO ₂ emission by heat pumps	24
Figure 2.4	Phase-out plan agreed in the Montreal protocol	28
Figure 2.5	CO ₂ heat pump	29
Figure 2.6	The COP of heat pumps	30
Figure 2.7	The GSHP with boreholes	33
Figure 2.8	Calculated underground temperature for Nottingham	34
Figure 2.9	Water-filled borehole system	36
Figure 2.10	Domestic use of water	39
Figure 2.11	Design image of domestic system	40

List of Figures

Figure 2.12	Measured rainwater temperature in Tokyo, 1993-1994	41
Figure 2.13	Rainwater heat collection system	44
Figure 2.14	Experimental apparatus with heat pipes	43
Figure 2.15	Roof pond with gunny bags	49
Figure 2.16	Deep injection process	55
Figure 2.17	Different packing geometry of carbon fibres	56
Figure 2.18	Cross-sectional diagram of the B480 heat flow meter (HFM) apparatus	59
Figure 2.19	Setup of dual-probe heat-pulse method (DPHP)	61
Figure 2.20	Example of the DPHP sensor unit	63
Figure 2.21	Spreadsheet to calculate thermal properties	69
Figure 2.22	Multi-needle heat-pulse method for fired tests	71
 <u>Chapter 3</u>		
Figure 3.1	Weather station in the University of Nottingham	100
Figure 3.2	Six year average weather data in the University of Nottingham	101
Figure 3.3	Comparison in soil temperature gradient	104
 <u>Chapter 4</u>		
Figure 4.1	Non-uniform layers around boundaries in FLUENT	108
Figure 4.2	Model for the mesh investigation	109
Figure 4.3	Results of cases with sub-soil	111
Figure 4.4	Results of case BL	112

List of Figures

Figure 4.5	Results of cases with copper	113
Figure 4.6	Results of case Mxd BL	114
Figure 4.7	Model for the verification	115
Figure 4.8	Comparison in required heat flux	118
Figure 4.9	Simulation model	119
Figure 4.10	Image of the end of rainwater down pipe	120
Figure 4.11	Model in Gambit	123
Figure 4.12	Model in FLUENT	124
Figure 4.13	Required amount of concrete bed	125
Figure 4.14	Simulation result without rainwater flow	130
Figure 4.15	Model with gaps between heat exchanger loops	134
Figure 4.16	Calculation results in FLUENT for case T-2	140
Figure 4.17	Heat flux and ratio between width and height	141
Figure 4.18	Eddies within tanks	142
Figure 4.19	Comparison in temperature contour	143
Figure 4.20	Results of sensitivity analysis	144
Figure 4.21	Comparison in different thickness of concrete bed	147
Figure 4.22	Comparison in different thermal conductivity of tank	149

Chapter 5

Figure 5.1	Image of a sample box	154
Figure 5.2	Calibration with agar	157
Figure 5.3	Derived distance between probes in calibration	158
Figure 5.4	Thermal properties of water after calibration	160

List of Figures

Figure 5.5	Electromagnetic sieve shaker	164
Figure 5.6	Automatic soil compactor	166
Figure 5.7	Soil sample covered with cling film	168
Figure 5.8	Particle distribution of the original soil	172
Figure 5.9	Particle distribution of the original soil less than 2 mm	173
Figure 5.10	The OMC of the original soil	174
Figure 5.11	Thermal conductivity measured by the HFM	176
Figure 5.12	Thermal conductivity against dry density	177
Figure 5.13	Thermal conductivity measurement with the DPHP	178
Figure 5.14	Thermal conductivity against dry density with the DPHP	179
Figure 5.15	Derived heat capacity and diffusivity for sample Pd1	180
Figure 5.16	Comparison between the HFM and the DPHP	181
Figure 5.17	Comparison between the HFM and the DPHP with dry samples	182
Figure 5.18	Comparison to Campbell's prediction for sample Pd1 and Pd2	184
Figure 5.19	Blended sample with more large particles	186
Figure 5.20	Setup of x-ray micro scanning	187
Figure 5.21	Preparation of specimen	188
Figure 5.22	Scanned images of the sandy and the gravelly soil	189
Figure 5.23	Pore size distribution	190
Figure 5.24	Comparison of thermal conductivity between the sandy and the gravelly soil	191
Figure 5.25	Comparison of thermal conductivity against dry density	192

List of Figures

Figure 5.26	Relation between compaction energy and density	193
Figure 5.27	Investigation of the OMC	195
Figure 5.28	Ideal curves with different n factor	196
Figure 5.29	Blending for the maximum packing	197
Figure 5.30	Compaction test of sample 0.225 and sample 0.33	198
Figure 5.31	Sampling points for water content	200
Figure 5.32	Compaction in thermal conductivity	201
Figure 5.33	Thermal conductivity against density	202
Figure 5.34	Effects of compaction energy on thermal conductivity	202
Figure 5.35	Effects of compaction energy after water mixing up to the OMC	204
Figure 5.36	Effects of high packing ratio at the OMC	205
Figure 5.37	Effects of high packing ratio at the OMC against dry density	206
Figure 5.38	Change of thermal conductivity through water absorption	208
Figure 5.39	Comparison to theoretically estimated thermal conductivity	209
 <u>Chapter 6</u>		
Figure 6.1	Simulation model in FLUENT	218
Figure 6.2	Thermal pillar in simulation model	221
Figure 6.3	Image of grout injection to create sub-roots added to thermal pillars	223

List of Figures

Figure 6.4	Calculation model with sub-roots, case Nsr-3	223
Figure 6.5	Calculation model without thermal pillars	225
Figure 6.6	Calculation model with thermal pillars	226
Figure 6.7	Heat flux with different depth of a slinky coil	228
Figure 6.8	Effects of thermal conductivity of thermal pillars	232
Figure 6.9	Temperature contour in three dimensional model with thermal pillars	235
Figure 6.10	Comparison against volume of excavation	236

Chapter 7

Figure 7.1	Comparison between case MR and case MS	245
Figure 7.2	Relation between ratio of the initial cost and ratio of required installation area	247
Figure 7.3	Monthly heating and cooling load	250
Figure 7.4	Trendline derived from experiments for soil at 1.5 Mg/m ³	252
Figure 7.5	Estimated loads in a year	255
Figure 7.6	Conditions around tube	256
Figure 7.7	Effect of soil modification against soil thermal conductivity	262
Figure 7.8	Design proposal to apply soakaways to modified underground structure	270

Appendix A

Figure A.1	Statistics of office buildings in the USA	296
Figure A.2	Plan of the model office building	297
Figure A.3	The COP characteristics of the selected heat pump	300
Figure A.4	Plan of the insulated office building	303
Figure A.5	Field data of soil moisture content and precipitation	304
Figure A.6	Phases of modelling and simulation	305

Appendix D

Figure D.1	Thermal transmission in the HFM	311
------------	---------------------------------	-----

Appendix F

Figure F.1	Relation between soil moisture content and rainfall in San Pedro River Valley	314
------------	--	-----

List of Tables

Chapter 1

Table 1.1	Situation of the GSHP in each region	7
-----------	--------------------------------------	---

Chapter 2

Table 2.1	Types of commercialised heat pumps	25
Table 2.2	Heat sources	26
Table 2.3	Characteristics of working fluids	27
Table 2.4	Temperature difference between raining and non-raining conditions	42
Table 2.5	Frequency and duration of rainfall	43
Table 2.6	Comparison of properties	52
Table 2.7	Calibration constants for measuring with silicon rubber mats	60
Table 2.8	Comparison between the HFM and the DPHP	70

Chapter 3

Table 3.1	Calculation of U-values	83
Table 3.2	U-values of the building models	84
Table 3.3	Calculation of sol-air temperature	86
Table 3.4	Demands caused by conduction	87
Table 3.5	Demands caused by solar gain	89
Table 3.6	Demands caused by air infiltration	90
Table 3.7	Demands caused by ventilation	91

List of Tables

Table 3.8	Demands caused by occupants	92
Table 3.9	Demands caused by electric appliances and lighting	92
Table 3.10	Design demands	93
Table 3.11	Specs of the selected heat pump	94
Table 3.12	Design demands for a four story office building	97
Table 3.13	Design demands for an insulated building model	98
Table 3.14	Data for estimating underground temperature gradient	103

Chapter 4

Table 4.1	Study cases for the mesh investigation	110
Table 4.2	Variation of calculation models	118
Table 4.3	Specs of calculation model	122
Table 4.4	Standard calculation conditions	127
Table 4.5	Calculation of Reynolds number	127
Table 4.6	Materials and their thermal conductivity	128
Table 4.7	Climatic data in Nottingham	129
Table 4.8	Cases with different ratio between width and height	132
Table 4.9	Study cases with different thermal conductivity of concrete bed	133
Table 4.10	Estimation of the total heat exchanger length for a half tank	135
Table 4.11	Study cases with different thermal conductivity in the surrounding soil	136
Table 4.12	Study cases with different thickness of concrete bed	137
Table 4.13	Study cases with different thickness of the surrounding	138

	soil	
Table 4.14	Study cases with different thermal conductivity of tank	139
Table 4.15	Simulation results among case T-1 to T-5	140
Table 4.16	Simulation results among case G-1 to G-3	144
Table 4.17	Simulation results among case M-1 to M-5	145
Table 4.18	Simulation results among case TG-1 to TG-4	146
Table 4.19	Simulation results among case TS-1 to TS-5	148
Table 4.20	Simulation results among case TT-1 to TT-5	148

Chapter 5

Table 5.1	Results of calibration of thermal characteristics	158
Table 5.2	Results of error analysis	161
Table 5.3	Conditions for calibration with cling film	168
Table 5.4	Comparison between estimated and measured thermal conductivity	169
Table 5.5	Moisture content of natural soil	175
Table 5.6	Correlation coefficient in measurement with the DPHP	180
Table 5.7	Results of analysis	189
Table 5.8	Results of compaction test at water content of $0.1 \text{ m}^3/\text{m}^3$	194
Table 5.9	Sectional moisture content in sample 4.5	207
Table 5.10	Comparison in thermal effusivity	211

Chapter 6

Table 6.1	Study cases with different depth of heat exchanger	219
Table 6.2	Study cases with different number of sub-roots	224

List of Tables

Table 6.3	Study cases with different thermal conductivity of thermal pillars	224
Table 6.4	Study cases with different depth and width of modified soil space	227
Table 6.5	Simulation results with different depth of a slinky coil	228
Table 6.6	Simulation results with solar gain	229
Table 6.7	Simulation results with different thermal conductivity of the modified soil space	230
Table 6.8	Simulation results with different length of thermal pillars	231
Table 6.9	Simulation results with different number of sub-roots	232
Table 6.10	Simulation results with different thermal conductivity of thermal pillars	232
Table 6.11	Simulation results with different diameter of thermal conductivity	233
Table 6.12	Comparison between with and without thermal pillars	234
Table 6.13	Simulation results with different width and depth of modified soil space	235
Table 6.14	Summary in effects of design parameters	237
 <u>Chapter 7</u>		
Table 7.1	Study cases	241
Table 7.2	Input data	241
Table 7.3	Cost estimation	242
Table 7.4	Heat flux with different combination of system components	244

List of Tables

Table 7.5	Comparison in required design specs	246
Table 7.6	Estimation of the change of load against ambient temperature	249
Table 7.7	Estimated thermal conductivity of sub-soil for each month	252
Table 7.8	Input data for each month	253
Table 7.9	Designing heat exchanger	254
Table 7.10	Conditions of heat exchange tube	256
Table 7.11	State of liquid thermal media	257
Table 7.12	Estimated temperature drop	257
Table 7.13	Estimation of extra electricity consumption at a pump in the existing design	260
Table 7.14	Estimation of heat collection capacity	261
Table 7.15	Comparison of annual electricity consumption	263
Table 7.16	Prediction of payback period with growing electricity prices	266
Table 7.17	Prediction of payback period with different construction cost	267
Table 7.18	Design suggestions to reduce payback period	267
Table 7.19	Estimation of practically feasible quartz mixture	268

Appendix A

Table A.1	Materials and conditions of the building model	297
Table A.2	Indoor conditions of the building model	298
Table A.3	Temperature settings to calculate design demands	299

List of Tables

Table A.4	Properties of 20 % ethylene glycol solution	301
Table A.5	Examples to improve U-values in the building model	301
Table A.6	Indoor conditions of the insulated building model	302
Table A.7	Comparison in ratio of window area	303

Appendix D

Table D.1	Results of calibration to obtain unique heater resistance	311
-----------	---	-----

Chapter 1 Introduction

Introduction

Recent global issues have been questioning basic supplies to our lives; energy and food. These items used to be believed that people could afford for reasonable price almost eternally. However, it seemed to be a myth and efforts for the sustainable future are required. The good news is that some sustainable technologies and methods have been developed and they would save the situation when the researches have reached feasible solutions for practical use. To begin with, required attitude and potential technologies for the usage of sustainable energy are summarised. The following sections attempt to propose an effective energy supply system. Finally, a structure of this research is presented.

1.1 Background

No explanation is necessary about global fear in association with the limitation of energy sources. The solution for human being to maintain our civilised life style seems to be a combination of two actions; reducing energy consumption and seeking new energy sources. With regard to the rapid growth of energy consumption as well as the rapid growth of population in some parts of the world, the two methods should be implemented immediately.

Some have been aware of the possible energy crisis earlier, and so alternative energy sources of fossil fuels have been surveyed. For instance, coal beds are rich in methane concentration; the potential amount of methane hydrates seems

large; substantial amount of energy might be generated in nuclear fusion (Fanchi, 2004). However, the feasibility differs for each source: some are far impractical both technically and economically, such as thermoelectric and methane hydrate (Durham, 1999). On the other hand, the most expected sources must be renewable energy, for instance, solar, wind, geothermal and oceanic. Each energy source is relatively easy handling and straightforward to be extracted and processed, which created more economic attraction recently. Not only for energy security, but incombustible types of renewable energy can remarkably contribute to reduce the greenhouse gases, such as CO₂.

Various kinds of strategies should be attempted to save the fossil fuels. The quickest and the easiest way is to modify our life style toward more energy-saving conscious one, for example, reducing hot water flow rate at radiators and wearing more layers of clothes in winter. When energy facilities require modification or replacement, installing highly efficient equipment is also essential. Due to the demand for more economic energy supply and the regulations to reduce energy consumption, more options to create highly efficient systems are available on the recent market. For instance, in the field of thermal energy generation, such as for air conditioning and chemical processes, heat pumps are advantageous due to the high efficiency.

The COP (Coefficient Of Performance) of vapour compression-type heat pumps can be more than 3.0, when wasteful or renewable energy is used as the heat source. When heat source is supplied to heat pumps via water (water source) instead of air, the COP reaches even 4.0 to 5.0 (IEA Heat Pump Centre, 2005).

It is obvious that air source is less selective in terms of available location for the operation than river / sea water and geothermal. However, water source must be worthwhile to consider when the local conditions allow.

Benefit of heat pump mechanisms from a practical viewpoint is the use of low grade energy, which does not have attractive energy density and temperature level. The efficient use of low grade energy is an inevitable issue in order to minimise the fossil fuels consumption. This objective is solved with simple and flexible components in heat pumps; evaporator, condenser, compressor and expansion valve. As a result, heat pumps convert the less valuable energy into the energy at more useful temperature, for instance, hot water at 40 to 60 °C and cold water at -20 to 10 °C (Zeneral Heat Pump Co. Ltd., 2006). For these reasons, heat pump systems with various kinds of renewables, such as air, solar, geothermal and river / sea water, have been successfully installed (Lund et al., 2004). A range of applications also becomes wider, from industrial facilities to residential buildings.

1.2 Objectives in the Use of Heat Pumps

A use of newly developed renewable sources for heat pumps has been a challenge. Tackling this new field needs to be started from clarifying the objectives. As an example, detailed circumstances of geothermal heat pump systems (also known as ground source heat pumps, GSHP) are introduced.

1.2.1 Objectives in the use of renewables

It is attractive to use the complimentary energy in practical energy supply

systems. However, available types and amount of renewables highly depend on geographic conditions; therefore, location and capacity of heat pump systems are sometimes limited. Furthermore, some renewables, for instance, ground source energy at great depth, are fairly unpredictable that a large investment on the field measurements is required to collect fundamental environment data (IEA Heat Pump Centre, 2005). Therefore, at least the system performance ought to be evaluated on the basis of reliable database for the local environment to minimise the negative effects of the selective and fluctuating characteristic. Both energy demand and available renewable energy input vary seasonally, and so year-round dynamic operation ought to be examined.

Another troublesome characteristic of renewables is their low energy density. Unlike fossil fuels, energy density is low; therefore, required energy needs to be collected from more space and with more time (The Scottish Government, 2009). Facilities with high energy demands are generally built in highly dense regions, where large space for the energy collection is difficult to expect, such as in the city centre. For this reason, high efficiency is crucial to overcome this dilemma.

One more immiscible viewpoint is economic feasibility. For instance, when only ground source energy is viable, heat exchangers need to be buried for a long distance horizontally or vertically to supply the energy stably. In case that long vertical heat exchangers (boreholes) are chosen, the initial costs for the practical depth, 50 to 100 m, generally discourage potential users

(Hellström, [no date]). However, it is always the case that new technologies require certain period of time and investment until they become economically available on the markets. Figure 1.1 demonstrates that all the renewables will be cost effective one day regardless of their current status. Moreover, European commission announces that the continuous rise in oil price will make renewable energy technologies reasonable in the future (Figure 1.2, 2003 a). In order to make the day come earlier, persistent efforts to reduce the initial costs are greatly needed.

1.2.2 Objectives in the use of geothermal energy

The GSHP shares all the three common objectives, which are reliable performance, high efficiency and economic feasibility as mentioned in the

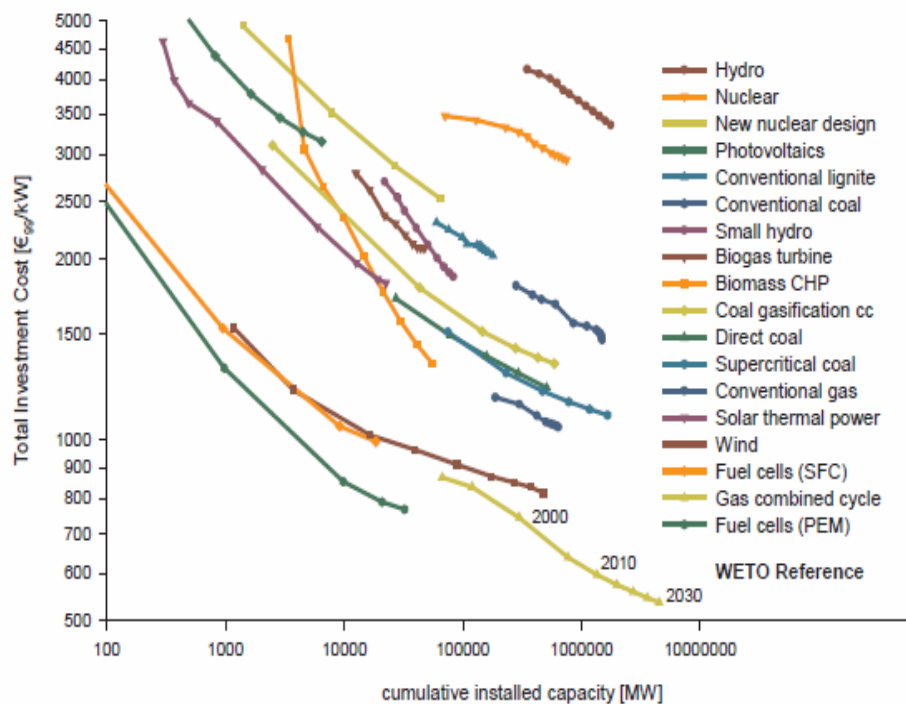


Figure 1.1 Learning curves for power generation technologies up to 2030 (European Commission, 2003 b)

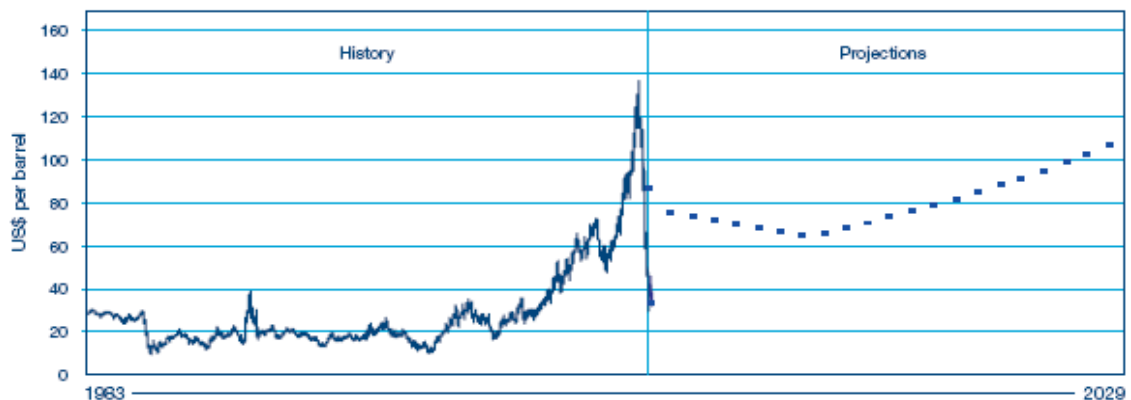


Figure 1.2 Historic oil price development (WTI) and forward projections between 1981 and 2029 (Wiegand et al., 2009)

previous section. Even if there are some barriers, the uptake of GSHP has spread globally. Since the use originally became common in North America and Europe in 1990s, the GSHP has continued to be well recognised in these regions (Lund et al., 2004). Subsequently, as energy issues have had more attention, the technology has one of the fastest growing markets, such as in Europe. However, the attention is still much lower in some countries, such as the UK and Japan (Table 1.1). The number of installed systems for different regions is subject to each unique situation. Although Japan is a leading country in the use of heat pumps, the development of the GSHP market is far behind. On the other hand, European nations tend to show a short term uptake.

The first explanation must be the geography-dominant characteristic. Since soil temperature approximately under 7 m deep is constant at the mean ambient temperature of the area (Doherty et al., 2004), locations with extreme climate would acquire more benefits (Lund et al., 2004).

Table 1.1 Situation of the GSHP in each region (Leech, 2006 and Nagano, 2006)

Region	Installation in 2007	Situation	Barriers
North America	more than 200,000	largest capacity	
Central or north/ west Europe	more than 60,000	increased significantly	
UK	500	increased for new residential houses	Biased image for existing houses and application for commercial facilities
Japan	125	not common yet	Reasonable electricity prices but fuel costs have increased

Nevertheless, Geo-Heat Centre ([no date]) suggests that geothermal energy is accessible in vast area, such as everywhere in the USA (Figure 1.3). If the use of the abundant energy is unexpectedly within the reach, an effective method to enjoy the benefits is awaited to be announced.

The other powerful factor is the policies issued by local governments. Many governments have launched funding schemes to the GSHP for the sake of energy security. For instance, Sweden and France increased the installation due to the governmental supports (Forsen et al., 2008). This driving force is influential, because of the economic barrier that the GSHP has had.

1.3 Design Example

Geothermal energy has potentials to become one of the flexible heat sources for heat pump systems. If there are approaches to enhance the benefits of the

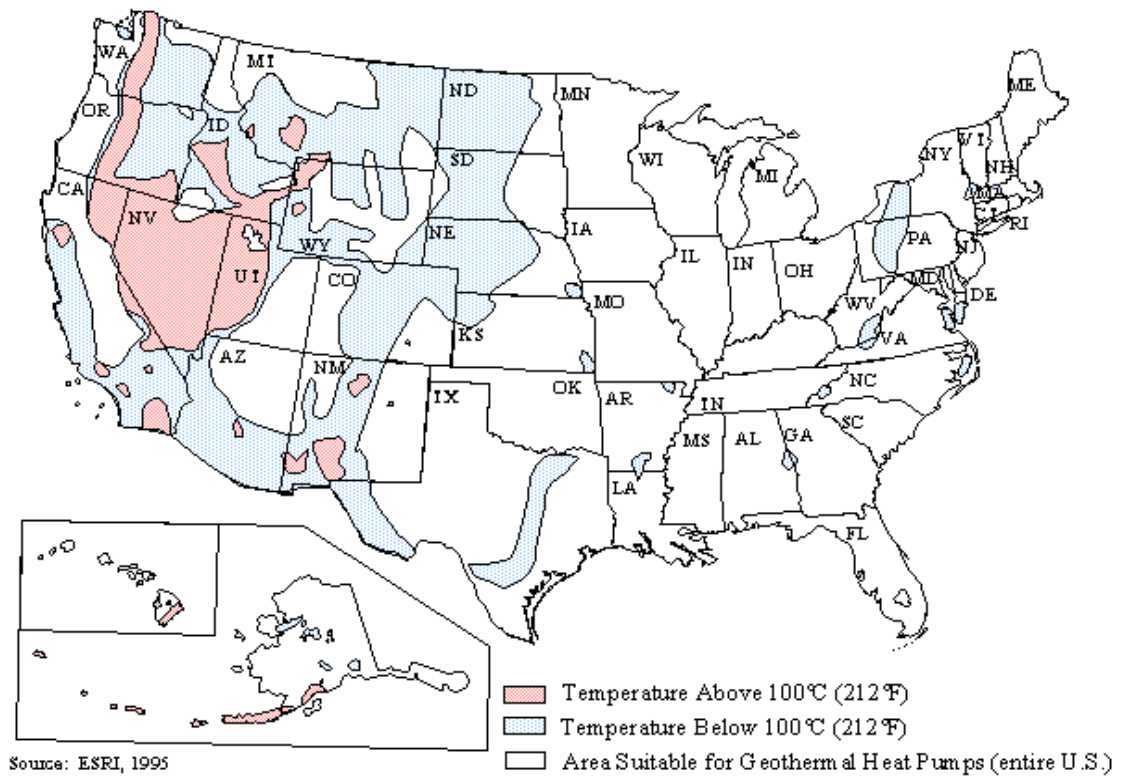


Figure 1.3 Ground source in the USA (Geo-Heat Center, 2008)

vastly available energy, the uptake would contribute to solve the global energy shortage. To achieve this, it is ideal that the GSHP becomes a feasible option without governmental subsidies. Therefore, further technical efforts should be made. This section intends to discuss a system idea in order to find a solution to the objectives that the GSHP has.

1.3.1 Considered system

A system is suggested to cover the weakness of the GSHP as illustrated in Figure 1.4. This idea allows designers to assemble the system using only the most beneficial of the available energy sources at the location. Preparing multiple sources enables provision of alternatives when energy shortage occurs at one source, which will make the system operation more

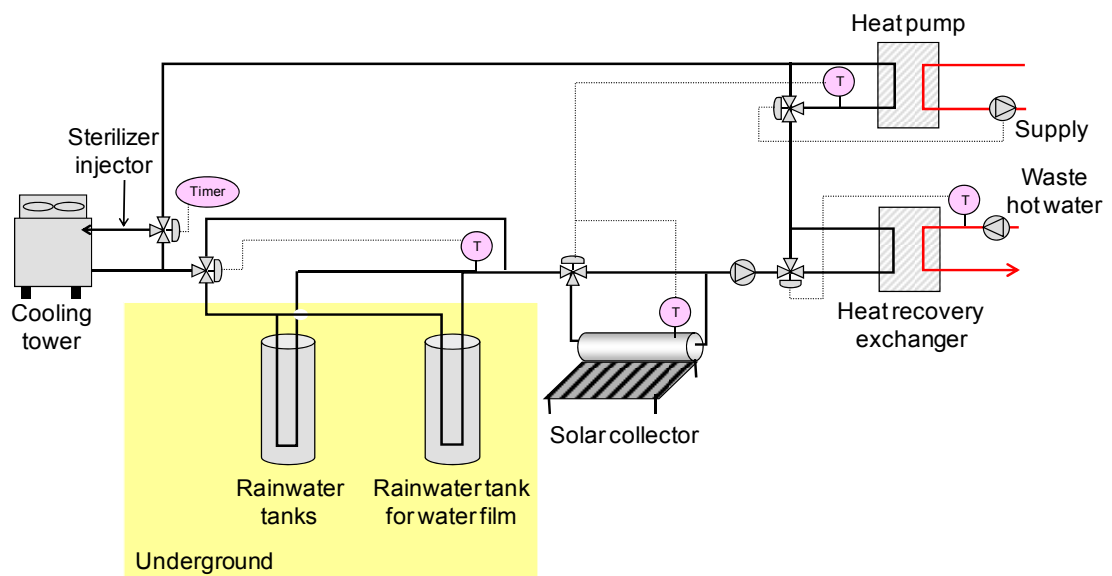


Figure 1.4 System example: circuit for heat sources

stable. A variety of heat source can compose the system with dependence on the local conditions and on required heat supply capacity. Possible additional sources are evaporative cooling through cooling towers, solar thermal collectors, energy recovered from drain and energy in rainwater and underground.

In this design, ground heat source collection is enhanced by making a use of thermal energy in rainwater. For instance, when cooling demand occurs, heat source at low temperature can be produced by cooling towers, ground heat source and rainwater thermal energy. Since rainwater stream is likely to stir the water in the tanks, the enhancement of heat transfer due to the convection is expected simultaneously. This strategy is a suggestion to the first objective pointed out in the previous section, stability of energy supply. Furthermore, selecting optimised combination of system components would maximise the operational efficiency.

This system is capable of storing energy into the rainwater tanks and the underground space during off operational hours by circulating the liquid medium. In case that night operation of the cooling towers can generate colder water than the daytime operation, the daytime COP will be improved by using the stored energy underground. Hence, the proposal is to stabilise the fluctuating energy supply by preparing a combination of sources and by storing energy.

There are several methods to utilise rainwater, for instance, as water source. However, the proposed system expects rainwater to contribute thermally. Rainwater is collected from the roof, facades or ground surface into the water tanks buried underground. Then, the useful temperature is maintained by the insulation of the soil. A heat exchanger is immersed in the tanks to collect the stored energy source for the heat pump. In case of rainfall, thermal energy can be immediately topped-up around the heat exchanger. This quick replenishment may lengthen the system operational time.

The School of the Built Environment in the University of Nottingham (52°94'N, 1.20°W) is equipped with a weather station. According to the collected data, the average ambient temperature during rainfall in the coldest month, December, was approximately 6.2 °C. This is not impressively high; however, it is certain that the rainwater inflow can delay the timing when the stored rainwater is frozen during the heat extraction. It is advisable to prevent the water from freezing, since the convective heat

transfer effect would be lost. Moreover, the frequency of precipitation is not little. The average chance during December in Nottingham is once in 11.9 hours. On the whole, the direct heat recovery from rainfall can be regularly expected with a reasonable frequency, such as once in a half day.

The last barrier is also required to be solved; therefore, the proposed system consists of the existing technologies and materials to minimise the initial costs. Needless to say, cooling towers, thermal collectors, heat recovery exchangers and rainwater collection tanks have been already developed. Commercially available heat exchangers, such as slinky coils, can be chosen to be installed within the rainwater collection tanks. Even if some additional functions become necessary, efforts ought to be made to maintain the economic feasibility.

1.3.2 Strategies to reduce cooling demand

Some regions have more cooling demand than heating. Though renewable energy has limits in terms of stable supply and energy density, the reduction of cooling demand should be attempted. If humidity in air is not considerably high, air temperature can be dropped by water evaporation, for example, at the neighbouring outdoor space of the buildings. Then, directly guiding the fresh and cool air into the buildings can contribute to air conditioning. For areas with high humidity as well as high temperature, one of the effective methods to minimise cooling load is again evaporative cooling, for instance, by making water film on the roof and the facades as shown in Figure 1.5. The stored rainwater is pumped up from the

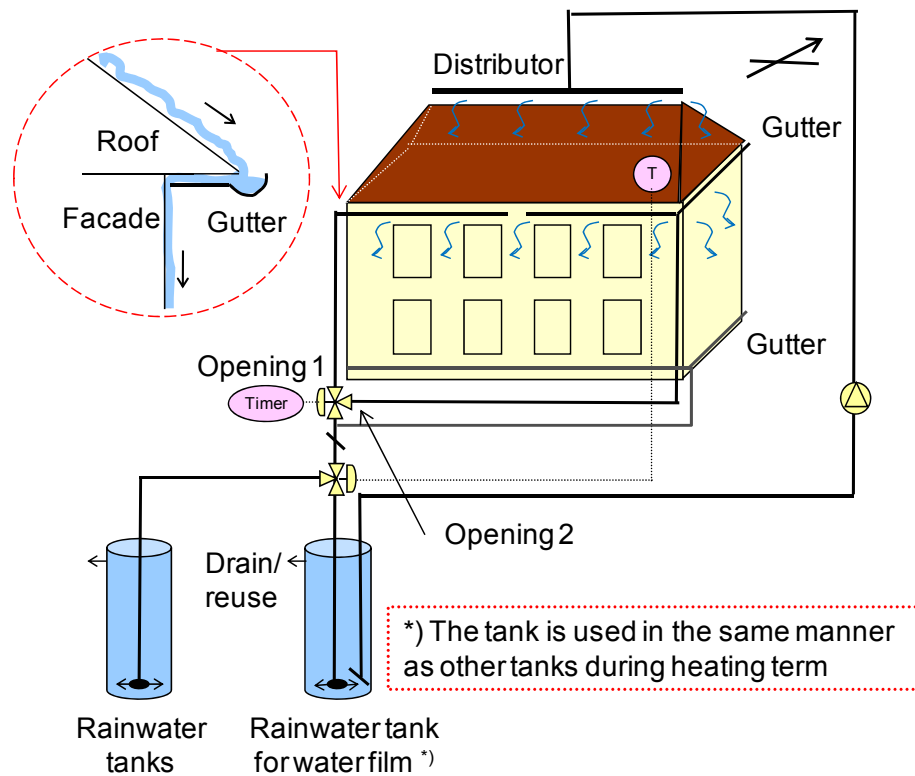


Figure 1.5 System example: circulation of rainwater

underground tanks and sprayed at the top of the roof. The water evaporates on the surface of the flowing water and decreases the outer surface temperature of the roof or facades. Consequently, excessive solar energy is absorbed in the evaporation process so as to lessen the amount of heat transferred through the building structure. This is another way to make effective use of rainwater and this strategy can be integrated into the proposed system as drawn in Figure 1.5. As mentioned in section 1.3.1, utilising cold water produced by the night storage operation will improve the efficiency of this rainwater evaporation cooling.

Evaporative cooling is the most suitable cooling method for the conventional roofs; however, there is also a fact that substantial amount of water supply is

required (Nahar et al., 2003). For instance, approximately 50 litres/m²/day is consumed in arid regions. For this reason, the use of rainwater to make the water film is suggested in this research project.

The rainwater harvesting system can be operated efficiently with a simple control method and a simple geometry. Figure 1.5 illustrates gutter, which is specially designed to provide evaporative cooling both on the roof and facades. Evaporative cooling on larger surface area is a more effective condition to minimise solar gain rather than utilising only the roof surface. When both Opening 1 and Opening 2 are closed, rainwater flow in the downpipes is blocked to make the rain over flow in the gutter. Consequently, the rainwater flows over the facades. A downpipe attached to the bottom of the facades is always open to direct the rainwater into the buried tanks. Efficient operations can be achieved by creating rainwater film when the façade is exposed to plenty of solar radiation. Therefore, shifting the operational facades following the movement of the sun must be worth considering. This function can be realised by controlling Opening 1 and Opening 2 with timer settings. When water evaporation on the facades is not necessary, both Opening 1 and Opening 2 are open so as to allow all the rainwater to flow into the downpipe and eventually into the rainwater collection tanks.

1.3.3 Strategies to enhance the underground heat collection

Low energy density of ground heat source requires to be covered by efficient heat transfer. Enhancement of underground heat collection has been

investigated, such as grouts with high thermal conductivity (Allan, 2000). Without doubt, even higher overall thermal conductivity than only highly conductive grout is preferable, if it is delivered economically. Hence, modifications, such as that to sub-soil surrounding the rainwater collection tanks, must be worth investigating. Mixing highly conductive substances is one of well approved strategies to accelerate the heat transfer. In this project, injection of highly conductive particles into soil is assessed as a novel approach.

An idea of injection is also selected from the aspect of economic feasibility. It is possible that an impact on the construction costs could be milder than that for digging up substantial amount of sub-soil to mix additional materials and returning them back to the underground. The soil injection could be also a useful instant modification method even after a certain period of operation.

1.4 Purpose and Approaches of Project

This thesis intends to investigate feasible design modifications of the GSHP to promote the uptake particularly for commercial and small industrial facilities. Though borehole systems have been relatively common, this project focuses on horizontal coiled loop (slinky coil) systems. Horizontal slinky coil systems have lower efficiency in underground heat collection; however, the impacts of the initial costs are less than those of borehole systems (Lund et al., 2004). Hence, improving operational efficiency by enhancing underground heat collection is the aim to be tackled.

Chapter 1 Introduction

The objective of investigation is to find design solutions to overcome the main three objections in the use of the GSHP. These are reliability of performance, high efficiency for compact required space and economic viability as introduced in section 1.2.2. Particularly, utilisation of one of the complimentary energy sources, rainwater, is assessed. Effects of thermal energy in rainwater and convective contribution to heat transfer within the rainwater collection tanks are evaluated for practical applications. A thorough design comparison is attempted as displayed in Figure 1.6.

Background circumstances of this project and design ideas of the GSHP are introduced in Chapter 1. Relevant fundamental information and issues are

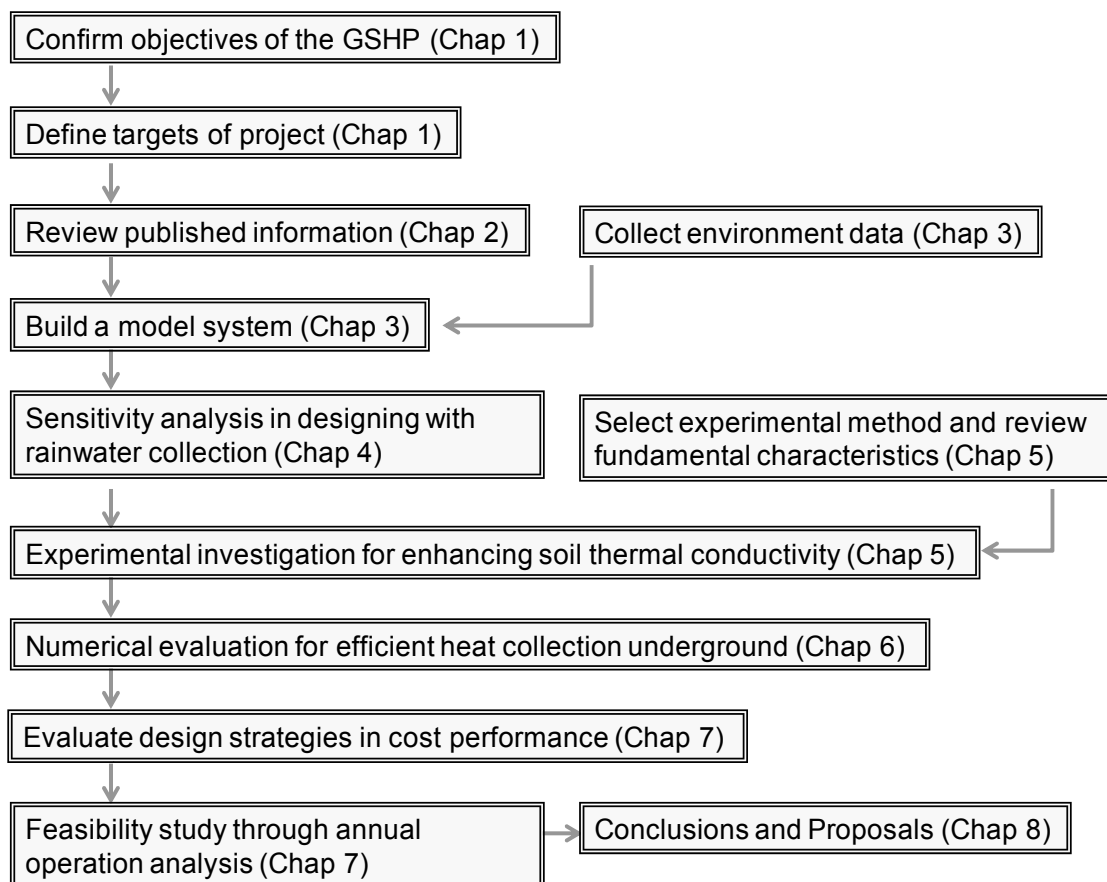


Figure 1.6 Flowchart of the procedure

derived from the past research about the system components; heat pumps, rainwater collection systems, evaporating cooling systems and highly conductive materials (Chapter 2). Background and reasons for chosen design ideas, for instance, the use of rainwater and graphite for the GSHP, are also explained with references. In addition, two measuring tools and two theoretical models to obtain soil thermal properties are introduced.

A GSHP model system is designed in Chapter 3, which enables this project to assess various kinds of design options on the same base. Office buildings with different design conditions are matched with a heat pump to recognise an applicable design range. Subsequently, Heating and cooling loads are calculated for a building which meets the approved document L2B. In order to evaluate with realistic operational conditions during simulation analysis, a methodology to obtain and process environmental database is presented.

System design with an underground rainwater collection tank is optimised with Computational Fluid Dynamics (CFD) in Chapter 4. The study starts with fundamental preparation; defining a method to determine the most effective mesh size, verification of the simulation model and setting up a simulation model and conditions. Sensitivity analysis compares the influences of components with different size and materials on the underground heat transfer. Consequently, effective design parameters to improve the overall heat transfer are extracted.

Practical design methods are investigated for one of the most essential design

factors, which are concluded in the previous chapter. Efficient enhancement of soil thermal conductivity is targeted through experimental investigation in Chapter 5. Setting up of one of the measuring methods, dual-probe heat pulse method (DPHP), is required including calibration and error analysis. Then, the investigation begins with selecting a more suitable methodology between the DPHP and heat flow meter (HFM). The evaluation is carried out by measuring soil thermal conductivity with various kinds of water content. Basic characteristics of soil are also understood by quantifying particle size distribution in wet sieving method, optimum moisture content (OMC) and thermal properties. Pore size is measured with x-ray micro scanning in order to specify the criteria for high soil thermal conductivity. After defining conditions to generate natural soil in lab, effective and economically practical modification strategies are outlined through case studies by varying compaction energy, packing ratio and water content gained from suction.

Underground structure with the derived soil modification method is optimised with the CFD in Chapter 6. At the beginning, possibility of incorporating convective heat transfer into the heat collection design is examined. Criteria for increasing the effects are studied from the past research results and a combined design with the existing obliged facility is proposed. The rest of discussion concentrates on conductive heat transfer through horizontal slinky coils, which are directly varied without a rainwater collection tank. Desirable depth of heat exchanger and thermal conductivity of the modified soil space are examined through a sensitivity analysis. After studying an effect of solar gain, design of thermal pillars containing carbon fibres is optimised with fifteen kinds of cases

with different length, number of sub-roots, thermal conductivity and diameter. Consequently, the advantages of thermal pillars over simple soil modification are concluded.

Six underground heat collection designs are compared through a simulation analysis for the insulated office building in Chapter 7. Benefits of a rainwater collection tank and soil modification are evaluated from an aspect of enhanced efficiency and installation costs. Subsequently, the most competitive solution is compared with the existing design in an annual operational analysis. The improved capacity of the ground heat source for each month is assessed in yearly electricity consumption and CO₂ emission. Possibilities of further improvements with different electricity price and initial costs are also discussed. Moreover, a design method to sustain water content in soil is proposed with a concern of economic feasibility.

The thesis finishes with reviewing conclusions from each chapter in Chapter 8. In addition, further research themes are suggested so as to ensure that the findings are eventually ready for real applications.

Chapter 2 Literature Review

Introduction

Some system components mentioned in the previous chapter, heat pumps and rainwater collection systems, have a long history. Throughout various kinds of study and operations, more convenient and efficient designs have been invented. However, there are always possibilities to update the techniques or to adopt these technologies into the current demands. Hence, the first two sections address features, issues, common operation and recent developments of heat pumps and rainwater collection systems. In particular, the GSHP is introduced in details. Moreover, some novel ideas are described in order to assess their feasibilities throughout this project. One of them is the use of thermal energy in rainwater in order to improve the heat collection capacity of GSHP.

Evaporative cooling and the use of highly conductive materials were chosen to enhance the performance of the suggested system. Techniques for these two ideas have been also well studied. There is no doubt that evaporative cooling could be one of the most efficient sustainable cooling strategies. However, the water source and effective methodologies to integrate evaporating cooling into systems ought to be discussed. On the other hand, the practical use of conductive materials also demands careful consideration in open systems, such as the proposed underground structure in this project. To avoid resulting in negative side effects on the environment, sufficient considerations in the selection of materials and design are inevitable. As a result, an idea to use one of the harmless substances, graphite, is explained on the basis of the past

research.

Experimental and theoretical methods to find soil thermal properties are introduced. Firstly, two accessible methods, heat flow meter (HFM) and dual-probe heat-pulse method (DPHP), are compared. Subsequently, two kinds of well referred theories, de Vrie's model and Campbell's model, are introduced. The information provides the basis for the investigation in Chapter 5.

2.1 Heat Pumps

Since heat pump technology was invented in the 19th century, commercially feasible systems have been gradually formed by various attempts. After more than two centuries, heat pumps are expected to solve the energy issues that the world has been facing. The mechanisms, positive impacts, variety of choices and suitable operational conditions are introduced in this section. The last part of this section explains various aspects of the GSHP, such as problems, common practices, features, efforts for effective designs especially with the use of underground water.

2.1.1 Advantages of heat pumps

Heat pumps work in a closed thermal cycle and have a distinctive flexibility to supply cooling energy, heating energy and both. The flexibility allows the systems to provide thermal energy at a required temperature in dependence on the demands all through a year. A year round utilisation of the systems shortens the payback period in comparison with installing heating and

cooling systems separately. Furthermore, installing the combined equipments both for heating and air conditioning saves the required space in machine rooms.

The systems normally consist of four main components; compressor, condenser, expansion valve and evaporator in case of vapour compression type as illustrated in Figure 2.1. There are other types, for instance, absorption / adsorption systems; however, the basic mechanisms are introduced with the vapour compression type here. Thermal energy is transported through the phase change of refrigerant, which is circulating in between. When cooling demand rises, the refrigerant is liquidised by the compressor and thermal energy by the phase change is removed at the condenser. The compressed vapour at lower temperature starts evaporating after going through the expansion valve and seizes enthalpy of vaporisation at the evaporator. Fluid thermal medium is flowing into the heat exchanger in the evaporator to gain the low temperature for air conditioning. This procedure is perfectly reversible. Heating operation

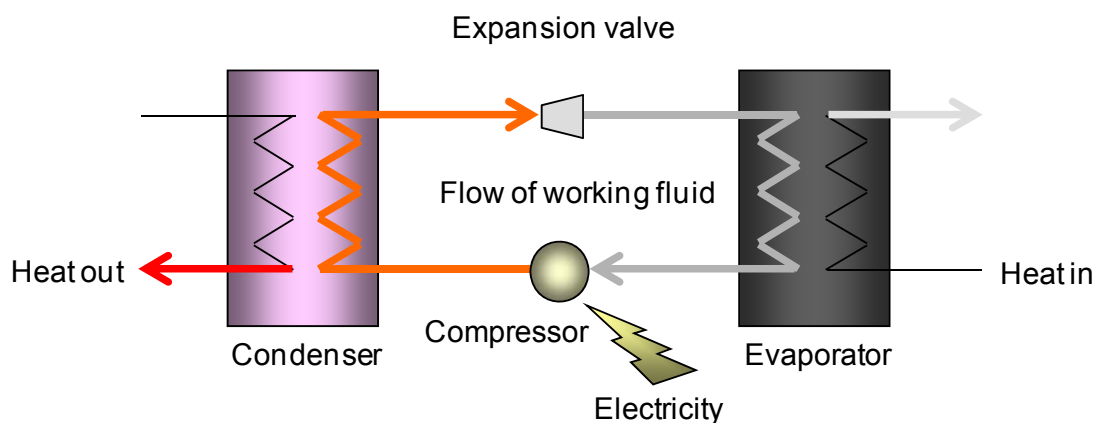


Figure 2.1 Electricity-powered heat pump (IEA Heat pump Centre, 2004)

can be achieved by a simple valve change to reverse the flow direction of the refrigerant.

Attractive characteristics of heat pumps are the high efficiency and the useful output temperature as introduced in section 1.1. In theory, the total output energy should be equal to the total input energy. In case of heating, input energy at the compressor and the evaporator should be the same amount as output energy at the condenser. In practical heat pump operations, the heat source is complimentary, such as ambient air or water from river, sea and waste and effluent from industry (IEA Heat Pump Centre, 2004). Therefore, only input energy at the compressor is normally counted. In an example of Figure 2.1, the compressor requires electricity and useful heat is extracted from the evaporator or / and the condenser. Electricity-driven heat pumps generally generate 100 kW of thermal energy out of 20 to 40 kW of input energy, which means 2.5 to 5.0 in the COP. Industrial heat pumps can operate even at the COP of 10.0 to 33.3. This is attributed to a combination of water heat source, an inverter controlled compressor and mechanical advantages in efficiency that large scale machines tend to obtain. The tendency of efficiency is described in section 2.1.3.

The uptake of heat pumps is expected to contribute in two manners; reduction of energy consumption and CO₂ emission. Electric heat pumps require less fuel than the conventional boilers by about 35 to 50 % (IEA Heat Pump Centre, 2004). Therefore, replacing the conventional energy supply

components by heat pumps would save energy. Figure 2.2 indicates the potential contribution of heat pumps in the UK. Due to the long term dominance of gas boilers, the UK market of heat pumps has been small (Forsen et al., 2008). Assuming almost no thermal energy was supplied by heat pumps in 2002, up to 44 % of energy consumption could have been trim downed by higher operational COP of heat pumps. Regarding that the UK government launched a policy, Low Carbon Buildings Programme (Department of Energy & Climate Change and Energy Trust, 2009), a remarkable improvement will be seen in the UK future.

The final point is an effect of operating heat pumps on the world CO₂ emission as shown in Figure 2.3. IEA Heat Pump Centre (2004) predicts that the total reduction will attain 5.4 % with heat pumps operated in the residential, commercial and industrial sectors. When power plants are operated at higher efficiency than the present condition, the joint reduction would reach up to 3.5 billion ton, which is equivalent to 16 % of the total

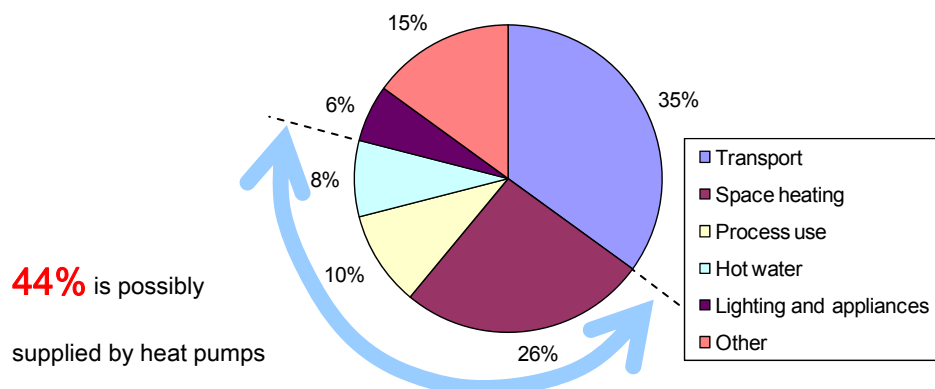


Figure 2.2 Energy consumption in the UK, 2002 (Energy White Paper, 2003)

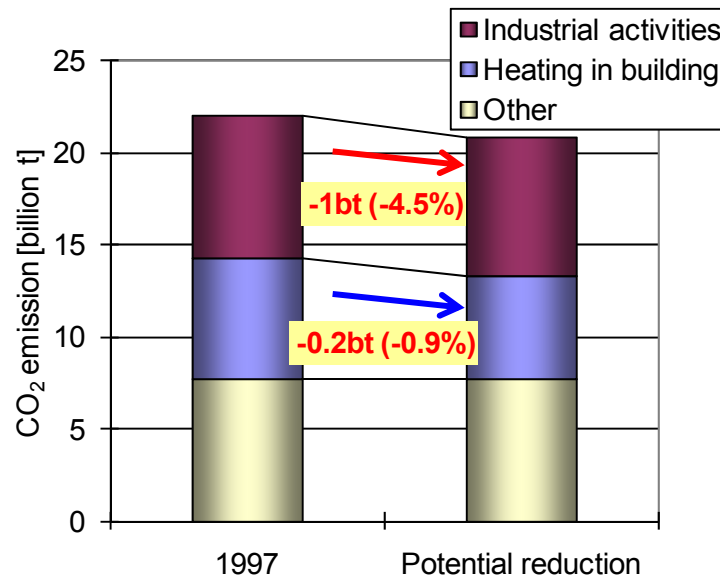


Figure 2.3 Potential reduction of CO₂ emission by heat pumps (IEA Heat Pump Centre, 2004)

emission in 1997. The United Nations (1998) obliged developed countries to reduce at least 5 % of reduction in comparison to the 1990 level was required in the Kyoto protocol. Hence, the estimated effect is also encouraging to modify heat pumps themselves for higher efficiency and to discover more efficient operational methods of heat pumps.

The positive impacts of heat pumps are good news for the nations which are struggling with the reduction of CO₂ emission, such as Japan. Japan made an optimistic commitment of 6 % reduction from the 1990 level by 2012 in the Kyoto Protocol. However, the CO₂ emission has been increasing due to the constant economic growth. As a result, the emission from the residential and commercial sectors rose up by 31.5 % and 37.9 % respectively in comparison to the 1990 levels (KIKO Network, 2006).

Therefore, further improvement in the efficiency of energy systems is one of the few strategies for the country which has already introduced basic environmental provisions.

2.1.2 Types of heat pumps

Types of heat pumps are categorised in terms of operational mechanisms, energy source and working fluid. This means that each heat pump can be identified with a combination of these features, for instance, electricity-driven heat pump with air heat source and with R-401A as working fluid.

Heat pumps are classified in terms of working mechanisms listed in Table 2.1. There are more technically available types; however, only commercially successful types are brought to a discussion here. Electricity-driven heat pumps are more commonly seen in the domestic and commercial use, while engine-driven systems tend to be applied for large scale industrial facilities (IEA Heat Pump Centre, 2004). Absorption systems overcame some inconveniences, such as the leak of the poisoning working fluid and the break of vacuum. Consequently, a potential for a

Table 2.1 Types of commercialised heat pumps (IEA Heat Pump Centre, 2004)

Category	Type		
Vapour compression	1)	Electricity-driven	
	2)	Gas/diesel engine-driven	
Absorption cycle		Working fluid	Absorbent
	1)	Water	Lithium bromide
	2)	Ammonia	Water

cascade use of waste heat has had attention.

Typical temperature range of each heat source is illustrated in Table 2.2. The availability and efficiency of heat sources largely depend on site conditions. In general, ambient air is applicable in most of the cases; however, the energy density is relatively low. On the other hand, the liquid heat sources potentially increase the operational efficiency of heat pumps; however, the geographic issues are more dominant over the available amount and the types. Therefore, selecting the most suitable heat sources is an essential process in designing heat pump systems.

The selection of working fluid has been a globally controversial issue. The main concern is the negative impact on the depletion of ozone layer and the green house effects. Table 2.3 indicates that a thoughtful choice of the working fluid enables to minimise the harms as well as to reduce the energy consumption by operating heat pumps. This idea has been introduced as the international regulations. Figure 2.4 illustrates the phased-out schedule

Table 2.2 Heat sources (IEA Heat Pump Centre, 2004)

Heat source		Temperature range		
		0	10	20
Air	Ambient	-10 to 15		
	Exhaust			15 to 25
Water	Lake	4 to 10		
	River	0 to 10		
	Sea	3 to 8		
	Waste and effluent			More than 10
Underground	Rock	0 to 5		
	Soil	0 to 10		

Table 2.3 Characteristics of working fluids (Pedersen, 2003)

Category	Substance	R-number	Chemical formula	ODP ¹⁾	GWP, 100 years ²⁾
CFCs	CFC-11	R-11	CFCl ₃	1.000	5,600
	CFC-12	R-12	CF ₂ Cl ₂	1.000	4,000
HCFCs	HCFC-22	R-22	CHF ₂ Cl	0.055	1,700
		R-401A	Mixture of R-22, HFC-152a and HCFC-124	0.000	1,082
Blends		R-407C	Mixture of HFC-32, HFC-125 and HFC-134a	0.000	1,526
		R-410A	Mixture of HFC-32 and HFC-125	0.000	1,725
HFCs	HFC-134a	R-134a	CH ₂ FCF ₃	0.000	1,300
	Ammonia	R-717	NH ₃	0.000	0
Natural	Water	R-718	H ₂ O	0.000	0
	Carbon dioxide	R-744	CO ₂	0.000	1

1) ODA, Ozone Depletion Potential, is expressed on the basis of the impact by CFCl₃. Hence, the ODP for certain substance is a ratio to the amount of ozone removed by a unit mass of CFCl₃, while the ODP for CFCl₃ is 1.

2) GWP, Global Warming Potentials, is the integrated radiative forcing over a certain period of time horizon, i.e. 100 years in this table. The value is expressed as a ratio to the integrated radiative forcing of CO₂. (Houghton et al., 2001)

agreed as the Montreal Protocol in 1987. The use of the CFCs (Chlorofluorocarbons) needed to be completely terminated by 1996 because of the large impacts both on the ozone layer and the global warming. The HCFCs (Hydrochlorofluorocarbons) have been also planned to be phased out by 2020, though the European Union has set the target at 2015. Moreover, the positive values of the GWP for the HFCs and the blended fluids have brought discussions. The UK government announced that the HFCs were not environmentally sustainable and alternative substances should have been discovered (Department for Environment, Food and Rural

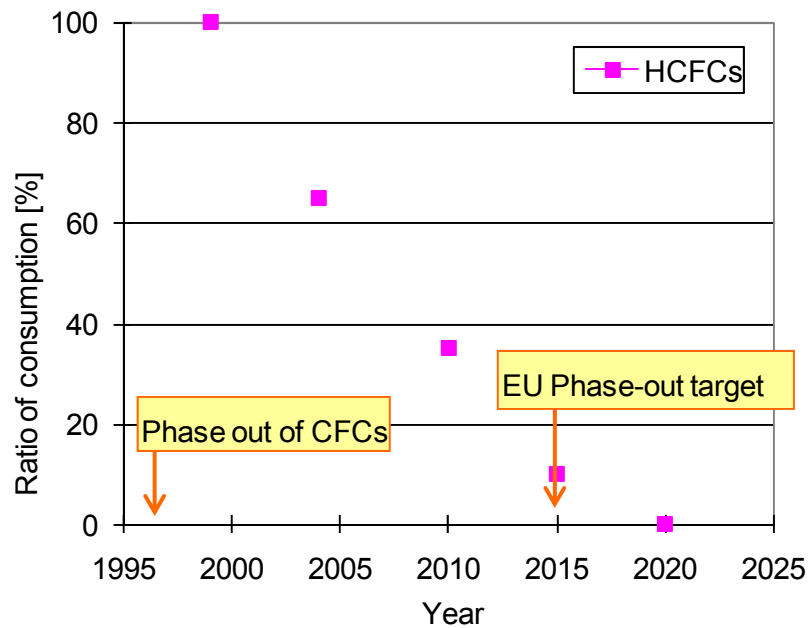


Figure 2.4 Phase-out plan agreed in the Montreal protocol (IEA Heat Pump Centre, 2004)

Affairs, 2006). Eventually, a Voluntary Agreement was implemented in 1996, in order to restrict the usage in the industrial sector (Department of the Environment, Transport and the Regions, 1999). This movement has changed the available types of heat pumps on the market.

The global discussions over the use of the HFCs lead to the new development of heat pumps with natural working fluid. Though there are technical barriers for each substance, heat pumps with CO₂ as working fluid had a break through to be successfully commercialised especially on the Japanese market. CO₂ heat pumps are marketed as alternative hot water generators. The COP currently attained 4.9, which is greatly ecological regarding that the COP for the conventional boilers is less than 1 (Figure 2.5, Sanyo, 2006).

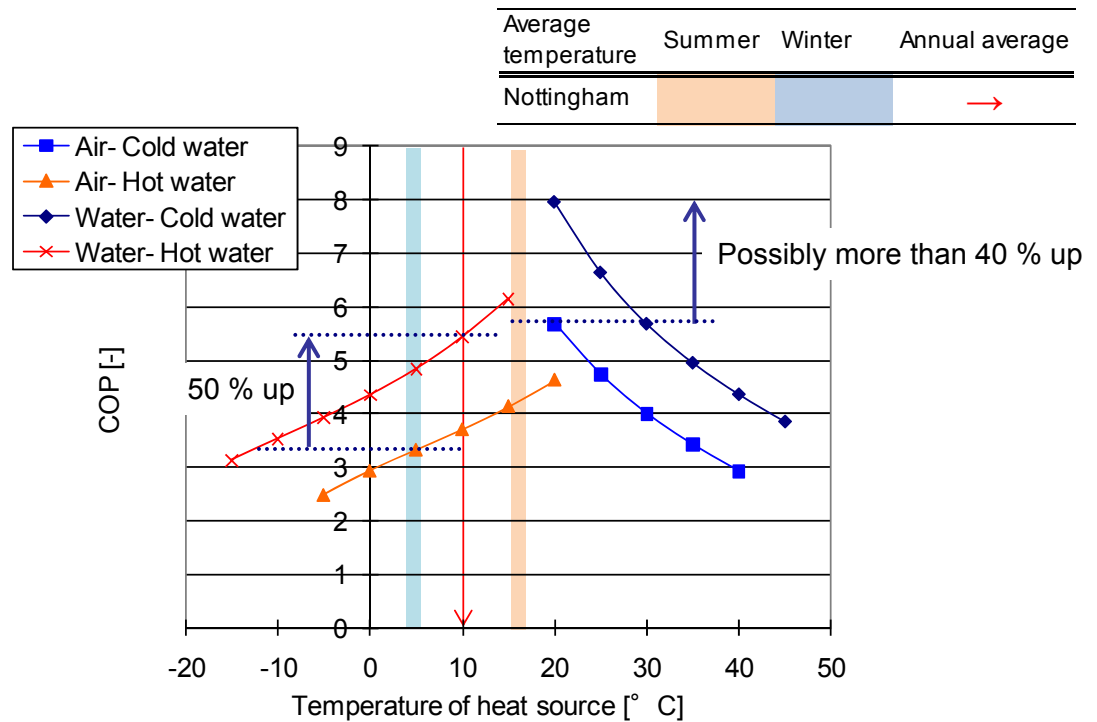


Figure 2.5 CO₂ heat pump (Sanyo, 2006)

This project, therefore, discusses heat pumps which will be acceptable in the future, in terms of availability on the market, practical heat source and ecological working fluid. With regard to that the commercial or small scale industrial use is targeted, electric heat pumps are imagined to be a part of the proposed system. In order to widen the possibility of practical applications, design solutions of the water-water heat pumps are investigated with only thermal energy in soil, rather than with combined heat sources. Finally, the working fluid needs to be either the blends, HFCs, or natural substances to meet the international agreement.

2.1.3 Conditions for efficient operation

The efficiency of heat pumps varies depending on operational conditions, such as the phase and temperature of heat source (Figure 2.6). A tendency of efficient input temperature of heat source differs between the



* The types of referred heat pump are ZQH-15A15-C and ZQH-15W15-C for air source and water source respectively. The conditions are as follows: current 50 Hz, medium R407C, cold water output 5 °C and hot water output 45 °C.
 * The monitored temperature range of the coldest / warmest three months in Nottingham is shown.

Figure 2.6 The COP of heat pumps (Zeneral heat pump Co Ltd., 2006)

heating and cooling cycle. On the whole, higher inlet temperature is more advantageous for heating, while lower temperature is for cooling. From the view point of heat source, heat pumps with water source have significantly higher COP. When the COP is compared at the same heat source temperature, heat pumps operated with water source (water source heat pumps) can operate more efficiently by 40 to 50%. It is calculated that the water source heat pumps normally have higher Seasonal Performance Factor (SPF) by 10 to 30% (IEA Heat Pump Centre, 2004).

Air source heat pumps have more drawbacks in terms of stable operation. Since ambient temperature is changeable, the capacity and efficiency become easily unstable. Besides, the low energy density in air requires frequent defrost during the operation in cold seasons. This process stops the operation temporarily and decreases the operational COP even more. As a result, it is clear that heat pump operation with water source supplied at advantageous temperature is preferable, if conditions permit.

These ideal operational conditions can be satisfied by utilising geothermal energy. As introduced in section 1.2.2, underground temperature below 7 m constantly keeps the average ambient temperature in the region. This creates an advantage against air source; the inlet ground source temperature at the heat pump is higher for heating and lower for cooling. Furthermore, liquid medium, which has higher heat transfer coefficient than gas medium, is normally applied to collect and transport the underground heat to the heat pump. When the ground temperature is referred to the mean ambient temperature, the potential COP rise for heating in Nottingham is up to 50 % (Figure 2.6). If cooling demand occurs, the effect is possibly more than 40 %. These remarkable potentials promote the recent uptake of the GSHP.

A combination between the COP characteristics of heat pumps and the trend of air or underground temperature explains why the GSHP could create more efficient operations. The biggest question is what sort of designs can achieve the effective use of underground temperature under 7 m with the

shallow heat collection systems.

2.1.4 Ground source heat pump (GSHP)

Though the system has a potential to become a popular sustainable strategy, further modifications are required as described in section 1.2.2. It should be said that the available capacity of ground heat source is unpredictable. Underground conditions frequently change and the design capacity is difficult to be guaranteed. An unwelcome scenario during the operation could be that the system has a shortage of heat source which would necessitate an emergency stop of the operation. If this happens during the heating process in cold regions, both soil and possibly the heat medium will be frozen and the system might have to wait for the warmer seasons to thaw the ice (IEA Heat Pump Centre, 2004). Consequently, larger heat exchange area is prepared taking large space, so as to secure the required amount of heat source. Figure 2.7 illustrates the GSHP with boreholes, which has been the most popular design for medium to large scale facilities. These boreholes are vertically buried up to 150 m deep (Office of Geothermal Technologies, 1999). Hence, drilling to great depth with heavy construction machines normally costs considerable amount of investment, though the maintenance costs are low (Hellström, [no date]). The large scale of construction work on sites also prevents potential users from taking the system into consideration.

There are some design strategies for the stable operation of the GSHP. Preparing larger heat exchange area is one of the conventional methods as

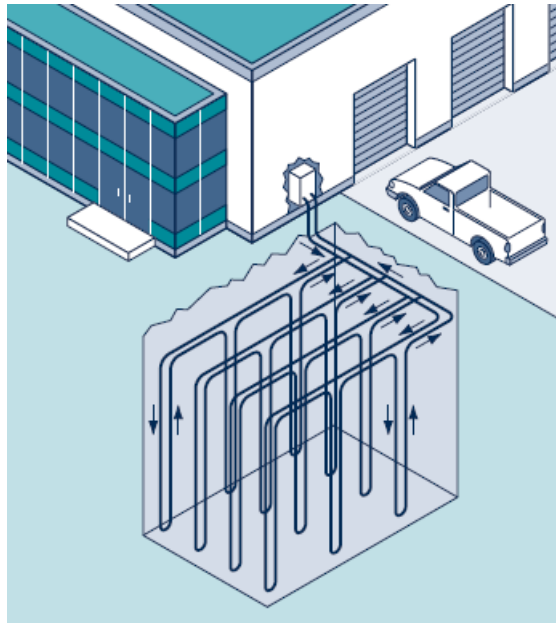


Figure 2.7 The GSHP with boreholes (Office of Geothermal Technologies, 1999)

described above. Another aspect is the depth of the heat exchangers for efficient heat collection. Figure 2.8 illustrates calculated underground temperature against depth for Nottingham. The method is introduced in section 3.2.2. The temperature near the soil surface is more influenced by the ambient temperature than the ground temperature below 7 m. Therefore, the soil deeper than 7 m stores more useful thermal energy for the GSHP. For this reason, installing long boreholes reduces the required exchange length by 30 to 50 % than burying shallow heat exchangers (Saif, 2004). Nevertheless, the dilemma with the intensive initial cost should be overcome.

Thermal energy for the GSHP can be separated from geothermal energy for electricity generation. The latter system extracts the energy transferred

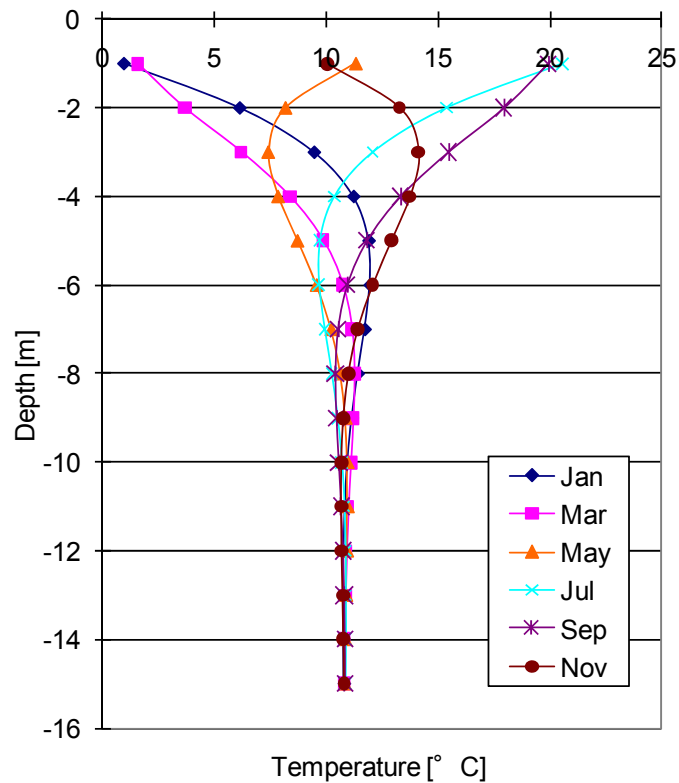


Figure 2.8 Calculated underground temperature for Nottingham

from the crust of the earth, where the wells up to 3,000 m deep collect energy at up to 500 °C (Barbier, 2002). On the other hand, energy for the GSHP is stored solar energy over the time. Therefore, the temperature gradient from the surface to soil at greater depth is the energy profile of the past several months (Figure 2.8). This may explain the peculiar trend. As more energy is transferred in the latest summer, higher temperature than the temperature below 7 m is seen in the gradient in the winter. This indicates that sub-soil is a useful substance for seasonal thermal energy storage.

Some research discovered other clues for the effective designs, for instance, Nidal (2000) finds that higher water content generates higher thermal

conductivity in soil. Furthermore, the flow of underground water potentially increases the thermal conductivity around the heat exchangers (Hellström, [no date]). To sum up, the effective use of water in sub-soil could reduce both required depth of the heat exchangers and the investment costs.

Various design strategies have been investigated, in order to enhance thermal conductivity between the heat source in soil and the heat exchangers. There are commercially available grout and heat exchangers, whose thermal conductivity was improved by adding conductive substances. Ordinary grouts have low thermal conductivity, such as 0.8 to 0.87 W/m/K with cement grout and 0.75 to 0.8 W/m/K with bentonite grout. However, grout made of a specific formulation of superplasticised cement-sand, Mix 111, enhances thermal conductivity up to 2.42 W/m/K (Allan, 2000). Besides, polyethylene is a practically selected material for heat exchangers, such as boreholes, due to the durability (Hellström, [no date]). There is a modified material mixed with highly conductive substances and this enables to thin the wall at the same time.

Groundwater flow is known as a desirable contributor to accelerate the total heat transfer. Some field measurements show 3 to 5 times as large thermal transfer as numerically calculated conductive transfer (Hellström, [no date]). However, the research points out the drawback, in which groundwater flow may also enlarge heat loss due to the greater heat transfer effect. To avoid this negative side effect, installing a water-proof screen is recommended in order to block the flow into the thermal energy collection area. This

probable benefit will encourage the active control of heat transfer by water movement in the practical applications. Nevertheless, this factor has been a potential bonus which will be revealed during the actual operation rather than a design strategy.

The active enhancement of convective heat transfer was eventually integrated into designs by creating natural convection around boreholes (Gehlin, 1998). Groundwater was poured into the borehole duct, in which U-tube was equipped as illustrated in Figure 2.9. As more heat was extracted from the U-tube, larger heat transfer was produced. The cause is presumed to be natural convection around the U-tube and the effect was even larger at higher temperature within U-tube (Hellström, [no date]).

Smith (2006) also implies the same effect by a pond type geothermal energy

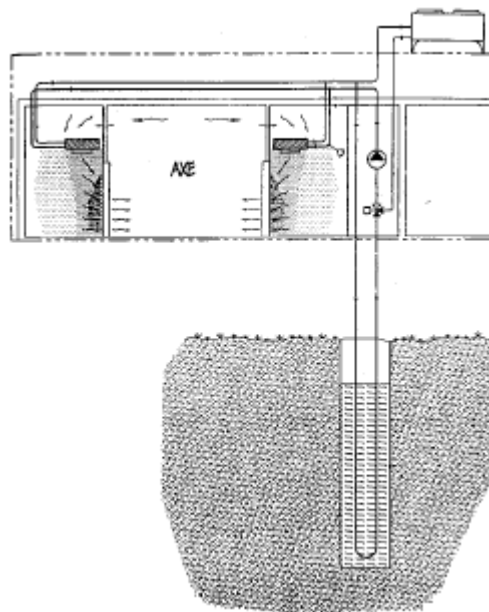


Figure 2.9 Water-filled borehole system (Gehlin, 1998)

collector. A slinky coil was placed in the centre of the geothermal storage area and effects of surrounding materials were compared among a pond, concrete filled space and others. The results show that the shallow pond extracted three times as much heat as the sand or concrete filled constructions during winter time. Forced convection heat transfer was unlikely in these tests; therefore, the advantage might be provided by natural convection.

This project ought to target constantly high efficiency in underground heat collection, instead of allowing the heat exchange area to be enlarged. Deep installation should be also given up for the sake of minimising the construction costs. Although mixing conductive materials has an effect, the applied amount needs to be the minimum for the same reason. Finally, efforts to make effective use of convective heat transfer are investigated through the CFD simulation for underground heat transfer models with a rainwater collection tank.

2.2 Rainwater Collection Systems

Rainwater has been utilised in simple systems since ancient time. However, the integration into modern buildings becomes more popular than before, due to the recent attention to the environmental issues. As the world population keeps growing on the top of the global warming, the sustainable use of water becomes of essence. Water had been thought as a basic source, which people did not doubt about the disappearance in the developed countries. However, these days the global water shortage in near future is predicted. Therefore, effective

strategies to use rainwater are more realistically needed. This section introduces expectations in the use of rainwater for the GSHP as well as the background and system designs of rainwater collection systems.

2.2.1 Usage of rainwater

Techniques of using rainwater have been applied for a long period of time in human history since the first use in Tibetan desert, which was documented 4,000 years ago (Li et al., 2003). In the UK, rainwater harvesting (RWH) has rapidly raised attention after 1985. Since water resource is limited and the water distribution system charges the users for the service, the RWH seems an economically sustainable solution as well as environmentally sustainable. A survey by OFWAT (The Office of Water Services, 2006) points out that water bills for residence have risen up by 39.1 % since 1989 in the UK. This lifted up the number of the RWH to three times as many as two years ago (envireau, 2006).

The applications of the RWH have a wide range, from flushing toilets to gardening, car washing, laundry and showering. The market has been expanding from the domestic sector to the commercial and industrial sectors. Figure 2.10 shows the ratios of water usage in residential buildings. In the case that rainwater is collected only for flushing toilets, gardening or car washing and laundry, 58 % of the mains water will be possibly saved. If sophisticated sterilising systems are equipped for hygiene reasons, the total contribution will be up to 98 %. The analysis also indicates that the RWH can meet 80 % of water demand in commercial buildings (envireau, 2006).

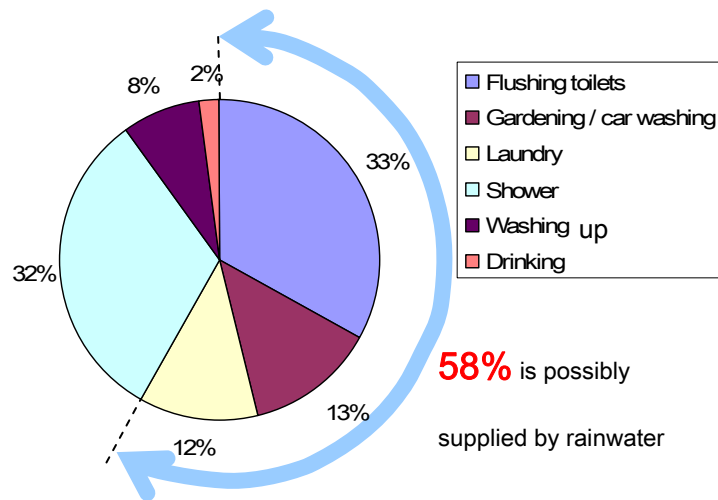


Figure 2.10 Domestic use of water (envireau, 2006)

These surveys support how significantly the RWH makes economical sense as well as environmental sense. An additional positive characteristic is that the RWH is adoptable even in remote or undeveloped regions.

2.2.2 System design

The RWH system mainly consists of drainage, a rainwater collection tank, a pump and filters. Figure 2.11 illustrates an example of direct systems, where a header tank is not installed unlike gravity systems. The rainwater collection tanks are mostly buried underground; therefore, a pump is required in the system.

The control panel automatically switches into the mains water supply in the event of rainwater shortage within the tank. Collecting cleaner rainwater makes the system operation more desirable, in terms of maintenance, quality of supplied water and a variety of applications. The most

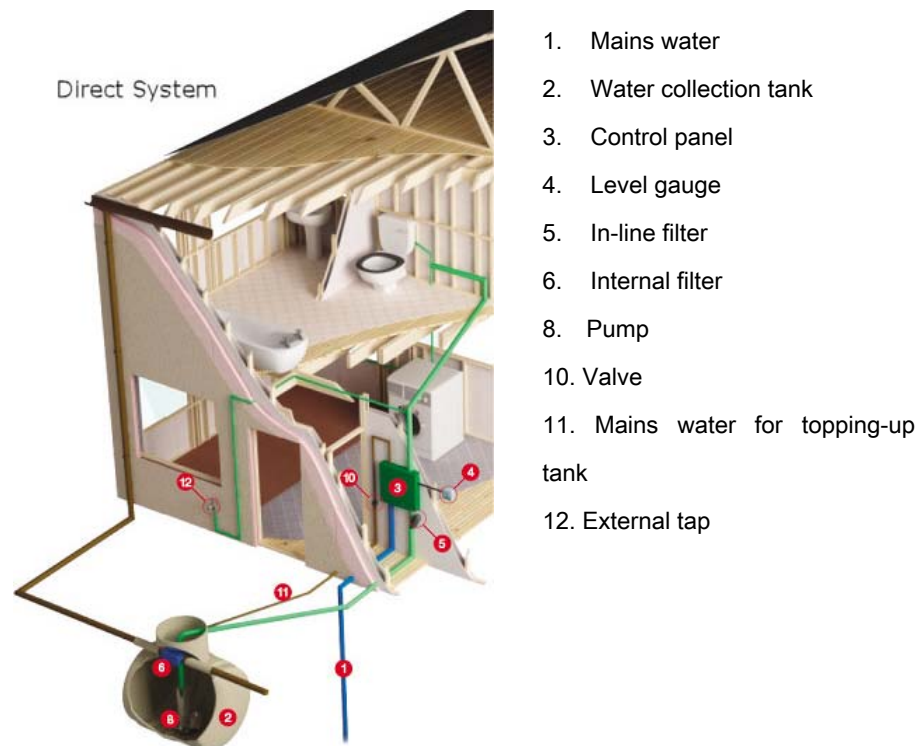


Figure 2.11 Design image of domestic system (envireau, 2006)

recommended collection area is roof; however, additional collection area on facades creates extra capacity as drawn in Figure 1.5.

2.2.3 Potentials of rainwater for the efficient heat collection in the GSHP

Some rainwater collection tanks are installed underground as Figure 2.11 illustrates. This indicates that rainwater can be used as a thermal media to collect ground heat source for heat pumps. In this case, rainwater contributes to improve the energy efficiency as well as to save the water bills. Simultaneously, thermal energy in rainwater can immediately top-up the stored energy in the tanks in the event of raining. This possibly makes the system operational time longer.

The effects can be estimated with meteorological data. Figure 2.12 demonstrates that rainwater temperature is similar to the ambient temperature during raining. It is rare to see database of measured rainwater temperature; hence, this assumption helps in predicting system operations.

The average ambient temperatures in the coldest and warmest month of Nottingham are listed in Table 2.4. The effects of thermal energy in rainwater can be roughly estimated with enthalpy, which is derived from the temperatures difference between rain and the ambient temperature. The rain temperature in December is nearly equivalent to the ambient temperature without rain. Therefore, energy in rain itself does not generate significant advantage to increase the COP of water source heat pumps in

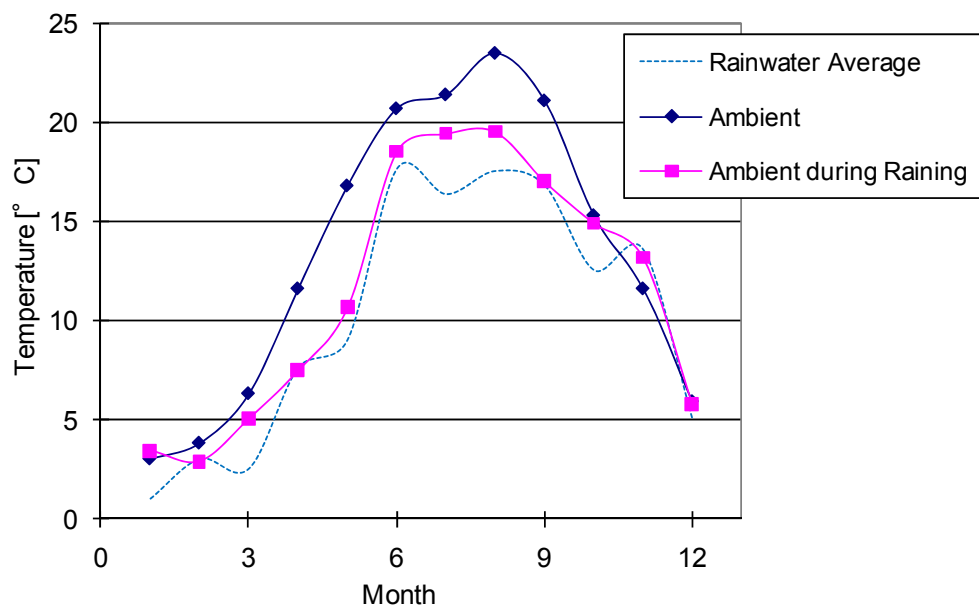


Figure 2.12 Measured rainwater temperature in Tokyo, 1993-1994

(Shokoku Sha, 2000 and Japan Meteorological Agency, 2006)

Table 2.4 Temperature difference between raining and non-raining conditions

Ambient temperature in °C							
Item		2001	2002	2003	2004	2005	Average
During raining	Dec	7.91	6.10	4.96	6.59	5.26	6.16
	July	14.12	14.45	14.57	13.91	12.69	14.69
Difference	Dec	2.26	-0.50	0.16	-0.21	-0.84	0.17
	July	-7.74	-4.45	-7.43	-5.29	-6.81	-6.34

1) Refer to Chapter 3.2 for database for Nottingham

2) Average ambient temperature is calculated with the climate data for 5 years. Then, the data in the coldest / warmest month is compared in table.

comparison to the COP of air source heat pumps. However, rainwater inflow at positive rain temperature, 6.16 °C, can prevent the system from stopping the operation due to frozen working fluid or soil.

The use of rainwater is a more attractive option in air conditioning. The rain temperature is lower than the average ambient temperature without rain by 6.34 °C. The reason must be that partial evaporation of rain decreases the ambient temperature and that rain cloud block sunshine. In this case, storing the rain underground has an advantage as the heat source can be sent to the heat pump at lower temperature. Simultaneously, water at high temperature within the underground tanks after the continuous operation will be replaced by rainwater at lower temperature straightaway.

Frequency of rainfall is another essential factor. Table 2.5 shows average chance of rainfall in the coldest and the warmest months in Nottingham. The frequency is less than one day. This regular rainfall is hopeful to fill the rainwater tanks with water at useful temperature. Parallel to this, stirring

Table 2.5 Frequency and duration of rainfall

Frequency of raining, in / hour ¹⁾

	2001	2002	2003	2004	2005	Average
Dec	16.2	4.8	8.8	17.5	12.2	11.9
July	12.6	7.2	7.0	10.1	12.0	9.8

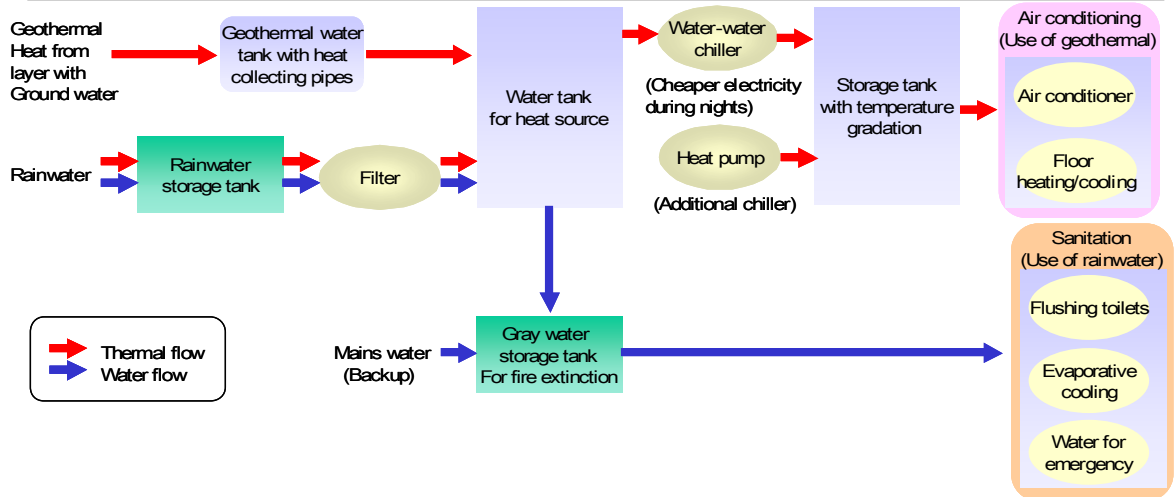
1) The total raining duration / the total hours in a month

2) Refer to Chapter 3.2 for database for Nottingham

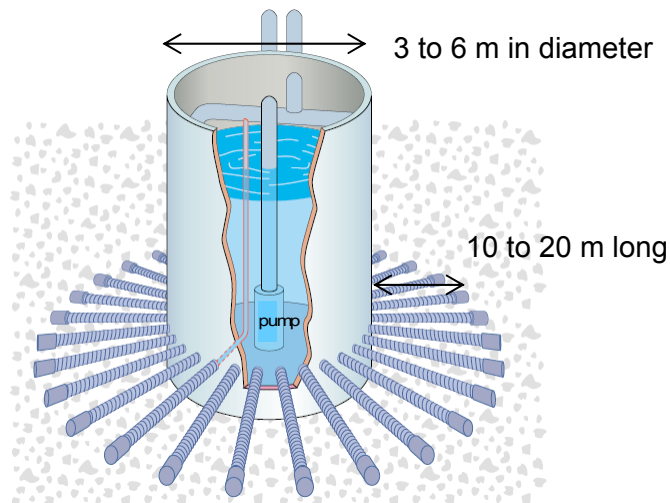
stored water by the rainwater flow will create convective heat transfer, which encourages heat transfer more effectively than conductive heat transfer.

The idea of utilising the thermal mass of rainwater for the GSHP is not common. Yet, a few systems are introduced, such as a system innovated by Sanken Setsubi Kogyo Co., Ltd (Figure 2.13). Stored rainwater in the underground tank circulates by a pump within the horizontally buried double tubes to collect geothermal energy. The thermal energy of rainwater is pumped up into the other tanks on the ground to be stocked until it is finally supplied to the heat pump as heat source. Rainwater flow within the double tubes is expected to enhance the energy collection efficiency by convection heat transfer. The system was installed in two governmental facilities. The operations reduced approximately 43 % of annual energy consumption and 38 % of running cost and CO₂ emission (Sanken Setsubi Kogyo Co., Ltd, 2005).

Al-Huthaili (2004) proposes to set heat pipes radially to create thermal bridge between rainwater in the buried tanks and the surrounding soil. Subsequently, it was experimentally proved that equipping heat exchange



(a) System flow of utilisation of geothermal heat and rainwater



(b) Geothermal water tank with heat collection pipes

Figure 2.13 Rainwater heat collection system (Sanken Satsubi Kogyo Co., Ltd, 2005)

plates around the solid bars improved the energy extract capacity (Figure 2.14, Chong, 2006). This result was affected by the enlarged total heat exchange area spread in sub-soil more than by the heat pipes without the plates. These two systems introduced above focus on different strategies to enhance the total capacity of thermal energy collection; convection heat

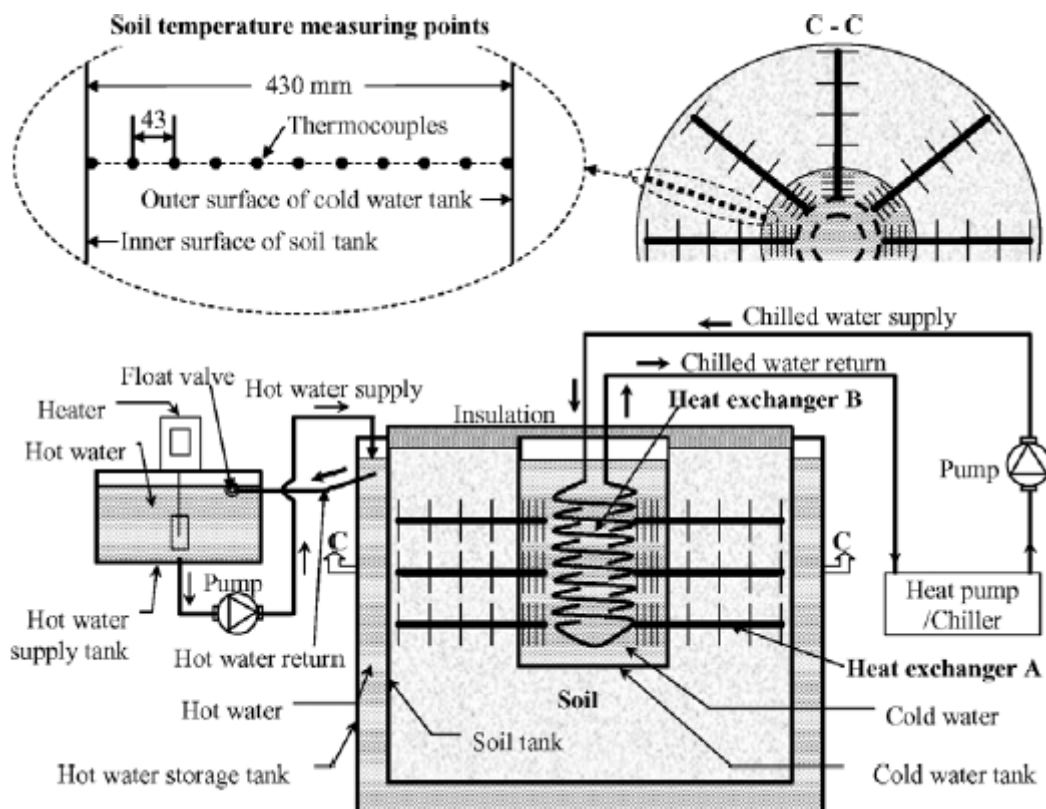


Figure 2.14 Experimental apparatus with heat pipes (Chong, 2006)

transfer in the former system and conductive heat transfer in the latter.

Thermal and mechanical energy of rainwater seems to have potentials to enhance operational efficiency in the GSHP. Though some of the design ideas prove that the use is beneficial, the cost performance is not either examined or disclosed. Since the economic evaluation is of great importance, this project reviews the technical advantages of the proposed designs and intends to discover the economically feasible solution.

2.3 Evaporative Cooling Systems

Some regions have more cooling demand than heating demand; therefore,

environmentally sustainable design techniques are essential. The use of water evaporation was invented in the ancient era. Nowadays, evaporative cooling has more attention as one of passive design strategies. As the system proposed in section 1.3.2 considers an integration of evaporative cooling, this section introduces the mechanisms and the applications for buildings.

2.3.1 Mechanisms of evaporative cooling

Evaporative cooling has been one of the most effective sustainable cooling methods. The system utilises a mechanism of temperature drop in environment through latent heat transfer, which is also known as enthalpy of vaporization. When liquid evaporates, required latent heat between the liquid and gas is taken from the water itself and the environment. Consequently, the temperatures decrease. The latent heat is 2,501 kJ/kg-water, while the sensible heat (specific heat capacity) is 4.22 kJ/kg-water/K (Holman, 2002). This indicates that more energy is involved in latent heat transfer, so that the system could be more compact. Furthermore, water has been the most popular substance in practical systems due to the convenience and from the economical point of view. Hence, evaporative cooling can be beneficial basically anywhere water evaporates.

The cooling effect by water evaporation is also subject to the allowance in the surrounding air. Theoretically, water can evaporate until the surrounding air reaches saturation. Therefore, dry environments have more chance to create effective cooling systems.

A major purpose of using this system is generating either cooled water or cool surrounding air. One of the well known gadgets in water cooling is cooling towers, which have been reliable and commercially successful. Consequently, numerous cooling towers have been installed in industrial / commercial facilities all over the world. Generating cooling air has been also utilised as one of human wisdoms since the ancient time.

2.3.2 Integration into building systems

There is more than one way to operate evaporative cooling systems in buildings. In general, there are three categories in calculating cooling demand; required energy to control fresh air conditions, to offset heat gain from indoor and to offset heat gain conducted through building structures (Down, 1969). Unless ambient temperature contains high humidity, the direct use of air cooled by evaporation is the most efficient solution. Since air has smaller specific heat, 1.006 kJ/kg/K, than water, 4.22 kJ/kg/K, air temperature is likely to drop more easily (Holman, 2002). Nevertheless, the criterion here is that the water content of conditioned air still remains in a range of comfort zone for occupants even after the evaporation.

When climate is hot and humid during warm seasons, indirect evaporative cooling is recommended. The options are either producing cold water or cooling down the building surface to reduce conductive thermal gain through walls. When the cold water is produced as the heat source of heat pumps, the energy supply system can utilise the cooling energy effectively. This is how evaporative cooling has been integrated into large energy supply

systems, such as air conditioning or process cooling systems in industrial or commercial facilities. As the conventional cooling towers have sufficient efficiency and economic variability, a combination between cooling towers and refrigerators has been a common strategy.

Regardless of that environment is dry or wet, it is effective if cooling demand is attempted to be reduced in the first place. Solar radiation which buildings receive from the outer surface is the main contributor to increase the cooling demand. Simultaneously, energy from warmed surrounding air transfers into the inside through building structures in accordance with the temperature difference in between. Though some passive methods, such as creating shadows on the surface, can assist, cooling the surface by water evaporation is a valuable strategy. This can be realised with relatively simple components as sketched in Figure 1.5, in comparison to installing a cooling system with several kinds of mechanical gadgets and an indoor control unit. Therefore, minimising cooling demand by cooling building surfaces would be reasonable.

2.3.3 Evaporative cooling on building surface

Various designs of evaporative cooling have been researched. It is said that almost a half of cooling demand occurs due to thermal gain from the roof in single story buildings. Hence, evaporative cooling on the roof has been studied well (Runsheng et al., 2003). The well known designs are water flow, water film by spraying, roof pond and green roof (Tiwari et al., 1994). The difference between the water flow and the water film is that

water is literally moving in the former method, while the sprayed water stays on the roof stand-still in the latter method. The roof pond is frequently combined with movable insulations, so as to enable the pond to be cooled by sky radiation at nights and to block unwelcome thermal gain during the day time (Anderson et al., 1996).

Runsheng et al. (2003) modify the water pond method with gunny bags or floating cloth on the water surface (Figure 2.15). This attempt shows a little better cooling performance and the daily task of moving the insulation is eliminated. The green roof has been known more these days as one of the effective passive cooling strategies. The additional layers on the roof including soil and plants work as extra insulation. One survey shows that the roof garden decreases temperature on the surface of roof slab from 60 °C to 30 °C in Japan (Onmura, 2001). This is equivalent to a reduction of thermal flux from the roof by some 50 %.

The effects of each evaporative cooling strategy have been compared with the others. Sodha et al. (1980) experimentally prove that the water flow method is more effective than the water film and the roof pond. Heat flux from each technique is compared using the standard structure, which has

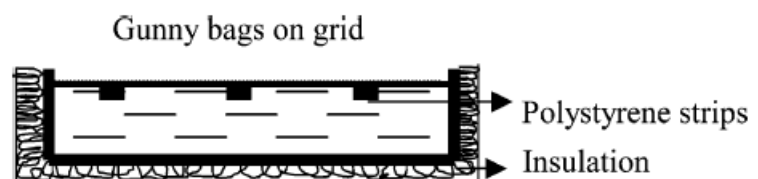


Figure 2.15 Roof pond with gunny bags (Runsheng et al., 2003)

only insulated roof in Delhi. 0.005 m thick of flowing water reduces the thermal transfer by 63.4 %, while the water film and the roof pond decrease by 58.4 % and 24 % respectively. It is also discovered that there is an ideal range of velocity to maximise the efficiency. Higher velocity is more efficient; however, the efficiency will be saturated at more than 0.02 m/s. Besides, a thick water layer discourages the evaporation and the heat flux becomes large. When the water is stand-still, thermal conductivity of water, 0.609 W/m/K, becomes dominant. Though water is relatively less conductive than other substances, the situation is recommended to avoid. If the water surface traps solar radiation and raises the temperature, the thermal gain will increase. The green roof shows less efficiency than the water flow technique in a numerical research (Nayak, 1982). Furthermore, the green garden encourages heat loss in cold seasons and requires seasonal maintenance, such as removing the layers (Nahar, 2003). Finally, the additional weight of the roof pond, thick water film and the green roof require stronger building structure which raises the investment costs. Consequently, the water flow method with a careful choice of velocity and layer thickness is advised to maximise the efficiency of evaporative cooling.

Evaporative cooling is one of the most effective sustainable cooling methods; however, there is one drawback. More efficiently the system works, the more a large amount of water is required (Nahar, 2003). Theoretically, 0.443 kg of water needs to evaporate to cool as much as 1 MJ. Nahar also reports that approximately 50 litres/m²/day of water is consumed for cooling in India. When this water source is provided from the mains

water, the running cost will not be practical. For this reason, the use of rainwater must be a satisfactory solution.

2.4 Highly Conductive Materials

Mixing highly conductive materials is a common strategy to enhance the total thermal conductivity. For the GSHP, the improvement of grout thermal conductivity has played an important role in the uptake as introduced in section 2.2.4. Hence, the characteristics have been well surveyed as well as some suggestions for successful applications. The adequate selection of conductive materials for the targeted GSHP systems is discussed to achieve environmentally undamaging systems. As a result, an effective use of graphite is proposed.

2.4.1 Comparison in thermal properties

Attempts to enhance thermal conductivity of the underground components are worthwhile to try. Table 2.6 lists thermal conductivity and other properties of solid materials, which have a possibility to be mixed into the heat exchanger, rainwater collection tank, grout and soil. Thermal effusivity is the ultimate indicator of how quickly the materials conduct and release the thermal energy (see section 5.8). In order to know the value, thermal conductivity is required to be measured. Three materials at the top of the table are known as highly conductive materials and the procurement is relatively easy. Some of the materials may be even available as scraps from factories for affordable price. Especially, graphite has distinctive thermal conductivity and thermal effusivity (see section 2.4.3 for the details).

Table 2.6 Comparison of properties (Holman, 2002 and Shokoku Sya, 2000)

Material	Density kg/m ³	Specific heat J/kg/K	Thermal conductivity W/m/K	Thermal effusivity ¹⁾ Ws ^{0.5} /m ² /K
Aluminium	2,707	905	237.00	580,611
Copper	8,954	384	398.00	1,368,458
Graphite ²⁾	1,730	710	3,000.00	3,684,900
Reference Polyethylene ³⁾	933	1,916	0.47	840
Concrete ⁴⁾	1,130		0.30	
Dry sand	1,700	836	0.20	284
Clayey soil	1,986	878	1.60	2,790
Wet soil	1,890	878	0.78-2.20	2,473
Quartz	2,640	743	6.21	12,181

1) $\beta_{eff}=(k/\rho C_p)^{0.5}$

2) Thermal conductivity (Choongho et al., 2006)

3) Medium density polyethylene (Brandrup et al., 1999)

4) (Dermirbođa et al., 2003)

On the contrary, the bottom six are references to the standard system components: the heat exchanger and the rainwater collection tank are made of polyethylene, grout is normally concrete and soil consists of the rest of the materials depending on location. It is obvious that mixing highly conductive materials is expected to improve the performance of the underground heat transfer.

2.4.2 Environmental issues

Mixing metals seems an easy strategy for the enhancement of heat transfer capacity; however, the environmental impact ought not to be neglected. Metallic ions might be leached from metals into soil and damage lakes and rivers by the generated acid. This phenomenon would happen only by a

directly buried metallic tank, due to the corrosion of the metal surface (Ismail et al., 2008). However, once the environment is polluted, there is little chance to be naturally healed (Sahu et al., 2004). Furthermore, a research discloses that these heavy metals deactivate earthworm, which is one of the most important elements in soil (Helling et al., 1999). Earthworm tends to accumulate these harmful substances inside of its body with high concentration. Considering that metallic ions might be carried by existence of water, the idea of using metals to enhance the underground heat transfer should be abandoned except that the components are perfectly waterproof. Using relatively conductive soil components is now one of the limited strategies. In case of soil modification around the underground heat exchangers, large underground space needs to be treated. Hence, only natural materials, for instance, sand, clay and quartz, may be economically feasible. If the original soil is assumed to be sandy, adding or partially replacing by silt and clay will raise the thermal effusivity up to approximately by 10 times (Table 2.6). The impact is much smaller than the expected improvement by metals; however, it must be worth considering. Especially quartz has the highest thermal effusivity among the environmentally friendly choices.

Quartz is the most common mineral on the planet and consists of silicon dioxide. It is partially crystallised and the use for semi-conductor has been popular. Due to the unique crystals inside, the thermal conductivity differs depending on measuring axis; 6.5 W/m/K for one axis and approximately 13 W/m/K for a perpendicular axis to the other axis under ambient temperature

(Gibert et al., 2009). In fact, the published values have a wide range from 6.21 W/m/K to 11.6 W/m/K (Holman, 2002). Because of this wide variety, selecting higher conductive type in an economic design is of essence. A possibility to use quartz in the underground heat collection system is discussed in section 7.5.2.

2.4.3 Graphite

It is discovered that carbon-based materials have the highest thermal conductivity among studied materials at moderate temperature (Chang et al., 2005). Though both diamond and graphite are representative materials, graphite is far more economically viable. Thermal conductivity of diamond, graphite and graphite fibres can be high as much as 3,000 W/m/K at 27 °C (Choongho et al., 2006). Furthermore, the numerical study comes to a conclusion that (10, 10) carbon nano-tube potentially has thermal conductivity of 6,600 W/m/K at ambient temperature (Chang et al., 2005).

The use of graphite particles seems to be harmless to the environment. Carbon fibres have strong resistance against corrosion and chemicals (Fukai et al., 2000); therefore, even direct mixing into soil may be acceptable. A simple way of mixing carbon graphite is digging out soil to mix the particles on the ground and bury them into the original place. However, there is an industrial method to inject fluid into soil. Injecting substances with hot air or steam is carried out to chemically neutralise polluted soil or to fill air voids for underground reinforcement (Uretek USA, 2004). Uretek USA provides a service to inject high density polymer into a depth of more than 9 m (Figure

2.16). This procedure shortens the required work time from days or weeks to hours and may cost less than the mixing process on the ground. If this technique works with high density polymer, injecting carbon fibres with fluid, for instance, grout, must be technically viable. In addition, this strategy is useful to modify soil conditions even after a certain period of operational time. The design ideas with the carbon fibre injection are explored through a series of simulation in Chapter 6.

The designs of underground particle distribution also need to be considered. Fukai et al. (2000) experimentally conduct a research in the efficiency of thermal energy transfer with different shapes of graphite (Figure 2.17). The

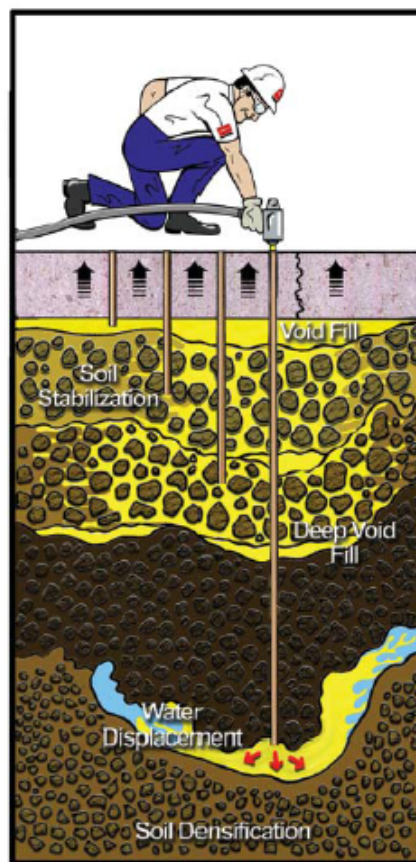


Figure 2.16 Deep injection process (Urettek USA, 2004)

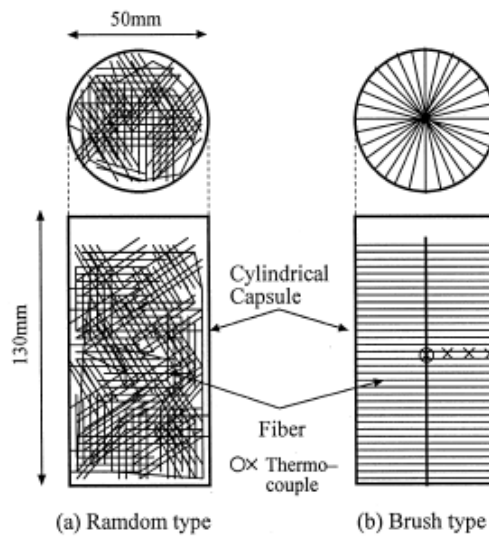


Figure 2.17 Different packing geometry of carbon fibres (Fukai, 2000)

results show that the brush type of carbon fibres enhances the thermal efficiency of the packed phase change material the most. The total heat transfer with 1 volume% of the brush type carbon fibres has almost the same as the random packing with 3 %. In addition, the length of carbon fibres influences little between 200 mm long and 5 mm long. This research implies that the average distance of physically touched fibres is more essential than graphite concentration. At the same time, the radial layout of fibres between the heat exchange surface touching the heat media within a controlled bath and the thermocouple in the centre of the sample could be another important factor. Therefore, even if the particles are equally dispersed, the random distribution is not necessarily the most efficient condition. As a result, the total thermal conductivity with the brush type shows that effective graphite content is 29 % higher than that in a simple estimation, which is obtained from volume content and thermal conductivity of each material.

$$k_{total} = \sum_{n=0}^i k_i \phi_i \quad (\text{Equation 2.1})$$

k	Thermal conductivity	W/m/K
φ	Volume fraction	-

Conversely, effective graphite content of the random packing is 70 % less than that of the simple estimation on average. This aspect is considered in planning the injection of carbon fibres in section 6.2.

Once the underground particle layout is determined, the design needs to be accurately realised during the injection process. A research discovers that the fluid permeates the pores in sub-soil effectively when it is injected at high concentration and at low flow rate by a probe with a small diameter (Moghadasi et al., 2004). The technique has been already industrialised, and so there must be practical methodologies to achieve the targets. Planning the construction carefully is of importance to minimise both investment and running costs.

2.5 Methodologies to Obtain Thermal Properties of Soil Samples

There are some categories in measuring thermal conductivity; steady state method, transient method and heat flow meter method (P. A. Hilton Ltd., 1994). Each has advantages and disadvantages, such as accuracy, cost, limits of samples and others. In this project, heat flow meter (HFM) and dual-probe heat-pulse method (DPHP), which is one of transient methods, are compared to select a suitable method for an experimental analysis in Chapter 5. The HFM has been one of the common methods, while the DPHP was invented relatively

lately. To start with, this section introduces the mechanisms and the differences between these two. Subsequently, two kinds of theories to estimate thermal conductivity are introduced.

2.5.1 Heat flow meter (HFM)

This method has been introduced in ISO 8301:1991. The system mainly consists of a controller, a chiller and a measuring part. A hot plate and a cold plate are attached to the inside of the measuring part and sandwich the soil sample as illustrated in Figure 2.18. Temperature at each plate is controlled by an installed programme and either the heater or the chiller to maintain the set value. When the temperature and the energy input achieve the steady state, thermal conductivity is calculated by inserting the stabilised energy input, mean temperature of the sample and calibration constants into the following theoretical equation (P. A. Hilton Ltd., 1994).

$$k = \frac{\ell_s \left[\left(c_1 + (c_2 \times \bar{T}) \right) + \left(\left(c_3 + (c_4 \times \bar{T}) \right) \times HFM \right) + \left(\left(c_5 + (c_6 \times \bar{T}) \right) \times HFM^2 \right) \right]}{dT}$$

(Equation 2.2)

ℓ_s	Specimen thickness	m
c_{1to6}	Calibration constants	-
\bar{T}	Average temperature between a hot plate and a cold plate	°C
HFM	Energy input	mV
dT	Temperature difference between a hot plate and a cold plate	°C

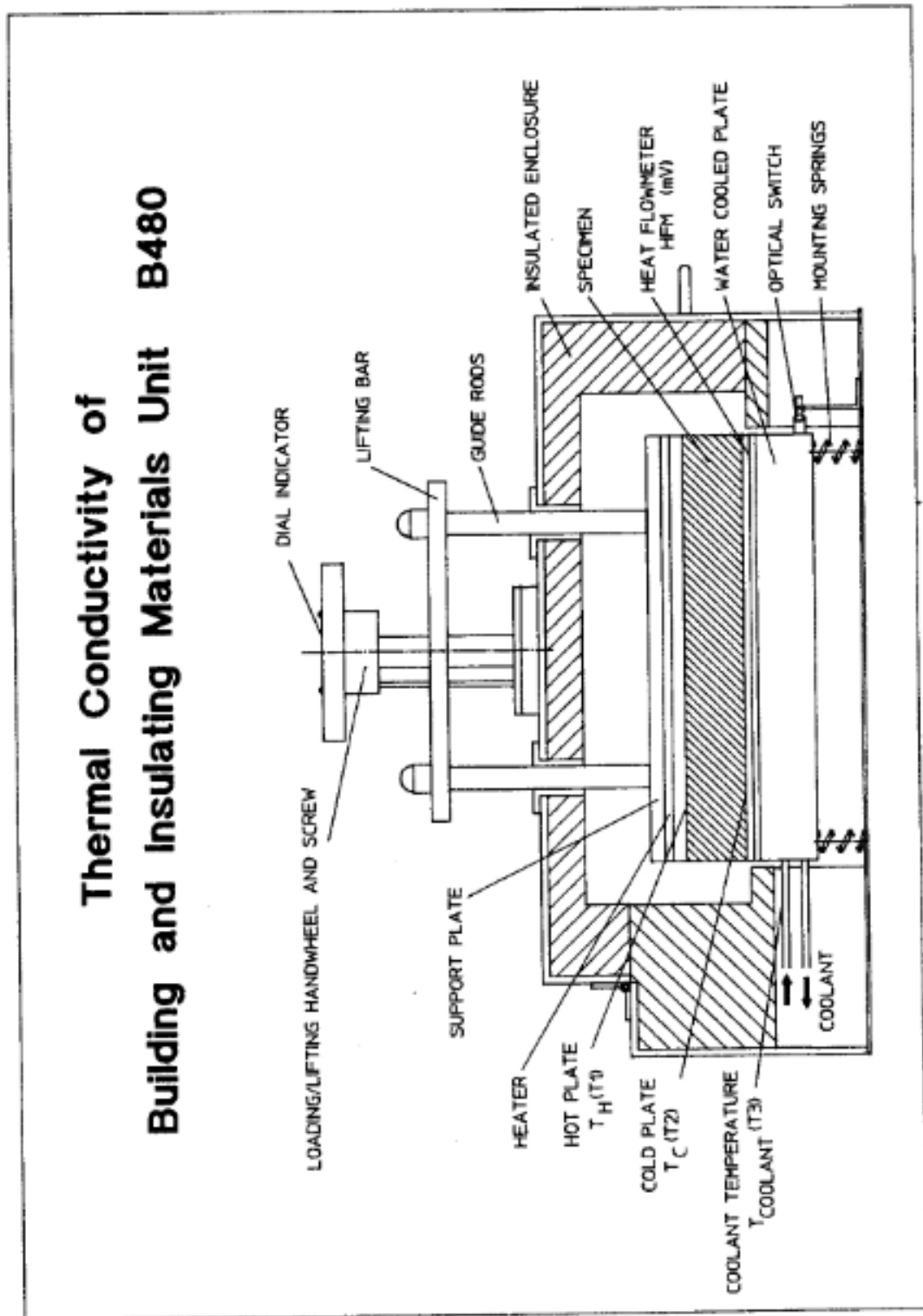


Figure 2.18 Cross-sectional diagram of the B480 heat flow meter (HFM) apparatus (P. A. Hilton Ltd., 1994)

Silicone rubber mats are set between the sample and the plates; therefore, the calibration contents for the mats are referred (Table 2.7).

Space for the sample tray is 7 cm in the measuring part and the maximum particle size in samples ought to be limited for accurate measurement. The common practice to determine the maximum particle size is less than one third of the tray height. During a course of experiments in Chapter 5, two trays were used; 1.5 cm and 5 cm high respectively. Hence, the samples need to be prepared to be less than 5 mm and 14 mm for each tray. The particle size is made sure to be under the maximum limit by sieving, which is the standard method to define the soil characteristics in the British Standard (1990).

2.5.2 Dual-probe heat-pulse method (DPHP)

The basic components of heat-pulse method are a unit of sensor buried into a soil sample in a test rig, a datalogger and a computer to collect the experimental data from the datalogger (Figure 2.19). The sensor normally contains a thermocouple and a wire. Electric energy is injected into the wire heater and the temperature rise is regularly detected at the

Table 2.7 Calibration constants for measuring with silicon rubber mats (P.

A. Hilton Ltd., 1994)

c_1	-31.7383	c_4	0.0558
c_2	0.4792	c_5	0.0279
c_3	6.6346	c_6	-0.0005

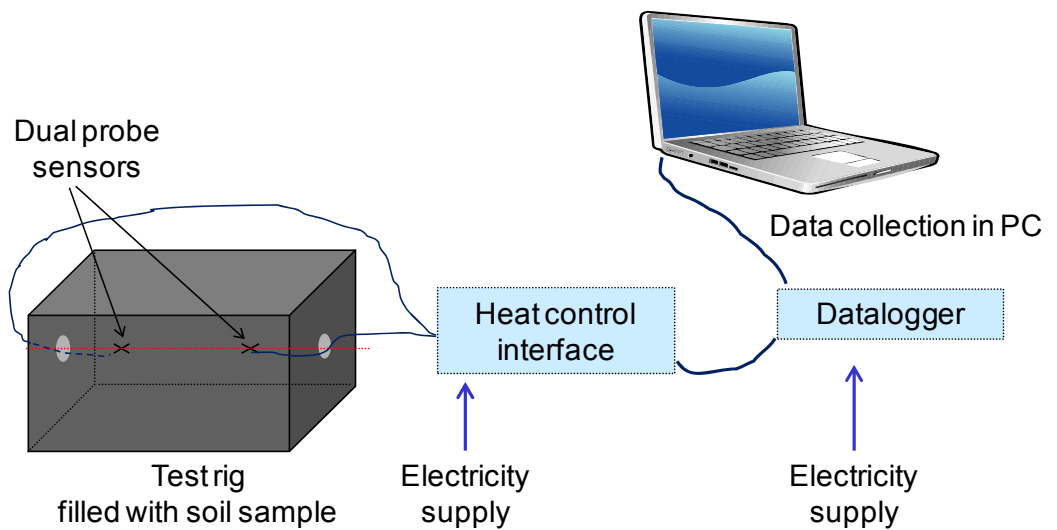


Figure 2.19 Setup of dual-probe heat-pulse method (DPHP)

thermocouple. Ultimately, thermal conductivity is calculated from the series of dynamic data, which is recorded by the datalogger. Though this method was discovered relatively lately, the DPHP has been accepted by the industries to measure thermal properties of fruits, foods and soil (Fontana et al., 1999). The remarkable features are the short measurement duration and the reasonable cost.

There are mainly three kinds of sensor types: single-probe method (SP), dual-probe heat-pulse technique (DPHP) and multi-needle probes. They were invented in the order as they are written above. Their features differ from each other. The SP has been well used since 1930s to 1940s; however, it requires separate measurement of volumetric heat capacity (Noborio et al., 2002). In addition, particle size data is not necessarily reliable to obtain accurate mineralogical information (Bristow, 1998). As a result, the derived thermal conductivity can be less accurate than the other

two methods. Subsequently, the DPHP was developed in 1990s (Nidal et al., 2000). An advantage of the DPHP is that volumetric heat and thermal diffusivity can be measured as well as thermal conductivity with a single unit (Noborio et al., 2002). Furthermore, the DPHP can reduce the resistance caused between soil and the heater probe, compared to the SP. This is because that water instantly evaporates on the surface of heater probe after large energy is inserted into the wire. Finally, the DPHP was modified into the multi-needle probe method. The sensor unit actually consists of four probes, in which two of them have the same functions as the probes in the DPHP. The method has more accuracy and can measure volumetric water content with an error range of $0.01 \text{ m}^3/\text{m}^3$ (Bristow et al., 2001). In addition, electrical conductivity can be even measured, when all the four probes are used. All of these three methods have a simple methodology and economic feasibility.

With regards to the accuracy of measurement and the purpose of the project, the DPHP has sufficient functions to apply. Therefore, thermal conductivity, volumetric heat, thermal diffusivity and water content of various kinds of soil mixture are measurable with the rig displayed in Figure 2.19.

The sensor unit consists of two probes made of stainless steel 304 as shown in Figure 2.20. These are fixed in parallel with a distance, r , approximately 6 mm in the test rig for this project. The electric heater is set in one of the probes (heater probe), while the thermocouple in the other probe (sensor probe). This unit is buried in soil samples as seen in Figure 2.19. At the

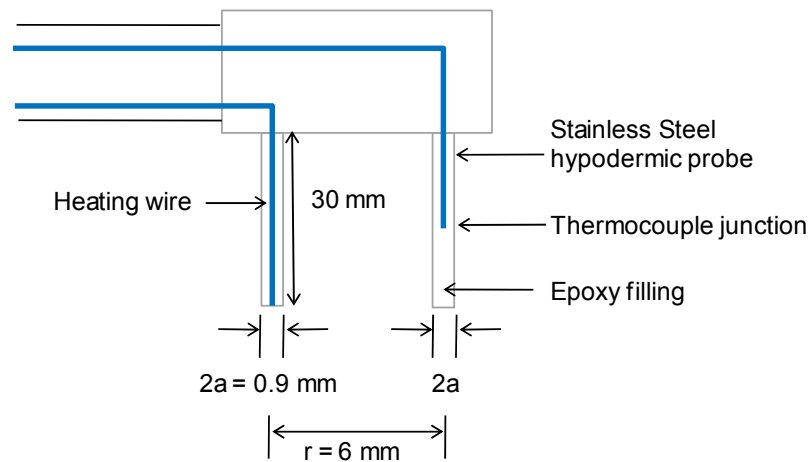


Figure 2.20 Example of the DPHP sensor unit (Fontana et al., 1999)

beginning of measurement, the pulse is sent, for 8 seconds in this project. The temperature difference between before and after the pulse is monitored at the sensor probe. The data is regularly recorded for certain period of time, every 1.0 sec and for 90 seconds respectively for this project.

2.5.3 Method for the analysis with the DPHP

Thermal properties are calculated by applying the obtained data into equations developed from theories and experiments. The calculation procedure is introduced below.

Determination of thermal diffusivity and volumetric heat capacity

The heat-pulse methodology is derived from a radial thermal conduction theory with an infinite line heat source. The environment is assumed to have equal features at equal temperature before the incident. This measuring method was originally invented by Campbell et al. (1991) with Equation 2.3.

$$\Delta T(r, t) = \frac{q}{4\pi\alpha\rho c} \exp\left(\frac{-r^2}{4\alpha t}\right) \quad (\text{Equation 2.3})$$

ΔT	Change in temperature	°C
r	Radial distance from the line source	m
t	Time	s
q	Energy input per unit length of heat per unit time	W/m
α	Thermal diffusivity	m ² /s
ρc	Volumetric heat capacity	J/m ³ /°C

Subsequently, Bristow et al. (1994) experimentally investigated the method and modified the equation, Equation 2.4. This shows a relationship between time and temperature change at certain distance from the heater, after the heat pulse is released for a short time.

$$\Delta T(r, t) = \frac{q}{4\pi\alpha\rho c} \left[Ei\left(\frac{-r^2}{4\alpha(t-t_0)}\right) - Ei\left(\frac{-r^2}{4\alpha t}\right) \right] \quad (\text{Equation 2.4})$$

t_0	Duration of a heat pulse	s
-------	--------------------------	---

Here, $-Ei(-x)$ is the exponential integral. This equation is followed by two other equations to obtain thermal diffusivity and volumetric heat capacity (Bristow et al., 2001).

$$\alpha = \frac{r^2}{4} \left(\frac{1}{t_m - t_0} - \frac{1}{t_m} \right) / \ln\left(\frac{t_m}{t_m - t_0}\right) \quad (\text{Equation 2.5})$$

$$\rho c = \frac{q}{4\pi\alpha\Delta T_m} \left[Ei\left(\frac{-r^2}{4\alpha(t_m - t_0)}\right) - Ei\left(\frac{-r^2}{4\alpha t_m}\right) \right] \quad (\text{Equation 2.6})$$

t_m Time to the maximum temperature change s

ΔT_m The maximum temperature change °C

Determination of thermal conductivity

Thermal conductivity is calculated from the obtained thermal diffusivity and the volumetric heat capacity as follows.

$$k = \alpha \cdot \rho c \quad (\text{Equation 2.7})$$

Determination of volumetric water content

Volumetric water content is calculated from the obtained volumetric heat capacity and the other soil data, which is referred to published database. de Vries introduced an equation to calculate thermal properties. In this equation, volumetric heat capacity, ρc , is a sum of heat capacity of each component in soil as described below (de Vries, 1963).

$$\rho c = (\rho c)_q \phi_q + (\rho c)_{rm} \phi_{rm} + (\rho c)_w \theta_v + (\rho c)_a \phi_a + (\rho c)_o \phi_o \quad (\text{Equation 2.8})$$

ρ Density kg/m³

c Specific heat J/g/K

θ_v Volumetric water content -

The subscript q, rm, w, a and o respectively mean quartz, minerals apart

from quartz, water, air and organic matter. This equation can be simplified to Equation 2.9, when the contribution of minerals, air and organic substances are ignored. In this equation, soil is described as a homogeneous substance and the porosity is expressed by introducing soil bulk density, ρ_b .

$$\rho c = \rho_b c_m + (\rho c)_w \theta_v \quad (\text{Equation 2.9})$$

ρ_b Soil bulk density kg/m^3

The subscript m indicates the average properties of the minerals. Hence, the water content can be extracted by inserting values in volumetric heat capacity, bulk density and specific heat.

Range selection to analyse experimental data

There are three kinds of methods to apply the experimental data to the methodology: one-point analysis method, all data adoption method and partial data adoption method (Noborio et al., 2002). In the first method, a pair of ΔT_m and t_m are selected from the collected data, in order to calculate thermal diffusivity and volumetric heat capacity with Equation 2.5 and Equation 2.6. In the second method, all the collected data is utilised to reduce an influence of the fluctuating experimental data. In the third method, a part of collected data is used, particularly the data around ΔT_m and t_m . Equation 2.4 is for an infinite linear heat source model, while the actual heat source is a finite line. Therefore, the measured temperature

possibly drops more significantly than the theoretical tendency, as time goes by. To sum up, it is inevitable to target a well balanced reference to the experimental data between the accuracy and the correct use of equations. For instance, Bristow et al. (1995) use 75 % of continuous data, which includes ΔT_m .

The past research directed by Noborio (2002) shows that the all data adoption method tends to obtain larger volumetric heat capacity and thermal conductivity than the other two methods by 10 to 20 %. The results from the other two methods match fairly well; therefore, either the one-point analysis method or the partial data adoption method is recommended. Since fitting with more than a point of data could increase the overall accuracy, the partial data adoption method with 66.7 % of continuous data including ΔT_m and t_m was selected for this project.

Computational handling of experimental data

The accuracy of curve fitting between the predicted and experimental data is crucial in the measurement with the DPHP. Therefore, finding a reliable set of data handling tools requires special attention for each test circumstance. Various handy and accurate methodologies have been proposed to obtain thermal properties. This is because the fundamental equation, Equation 2.4, contains the exponential integral, which is difficult to calculate in an easy and accurate manner. Besides, a use of spreadsheet is also a popular option rather than running a complex calculator. However, selecting a simplified methodology potentially leads to a less accuracy and less

flexibility for various kinds of samples. Hence, a satisfactory calculation method with Equation 2.4 was investigated.

A handy calculation base was chosen, for instance, spreadsheet type software such as Microsoft Excel. For calculating the exponential integral, free software, xnumb56, was installed. This software could work on Excel spreadsheets and provided fairly accurate results (see Figure 2.21 for the appearance). The curve fitting between the experimental data and predicted data was run by a solver function in Excel. The target was set to minimise a sum of squared error (SSE) in between.

$$SSE = \sum_{t=t_0}^{t=60} [\Delta T(r, t_{measured}) - \Delta T(r, t_{predicted})]^2 \quad \text{(Equation 2.10)}$$

t	Time	s
t_0	Duration of a heat pulse	s
ΔT	Change in temperature	°C
R	Radial distance from the line source	m

The thermal diffusivity and the volumetric heat capacity could be calculated from Equation 2.5 and Equation 2.6 respectively. However, since these parameters are essential to acquire thermal conductivity in the end, these were set as adjustable values in the solver (reference number).

The solver has an inconvenient feature, in which the results are largely affected by reference numbers. This means that different sets of inserted numbers for thermal diffusivity and volumetric heat capacity may conclude

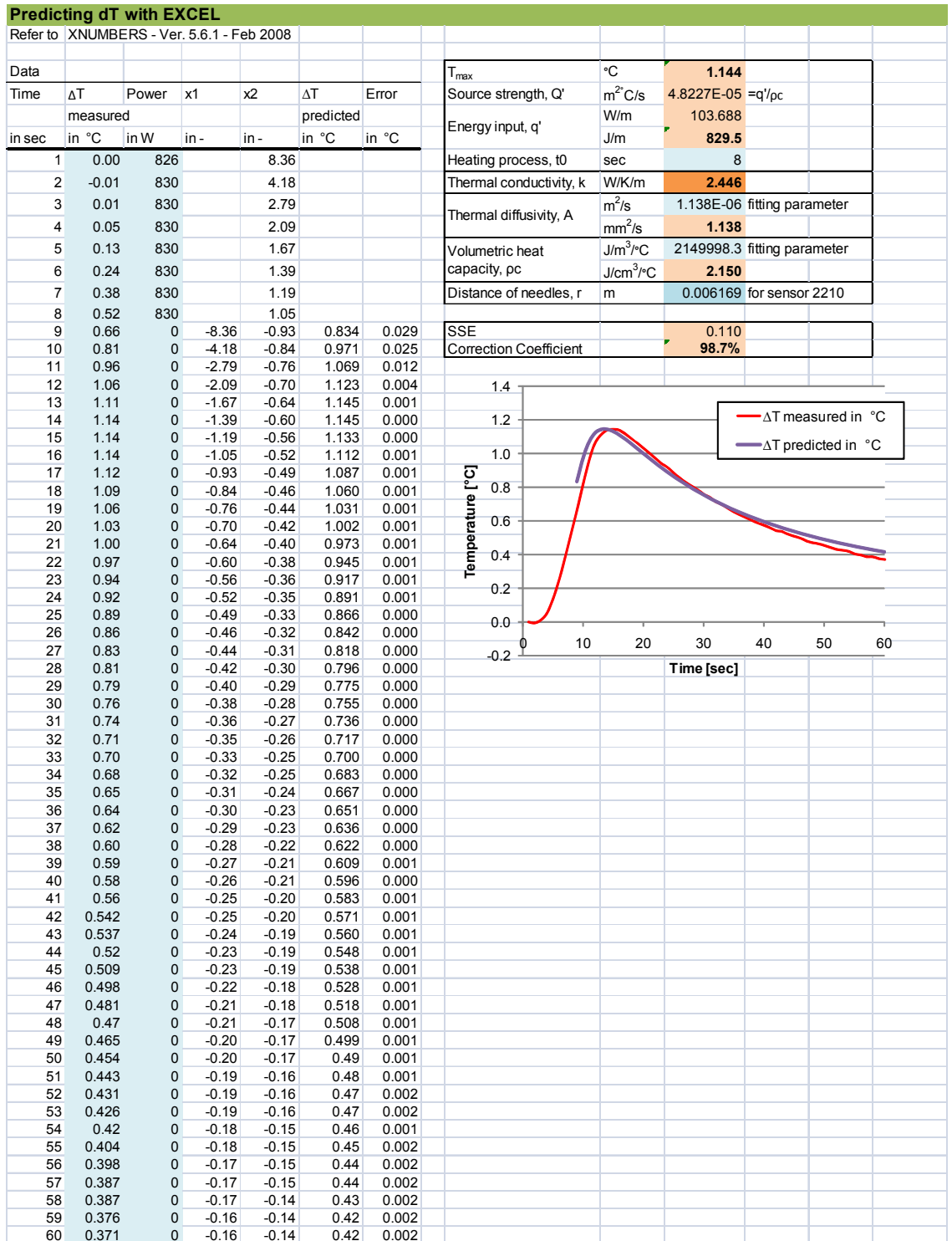


Figure 2.21 Spreadsheet to calculate thermal properties

differently. The difference can be quantified in a value expressing how similar the two curves shape, correction coefficient. Accordingly, various

sets of reference numbers were tried to maximise the correction coefficient. The uncertainty of the measurement with the DPHP is calculated in section 5.1.3.

2.5.4 Comparison between the HFM and the DPHP

Comparison of the characteristics between the HFM and the DPHP is presented in Table 2.8. The yellow cells indicate the inferior points to the other method, while the pink cells are the superior features. Though the

Table 2.8 Comparison between the HFM and the DPHP

		The HFM	The DPHP
Background	Year of discovery		1991
Size ¹⁾	unit	0.46 m ³	0.0022 m ³
Weight ¹⁾	unit	143 kg	1 kg
Mobility		Difficult	Outdoor is available
Price ¹⁾	unit	£16,000 ²⁾	£1,160
Measurable properties		Thermal conductivity	Thermal conductivity, Heat capacity, Thermal diffusivity and Water content
Duration		Several hours to days	90 sec
Samples	Maximum particle size	23 mm	2 mm
		Solid only	liquid or solid which can be touched to probe
Accuracy	Thermal conductivity	± 3 % for 0.1~1.4 W/m/K	up to ± 5 % ³⁾ , no technical limit in measurable range
	⁴⁾	Suitable for dried sample	Accurate even for samples with high water content
			Methodology of analysis should be carefully selected
Applications		Building materials etc.	Soil mixture or fruits

1) Except the data collection computer

2) For educational facilities

3) Refer to the error analysis presented in Chapter 5.1.3

4) Discussed in Chapter 5.3.4

HFM is a well known method and has impressive accuracy, the flexibility is dissatisfying, such as the immobility, price, measurable thermal properties and required duration for the measurement. On the contrary, the DPHP seems a more attractive measuring option. However, a methodology for the analysis still requires investigations to obtain satisfactory accuracy. The dynamic data is so sensitive that the handling conditions easily affect the results. Therefore, it seems that it is difficult to conclude a perfect methodology which will work for any experimental condition. Regarding the criteria for soil samples, the DPHP fundamentally has more flexible limit in the maximum particle size of the samples. The sensor is easily magnified for the field test, as Figure 2.22 provides an example with the multi-needle heat-pulse method.

The comparison is carried out with basic samples to determine more suitable measuring method for this project in Chapter 5.



Figure 2.22 Multi-needle heat-pulse method for field tests (Puedue University School of Civil Engineering, 2002)

2.5.5 Theories to predict thermal conductivity of sub-soil

Methods to predict soil thermal conductivity have been studied through theories with supportive experiments. There are two well respected theories; de Vries's model and Campbell's model. These have been used to compare with the experimental results acquired from the DPHP. The features of each theory are presented below.

de Vries's theory

This estimation method has been inspected for many samples, which are both saturated and non-saturated soil, since this theory was introduced (de Vries, 1963). The fundamental idea is that thermal conductivity can be expressed by the thermal conductivity and the shape of soil constituents.

$$k_{soil} = \frac{\phi_w \xi_w k_w + \phi_g \xi_g k_g + \phi_m \xi_m k_m}{\phi_w \xi_w + \phi_g \xi_g + \phi_m \xi_m} \quad \text{(Equation 2.11)}$$

k	Thermal conductivity	W/m/K
ϕ	Volume fraction	-
ζ	Weighting factor	-

The subscripts w, g and m mean water, gas and minerals. This equation indicates that larger thermal conductivity of gas and minerals is advantageous to achieve high total thermal conductivity (Campbell et al., 1998).

High thermal conductivity of gas is influenced by the vapour transfer within the pores between soil particles. This factor is expressed in the modified

Fick's law.

$$\lambda E = -\lambda \bar{\rho} D_v h_r \frac{\Delta}{p_a - e_a} \frac{dT}{dz} \quad (\text{Equation 2.12})$$

λ	Latent heat of water vaporisation	J/kg
E	Evaporation rate	mol/s/m ²
$\bar{\rho}$	Molar density of air	mol/m ³
D_v	Vapour diffusivity of soil	m ² /s
h_r	Relative humidity in soil	-
Δ	Slope of the saturation vapour pressure function	kPa/°C
p_a	Total atmospheric pressure	kPa
e_a	Vapour pressure in atmosphere	kPa
dT	Temperature difference	°C
dz	Difference of length	m

The powerful elements here are degree of saturation, Δ , and vapour diffusivity of soil, D_v . More water content creates more active heat transfer by the evaporation and the condensation in the air voids. The other past researches support the fact that thermal diffusivity increases when water content rises and slowly decreases around the saturation of water (Bristow, 1998). On the other hand, vapour diffusivity is dependent on temperature. In addition, the value is higher when soil is drier and larger air voids exist.

Handling of return water into soil pores is also expressed. This

phenomenon is seen, for instance, when soil humidity is decreasing. The return flow of liquid water is likely to drop significantly before the actual drop of soil humidity. There had been no theory to express this incident; however, Campbell introduced a dimensionless factor in 1994 (Campbell et al., 1998).

$$f_w = \frac{1}{1 + \left(\frac{\theta}{\theta_0}\right)^{-q}} \quad \text{(Equation 2.13)}$$

f_w	Dimensionless flow factor	-
θ	Water content	-
θ_0	Water content where return flow cuts off	-
q	Factor to express how quickly cutoff occurs	-

Ultimately, thermal conductivity derived from the vapour activity and fluid conductivity is presented respectively.

$$k_g = k_a + \frac{\lambda \Delta h_r f_w \widehat{\rho} D_v}{p_a - e_a} \quad \text{(Equation 2.14)}$$

$$k_f = k_g + f_w (k_w - k_g) \quad \text{(Equation 2.15)}$$

One of the unique factors, weighting functions, can be finally calculated with the following equations.

$$\begin{aligned}\xi_g &= \frac{2}{3 \left[1 + g_a \left(\frac{k_w}{k_f} - 1 \right) \right]} + \frac{1}{3 \left[1 + g_c \left(\frac{k_g}{k_f} - 1 \right) \right]} \\ \xi_w &= \frac{2}{3 \left[1 + g_a \left(\frac{k_w}{k_f} - 1 \right) \right]} + \frac{1}{3 \left[1 + g_c \left(\frac{k_w}{k_f} - 1 \right) \right]} \\ \xi_m &= \frac{2}{3 \left[1 + g_a \left(\frac{k_w}{k_f} - 1 \right) \right]} + \frac{1}{3 \left[1 + g_c \left(\frac{k_m}{k_f} - 1 \right) \right]}\end{aligned}\quad \text{(Equation 2.16)}$$

g_c Shape factors, $1-2g_a$ -

These equations tell that weighting factor depends on particle shape, thermal conductivity and volume fraction. Shape factor is given only for particles, for instance, 0.1 for minerals and 0.33 for organics (Campbell et al., 1998).

This method has been referred by numerous researchers; however, the practicality has been questioned. This semi-theoretical model requires many parameters, which need to be precise to achieve accurate results (Lu et al., 2007). Nevertheless, this method elects three essential elements to raise soil thermal conductivity; degree of saturation, thermal conductivity and fraction of soil components and vapour diffusivity of soil. The first element is easier to apply for samples; therefore, the experimental investigation with different water content is conducted as a start in Chapter 5. In fact, some equations calculate thermal conductivity from only this parameter, which indicates that water content is dominant (Rees et al., 2000). The second point is discussed in Chapter 6. The final point is difficult to be applied in

this project, as the underground temperature is not actively controlled in the practical operation.

Campbell's theory

The base of the empirical model was created by Mc-Innes and subsequently applied for soil properties by Campbell (1985).

$$k = A + B\theta_v - (A - D) \exp\left[-(C\theta_v)^E\right] \quad \text{(Equation 2.17)}$$

θ_v Volumetric water content -

A to E depend on soil characteristics including quartz. The theory also indicates that water content is an influential factor on thermal conductivity. Campbell concludes that the quartz fraction can be ignored for most of the soils containing minerals. This is a different aspect from de Vries's theory. In fact, Bristow (1998) experiences that defining mineralogy from particle distribution could cause substantially inaccurate results. He also discovers that the obtained volume fraction of quartz matches between Campbell's theory and a measurement with X-ray diffraction. As a consequence, factor A to E are obtained with concerns about quartz fraction.

$$A = (0.57 + 1.73\phi_q + 0.93\phi_{rm}) / (1 - 0.74\phi_q - 0.49\phi_{rm}) - 2.8\phi_s(1 - \phi_s) \quad \text{Equation 2.18}$$

$$B = 2.8\phi_s \quad \text{(Equation 2.19)}$$

$$C = 1 + 2.6 / (m_c^{0.5}) \quad \text{(Equation 2.20)}$$

$D = 0.03 + 0.7\phi_s^2$	(Equation 2.21)
--------------------------	-----------------

$E = 4$	(Equation 2.22)
---------	-----------------

ϕ	Volume fraction	m^3/m^3
--------	-----------------	-----------

m_c	Clay fraction	-
-------	---------------	---

where the subscripts q, rm and s indicate quartz, remaining minerals and solids, which are the average properties of the minerals. Lu et al. (2007) criticise that some of the five parameters in this model are difficult to obtain. However, this model is easier than de Vries's model. Hence, a comparison with the experimental data derived with the DPHP is attempted in section 5.3.5.

2.6 Conclusions

Heat pumps have had more attention nowadays for reducing energy consumption and CO₂ emissions. Heat pump systems with potentially higher operational efficiency have been developed, such as a combination between the use of underground thermal energy and water source heat pumps. In order to solve the costly construction and operation, some strategies have been investigated, for instance, the enhancement of conductive and convective heat transfer around the underground heat exchangers.

Rainwater harvesting system has been more important as the predicted water shortage in near future has become more realistic in the world. This complimentary water also enables to improve the performance of the GSHP by playing a role as the heat source or generating convective heat transfer. There

are only a few proposed systems; therefore, more research is required to discover practically attractive system designs, which meet all the criteria of the GSHP.

Various kinds of techniques have been investigated in building integrated evaporative cooling. Some researchers conclude that creating water flow on the surface of the buildings at adequate flow speed can be the most effective strategy even for hot and humid regions. Since the evaporation requires substantial amount of water, the use of collected rainwater is preferable.

The other method to improve the performance of the GSHP is the enhancement of thermal conductivity between soil and the heat exchangers. Though heavy metals have fairly attractive thermal conductivity, their negative environmental impacts should not be neglected. Therefore, the injection of graphite fibres and creating highly conductive soil out of harmless substances are advised to be studied.

There are several methods to measure and several theories to predict the thermal properties of soil samples. The HFM and the DPHP are used in the experiments presented in Chapter 5, while thermal conductivity is predicted from Campbell's theory. As de Vries's theory suggests, high water content and highly conductive soil components are taken into consideration to raise thermal conductivity in Chapter 5 and section 6.2 respectively.

Investigation after Chapter 3 is conducted on the basis of a sample system of the

Chapter 2 Literature Review

GSHP. The climate data of assumed location, Nottingham, is analysed to calculate the yearly heating and cooling loads for the office building. Thereafter, a sensitivity study is attempted to obtain essential design parameters to improve the overall heat transfer.

Chapter 3 Building a Model for Case Studies

Introduction

Section 2.2.3 indicated that a key to achieving the objectives of the GSHP lies in designing the underground heat collection system. Hence, numerous design strategies are investigated after this chapter. In order to make comparison between the results derived from different chapters, each case study is evaluated on the basis of the same model system. This chapter introduced the construction of the model system.

The specs of the system are defined regarding a balance between the capacities of commercialised water source heat pumps and office buildings in standard running conditions. Structure and size of the building are determined to match an available heat pump on the market and to meet the approved document L2B. Subsequently, required environmental data is selected and analysed to be used in simulation.

3.1 Characteristics of Building

A model system is not referred to existing systems or buildings; however, the designs and operating conditions are presented in as much detail as possible. A range of applicable building examples is shown to combine with a particular heat pump.

3.1.1 Background of the model

A model for the investigation was composed for a typical office building in the

UK. Water source heat pumps are efficient and the large capacity is suitable for small to medium size facilities. In accordance with the statistics displayed in Figure A.1, the majority of office buildings have floor space of 93 to 465 m² and one-story or two-stories. This hypothesised office was assumed to be located in Nottingham, UK (52°94'N, 1.20°W).

3.1.2 Plan and building components

A two story office building with flat roof was selected as a study model. The building plan was referred to a simulation model used by the past research (Ansari et al., 2005, Figure A.2). Each floor was assumed to be 7.1 m X 7.1 m; therefore, the total floor area was 100.8 m². The height of each floor was set as 4 m.

The materials of building components were set with the values of a typical existing office building (Table A.1). The operational conditions were also determined following standard office conditions as listed in Table A.2. U-values of building components were calculated with a standard equation for the overall heat transfer coefficient (Holman, 2002) and with the collected data by Down (1969).

$$U = \frac{Q}{A\Delta T} = \frac{1}{\frac{1}{h_{out}} + \sum_{m=1}^{m=n} \frac{L_n}{k_n} + \frac{1}{h_{in}}} \quad \text{(Equation 3.1)}$$

U	Overall heat transfer coefficient	W/m ² /K
Q	Rate of heat transfer	W
A	Area	m ²

ΔT	Temperature difference between external and internal air temperature	°C
h_{out}	Heat transfer coefficient on outer surface	W/m ² /K
m	Layer of materials	-
n	Number of layers	-
L	Thickness of layer	m
k	Thermal conductivity	W/m/K
h_{in}	Heat transfer coefficient on internal surface	W/m ² /K

Some examples are shown in Table 3.1. U-value for the roof was obtained with Equation 3.1 as follows;

$$\begin{aligned}
 U &= \frac{1}{\frac{1}{h_{out}} + \left(\frac{L_{board}}{k_{board}} + \frac{L_{aggregate}}{k_{aggregate}} \right) + \left(\frac{1}{h_{in}} + \frac{1}{h_{roofspace}} \right)} \\
 &= \frac{1}{28.4 \text{ W/m}^2 \text{ K} + \left(\frac{0.0160 \text{ m}}{0.375 \text{ W/mK}} + \frac{0.102 \text{ m}}{0.303 \text{ W/mK}} \right) + \left(0.150 \text{ W/m}^2 \text{ K} + \frac{1}{5.28 \text{ W/m}^2 \text{ K}} \right)} \\
 &= 1.33 \text{ W/m}^2 \text{ K}
 \end{aligned}$$

The obtained U-values for the integrated building components were much larger than the values specified by the approved document L2B as compared in Table 3.2. The differences of the U-values indicate that heat loss from the non-insulated building model would be substantial. Hence, a building sample designed with acceptable U-values is also presented in section 3.1.5.

Table 3.1 Calculation of U-values

Component	Thickness d m	Thermal conductivity k W/m/K	Heat transfer coefficient h W/m ² /K	Thermal resistance =d/k m ² K/W
Roof				
Summer	1) Gypsum or Plaster Board, Vermiculite Aggregate	0.02	0.37	0.04
	2) Sand and Gravel or Stone Aggregate	0.10	0.30	0.34
	3) Still Air, Heat Flow Down, inside air			0.15
	4) 7.5 MPH Wind, outside air film			28.39
	5) In Roof Air Space, Heat Flow Down			5.28
	Total thermal resistance			
	U in W/m ² /K			1.33
Wall				
Summer	1) Common brick	0.10	0.81	0.00
	2) Still Air, Heat Flow Horizontal			0.12
	3) 7.5 MPH Wind, outside air film			28.39
	Total thermal resistance			0.28
	U in W/m ² /K			3.54
Floor				
Winter	1) Concrete Block, Sand and Gravel Aggregate	0.15	1.44	0.11
	2) Still Air, Heat Flow Up, inside air film, 2 films			0.21
	Total thermal resistance			0.32
	U in W/m ² /K			3.15
External door				
Summer	1) Plywood	0.04	0.14	0.00
	2) Still Air, Heat Flow Horizontal			0.12
	3) 7.5 MPH Wind, outside air film			28.39
	Total thermal resistance			0.41
	U in W/m ² /K			2.43

1) Data for thermal conductivity and heat transfer coefficient was referred to Down (1969)

3.1.3 Estimation of design demands

Obtaining the design demand was the next step. The target indoor conditions and the design outdoor temperatures are listed in Table A.3. Though the target cooling temperature could be lower, such as 23.9 °C for transient work (Down, 1969), generating a cooling effect by the indoor air flow was considered. This strategy is studied in comparison to comfort zone for occupants and the results are believed to suggest the reduction of

Table 3.2 U-values of the building models (Office of the Deputy Prime Minister, 2000)

integrated value in W/m²/K

Components	Conditions	Acceptable values in document L2B	Calculation model	
			Non-insulated building	Insulated building
Wall	Summer	0.35	3.54	0.35
	Winter	0.35	3.72	0.35
Door	Summer		2.43	2.12
	Winter		2.51	2.18
Roof	Summer	0.25	1.33	0.24
	Winter	0.25	1.56	0.24
Ground base	Winter	0.25	3.15	0.25
Glass ¹⁾	Exposed to the sun	2.20	5.70	2.20

1) Glass for a non-insulated building was referred to Pilkington Architectural Product Guide ([no date])

the required cooling equipments (Arens et al., 1998). Another plan to diminish the cooling demand was a use of low outdoor temperature, 23.3 °C. When the outdoor temperature was lower than 27.3 °C, the cooling demand was assumed to be handled by ventilation with fresh air and the indoor air movement.

Both heating and cooling demands were calculated for the created office building mainly following a guide summarised by Down (1969).

Demand caused by conduction

Heating and cooling load is basically calculated with the following equation.

$$Q = UA\Delta T \tag{Equation 3.2}$$

Chapter 3 Building a Model for Case Studies

However, when building facades are exposed to sunshine, a part of the solar energy is transmitted into the building through the structure. This effect can be estimated using a concept of sol-air temperature (Down, 1969).

$$t_e = t_0 + \frac{\sigma I_s}{C_{so}} \quad (\text{Equation 3.3})$$

t_e	Sol-air temperature	°C
t_0	Outside air temperature	°C
σ	Absorption factor	-
I_s	Radiation intensity normal to surface	W/m ²
C_{so}	Outside surface coefficient	W/m ² /K

Time lag from the solar radiation and the decrease of the intensity are considered in the calculation. The obtained value can be used as an equivalent outside air temperature in Equation 3.2. Surface radiation intensity can be obtained from Equation 3.4 for horizontal surfaces and from Equation 3.5 for vertical surfaces.

$$I_s = I_d \sin \alpha \quad (\text{Equation 3.4})$$

$$I_s = I_d \cos \alpha \quad (\text{Equation 3.5})$$

I_d	Direct solar intensity	W/m ²
α	Solar altitude	Degree

In this design load estimation, Equation 3.4 was applied for the walls, doors and glass, while Equation 3.5 was used for the roof (Table 3.3). Sol-air temperature for vertical components under winter conditions was derived as

follows;

$$\begin{aligned}
 t_e &= t_0 + \frac{\sigma I_d \cos \alpha}{C_{so}} \\
 &= -3.33^\circ\text{C} + \frac{0.650 \times 446 \text{ W/m}^2 \times \cos(11.0^\circ)}{28.7 \text{ W/m}^2 \text{ }^\circ\text{C}} \\
 &= 6.60^\circ\text{C}
 \end{aligned}$$

The demands sourced by conduction were, therefore, calculated for each component as presented in Table 3.4. Referring to Equation 3.2, demand at the northern walls was obtained as follows;

$$\begin{aligned}
 Q &= UA(T_{\text{internal}} - T_{\text{external}}) \\
 &= 3.72 \text{ W/m}^2 \text{ K} \times 44.8 \text{ m}^2 \times \{20.0^\circ\text{C} - (-3.33^\circ\text{C})\} \div 1000 \\
 &= 3.88 \text{ kW}
 \end{aligned}$$

Table 3.3 Calculation of sol-air temperature

Operation			Heating	Cooling	
Outside temp	°C	t_0	-3.33	23.33	
Absorption factor ²⁾	-	σ	0.65	0.65	
Direct solar radiation ³⁾	W/m ²	I_d	446.00	516.00	
Solar altitude ³⁾	degree	α	11.00	55.00	
Outside surface coefficient ⁴⁾	W/m ² /°C	C_{so}	28.66	28.66	
Vertical component	Radiation intensity	W/m ²	I_s	437.44	296.10
	Raise of temperature	°C	dt	9.92	6.72
	Sol-air temperature	°C	t_e	6.60	30.00
Horizontal component	Radiation intensity	W/m ²	I_s	85.03	422.87
	Raise of temperature	°C	dt	1.93	9.59
	Sol-air temperature	°C	t_e	-1.40	32.90

1) Data for absorption factor, direct solar radiation and solar altitude was referred to Down (1969)

2) Red brick and tile, concrete and stone, dark paints

3) Designed for the midday in the hottest month, July, for cooling and in the coldest month, December, for heating

4) (Blanuša et al., 1999)

Table 3.4 Demands caused by conduction

	Surface area, A			Temperature difference, ΔT ²⁾					
	m ²			°C			°C		
				Heating			Cooling		
	North	East, south and west	Total	North	East, south and west	Total	North	East, south and west	Total
Walls	44.8	146.4	191.2						
Doors	0.0	3.2	3.2	23.33	13.41		-3.97	2.75	
Glass	12.0	24.0	36.0						
Roof			50.4		21.40			5.62	
Floor ¹⁾			113.6	15.26					

	Demand, Q			Demand, Q		
	kW			kW		
	Heating			Cooling		
	North	East, south and west	Total	North	East, south and west	Total
Walls	3.88	7.29	11.18	-0.63	1.42	0.79
Doors		0.11	0.11		0.02	0.02
Glass	1.60	1.83	3.43	-0.27	0.38	0.10
Roof	1.68		1.68	0.38		0.38
Floor	5.47		5.47			

1) Calculated only for heating. Ground temperature was set as 4.74 °C. The total outer walls in the first floor were applied.

2) Difference between indoor temperature and sol-air temperature cfor exposed area to sunshine

With regard to that the influence was derived from the direct solar radiation, the calculation was applied for vertical components in the east, south and west.

Demand caused by solar gain

Glass area allows solar energy to penetrate to the inside of the building. The effect by both direct and indirect radiation, such as radiation diffused by clouds and reflected on ground (Tao, 2001), is taken into consideration in the estimation.

$$Q = (I_{sdi} + I_{sin})AC_s F_{cl} \tau \tag{Equation 3.6}$$

Chapter 3 Building a Model for Case Studies

I_{sdi}	Direct solar radiation	W/m ²
I_{sin}	Indirect solar radiation	W/m ²
C_s	Shading coefficient of window	-
F_{cl}	Cooling load factor	-
τ	Transmission factor	-

The cooling demand was calculated for three windows facing the east, south and west (Table 3.5). Equation 3.6 was adapted to the assumption for the calculation model in which the northern walls do not receive direct solar radiation.

$$\begin{aligned}
 Q &= (I_{sdi} A_{esw} \tau_{direct} + I_{sin} A_{north} \tau_{indirect}) C_s F_{cl} \\
 &= (296 \text{ W/m}^2 \times 24.0 \text{ m}^2 \times 0.750 + 42.0 \text{ W/m}^2 \times 30.0 \text{ m}^2 \times 0.800) \times 0.660 \times 0.570 \div 1000 \\
 &= 2.39 \text{ kW}
 \end{aligned}$$

Demand caused by infiltration and ventilation

Demand by infiltration can be calculated from air filtration ratio, which expresses air tightness of buildings.

$$Q = V_{bul} R_{inf} C_p \Delta T \quad \text{(Equation 3.7)}$$

V_{bul}	Building volume	m ³
R_{inf}	Infiltration ratio	-
C_p	Specific heat	J/kg/K
ΔT	Temperature difference between inside and outside	°C

Infiltration load in heating conditions was calculated as follows;

Table 3.5 Demands caused by solar gain

Window area	East, south and west		24 m ²
	Total	A	30 m ²
Solar intensity	Direct	I_{sdi}	296 W/m ²
	Indirect ²⁾	I_{sin}	42 W/m ²
Transmission factor	Direct	τ	0.75 -
	Indirect	τ	0.80 -
Solar heat gain	Direct		5,330 W
	Indirect		1,017 W
	Total	Q	6,346 W
Shading factor ³⁾		C_s	0.66 -
Solar heat gain coefficient ³⁾		F_{cl}	0.57 -
Total glazing cooling load		Q	2.39 kW

1) Data for solar intensity and transmission factor was referred to Down (1969)

2) Indirect radiation was referred to a value at 30 degrees lower from the sun's position

3) (Pilkington Building Products, [no date])

$$\begin{aligned}
 Q &= V_{bul} R_{inf} C_p (T_{inside} - T_{outside}) \times (density_{air}) \\
 &= 403.3m^3 \times 0.6000 \times 1006 J/kgK \times \{20.00^\circ C - (-3.330^\circ C)\} \times 1.261kg/m^3 \\
 &\div 1000 \div 3600 \\
 &= 1.990kW
 \end{aligned}$$

On the other hand, demand by ventilation is based on the required fresh air to maintain comfort for occupants.

$$Q = m_{air} C_p \Delta T \quad \text{(Equation 3.8)}$$

m_{air} Required ventilation air kg/s

Heating load for very light work was obtained as follows;

Chapter 3 Building a Model for Case Studies

$$\begin{aligned}
 Q &= (\text{NumberOfOccupants}) \times (\text{RecommendedVentilation}) \times (\text{density}_{\text{air}}) C_p \\
 &\quad (T_{\text{inside}} - T_{\text{outside}}) \\
 &= 4.000 \text{ people} \times 7.080 \text{ litre/person} \times 1.260 \text{ kg/m}^3 \times 1006 \text{ J/kgK} \\
 &\quad \times \{20.00^\circ\text{C} - (-3.330^\circ\text{C})\} \div 1000.0 \\
 &= 2.240 \text{ kW}
 \end{aligned}$$

Infiltration and ventilation have similar consequences, the intake of fresh air. The difference is that ventilation is required while infiltration is unwelcome. If it is certain that building is pressurised enough, for instance, by ventilation, air inflow by infiltration would be prevented. For this calculation, it was assumed that the building was not particularly pressurised. The results are listed in Table 3.6 and Table 3.7.

Demand caused by internal heat gain

Three kinds of internal heat gain were calculated for the estimation; heat

Table 3.6 Demands caused by air infiltration

		Heating	Cooling	
Building volume	V_{bul}		403.3	m^3
Temperature difference between outdoor and indoor	ΔT	23.33	-3.97	$^\circ\text{C}$
Mean temperature between outdoor and indoor		8.34	25.30	$^\circ\text{C}$
Infiltration ratio ²⁾	R_{inf}	0.60	0.30	-
Outside air inflow		241.97	120.98	m^3/h
Air property	Specific heat capacity ³⁾ C_p	1,006.00	1,007.00	J/kg/K
	Density	1.26	1.18	kg/m^3
Infiltrating air		305.12	142.40	kg/h
Infiltration load	Q	1.99	-0.16	kW

1) Data for infiltration ratio and air property was referred to Down (1969) and Holman (2002) respectively

2) For a tight building. The ratio is larger when wind speed is larger, i.e. In winter.

3) For mean temperature between outdoor and indoor

Table 3.7 Demands caused by ventilation

			Heating	Cooling	
Number of occupants		Very light work		4	people
		Light work		4	people
Recommended ventilation		Very light work		7.08	L/s/person
		Light work		11.80	L/s/person
Required ventilation		Very light work		0.028	m ³ /s
		Light work		0.047	m ³ /s
	W_{air}	Very light work	0.04	0.03	kg/s
		Light work	0.06	0.06	kg/s
Ventilation load	Q	Very light work	0.84	-0.13	kW
		Light work	1.40	-0.22	kW
		Total	2.24	-0.36	kW

1) Data for recommended ventilation was referred to Down (1969)

gain from occupants, electric appliances and lighting. The calculation referred to cooling load factor as well as the standard ratios of heat gain. This factor is multiplied by the standard heat gains when the internal heat gain occurs intermittently, for instance, heat from occupants affects only during working hours in this case study. The office was assumed to be used from 9 am, while the system was designed with conditions at noon. Hence, the factor to estimate the effect after three hours operation, 0.8, was chosen according to the research results (Kreith et al., 2005). This element was added to the demand calculation by multiplying by this factor (Table 3.8 and Table 3.9).

Some sample calculations are introduced here. Firstly, latent heat gain in heating operation was derived as follows;

Table 3.8 Demands caused by occupants

		Heating	Cooling		
Number of occupants	Very light work		4	people	
	Light work		4	people	
Cooling load factor			0.80	-	
Indoor temperature		20.00	27.30	C	
Latent heat gain	Very light work	21.49	48.53	W	
	Light work	43.30	76.80	W	
Sensible heat gain	Very light work	81.08	54.05	W	
	Light work	88.59	55.08	W	
		Latent heat	0.26	0.50	kW
Total heat gain	Sensible heat	0.68	0.44	kW	
	Total	0.75	0.75	kW	

1) Data for cooling load factor and heat gain was referred to Kreith et al. (2005) and Down (1969) respectively

Table 3.9 Demands caused by electric appliances and lighting

Cooling load factor		0.8 -
Electric applicants	Total emission	8.0 kW
	Use factor	0.8 -
	Total demand	5.1 kW
Total electric consumption		2.15 kW
Lighting	Ballast factor ²⁾	1.20
	Total demand	2.07 kW

1) Data for cooling load factor was referred to Kreith et al. (2005), while use factor and ballast factor was referred to Down (1969)

2) For fluorescent light

$$Q = \left\{ \begin{array}{l} (NumberOfOccupants) \times (LatentHeat_{verylightwork}) + \\ (NumberOfOccupants) \times (LatentHeat_{lightwork}) \end{array} \right\} \times (CoolingLoadFactor)$$

$$= (4.00 \text{ people} \times 21.5 \text{ W/person} + 4.00 \text{ people} \times 43.3 \text{ W/person}) \times 0.80 \div 1000$$

$$= 0.260 \text{ kW}$$

Secondly, heat gain from electric applicants was obtained as follows;

$$\begin{aligned}
 Q &= (TotalEmission) \times (UseFactor) \times (CoolingLoadFactor) \\
 &= 8.0kW \times 0.80 \times 0.80 \\
 &= 5.1kW
 \end{aligned}$$

Finally, heat gain from electric applicants was obtained as follows;

$$\begin{aligned}
 Q &= (TotalElectricConsumption) \times (BallastFactor) \times (CoolingLoadFactor) \\
 &= 2.15kW \times 1.20 \times 0.800 \\
 &= 2.07kW
 \end{aligned}$$

Design demands

Demand from each category was summed up to acquire the total heating and cooling demands (Table 3.10). The heating demand was a subtraction between the heat loss through the poorly insulated structure, 26.1 kW, and the heat gain from the inside, 7.9 kW. Since the outdoor temperature was

Table 3.10 Design demands

in kW			
Category		Heating	Cooling
Conduction	Walls	11.18	0.79
	Doors	0.11	0.02
	Walls below grade	5.47	
	Roof	1.68	0.38
	Glass	3.43	0.10
Solar gain	Glass		2.39
Infiltration and ventilation	Infiltration	1.99	-0.16
	Ventilation	2.24	-0.36
Internal heat generation ¹⁾	Lights	-2.07	2.07
	Electronic equipment	-5.12	5.12
	Occupants	-0.75	0.75
Total demand		18.15	11.11

1) Total internal heat gain; 7.94 kW

lower than the target indoor temperature in summer, the heat loss by the conductive heat transfer through the building structure was small. As a result, the major contributors to the cooling demand were solar gain and internal heat generation.

3.1.4 Selection of heat pump

Water source heat pumps designed for the GSHP were referred (Zeneral Heat Pump Co.Ltd, 2005). The smallest heat pump with parallel flow passes and R-407C of working fluid, ZQH-10W10-R-C, provided a sufficient performance (Table 3.11). R-407C is one of the blended types; therefore, the negative impact on the ozone depletion is zero (section 2.1.2).

The heat pump contains an inverter controlled compressor. Unlike a vane controlled compressor, the compressor can maintain the COP even if the load goes down at the same inlet temperature of heat source. The COP finally goes down when the control is shifted to a combination with the vane

Table 3.11 Specs of the selected heat pump

Condition	Operation	Capacity kW	COP ¹⁾	Outlet / inlet temperature		Electric consumption kW	Heat source kW	Flow rate for 5 °C difference ²⁾³⁾ m ³ /h
				Supply °C	Heat source °C			
Original	Cooling	24.9	4.6	7 / 12	30 / 25	5.4	19.5	3.5
	Heating	28.8	3.9	45 / 40	12 / 7	7.4	21.4	3.9
Design	Cooling	22.8	4.6	7 / 12	30 / 25	4.9	17.9	3.3
	Heating	18.0	2.5	45 / 40	-5 / 0	7.2	10.8	2.0

1) COP differs with dependence on the outlet temperature of heat source

2) Properties for 20% ethylene glycol solution was referred

3) Flow control depending on operation mode was not considered; therefore, the flow rate for cooling in the design was also 3.3 m³/h. Therefore, design temperature difference for heating was 3 °C. Though the selected flow rate could supply up to 30.1 kW with 5 °C, the maximum capacity of the system was capacity of heat pump, 28.8 kW.

control; however, the load is normally less than 40 % of the full capacity. Therefore, the design COP was assumed to be the same as that of the nominal value.

The mean ambient temperature is approximately 10.8 °C in Nottingham (section 3.2.1); hence, it is unrealistic to expect the inlet temperature of heat source to be 12 °C. Hence, the design inlet temperature of the heat source was set as the freezing point of moisture in soil, 0 °C. In fact, ordinary liquid has a supercooling process before it freezes. The temperature during this process normally goes down; therefore, limiting the temperature of the working fluid at 0 °C should avoid freezing. Once the moisture in soil is frozen, effective heat transfer between the evaporation and the condensation, which was introduced in section 2.5.5., would be reduced. When the system requires safe enough operational allowance, the operational limit temperature is advised to be set at higher than 0 °C. However, a condition to discover the heat collection capacity as large as possible was selected for this analysis.

The COP is affected by the outlet temperature of heat source and the supply temperature (Figure A.3). Since the design input temperature of heat source was lower than the original value, the design COP for heating went down to 2.5 as shown in Table 3.11. The design COP is a source to estimate the electric consumption and the required amount of heat source. Table 3.11 shows design demands and the required heat source for an insulated office building, which is described in section 3.1.5.

Chapter 3 Building a Model for Case Studies

It is more economical to use water as liquid medium between the underground energy and the heat pump. However, as the temperature of the working fluid was designed to be below 0 °C, anti-freezing liquid, brine, ought to be applied. For this investigation, 20 % solution of ethylene glycol was chosen to have the freezing limit of less than -8 °C (M. Conde engineering, 2002). On the basis of the properties (Table 3.11), the operational flow rate was quantified to obtain 5 °C of temperature difference between the inlet and the outlet at heat exchanger of the heat pump (Table 3.11). Since the pump was assumed to be operated at the same flow rate, the larger required flow rate between heating and cooling operation, 3.3 m³/h, was set as the design value. Therefore, the heat pump can supply hot water for heating up to the maximum capacity, 28.8 kW with temperature difference of 4.8 °C.

The selected heat pump has larger capacity than the demands for the two story office building. Therefore, the maximum building size was estimated to know a range of applicable buildings, which the same heat pump can provide the sufficient heating and cooling energy. Consequently, it was found that the heat pump could meet the demands of a four story office building with the same building components and operating conditions (Table 3.12).

3.1.5 Building example to meet the approved document L2B

The structure of the building model had poor insulation effect to meet the acceptable level regulated by the approved document L2B. Therefore, an insulated building model was explored. Each building component was

Table 3.12 Design demands for a four story office building

kW			
Category		Heating	Cooling
Conduction	Walls	23.39	1.42
	Doors	0.11	0.02
	Walls below grade	5.47	
	Roof	1.68	0.38
	Glass	5.26	0.48
Solar gain	Glass		4.77
Infiltration and ventilation	Infiltration	3.98	-0.32
	Ventilation	3.35	-0.53
Internal heat generation ¹⁾	Lights	-4.16	4.16
	Electronic equipment	-10.32	10.32
	Occupants	-1.13	1.13
Total demand		27.63	21.83
Heat pump capacity		28.80	24.90

1) Total internal heat gain; 15.6 kW

assessed to have the acceptable U-values as listed in Table 3.2. Examples of the refurbishment are expressed with the coloured parts in Table A.5.

It was revealed that the insulated building needed no additional heating, since the insulation was sufficient to balance with the internal heat gain. Therefore, the unit values for the office operation were tolerated to find the conditions, with which the selected heat pump was not oversized both in heating and cooling (Table A.6). As a result, only very light work was assumed to occur in the insulated building. In addition, the space per worker was doubled to be 1 person / 30 m², compared to the non-insulated building. This is equivalent to the German average and the most spacious layout in Europe (Weber, 2006). Simultaneously, the density of lighting and electric appliances was halved. When a plan for a typical office block was

Chapter 3 Building a Model for Case Studies

taken from the past research as illustrated in Figure A.4, the building could have seven stories to assemble a system with the selected heat pump capacity. As a result, the total floor area became $105 \text{ m}^2 \times 7 \text{ story} = 735 \text{ m}^2$, while the ratio of the total window area against the total wall area remained nearly the same (Table A.7).

The obtained design demands showed different balance between heat loss and heat gain from the non-insulated building (Table 3.13). Heat loss by conduction was reduced compared with the four story office building, even though the total floor area became approximately 1.8 times as large. Though unit internal heat gain was reduced, the total value, 17.7 kW, was larger due to approximately 2.2 times more occupants. These features contributed to make the total heating load smaller than that of the

Table 3.13 Design demands for an insulated building model

kW			
Category		Heating	Cooling
Conduction	Walls	7.23	-0.51
	Doors	0.13	-0.01
	Walls below grade	0.67	
	Roof	0.55	0.14
	Glass	7.14	0.46
Solar gain	Glass		7.97
Infiltration and ventilation	Infiltration	14.50	-1.15
	Ventilation	5.45	-0.87
Internal heat generation ¹⁾	Lights	-3.81	3.81
	Electronic equipment	-11.76	11.76
	Occupants	-2.13	2.13
Total demand		17.96	22.82
Heat pump capacity		28.80	24.90

1) Total internal heat gain; 17.7 kW

non-insulated building.

The design exercise reconfirmed a large impact of U-values on design cooling and heating demands. It was indicated that the same heat pump system could meet demands for a larger office building with more occupants, if the building was well insulated with the minimised internal heat gain.

3.2 Environment Data

Environment data is the most essential information in considering the use of renewable energy. The required data is, for instance, soil temperature and climatic data, such as ambient temperature, humidity, solar radiation, wind speed and precipitation through a year. The micro climate changes significantly, with dependence on a change of thermal mass in buildings or the movement of underground water around the operational site.

3.2.1 Weather data in Nottingham

The weather data in Nottingham has been collected since January 2001 by a weather station at the School of the Built Environment in the University of Nottingham (Figure 3.1). Ambient temperature, humidity, solar radiation, wind speed and precipitation had been automatically saved into the hard disk of computer every minute. Then, the data was summarised as the hourly average to be used for the design investigation of the building model.

Figure 3.2 shows the average monthly temperatures and precipitation from 2001 to 2006. The monthly lowest temperature went below 0 °C for about 4 months. Besides, the lowest temperature was below 10 °C even in



1) Measuring tools on Marmont Centre



2) Precipitation measuring equipment on the adjacent building



3) Data collection computer

Figure 3.1 Weather station in the University of Nottingham

summer, though the highest temperature rose to nearly 30 °C. This temperature difference over days or seasons can be effectively used in the

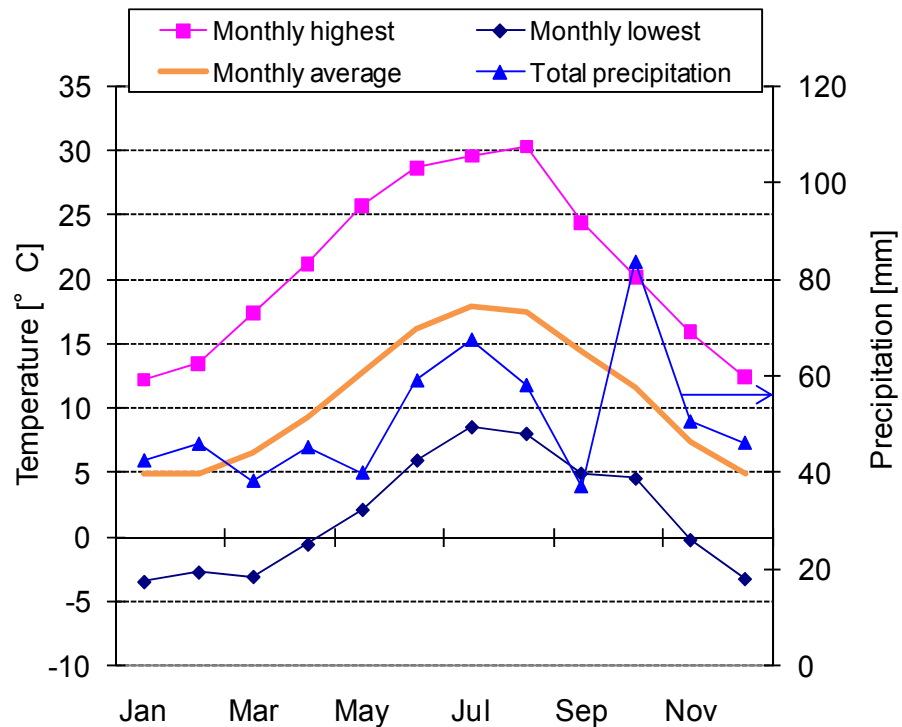


Figure 3.2 Six year average weather data in the University of Nottingham

GSHP. As explained in section 2.1.4, ground heat source is stored from sunshine and ambient temperature. For instance, it is effective to store cooling energy from low ambient temperature and to release the energy when cooling loads occur.

The precipitation seems to have a mild seasonal change. It is studied that soil water content is synchronised with precipitation as displayed in Figure A.5 (Zreda et al., 2008). Hence, it can be expected that the relatively constant precipitation through a year may prevent soil water content from becoming extremely low. Maintaining water content is one of the directions for high soil thermal conductivity as understood through de Vries's theory in section 2.5.5.

3.2.2 Estimation of soil temperature

Soil temperature is another essential data for the design optimisation of the GSHP. However, it is not easy to find published data for specific micro environment. Equally, measuring the locally unique data is not always practical, regarding the required time and budget. Data at greater depth is required to be monitored for at least a year in order to understand the variation. Even if situation allows the data collection, there is no guarantee that the data does not fluctuate depending on the environmental events, such as rainfall, the movement of water table or possible installation of energy systems in the neighbours. Therefore, one of the useful options is the use of models derived from a research to understand underground temperature gradient at specific locations.

There is a useful equation to describe seasonal variations of soil temperature (Kusuda et al., 1965).

$$T(x, t) = T_m - T_a \times e^{[-x(\pi/365\alpha)^{0.5}]} \times \cos\left\{2\pi/365 \times \left[t - t_{cd} - x/2 \times (365/\pi\alpha)^{0.5}\right]\right\}$$

(Equation 3.9)

T	Temperature	°C
T_m	Mean air temperature	°C
T_a	Temperature amplitude of air, $\frac{1}{2} (T_{\max} - T_{\min})$	°C
x	Depth from ground level	m
α	Soil diffusivity	m ² /day
t	Day of year	-
t_{cd}	Day of year when the coldest air temperature occurs	-

This equation is applicable, when yearly data of ambient temperature and thermal diffusivity of soil are collectable. The results are shown in Figure 2.8 for Nottingham. The values used for this estimation are listed in Table 3.14.

Figure 3.3 compares estimated temperature gradient for November (data A) to data in other researches for the UK. Viessmann Limited (2004, data B) and Busby (2005, data C) carried out the measurement in the UK, while Doherty et al. (2004, data D) calculated with Equation 3.9 for Nottingham.

Each trend differs from each other; however, the maximum temperature difference of data A, 4.1 °C, was in the same range as those from experimental data B and data C. Though the same formula was referred, the value of data D was approximately double, 8.0 °C. Nevertheless, two kinds of experimental data disagreed with each other by up to 63 %. This suggested a difficulty to define representative soil temperature even with experiments. Furthermore, the experiments demonstrate typical temperature gradient in the UK, which was too broad to verify the estimated

Table 3.14 Data for estimating underground temperature gradient

Item			
Mean air temperature	T_m	°C	10.8
Maximum air temperature	T_{max}	°C	31.2
Minimum air temperature	T_{min}	°C	-2.0
Temperature amplitude of air	T_a	°C	16.6
Day of T_{min}	t_{cd}	-	17
Soil diffusivity ¹⁾	α	m ² /day	0.05

1) Effective value for wet sand (Singh et al., 1991)

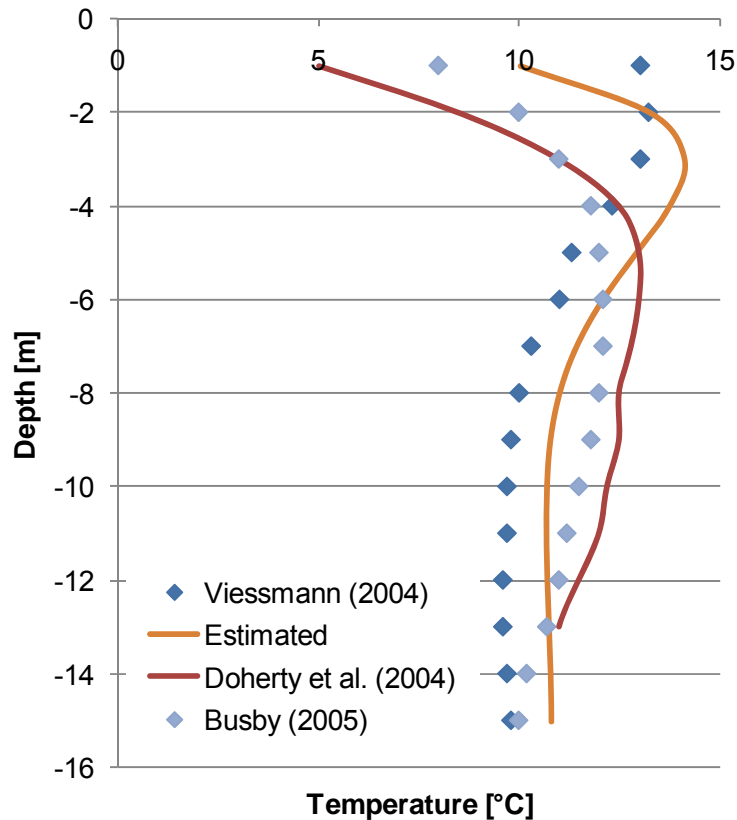


Figure 3.3 Comparison in soil temperature gradient

results for Nottingham. Beside, the difference between the estimation and data B and C was $\pm 24.6\%$ and $\pm 29.5\%$ respectively. The data derived from the formula did not convincingly match the experimental data and the maximum temperature was higher than experimental values. However, the estimation refers to soil diffusivity and variation of ambient temperature, which interprets the unique characteristics of operational sites. Hence, this method could be more reasonable than referring to the generalised experimental data when site measurement is not available. The estimated soil temperature gradient was referred for the simulation analysis in this project.

3.3 Conclusions

A system example was presented to be used for the design optimisation to enhance the underground heat collection throughout this project. Office buildings with common size and standard operating conditions were demonstrated with and without insulated structures. This provided an applicable variation with the same water source heat pump. Consequently, design loads for heating and cooling were calculated for an insulated office building.

The environment data collected in the University of Nottingham was analysed to estimate the operation of the GSHP. As the soil temperature data had not been measured in the university, the monthly variations were predicted with a published empirical equation.

Chapter 4 Design Optimisation of Rainwater Collection Tank for the GSHP Application

Introduction

A system model, design loads and environmental data were identified in the previous chapter. Therefore, design optimisation of the underground structure is carried out after this chapter. The target design criteria need to be a solution which meets three essential objectives; consistent performance, feasible construction costs and high system efficiency. As discussed in section 2.2.3, the use of thermal energy in rainwater is one of the hopeful strategies to tackle these barriers. Potential acceleration of the underground heat transfer by rainwater convection is another point to evaluate. Therefore, a GSHP system combined with a rainwater collection tank is studied.

The design optimisation is attempted through a sensitivity analysis with the CFD. Simulation is convenient to obtain rough ideas through a parametric design analysis, since neither facility nor test rig is required to be built. Even though some settings need to be interpreted differently from the reality into models, time and budget can be hugely saved for studying many kinds of design parameters.

As a preparation, a methodology to determine mesh size is explored for accurate calculations in FLUENT 6.1.18 software. This analysis is accomplished by comparing diverse calculation conditions with a simple calculation model. In addition, verification of simulation models is conducted to confirm resemblances to theoretical calculation.

A series of sensitivity analysis is conducted with different operational conditions. In order to extract influential design parameters, six design parameters are picked up; tank shape, thermal conductivity of concrete bed, soil surrounding the tank and tank itself and thickness of concrete bed and the surrounding soil. Design modification to maximise the positive effects of the essential parameters is investigated after Chapter 5.

4.1 Investigation of Meshing

The use of simulation was chosen in order to examine influential design factors in the considered GSHP systems; however, the CFD fundamentally has some sources of errors in its characteristics (American Institute of Aeronautics and Astronautics, 1998). The common acknowledged errors are, for instance, round-off error in the digital computation and error when the geometry of models is simplified. These cannot be completely solved; therefore, efforts to minimise the occurrence of the potential errors are at least required. Since FLUENT 6.1.18 software leaves meshing optimisation to users, the investigation was needed as a preparation.

4.1.1. Indications for accurate meshing

One of the most crucial preparations is the determination of mesh size. Holman (2002) advises to investigate different mesh size to discover the small enough size to meet the actual thermal transfer rate. It is said that smaller mesh size can generate more accurate results, while larger mesh size terminates the simulation more quickly. Nevertheless, the American Institute of Aeronautics and Astronautics (1998) points out that even this size refinement could trigger the potential errors in the CFD. Therefore, a

methodology to determine mesh size was explored.

Majumdar (2005) suggests that non-uniform cell size is more efficient than uniform cell size. Non-uniform layers can be set in FUEENT as displayed in Figure 4.1. The width of each non-uniform layer is determined through multiplying by a growth ratio. In Figure 4.1, the widths of layers become larger from the boundary to the rest of the calculation area by 1.5 times up to the layer 8th. Since more active heat transfer occurs around boundaries, sharper variation of temperature near the boundaries can be effectively captured. Thus, the use of non-uniform boundary layers could be a smart strategy to accurately express the significant change of heat transfer and to avoid increasing the number of calculation cells for the entire model.

The theories suggest directions to effectively set accurate meshes; however, other influences ought to be also examined in advance. One of the purposes through the sensitivity analysis is to evaluate heat collection

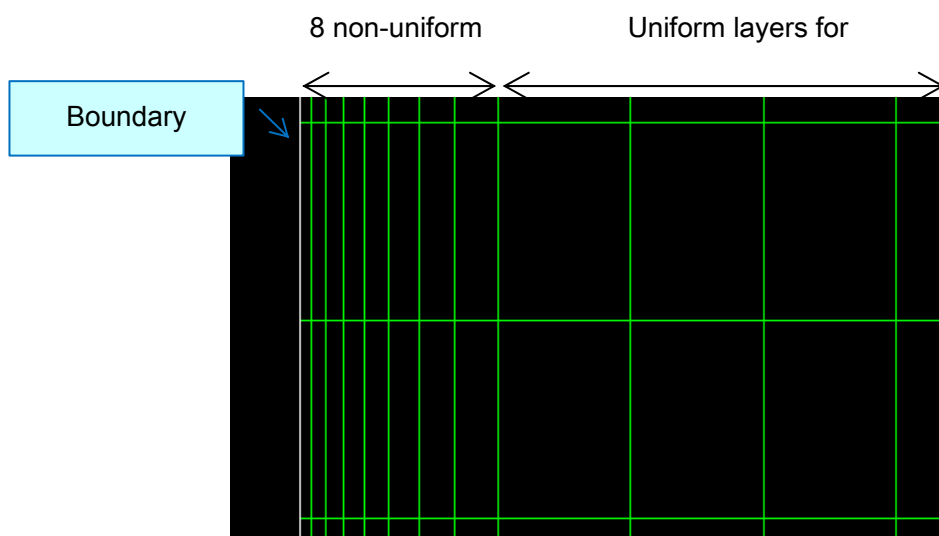


Figure 4.1 Non-uniform layers around boundaries in FLUENT

capacity with dependence on high thermal conductivity of components in the underground system. This may cause extreme heat transfer and the calculation could be unstable. Therefore, to clarify the effects of high thermal conductivity in the calculation models is required. The results would determine a valid range of thermal conductivity in the sensitivity analysis.

4.1.2. Case study

A simple model was built to resolve the effects of mesh size as drawn in Figure 4.2. Similar size and conditions to the actual calculation models were selected to predict the features. Studied cases are defined in Table 4.1. Higher thermal conductivity was applied to solid area 2 to compare with the cases with ordinary soil thermal conductivity. Various numbers of boundary layers were attempted for each case. The results were

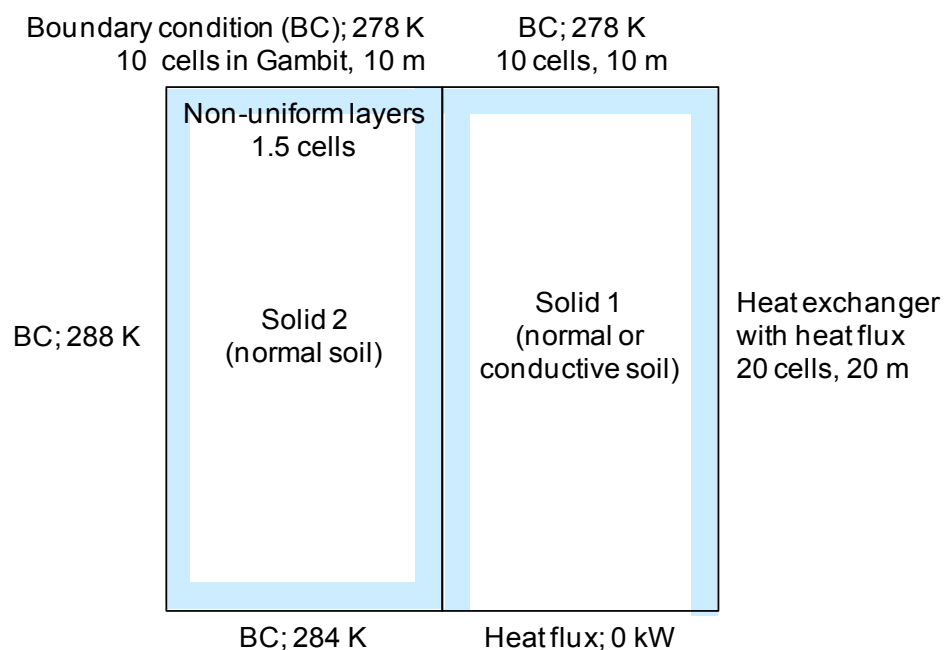


Figure 4.2 Model for the mesh investigation

Table 4.1 Study cases for the mesh investigation

Case name	Mesh size for non-boundary area m	Material ¹⁾ Solid 1	Material ¹⁾ Solid 2	Heat flux W/m ²	Comment
Stn	No boundary layer				Standard
BL	1.00				
BL 0.5	0.50		Sub-soil	-1	
BL 0.2	0.20				
Mxd Stn	No boundary layer	Sub-soil			
Mxd BL	1.00				
Mxd BL0.5	0.50		7% copper	-5	Mixture between sub-soil and 7 vol% of copper
Mxd BL0.2	0.20				
Mxd BL0.08	0.08				

1) Thermal conductivity of sub-soil and copper mixture were 1.7 W/m/K and 21 W/m/K respectively. The latter was calculated regarding effective conductivity in random packing was 70 % of the actual volume fraction (section 2.4.3).

compared with the minimum temperature in the calculation area at the fixed heat flux; -1 W/m² for the models with only sub-soil and -5 W/m² for the models mixed with copper respectively. The different heat flux allows the results to be compared in the same temperature range.

All the simulation for this project was conducted on Windows. Some say that FLUENT exerts itself on Unix, which FLUENT was originally developed for. Therefore, operating on Windows might cause limits or troubles. Hence, the mesh investigation was carried out to optimise for operating on Windows.

4.1.3 Calculation results

The change of the minimum temperature in case Stn is plotted in Figure 4.3. The result was almost stable with larger mesh size than 0.2 m for the non-boundary area; however, smaller mesh size did not bring the

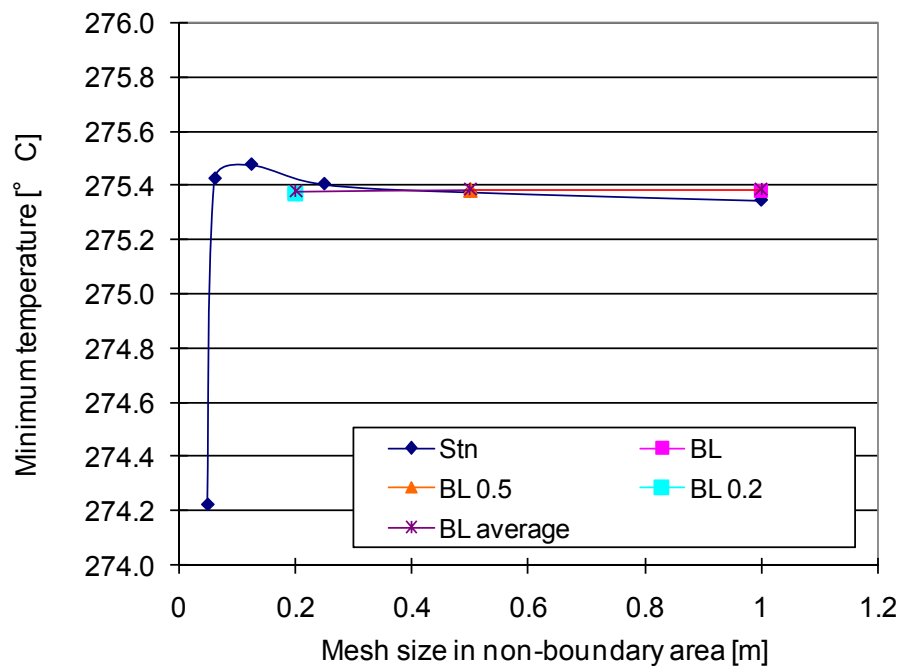


Figure 4.3 Results of cases with sub-soil

convergence as the theory suggests. It seemed that too small mesh size led to divergence in FLUENT. The reason could be that the tested small mesh was too fine for the calculation conditions and lured the computational errors in FLUENT as pointed in section 3.1.1.

The results with non-uniform boundary layers in case BL are displayed in Figure 4.4. The result looked consistent regardless of different number of layers. This may be because the existence of the boundary layers effectively captured the sharp temperature variation near the boundaries and achieved the stable calculation without refining the mesh size for the rest of the calculation model. The calculation was conducted with up to 16 layers for case BL 0.5 and case BL 0.2 as well. In these cases, the results were also stable as shown in Figure 4.3. The models with non-uniform boundary

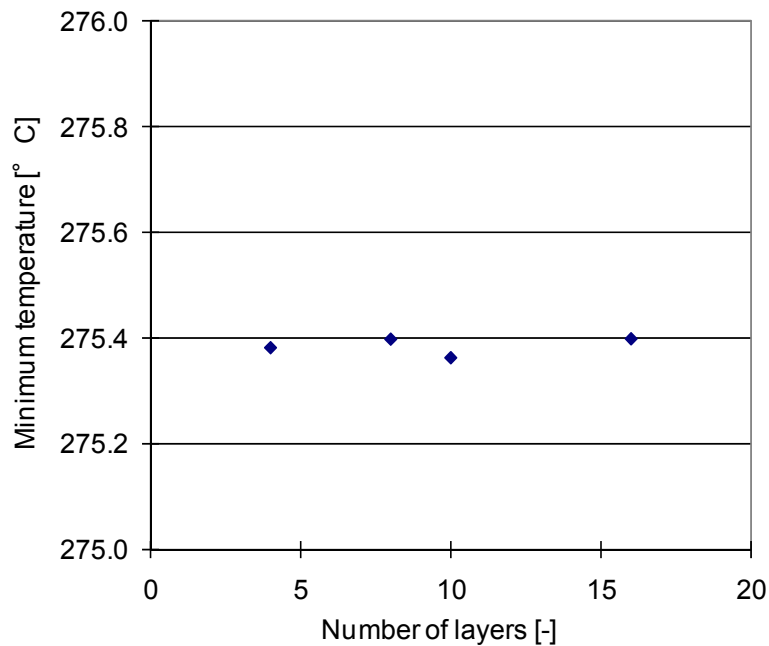


Figure 4.4 Results of case BL

layers tended to exhibit more stable results than the model without boundary layers, case Stn. A range of the minimum temperature among the cases with different number of boundary layers was subtle even with a smaller mesh size for the non-boundary area in case BL 0.2. This advised to use non-uniform boundary layers to attain converged results. When this finding is combined with the theory developed by Holman, more accurate results would be delivered with smaller mesh size among the calculation cases with non-uniform boundary layers.

The result of case Mxd Stn showed similar tendency to that of case Stn (Figure 4.5). The minimum temperature rose and dropped suddenly with small mesh size. This characteristic was stronger than the cases only with sub-soil and no stable part was seen in the profile.

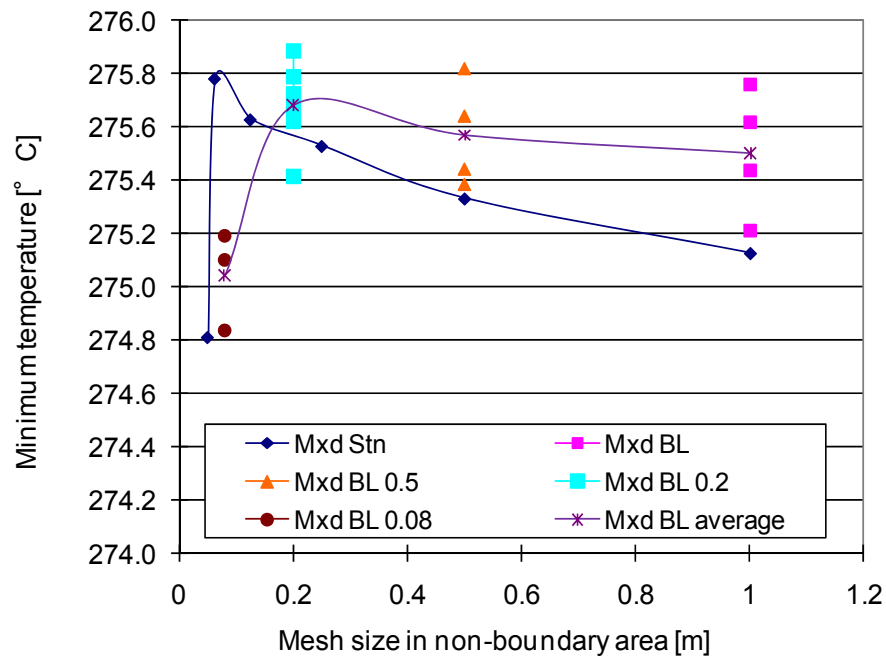


Figure 4.5 Results of cases with copper

Fluctuating results with dependence on different number of layers can be pointed out in Figure 4.6. Unlike case BL, converged result was not indicated. The results did not even show clear tendency and the profile looked partially random. This suggests that the calculation was possibly diverged.

Case Mxd BL 0.5, Mxd BL 0.2 and Mxd BL 0.08 also showed the same diverged results against the number of layers as seen in Figure 4.5. The average of the cases with non-uniform boundary layers showed a similar tendency to that from case Mxd Stn. To sum up, even if non-uniform boundary layers were applied, FLUENT did not necessarily acquire converged results when thermal conductivity in the calculation model went beyond a certain level.

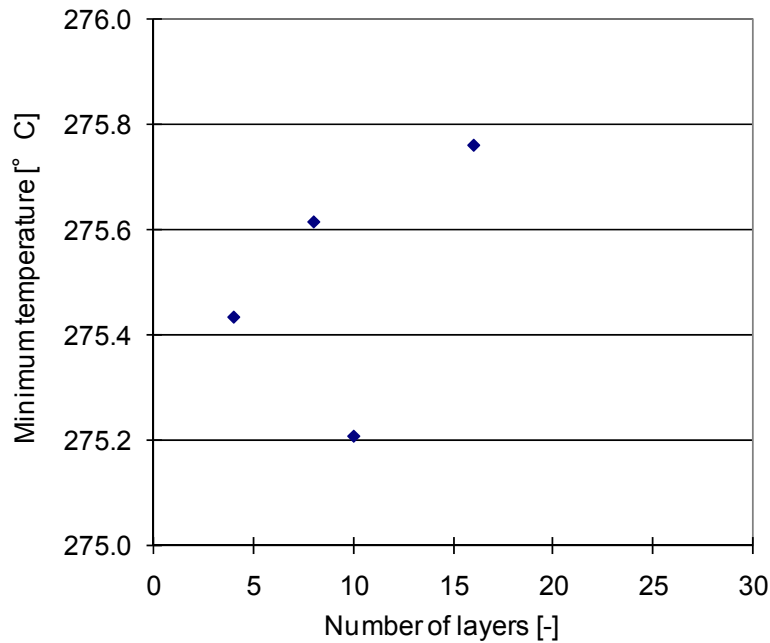


Figure 4.6 Results of case Mxd BL

4.1.4 Conclusion

The effects of mesh size and thermal conductivity setting were investigated with simulation models in FLUENT, which was operated on Windows. Though in theory setting smaller mesh size results in accurate calculation, the results fluctuated when smaller mesh size than a certain value was set. However, non-uniform boundary layers effectively led to converged results with medium thermal conductivity. In this case, selecting smaller mesh size for the non-boundary area might bring more accuracy among the cases with non-uniform boundary layers.

Cases with higher thermal conductivity generated scattered results, which were sometimes impossible to obtain the converged solution even with non-uniform boundary layers.

4.2 Verification of Simulation Models

Before discussing the impacts of design parameters, it is important to assess the accuracy of calculation with the simulation software. There are two main categories to investigate the accuracy; validation and verification (American Institute of Aeronautics and Astronautics, AIAA, 1998). Verification determines the accuracy of conceptual interpretation into simulation model, while validation evaluates the accuracy against the real world (Figure A.6). For the following simulation analysis, verification is attempted.

4.2.1 Method

Even if the best effort is made in the mesh size optimization, simulation with the CFD still has a potential for errors. Therefore, verification expressed the difference from the results from theoretical calculation. To begin with, mesh size and the number of boundary layers were examined. A simple model was chosen to compare between theoretical and simulation results (Figure 4.7). Though the targeted problems are simplified for small area, verification with highly accurate theoretical solutions is recommended by the

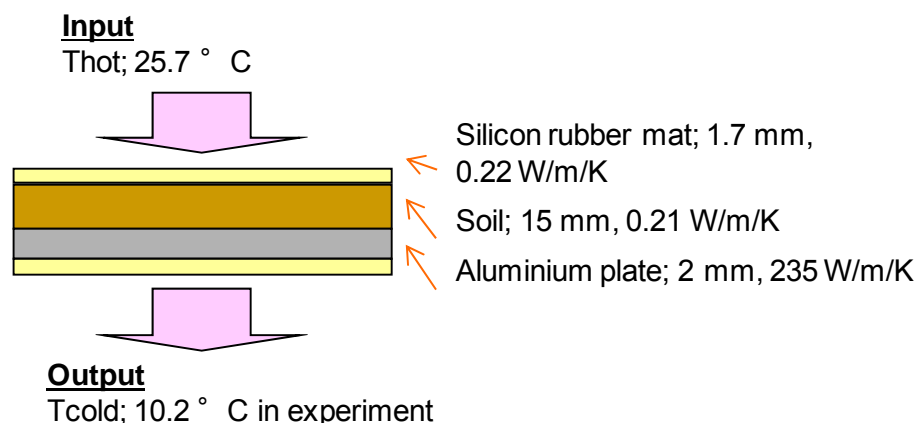


Figure 4.7 Model for the verification

AIAA. This condition enables to evaluate the computational errors with the most accuracy and reliability.

The geometry was based on an experiment conducted with heat flow meter (HFM, see Chapter 5). The soil sample was completely oven-dried sand, which was sieved to granules of a size no greater than 2 mm (2 mm sand). Since the sand was granular, the sample was shaped by a wooden tray with 15 mm high sides and a 5 mm thick aluminium plate base.

The mechanism of the HFM was explained in section 2.5.1. In the real measurement with the HFM, the sample tray is sandwiched by silicon mats, so as to fill air gap between the sample and the hot or cold plate. Thickness of the mats was measured with an electric thickness gage. For the verification, these layers were assumed to be infinite. Therefore, both sides of the calculation model were set as symmetric and the impact of the wooden tray was disregarded.

The thermal conductivity of the silicon rubbers and the aluminium plate were taken from the standard values (Ramirez et al., 2009 and Holman, 2002). The thermal conductivity for the dry sand was measured during the experiment presented in Chapter 5. The temperatures on the hot and cold plate were also measured values at steady state. Since the energy input to the heater and the chiller to reach the temperature gradient was unknown, the required heat flux per area was not available from the experiment itself. Therefore, validation was not conducted with this model.

A theory discovered by Fourier was selected to estimate the heat flux to realise the temperatures on both sides of the sample layers with the following equations (Lienhard et al., 2006). This theory is categorised as a benchmark numerical solution to ordinary differential equation, ODE, by the AIAA. The ODEs are more accurate than other theoretical solutions, which are analytical solutions and benchmark numerical solutions to partial differential equations.

$$Q = -k_{total} A \frac{\Delta T}{\Delta x_{total}} \quad (\text{Equation 4.1})$$

$$k_{total} = \frac{\Delta x_{total}}{R_{total}} \quad (\text{Equation 4.2})$$

$$R_{total} = \frac{\Delta x_1}{k_1} + \frac{\Delta x_2}{k_2} + \frac{\Delta x_3}{k_3} \quad (\text{Equation 4.3})$$

Δx	Thickness of layer	m
R_{total}	Total thermal resistance	m^2K/W

, where subscript 1, 2, 3 means each layer.

A series of simulation with FLUENT could quantify the required heat flux using the programmed equations. The calculation model was created with Gambit 2.0 software. 1 mm in the actual size was expressed by a cell and 2 cells of boundary layer area were prepared. Then, various kinds of heat flux were attempted with the fixed hot plate temperature, until the cold plate temperature reached the experimental value.

4.2.2 Results

Combinations between the number of boundary layers and mesh size in the

non-boundary area were determined to create a smooth gradient of mesh size (Table 4.2). The required heat flux varied when the mesh size changed (Figure 4.8). Though boundary layers were applied, the impacts of simulation errors seemed to be significant in the cases with small mesh size. As a consequence, the result derived from a case with mesh size 0.5 mm was considered to be the most accurate answer, since the results were stable in the cases in which the mesh size was larger than 0.5 mm.

Table 4.2 Variation of calculation models

Mesh size in mm	Number of boundary layers ¹⁾
0.05	12
0.10	10
0.50	6
1.00	5

1) The growth ratio was 1.2

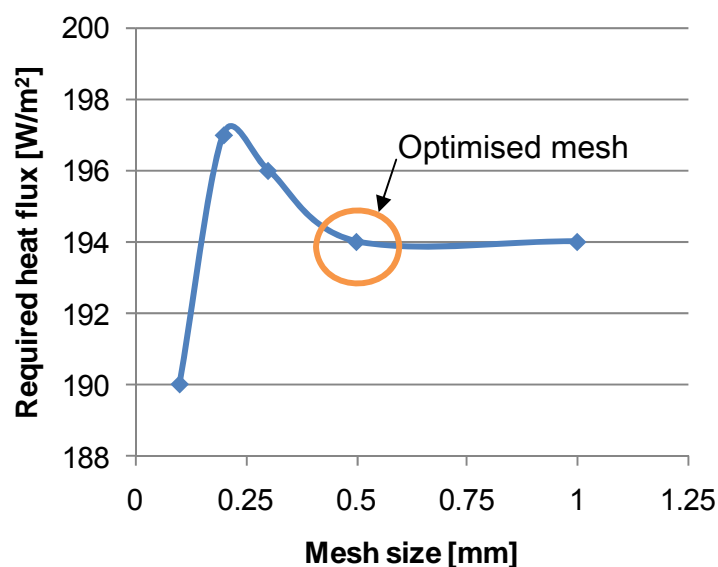


Figure 4.8 Comparison in required heat flux

While the required heat flux was 194 W/m^2 in the simulation, the theoretical calculation quantified the heat flux as 178.35 W/m^2 . Therefore, the difference 8.8 % indicated the accuracy of the simulation in comparison to Fourier's law. As a result of the verification, it was concluded that the uncertainty of the simulation was $\pm 8.8 \%$.

4.3 Preparation for Design Optimisation

For successful sensitive analysis, setting realistic simulation model is of essence. This section describes the features.

4.3.1 Simulation model

The standard simulation model was built only for the underground heat collection system, comprising of a rainwater collection tank, heat exchanger within the tank, concrete bed, soil and air near the ground line as illustrated in Figure 4.9. Though most of the large commercial tanks for rainwater harvesting shape horizontal columns, a vertical tank was investigated in this

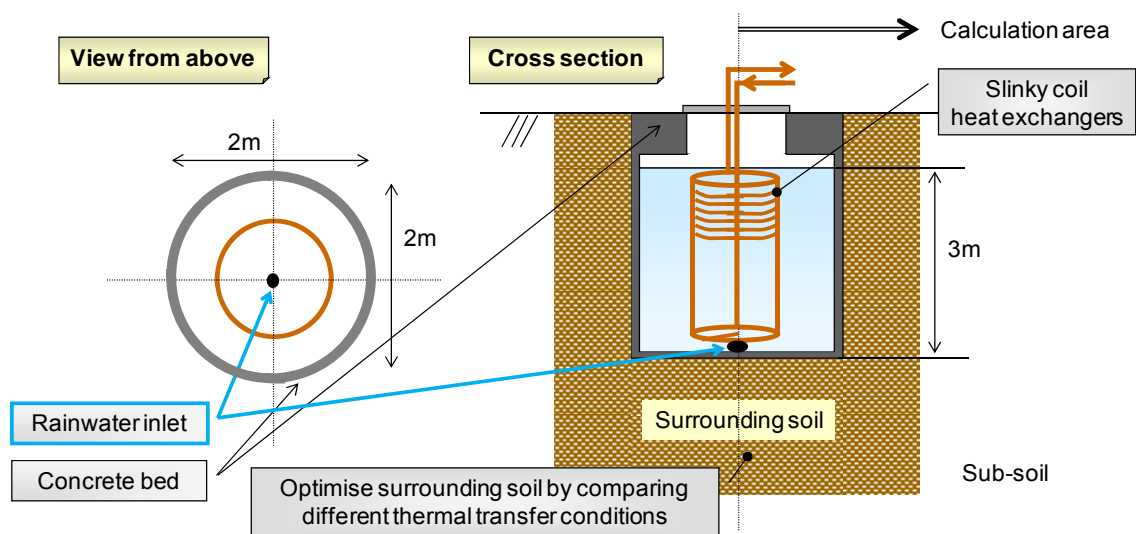


Figure 4.9 Simulation model

simulation. As pointed out in section 2.1.4, soil temperature at greater depth is more useful and stable throughout a year. Therefore, the long tank was expected to collect thermal energy more efficiently.

The first comparison over tank shape was conducted in a two dimensional symmetric model. The centre line of the tank was set as the symmetric line to reduce the calculation load and duration. After the second sensitivity analysis over the thermal conductivity of concrete bed, the centre line of the tank was set as the axisymmetric line. Hence, the rainwater tank was assumed to be a vertical column tank as drawn in Figure 4.9.

The design contained the following ideas. Rainwater was guided to enter the tank from the bottom. The inlet was set at the bottom centre of the tank to encourage equal rainwater circulation around the heat exchanger. For the equal distribution, horizontal rainwater inflow could be intentionally encouraged, for instance, with a disk shaped distributor at the end of the rainwater down pipe (Figure 4.10). It is also ideal to bury the piping underground, and so more thermal energy would be transferred into the piping when rainwater flows into the tank. Nevertheless, this strategy was not taken into consideration for this simulation analysis. Therefore, the inlet

e.g. 0.1 m diameter

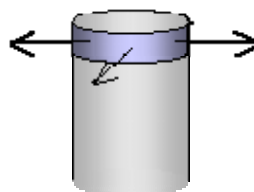


Figure 4.10 Image of the end of rainwater down pipe

rainwater temperature was set to be equal to the monthly average ambient temperature during raining. Besides, the water level was restricted by the drain near the tank neck. Therefore, when abundant rainwater comes into the tank, the excessive amount would overflow to prevent floods.

Thermal energy in soil and rainwater was extracted through the heat exchanger between the rainwater and the fluid heat media within the heat exchanger. The media, such as brine, circulated to transport the energy to the heat pump. The heat exchanger was assumed to be vertically piled up slinky coil, since the cost of slinky coil has been commercially reasonable. This would avoid increasing the payback period by adding expensive order-made heat exchangers.

Soil around the tank was divided into two parts in the model; the surrounding soil and sub-soil. This allowed the calculation model to explore the effects of modification of thermal conductivity in the surrounding soil. The sub-soil could have a range of thermal conductivity, for instance, between 0.2 and 2.2 W/m/K as displayed in Table 2.6. If there are handy techniques to create preferable thermal conductivity of the surrounding soil space, the design reliability will be improved.

Specs related to the rainwater collection were determined as listed in Table 4.3. The total collection area was the roof area, 105 m². From the rainwater inlet size and the average rainfall in December of Nottingham, 0.96 mm/h/m², the inlet velocity was calculated as 0.0035 m/s. The required tank size was determined to have 2 to 3 times larger volume of the stored

Table 4.3 Specs of calculation model

Item	Value	
Building	Roof area ¹⁾	105.0 m ²
	Height of floor	4.0 m
Rainwater flow	Average rainfall in December ²⁾	0.96 mm/h/m ²
	Collectable rainfall	0.10 m ³ /h
	Diameter of inlet in tank ³⁾	0.10 m
	Velocity of rainwater inflow	0.0035 m/s
Rainwater tank	Flow rate for cooling ⁴⁾	3.3 m ³ /h
	Design volume ⁵⁾	9.4 m ³

1) Flat roof, refer to Figure A.4

2) Refer to average rainfall between 2001 and 2005 in Winter, Nottingham

3) e.g. rainwater down pipe of a 0.1 m diameter

4) Calculated in Chapter 3.1.4

5) 2 to 3 times more rainwater than the required heat source capacity per hour was supposed to be stored. e.g. a vertical column with a 2 m diameter and a 3 m height

rainwater than the required heat source per hour, 3.3 m³/h. In case of a vertical column, the diameter and the height could be 2 m and 3 m respectively as illustrated in Figure 4.9.

These design ideas were contained in a calculation case in Gambit and in FLUENT as shown in Figure 4.11 and Figure 4.12 respectively. The calculation area was limited up to 2 m from the ground level in air, up to 7 m of horizontal distance from the centre of the tank and up to a 12 m depth underground. A sufficient distance was deliberately kept between the tank and the boundaries to reduce the influences of the boundary conditions on the heat transfer. A growth ratio of boundary layers was set as 1.2 throughout the calculation analysis.

Water level in the tank may change during the operation, when the stored

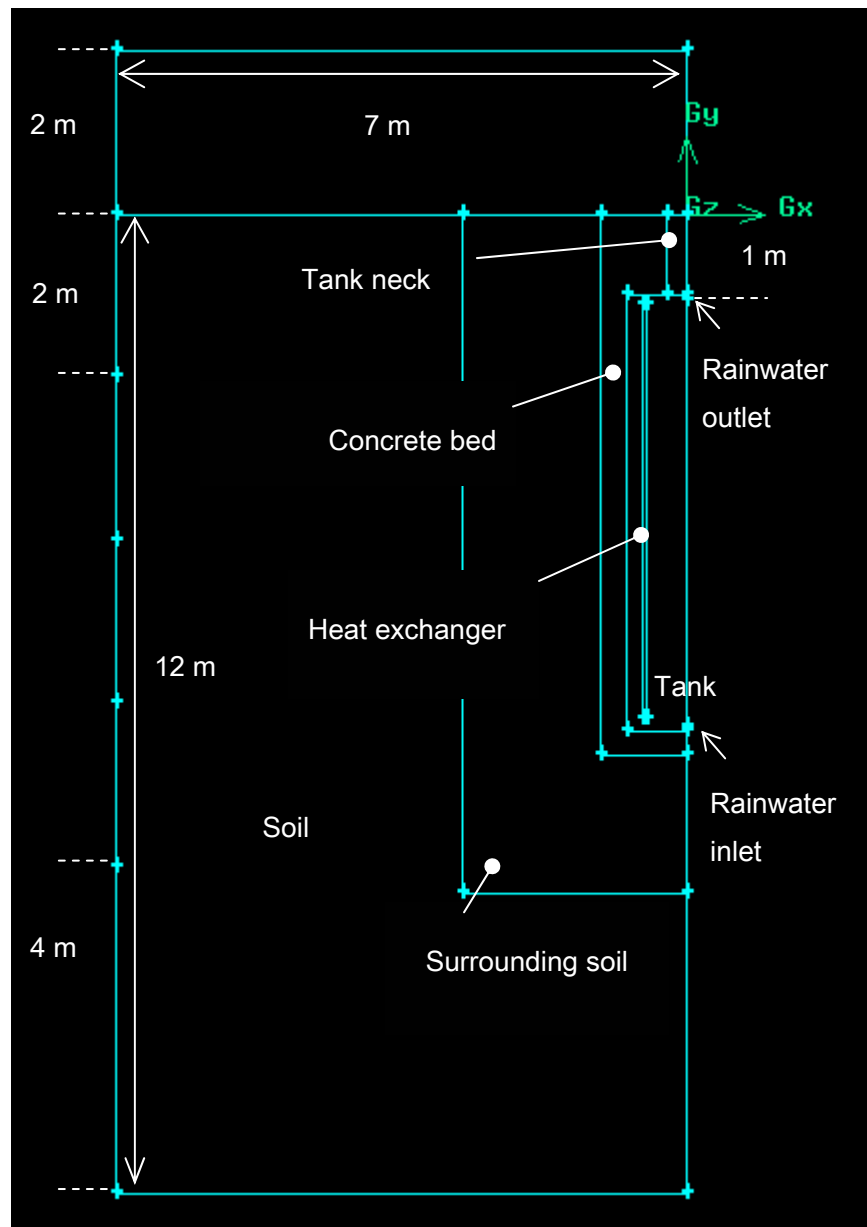


Figure 4.11 Model in Gambit

water is used, for instance, for flushing toilets. However, the tank was assumed to be always filled with water in the calculation model. The tank needs an access from the ground level for maintenance. This was modelled as a vertical pipe of a 0.5 m diameter and assumed to be filled with air (tank neck). Since FLUENT cannot handle more than two kinds of fluid in the same calculation, air was counted as a solid substance with air

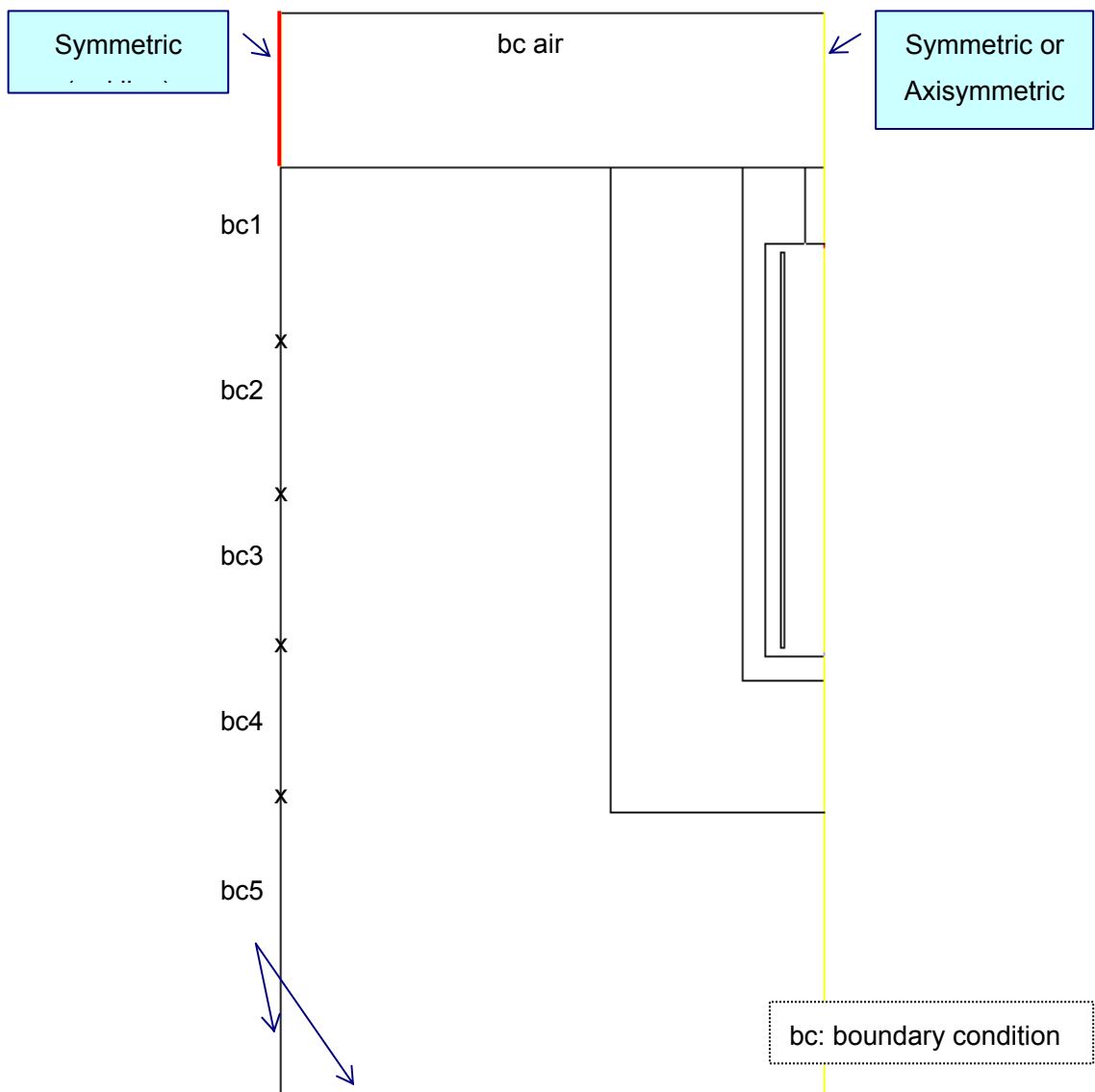


Figure 4.12 Model in FLUENT

properties. This setting was applied to the air both above the ground level and within the tank neck. Hence, wind was disregarded and the ambient air space had a temperature setting only at the top.

Some sizes in the calculation model were based on the practical data. One of the commercialised slinky coils has a 0.019 m diameter (Smith, 2006), which was too small in comparison to the whole model area. Hence, the

diameter was rounded up to 0.05 m to guide the calculation to smooth convergence. A cross section of the heat exchanger was simplified to be a rectangular as the calculation model shows in Figure 4.11, rather than a number of circles as the design concept meant. Therefore, the actual total heat exchange area could be larger than that in the calculation model, even if a part of each loop is touched and heat is transferred indirectly between the working fluid and the water in the tank.

Adequate thickness of concrete bed was calculated with the data supplied by a manufacturer of rainwater collection tanks (Figure 4.13). An equation was derived to relate the tank size with the required volume of concrete as follows.

$$V_c = -0.0004 \times V_t^2 + 0.409 \times V_t + 1.8616 \quad \text{(Equation 4.4)}$$

V_c Required volume of concrete m^3

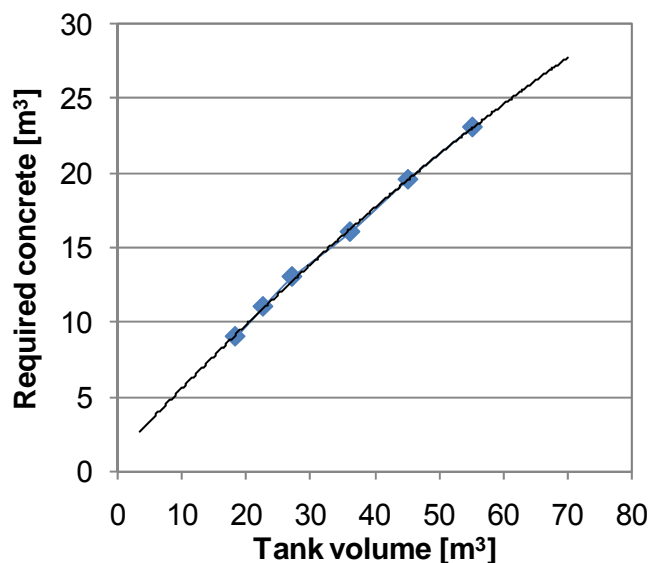


Figure 4.13 Required amount of concrete bed (Klargester, [no date])

V_t	Tank volume	m^3
-------	-------------	-------

Concrete was assumed to fill around the tank neck in the calculation model. Hence, the required concrete volume was determined to support the main body, the bottom and the tank neck.

A column tank in consideration was $9.4 m^3$; therefore more than $5.7 m^3$ of concrete was advised for the mechanical support. For a tank with a 2 m diameter and a 3 m high, a 0.11 m thickness met the requirement. The tank surface area varies in dependence on a ratio between the width and the length, and the wider tanks need thicker concrete layer. In case of the widest tank in the first sensitivity analysis described in section 3.6.1, a 0.13 m thickness satisfied the requirement. Since the fourth sensitivity analysis examines the effects of concrete bed thickness, 0.3 m was used as the standard thickness throughout the first three sensitivity analysis.

Soil has continuous temperature gradient in dependence on the depth in reality. Notwithstanding, boundary conditions for soil temperatures were simplified into five representative sections; bc1 to bc 5 as shown in Figure 4.12. Soil temperature was estimated every 1 m with Equation 3.9 and the average values were obtained for every 2 m.

4.3.2 Standard conditions

The sensitivity analysis was carried out based on the standard calculation conditions as listed in Table 4.4. Reynolds number was calculated using Equation 4.5 in Table 4.5 (Lienhard IV et al., 2006).

Table 4.4 Standard calculation conditions

Tool bar	Contents	Items	Setting	
Grid	Scale Grid	Scale Factors	0.1 for both x and y axis	
Define	Models/Energy	Energy Equation	On	
	Models/Viscous Model	Model	Laminar	
	Materials	Density	Constant	
	Operating Conditions	Gravity ¹⁾	Off	
	Boundary Conditions/Velocity Inlet	Velocity Specification Method	Components	
		Velocity for air		X=0 m/s
		Velocity for water ²⁾		X=-0.0035, Y=0 m/s
		Temperature ³⁾		279.3 K
	Boundary Conditions/Pressure Outlet	Temperature ³⁾		278.0 K
	Boundary Conditions/Heat exchanger	Wall Thickness		0 m
	Boundary Conditions/Tank	Wall Thickness		0.01 m
	Boundary Conditions/Tank lid	Material		Polyethylene
		Wall Thickness		0.05 m
	Boundary Conditions/Concrete bed surface	Material		Concrete
Wall Thickness			0 m	
Boundary Conditions/Outer area surface	Material		Grass	
	Wall Thickness		0.05 m	

1) Natural convection was not considered, since density does not affect in two-dimensional calculations in FLUENT.

2) In case of calculation with rainwater flow. Refer to Table 4.5 for the calculation procedure

3) Referred to the data for winter in Nottingham

Table 4.5 Calculation of Reynolds number

Case	at inlet	in tank	
Velocity ¹⁾	0.0035	0.0003	m/s
Diameter / distance ²⁾	0.0500	2.0000	m
Density		1,000	kg/m ³
Viscosity ³⁾		0.001791	kg/m/s
Reynolds number	98	326	-

1) A value for the tank was calculated from rainwater flow, 3.3 m³/h and a column tank of a 2 m diameter.

2) The outlet of the rainwater distributor was assumed to be 0.05 m

3) (Holman, 2002)

$$Re = \frac{\rho V \ell}{\mu} \quad \text{(Equation 4.5)}$$

<i>Re</i>	Reynolds number	-
ρ	Density	kg/m ³
<i>V</i>	Velocity	m/s
<i>ℓ</i>	Length	m
μ	Dynamic viscosity	kg/m/s

Reynolds numbers were less than 2,000 both near the rainwater inlet and the rest of space inside the tank; therefore, viscosity model was set for laminar flow.

Table 4.6 shows standard materials for each component of the simulation model and their thermal conductivity. The sensitivity analysis was held with the winter conditions in Nottingham (Table 4.7). The maximum heat

Table 4.6 Materials and their thermal conductivity

Thermal conductivity, W/m/K		
Component	Value	Comment
Air ¹⁾	0.024	
Soil ²⁾	1.700	Clay and fine sandy silt
Surrounding soil ²⁾	1.700	Soil in standard model
Concrete bed ³⁾	0.300	Concrete
Tank ⁴⁾	0.470	Polyethylene
Inside of tank ¹⁾	0.600	Water
Grass ⁵⁾	0.500	

1) Referred to FLUENT (2001)

2) Wet soil given by Holman (2002)

3) Lightweight concrete (Dermirbođa et al., 2003)

4) Average in a range between 0.42 and 0.51 (Al-Huthaili, 2004)

5) Referred to the minimum value for soil surface covered with grass (Lipiec et al., 2007)

Table 4.7 Climatic data in Nottingham

Item		Summer	Winter
Representative month		July	Dec
Average ambient temperature ¹⁾	°C	17.90	4.90
Average precipitation ¹⁾	mm/h/m ²	1.82	0.96
Average soil temperature ²⁾	1-2 m K	291.10	280.30
	3-4 m K	284.40	285.50
	5-6 m K	282.80	285.60
	7-8 m K	283.20	284.60
	9-10 m K	283.80	284.10

1) Refer to the monitored data between 2001 and 2005 in Nottingham

2) Refer to the calculation result introduced in Chapter 3.2.2

collection capacity was explored for each study case under a constant heat flux which was charged at the heat exchanger. Since thermal energy was absorbed in winter, the input heat flux is negative.

Calculation without rainwater inflow showed fairly little thermal transfer (Figure 4.14). The highest underground temperature was seen in the middle between the ground line and soil at greater depth, due to the stored solar energy as explained in section 2.1.4. The problem was that calculation with the stand-still water did not show a clear difference between the study cases. Water between the inner walls of the heat exchanger was stagnated and the temperature easily dropped below the minimum acceptable temperature for this test calculation, 276 K. Though this problem in modelling was solved in section 3.6.2, it was determined that simulation results were compared with the presence of rainwater flow for this stage. This indicated that results are affected by water circulation within the

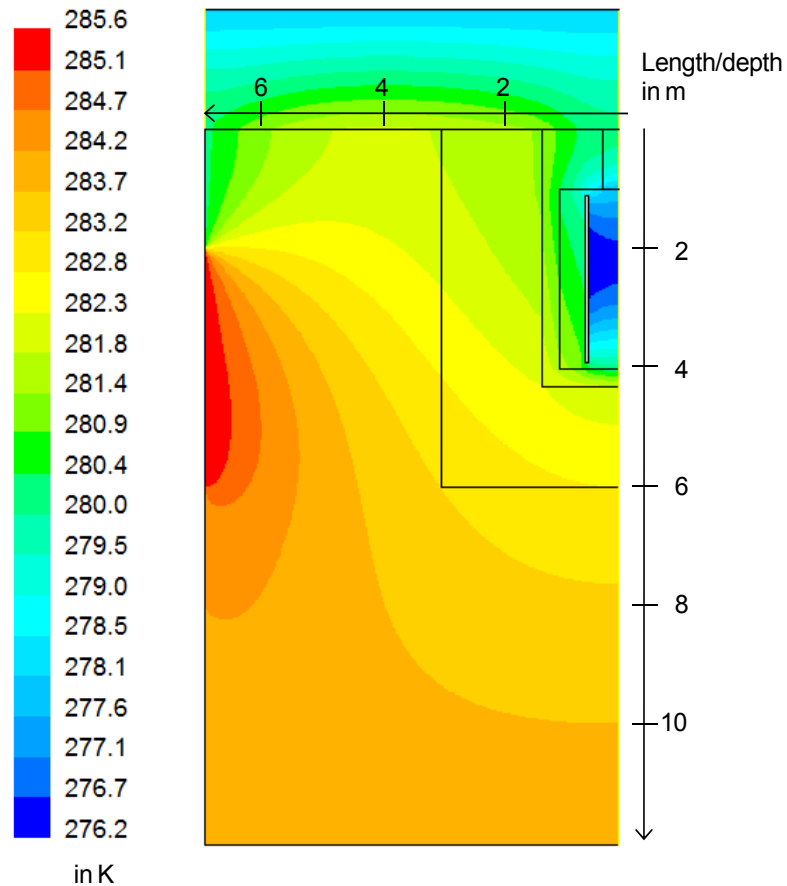


Figure 4.14 Simulation result without rainwater flow

tank as well as by conductive heat transfer.

Installing an additional motor to stir water in the tank will make the system less economic; hence, holding rainfall within downpipes and releasing it for a long time would be a more feasible strategy. The possible gadget is a controlled valve or a cleverly designed rainwater stopper in the vertical downpipe. When the gutters and the downpipes are installed in common size for roof of 105 m^2 (Angel Plastics, [no date]), 0.6 m^3 of rainwater can be held in the insulated office building. In case that the largest size is selected, the storage capacity will be 1.4 m^3 . Regarding the average rainfall and

frequency in December of Nottingham (Table 4.7 and section 1.3.1), the storable rainwater is equivalent to rainfall for 3 days and 7 days respectively. The gadget should be also designed to release the excessive amount of rainfall to avoid flooding. Thus, the operational efficiency of thermal energy transfer might be raised.

Each study case was calculated until two criteria were achieved; the calculation was converged and the thermal condition, such as the minimum water temperature, reached the set operational limit. Judging convergence was another vital point in simulation. The minimum water temperature was monitored every more than 1,000 iterations. When the temperature difference from the previous value became less than 0.005 °C, the calculation was judged to be stable enough to declare convergence and the simulation was terminated. 0.005 °C was equivalent to 0.066 % of the maximum temperature difference in the simulation model.

4.4 Variations for Sensitivity Analysis

There are six design parameters: tank shape, thermal conductivity of concrete bed and the surrounding soil, thickness of concrete bed and the surrounding soil and finally material of tank. A relation between the thermal output from the rainwater tank and the design parameters was acquired to discover the most desirable design specs.

4.4.1 Effects of tank shape

Tank shape is presumably one of the most important items, since this affects the efficiency of the underground heat collection and the economic

characteristics of the design. The longer the tank becomes, the closer the features would be to boreholes. However, boreholes have had economic disadvantages due to the restrictive construction costs. On the other hand, shallow tanks enable to collect energy only near the ground surface where soil temperature is normally close to ambient air. This smaller temperature contrast in between potentially reduces the system efficiency. Therefore, it is required to find out a tank shape, with which the cost performance is attractive.

Several cases were compared as shown in Table 4.8. Five different ratios between the width and height of rainwater tank were picked up on the bases of a column tank of 9.4 m³. The yellow line in Figure 4.12 was set to be symmetric. The minimum water temperature needed to be kept over 0 °C, in order to avoid that rainwater is frozen to block the piping. Hence, the heat collection capacity was determined when the minimum water temperature in the tank reached 3 °C.

Table 4.8 Cases with different ratio between width and height

Case	Width	Height	Surface area	Height of heat exchanger	Heat exchange area
	m	m	m ²	m	m ²
T-1	1.3	7.1	36.9	6.9	41.5
T-2	1.5	5.3	32.0	5.1	30.7
T-3	2.0	3.0	24.0	2.8	17.0
T-4	2.5	1.9	19.2	1.7	10.4
T-5	3.0	1.3	16.0	1.1	6.9

*) Diameter of heat exchanger was 1 m for all cases

4.4.2 Effects of thermal conductivity of concrete bed

The effect of enhanced thermal conductivity of concrete bed on the underground heat extraction was investigated. As introduced in section 2.1.4, thermal conductivity of grout has been enhanced by using effective chemical bonding. Three cases were compared as listed in Table 4.9.

The standard tank shape was selected in accordance to the results of the comparison in the previous case study. In order to highlight the effect of thermal conductivity of concrete bed, rainwater flow was not counted. In order to remove overpowering influence by the simplified shape of heat exchanger, small gaps between the heat exchange loops were reflected into the calculation model (Figure 4.15). Otherwise, the water between the inner surfaces of the heat exchange loops would soon lose thermal energy and reach the lowest temperature limit as seen in section 3.5.2.

Small distance between loops was selected, so as to prevent from a too optimistic model. Referring to the diameter of slinky coil, 0.019 m, gaps of a 0.02 m length were prepared every 0.18 m. In case of a tank with heat exchanger of a 5.1 m length for case T-2, the total heat exchange area per

Table 4.9 Study cases with different thermal conductivity of concrete bed

Case	Thermal conductivity W/K/m	Material
G-1	0.90	Cement (standard)
G-2	1.66	Middle of G-1 and G-3
G-3	2.42	Mix 111, refer to Chapter 2.1.4

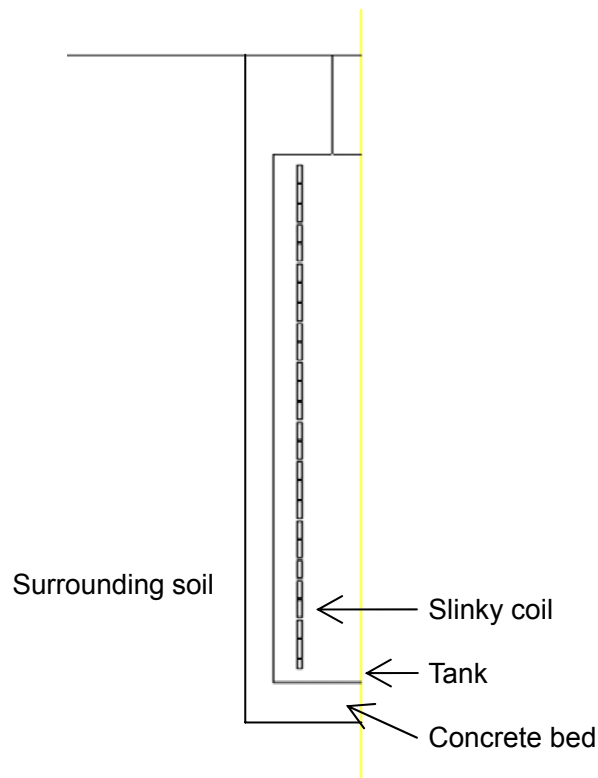


Figure 4.15 Model with gaps between heat exchange loops

calculation area, which is for a half tank, was approximately 11.8 m as shown in Table 4.10. In the real condition, the total area is a sum of outer coil area which touches the water directly. When 5 % of the outer surface area was assumed to be covered by the adjacent loops, the total heat exchange area could be 15.2 m² for a half tank. This was still 47 % larger than the value in the calculation model; therefore, the calculation condition was not necessarily too optimistic. All of the heat exchange area touching water may not be uniformly active; therefore, the details ought to be studied for the precise model construction as one of the future objectives. An effective design strategy could be achieved by creating gaps intentionally with simple spacers between the loops.

Results were compared in the maximum heat output, which was defined as

Table 4.10 Estimation of the total heat exchange length for a half tank

Item		Real	Model with gaps
Diameter of coil	m	0.019	0.050
Number of coils ¹⁾	-	268.0	
Touched coils ²⁾	m%	5.0	
Length for direct heat exchange ³⁾	m/a half tank	15.2	11.8
Ratio of advantage	%	47.0	

1) Length of heat exchanger was 5.1 m to leave space of 0.1 m from the tank walls

2) Points not for the direct heat transfer

3) Outer coil area touched water in the tank. The length was compared for the simulation area, which was for a half tank.

the capacity when the average temperature on the heat exchanger surface reached 0 °C. The tank was calculated as a column as illustrated in Figure 4.9. Therefore, the centre line was set as an axisymmetric boundary. These conditions were applied for the rest of sensitivity analysis.

4.4.3 Effects of thermal conductivity of the surrounding soil

The degree of influence by enhanced thermal conductivity in the surrounding soil was investigated. The possible first step of the construction is removing sub-soil to secure the space for the tank, concrete bed and the modified surrounding soil. Then, the excavated soil is modified on the ground and returned to fill the space between the concrete bed and sub-soil. As mentioned in section 2.4.2, mixing metals may cause negative environmental impacts. Therefore, the change of thermal conductivity in the surrounding soil was assumed to be brought by different soil status.

Thickness of the surrounding soil was determined to make the total distance

between the outer surfaces of the tank and sub-soil 2 m. Since the standard concrete bed thickness was set as 0.3 m, a 1.7 m thickness of the surrounding soil was assumed to be modified.

The maximum thermal conductivity that sub-soil can achieve was unknown. Therefore, the comparison was conducted up to the largest thermal conductivity which the calculation could be converged. The study cases were picked up as listed in Table 4.11.

4.4.4 Effects of thickness of concrete bed

The influences of size of the underground components were also studied. The first element was thickness of concrete bed. Thermal conductivity of concrete bed was fixed at the best value that can be obtained from the current market, 2.42 W/m/K.

Calculation with a smaller concrete thickness was studied, in order to

Table 4.11 Study cases with different thermal conductivity in the surrounding soil

Case	Thermal conductivity W/K/m	Material
M-1	1.70	Soil (standard)
M-2 ¹⁾	2.31	Clayey till water content 16.8 %
M-3	3.47	50% up from M-2
M-4	5.21	50% up from M-3
M-5	6.51	25% up from M-4

¹⁾ (Hevacomp, 2006)

compare the effects of the standard value, 0.3 m. Calculation for a required volume of concrete bed is dependent on material strength and manufacturing conditions; therefore, the information should be confirmed by the suppliers. Hence, a trend with concrete bed of 0.13 m thick was investigated against the same change of thermal conductivity of the surrounding soil as listed in Table 4.12.

The total thickness of concrete bed and the surrounding soil was remained the same as the original as mentioned in section 3.6.3, 2 m. Therefore, thickness of the surrounding soil was changed to 1.87 m. The referred tank after the first sensitivity analysis had a 1.5 m diameter and a 5.3 m length. This column tank required a 0.13 m thickness of concrete bed to satisfy the recommended value. For this project, the value was calculated with Equation 4.4. Results were discussed among the study cases, which were converged during the mesh investigation process.

4.4.5 Effects of thickness of the surrounding soil

The next element of changeable thickness was thickness of the surrounding

Table 4.12 Study cases with different thickness of concrete bed

Case	Thermal conductivity of the surrounding soil W/K/m	Material
TG-1	1.70	Soil (standard)
TG-2 ¹⁾	2.31	Clayey till water content 16.8 %
TG-3	3.47	50% up from M-2
TG-4	4.34	25% up from M-3

¹⁾ (Hevacomp, 2006)

soil. Thickness of concrete bed was chosen out of the previous sensitivity analysis between two different thicknesses. Thermal conductivity of concrete bed and the surrounding soil was set at 2.24 W/m/K and 3.47 W/m/K respectively. Here, thermal conductivity of the surrounding soil was selected not to be too idealistic. It can be easily imagined that thicker surrounding soil area would be more efficient, when the thermal conductivity is larger than that of sub-soil. Hence, the main objective of this sensitivity study was to obtain an effective range. The study cases are shown in Table 4.13.

4.4.6 Effects of thermal conductivity of tank

The final design element was thermal conductivity of tank. The same thickness of concrete bed, thermal conductivity of concrete bed and the surrounding soil were used. Practically effective thickness of the surrounding soil was chosen from the results in the previous sensitivity analysis. The set tank thickness, 0.01 m, was not particularly thick; however, the degree of effects was worthwhile to recognise. The study cases are shown in Table 4.14.

Table 4.13 Study cases with different thickness of the surrounding soil

Case	Thickness of surrounding soil m	Comment
TS-1	0.70	
TS-2	1.20	
TS-3	1.70	The original value (standard)
TS-4	2.20	
TS-5	2.50	

Table 4.14 Study cases with different thermal conductivity of tank

Case	Thermal conductivity of tank W/m/K	Comment
TT-1	0.47	Polyethylene (standard)
TT-2	2.42	Conductive grout (Mix 111) ¹⁾
TT-3	15.00	Stainless steel

1) Concrete bed was remained

4.5 Simulation Results

Results for each sensitivity analysis and the discussion are presented below.

4.5.1 Comparison in different tank shape

One of the calculation results in FLUENT, case T-2, is displayed in Figure 4.16. The result is shown as a mirror image at the symmetric border line in the centre of the tank. The temperature contour indicates a reasonable temperature gradient around the tank.

The results were compared among five cases in Table 4.15 and Figure 4.17. It is clear that smaller ratio between width and height encouraged larger heat transfer. Especially, the improvement ratio indicated that longer tanks with more than a 3 m depth increased the total heat collection more effectively.

The advantages of longer tanks must be the larger heat exchanger surface area as calculated in Table 3.21 as well as the larger tank surface area. In addition, the stable underground heat source under 7 m was also accessible for the relatively long tanks. On the whole, this condition enlarged the ability of underground heat collection.

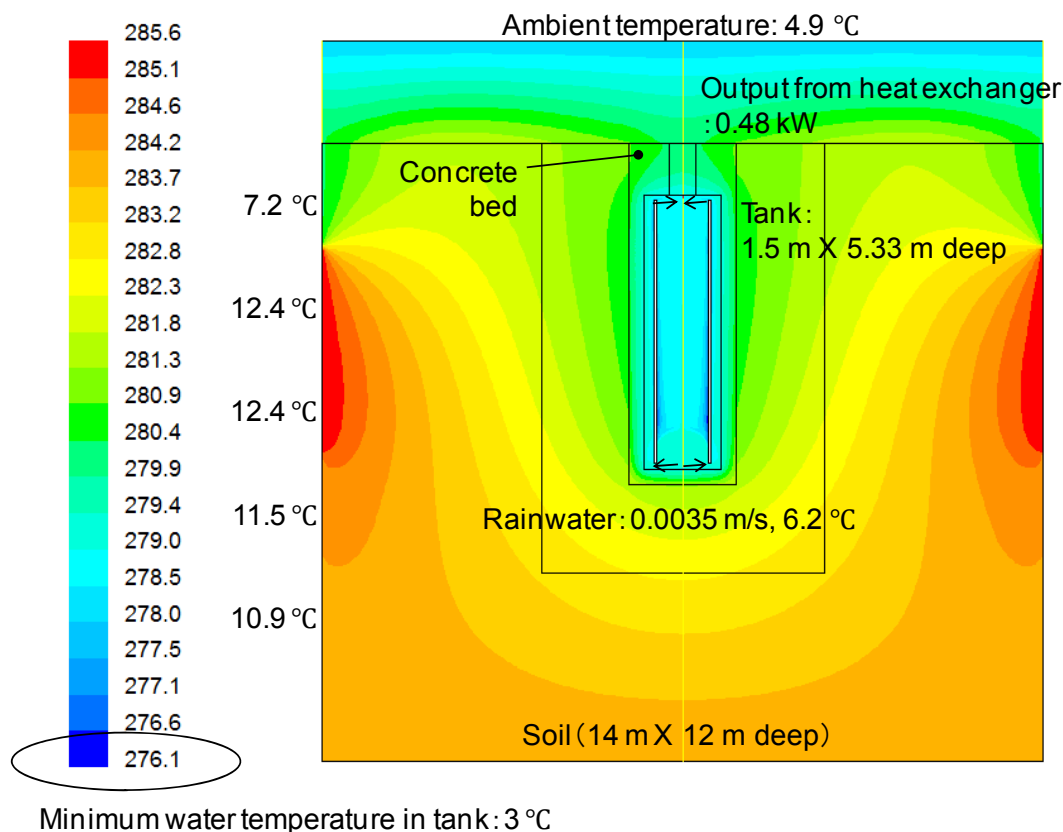


Figure 4.16 Calculation results in FLUENT for case T-2

Table 4.15 Simulation results among case T-1 to T-5

Case		T-1	T-2	T-3	T-4	T-5
Width	m	1.3	1.5	2.0	2.5	3.0
Height	m	7.1	5.3	3.0	1.9	1.3
Required excavation ¹⁾	m	8.4	6.6	4.3	3.2	2.6
Ratio between width and height	-	0.2	0.3	0.7	1.3	2.3
Heat flux ²⁾	W/m ²	-15.0	-15.5	-18.0	-16.0	-27.5
Heat transfer rate ³⁾	kW	0.62	0.48	0.31	0.17	0.19
Improvement ratio ⁴⁾	kW/m	0.08	0.07	0.13	-0.04	

1) Additional 1.3 m (tank neck of 1 m and concrete bed of 0.3 m under the base) was also required

2) The maximum heat extract, in which the minimum water temperature reached 3 °C

3) Heat transfer rate was multiplied by the surface area of heat exchanger

4) Improvement of total flux per increase of height

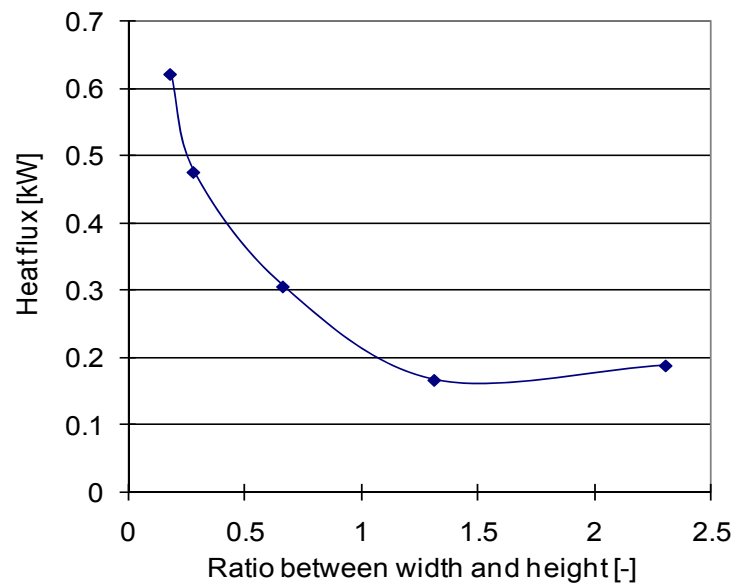


Figure 4.17 Heat flux and ratio between width and height

Another reason of larger heat flux with the longer tanks seemed to be a characteristic of the internal flow. Figure 4.18 displays the directions and the relative velocity of water stream with vectors at different locations. The design of case T-5 encouraged larger eddies, which may accelerate more powerful convection heat transfer at most of the internal tank space. In fact, the average velocity within the tank in case T-5 was 0.000636 m/s, which was 25.7 % larger than that in case T-2. However, the temperature contour indicates that the created active heat transfer near the ground surface allowed the low ambient temperature to influence the underground heat transfer (Figure 4.19). Hence, it can be graphically understood that a case with a longer tank had the most active heat transfer area farther from the ground level and decreased the influence by ambient temperature.

The unique development of the internal streams in each tank shape seemed

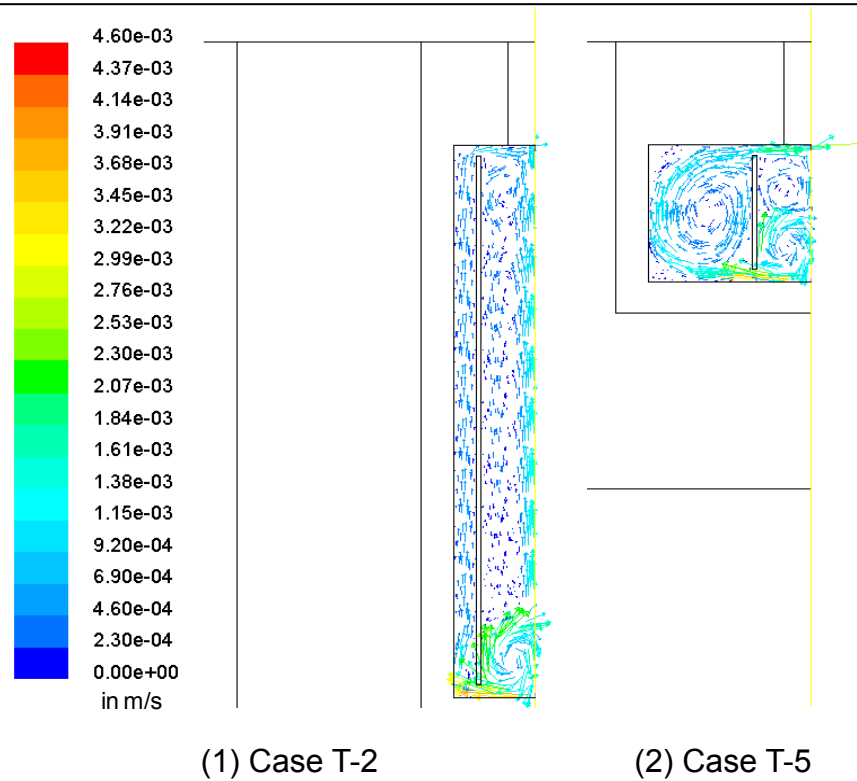


Figure 4.18 Eddies within tanks

to be a reason why heat flux in case T-4 was less than that in case T-3. The distribution of eddies created larger dead space in case T-4. This indicated that the prediction of the internal streams in dependence on a balance between the internal design of tank and design rainwater inflow also required attention.

One of the objectives in this project is to find out economically practical design criteria. Therefore, the optimised tank shape needs to be both efficient and economically feasible. Longer tanks are more likely to increase the initial costs due to the more unique shape and due to deeper excavation of sub-soil. With reference to published excavation cost per depth, unit price below 5 m is double of that above 5 m (Langdon, 2006). As a consequence, one of the most efficient cases with less impact of

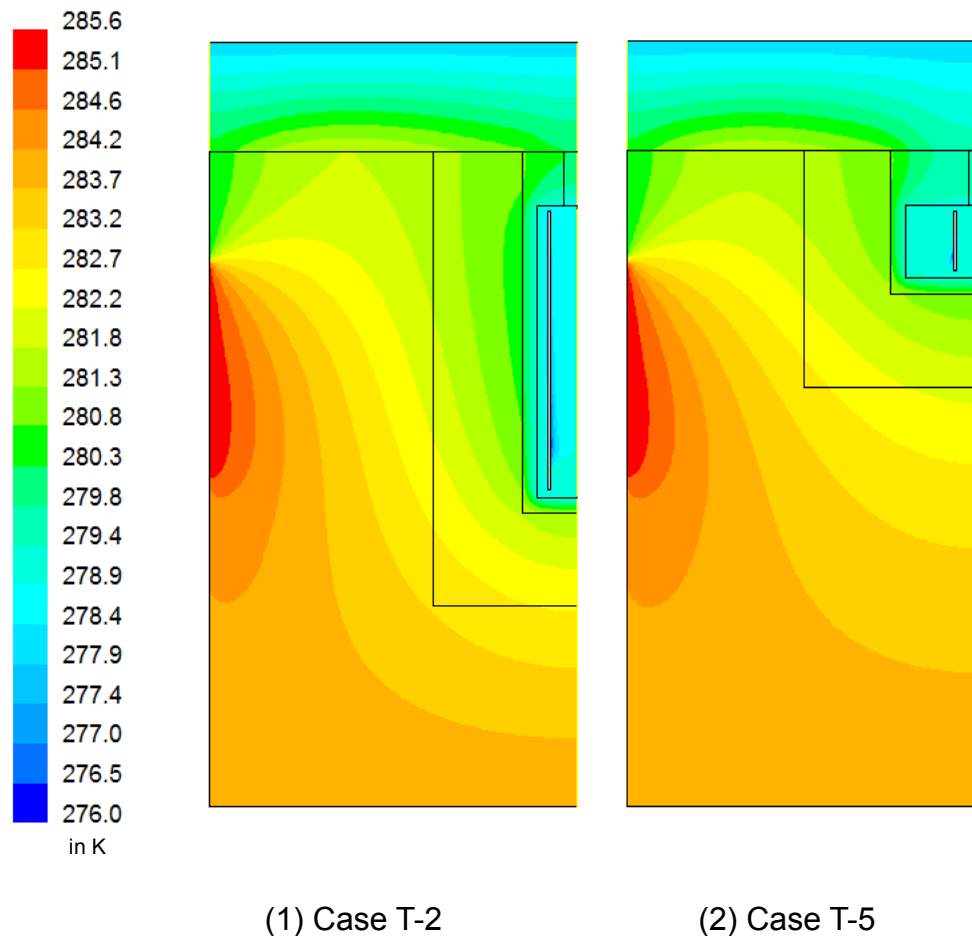


Figure 4.19 Comparison in temperature contour

excavation cost for below 5 m, case T-2, was chosen as the standard model for the rest of sensitivity analysis.

4.5.2 Comparison in different thermal conductivity of concrete bed

The obtained heat output for each case is displayed in Table 4.16 and Figure 4.20. Higher thermal conductivity of concrete bed had a potential to enhance the efficiency of underground heat transfer. From a comparison between case G-1 and G-3, 2.7 times larger thermal conductivity might increase the heat collection up to 12 %.

Table 4.16 Simulation results among case G-1 to G-3

Case		G-1	G-2	G-3
Thermal conductivity of concrete bed	W/m/K	0.9	1.66	2.42
Heat flux ¹⁾	W/m ²	-4.1	-4.50	-4.60
Heat transfer rate ²⁾	kW	0.29	0.32	0.32
Improvement ratio ³⁾	kW/(W/m/K)		0.04	0.01

1) The maximum heat extract, in which the average temperature on the heat exchanger surface reached 0 °C

2) Heat transfer rate was multiplied by the surface area of heat exchanger

3) Improvement of total flux per increase in thermal conductivity of concrete bed

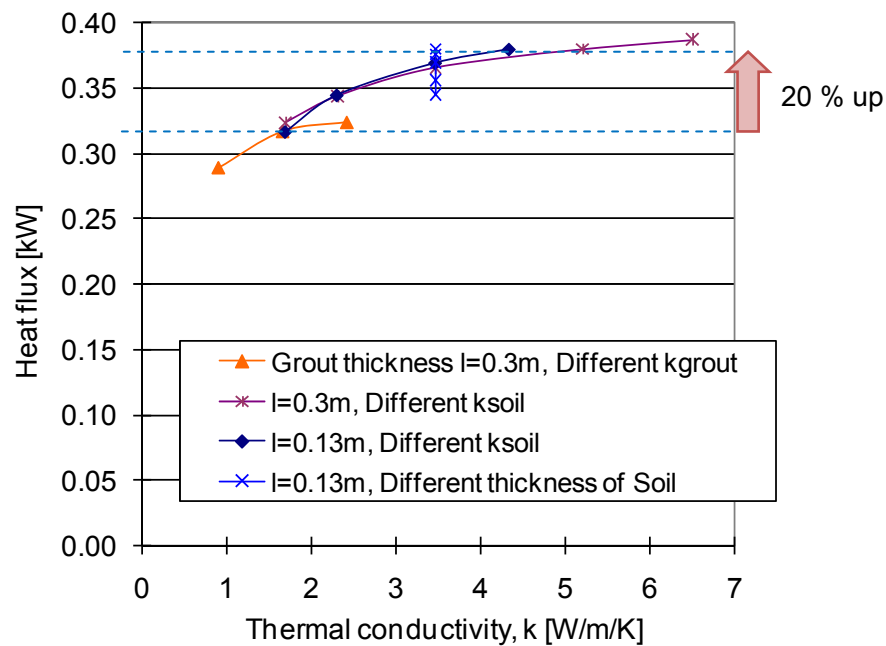


Figure 4.20 Results of sensitivity analysis

When a better condition was found through each sensitivity analysis, the modified condition was used for the following analysis. Improvement ratio from case G-1 to case G-2 was larger than that from case G-2 to case G-3. Since the commercial use of Mix 111 becomes cost effective in the GSHP (U. S. Department of Energy, 1999), the largest grout thermal conductivity, 2.42

W/m/K in case G-3, was used after the next sensitivity analysis.

4.5.3 Comparison in different thermal conductivity of the surrounding soil

The results are shown in Table 4.17 and Figure 4.20. The collected amount rose up, as the surrounding soil became more conductive. The calculation model became incapable of achieving convergence after thermal conductivity of the surrounding soil went higher than a certain value. This phenomenon was explained in section 3.3. Therefore, the study cases were compared within the valid thermal conductivity, 1.70 to 6.51 W/m/K. While thermal conductivity of the surrounding soil became 3.82 times larger from case M-1 to case M-5, the thermal energy output increased by approximately 20 %. This parameter was as powerful as thermal conductivity of concrete bed.

4.5.4 Comparison in different thickness of concrete bed

A change of heat output with 0.13 m thick concrete bed was investigated (Table 4.18). The calculation was stable as far as thermal conductivity of

Table 4.17 Simulation results among case M-1 to M-5

Case ¹⁾		M-1	M-2	M-3	M-4	M-5
Thermal conductivity of surrounding soil	W/m/K	1.70	2.31	3.47	5.21	6.51
Heat flux ²⁾	W/m ²	-4.60	-4.89	-5.20	-5.40	-5.50
Heat transfer rate ³⁾	kW	0.32	0.34	0.37	0.38	0.39
Improvement ratio ⁴⁾	kW/(W/m/K)		0.03	0.02	0.01	0.01

1) Case M-1 was the same as case G-3

2) The maximum heat extract, in which the average temperature on the heat exchanger surface reached 0 °C

3) Heat transfer rate was multiplied by the surface area of heat exchanger

4) Improvement of total flux per increase in thermal conductivity of surrounding soil

Table 4.18 Simulation results among case TG-1 to TG-4

Case		TG-1	TG-2	TG-3	TG-4
Thermal conductivity of surrounding soil	W/m/K	1.70	2.31	3.47	4.34
Heat flux ¹⁾	W/m ²	-4.50	-4.90	-5.25	-5.40
Heat transfer rate ²⁾	kW	0.32	0.34	0.37	0.38
Improvement ratio ³⁾	kW/(W/m/K)		0.05	0.02	0.01

1) The maximum heat extract, in which the average temperature on the heat exchanger surface reached 0 °C

2) Heat transfer rate was multiplied by the surface area of heat exchanger

3) Improvement of total flux per increase in thermal conductivity of surrounding soil

the surrounding soil was less than 4.34 W/m/K. In comparison to the results for a 0.3 m thickness, the thermal output was larger after around 2.4 W/m/K of thermal conductivity in the surrounding soil as displayed in Figure 4.21. This was because thicker concrete bed contributed to raise the total thermal conductivity when the thermal conductivity was larger than that of the surrounding soil. However, when the surrounding soil was more conductive, designers ought to make sure thickness of concrete bed is the minimum.

The desirable concrete thickness for the column tank, 0.13 m, was used for the rest of the analysis. Furthermore, improvement ratio dropped notably and seemed gradually saturated after case TG-3; therefore, 3.47 W/m/K for case TG-3 was selected to be used as well.

4.5.5 Comparison in different thickness of modified soil

The results suggested that larger space for modified soil increased the thermal output, when the thermal conductivity was larger than sub-soil

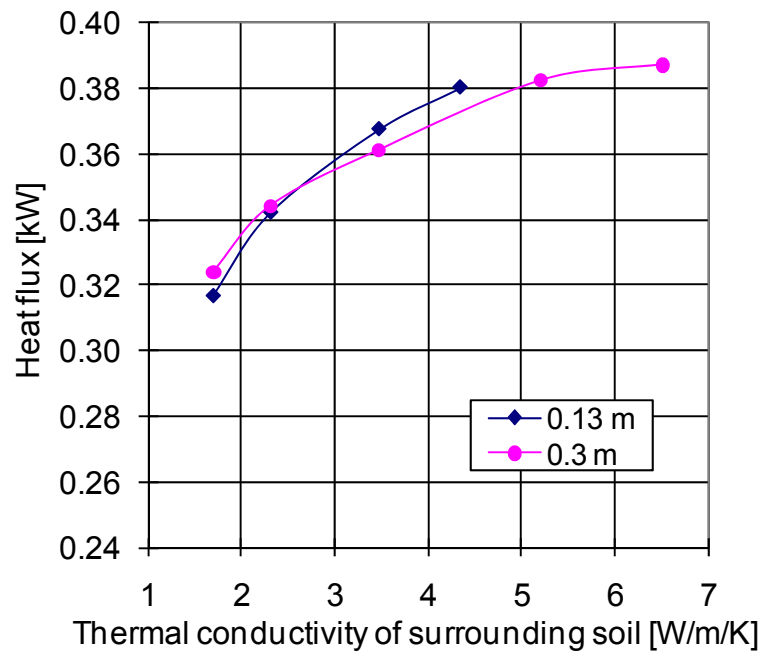


Figure 4.21 Comparison in different thickness of concrete bed

thermal conductivity; 3.27 W/m/K and 1.7 W/m/K respectively in this calculation (Table 4.19, Figure 4.20). According to the comparison between case TS-1 and TS-5, approximately 3.6 times thicker surrounding soil would improve the heat extraction capacity up to 10 %.

Larger modified space requires more construction, such as digging a larger hole and treating larger volume of soil. Hence, the size ought to be selected for the best cost performance. Improvement ratio dropped after case TS-4; therefore, 2.2 m for case TS-4 was chosen for the last analysis.

4.5.6 Comparison in different thermal conductivity of tank

The results are shown in Table 4.20 and Figure 4.22. No improvement of heat collection capacity was seen even if thermal conductivity of tank rose. Thermal conductivity of tank needed to be 32 times as large as the original

Table 4.19 Simulation results among case TS-1 to TS-5

Case ¹⁾		TS-1	TS-2	TS-3	TS-4	TS-5
Thickness of modified soil m		0.70	1.20	1.70	2.20	2.50
Heat flux ²⁾	W/m ²	-4.90	-5.06	-5.25	-5.34	-5.40
Heat transfer rate ³⁾	kW	0.34	0.36	0.37	0.38	0.38
Ratio of improvement ⁴⁾	kW/m		0.03	0.03	0.01	0.01

1) Case TS-3 was the same as case TG-3

2) The maximum heat extract, in which the average temperature on the heat exchanger surface reached 0 °C

3) Heat transfer rate was multiplied by the surface area of heat exchanger

4) Improvement of total flux per increase in thickness of modified soil

Table 4.20 Simulation results among case TT-1 to TT-5

Case ¹⁾		TT-1	TT-2	TT-3
Thermal conductivity of tank	W/m/K	0.47	2.42	15.0
Heat flux ²⁾	W/m ²	-5.34	-5.42	-5.40
Heat transfer rate ³⁾	kW	0.38	0.38	0.38
Improvement ratio ⁴⁾	kW/(W/m/K)		0.00	0.00

1) Case TT-1 was the same as case TS-4

2) The maximum heat extract, in which the average temperature on the heat exchanger surface reached 0 °C

3) Heat transfer rate was multiplied by the surface area of heat exchanger

4) Improvement of total flux per increase of tank thermal conductivity

to gain 1 % larger heat extract.

4.5.7 Summary of design analysis

The parametric analysis was useful to extract powerful design elements.

The parameters can be categorised into three groups; tank shape, thickness of components and thermal conductivity of components. The most influential parameter was tank shape and longer tanks could collect larger thermal energy. This was partially because shorter tanks encouraged

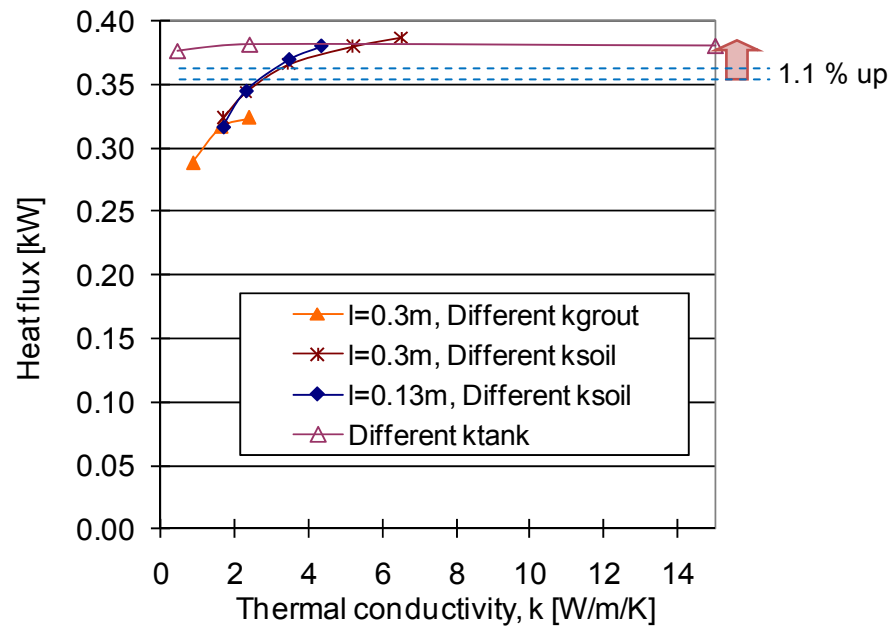


Figure 4.22 Comparison in different thermal conductivity of tank

convection heat transfer near the ground line, which enlarged the influence of low ambient temperature.

The other design category was thickness of the underground components. It was confirmed that thinner concrete bed created more heat transfer, when the thermal conductivity was smaller than that of the surrounding soil. In addition, more modified soil space was advantageous. While the concrete thickness needed to be met the minimum requirement for the sake of reinforcement, thickness of the modified soil space was advised to be expanded as much as the construction financially made sense.

Another powerful design category was thermal conductivity of the underground components. Higher thermal conductivity in general improved the efficiency of thermal energy collection from underground. Especially,

higher thermal conductivity of concrete bed and the surrounding soil created a significant difference. 20 % more heat output was seen by modifying the surrounding soil to be 2.55 times more conductive with the most conductive commercialised concrete. Nevertheless, the upper limit of the parametric study was determined only by stable calculation conditions, while a range for the other components was selected on the basis of the existing materials. Therefore, the next objective was to define the detailed method to realise high soil thermal conductivity. For this reason, an experimental study for enhancing soil thermal conductivity is presented in the next chapter.

4.6 Conclusions

An effective method to mesh in FLUENT was explored with a simple calculation model. The investigation suggested that a combination between non-uniform boundary layers and uniform mesh in the rest of model could realise convergence stably. Though setting smaller mesh size theoretically increases accuracy, it needed to be aware that small mesh size could lure the errors of computational calculation. In the studied models, calculation with high thermal conductivity seemed to expand the possibility of the potential errors. As a consequent, mesh investigation was advised to be conducted for discovering the most accurate and stable calculation conditions.

A degree of the difference between the calculations of heat transfer with FLUENT and with a theoretical formula was investigated. A simple conductive heat transfer model was built in FLUENT to compare the result derived from Fourier's law. With regard to the required heat flux over the layers of materials, the uncertainty was understood to be ± 8.8 %.

The effects of six kinds of design parameters on underground heat collection were studied through series of sensitivity analysis in FLUENT. The underground structure contained a rainwater collection tank. The results revealed that tanks with a larger ratio of the depth against the width would provide more capacity. The expected effects of combining a rainwater collection tank to the system are discussed in section 7.1.2. Furthermore, higher thermal conductivity in concrete bed and soil surrounding the tank showed significant impact. Since achievable soil thermal conductivity was unknown, an experimental investigation was required to define a realistic effect of the soil modification. Therefore, the next chapter intends to seek practical methods to enhance the conductivity as much as possible.

Chapter 5 Optimisation of Soil Thermal Properties for the GSHP

Introduction

Sensitivity analysis presented in Chapter 4 indicated the positive effects of high thermal conductivity in the surrounding soil space. Nevertheless, concrete methods to obtain high soil thermal conductivity are required for practical designs. As warned in section 2.4.2, there are fairly limited environmentally friendly substances to blend with sub-soil for creating high thermal conductivity. Consequently, mechanical options using locally available substances are targeted.

Experimental analysis is chosen as a realistic approach. To begin with, a procedure to set a test rig with dual-probe heat-pulse method (DPHP) is displayed. The sensors are calibrated in two kinds of parameters, heater resistance and of distance between the probes. The results are expressed as an overall uncertainty of the measurement including the use of a theoretical model and spreadsheet calculation with a solver function.

Soil is sampled to examine the characteristics; particle size distribution in wet sieving method, optimum moisture content (OMC) and thermal properties. Then, soil thermal conductivity is measured with the DPHP and the HFM with various kinds of water content to verify the features. As de Vries's theory indicates in section 2.5.5, the effects of degree of saturation on thermal conductivity are investigated as the first clue. The results from the chosen

Chapter 5 Optimisation of Soil Thermal Properties for the GSHP

measuring method and one of the theoretical solutions, Campbell's model, are discussed.

Two soil samples, the original soil and a sample with more large particles, are examined in pore size distribution and soil thermal conductivity. This is to comprehend the advantages of the latter sample.

A method to reproduce natural soil in lab is sought to evaluate the advancement of the modified soil. Then, three more parameters, compaction, packing ratio and water content gained from suction, are investigated the effect on soil thermal conductivity. In the end, feasible modification methods are proposed by comparing some design options with natural soil. The result is led with heat transfer efficiency, which expresses a balance between underground storage and heat transfer.

5.1 Methodology

Two kinds of methods to measure soil thermal properties were introduced and compared in section 2.5. This section describes the details of a test rig with the DPHP as well as a process and results of the calibration. Overall uncertainty of the DPHP analysis is eventually evaluated as an outcome of calibration consisting of two steps.

5.1.1 Setup of the DPHP

The test rig was assembled with a set of specific heat sensors (Model Sh2, East 30 Sensors, Pullman, WA), a heater controller (Model HC1, East 30

Chapter 5 Optimisation of Soil Thermal Properties for the GSHP

Sensors, Pullman, WA), a datalogger (CR1000, Campbell Scientific Ltd., Loughborough, UK), a sample box and a data collection computer (Figure 2.19). The probes measured 30 mm long and 0.9 mm of diameter with a 6 mm distance in between as illustrated in Figure 2.20. For this size of sensor, samples were required to be sieved to limit the largest particles under 2 mm for the sake of accuracy. Soil samples were packed into the test box up to the top and the sensors were buried in the centre of the box. Thus, enough distance between the measuring points and the walls of the box was secured to prevent thermal interference from the outside of the box as much as possible. With reference to other studies, the minimum distance seems to be set between 0.043 m and 0.1 m (Nidal et al., 2000 and Noborio et al., 2002). Therefore, the size of two boxes were determined, such as 0.25 m x 0.15 m x 0.15 m high and 0.15 m x 0.15 m x 0.15 m high respectively as illustrated in Figure 5.1. The bigger box was designed to operate with two sets of sensors, while the smaller one for one set. The interior walls were varnished to be water-proof; however, samples were set into a plastic bag both for easy removal after measurements and for doubly making sure that the moisture inside of the samples were enclosed.

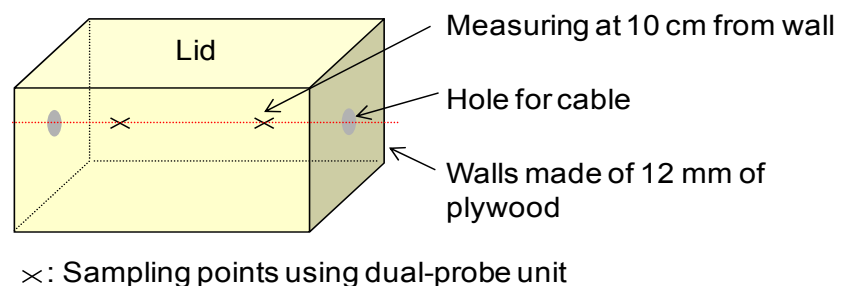


Figure 5.1 Image of a sample box

Chapter 5 Optimisation of Soil Thermal Properties for the GSHP

The sensors were connected to the datalogger. All the measuring process was controlled by a programme installed in the datalogger. Programme was written in the original computer language, CRBasic, which was created based on Basic. The original programme provided by the supplier was revised up for the measurement (Appendix B). The wire heater was electrically charged for 8 seconds, and then the energy input and temperature at the thermocouple were recorded every second for 90 seconds. The partial data adoption method with 67 % of data, for 60 seconds, was applied to calculate thermal properties as discussed in section 2.5.3. A sample of the obtained dynamic data can be referred in Figure 2.21.

5.1.2 The DPHP calibration with agar

Two types of calibration were conducted; calibration of heater resistance and distance between the probes. The first method followed a theoretical equation, which shows a relation between heater resistance, R_h , heat input and reference resistance, R_r (East 30 Sensors, 2007).

$$q = t \cdot \frac{E_r^2}{R_r^2} \cdot \frac{R_h}{L} \quad (\text{Equation 5.1})$$

q	Energy to heat probe per heater length	J/m
t	Time	sec
E_r	Voltage	V
R	Resistance	Ω
L	Heat unit length	m

Chapter 5 Optimisation of Soil Thermal Properties for the GSHP

Two units of sensors were calibrated by the manufacturer using a programme (Appendix C). The results provided both reference resistance and heater resistance as listed in Table D.1. Thus, the heat input could be calculated more accurately by using the derived calibration constants.

The accuracy of measuring soil thermal properties was also refined by the other calibration method. The used equation was derived from Equation 2.2 after the differentiation with respect to time (Kluitenberg, [no date]).

This led to the relation where the maximum temperature rise, ΔT_m , is seen when t is equal to $\frac{r^2}{4\alpha}$.

$$\rho c = \frac{q}{e\pi r^2 \Delta T_m} \quad \text{(Equation 5.2)}$$

ρc	Volumetric heat capacity	J/m ³ /°C
r	Radial distance from the line source	m
ΔT	Change in temperature	°C

Heat pulse was sent to detect the dynamic change of temperature in samples. As a result of the calibration, distance between the probes was adjusted. Water was used as a calibration sample and the published heat capacity of water, 4,17 kJ/m³/K at 25 °C, was referred (Holman, 2002). Though water is one of the most reliable standard substances, even small thermal interference can generate convection heat transfer around the heater. This condition is likely to lower the accuracy of measurement of thermal conductivity. Hence, making jelly with agar is usually used to

Chapter 5 Optimisation of Soil Thermal Properties for the GSHP

immobilise currents within the sample. Agar is a gelatinous substance derived from red algae. Ochsner et al. (2003) report that 6 g of agar per one litre of water stabilises calibrated probe distance regardless of different maximum temperature rise, compared to the results by Campbell with 2 g/litre. Hence, two sensors were buried into a litre of water jellied by 6 g of agar and the same test was repeated 13 times for each sensor.

A photo of the calibration is presented in Figure 5.2 and the results are displayed in Table 5.1 and Figure 5.3. The obtained distance was around 6 mm as it was manufactured; however, the data was not stable against the maximum temperature rise. The test sample seemed not to be visually fluidised anymore. However, there might have been free water which was thermally charged to create convection in the micro space as Ochsner et al. (2003) reason. Representative distance was determined by calculating the



Figure 5.2 Calibration with agar

Chapter 5 Optimisation of Soil Thermal Properties for the GSHP

Table 5.1 Results of calibration of thermal characteristics

Sensor	Item	Number	1	2	3	4	5	6	7	
2209	Power to probe	q	J/m	828.6	828.6	828.6	828.5	828.5	828.5	828.6
	Maximum temperature rise	ΔT_m	°C	0.527	0.631	0.576	0.574	0.568	0.596	0.563
	Distance between needles	r	m	0.0066	0.0061	0.0064	0.0064	0.0064	0.0062	0.0064
2210	Power to probe	q	J/m	830.0	830.0	830.0	830.0	830.0	830.0	830.0
	Maximum temperature rise	ΔT_m	°C	0.601	0.585	0.598	0.623	0.601	0.524	0.618
	Distance between needles	r	m	0.0062	0.0063	0.0062	0.0061	0.0062	0.0067	0.0061
Sensor	Item	Number	8	9	10	11	12	13	Average	
2209	Power to probe	q	J/m	828.5	828.5	828.6	828.6	828.5	828.3	
	Maximum temperature rise	ΔT_m	°C	0.518	0.535	0.543	0.586	0.534	0.586	
	Distance between needles	r	m	0.0067	0.0066	0.0065	0.0063	0.0066	0.0063	
2210	Power to probe	q	J/m	830.0	830.0	830.0	830.0	830.0	830.0	
	Maximum temperature rise	ΔT_m	°C	0.585	0.618	0.557	0.605	0.790	0.650	
	Distance between needles	r	m	0.0063	0.0061	0.0065	0.0062	0.0054	0.0060	

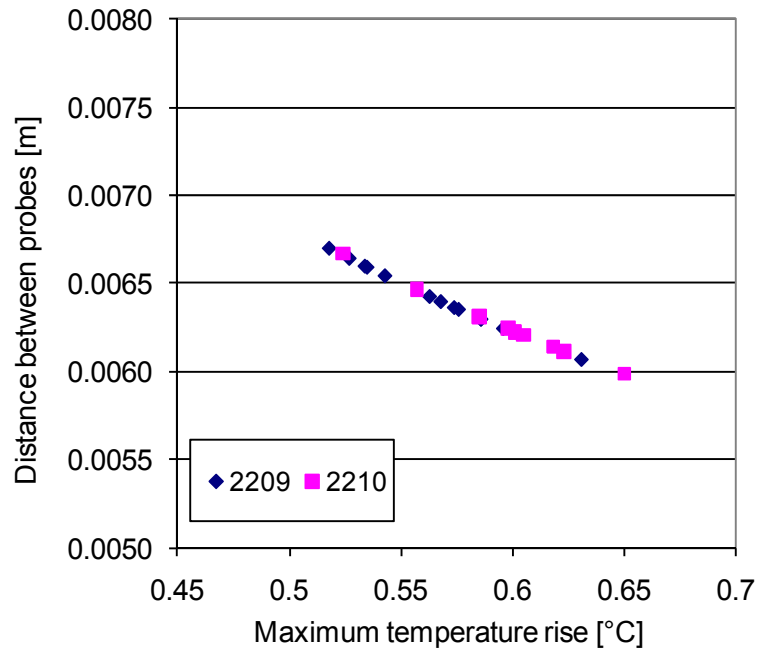


Figure 5.3 Derived distance between probes in calibration

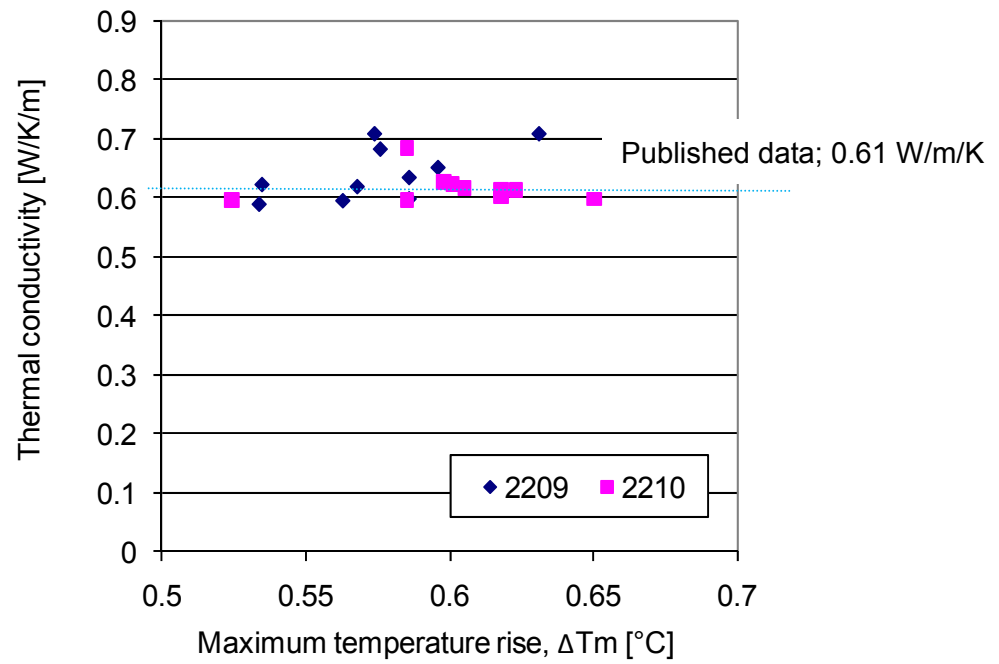
Chapter 5 Optimisation of Soil Thermal Properties for the GSHP

average among 13 test results; 0.00641 m for sensor 2209 and 0.00619 m for sensor 2210 respectively.

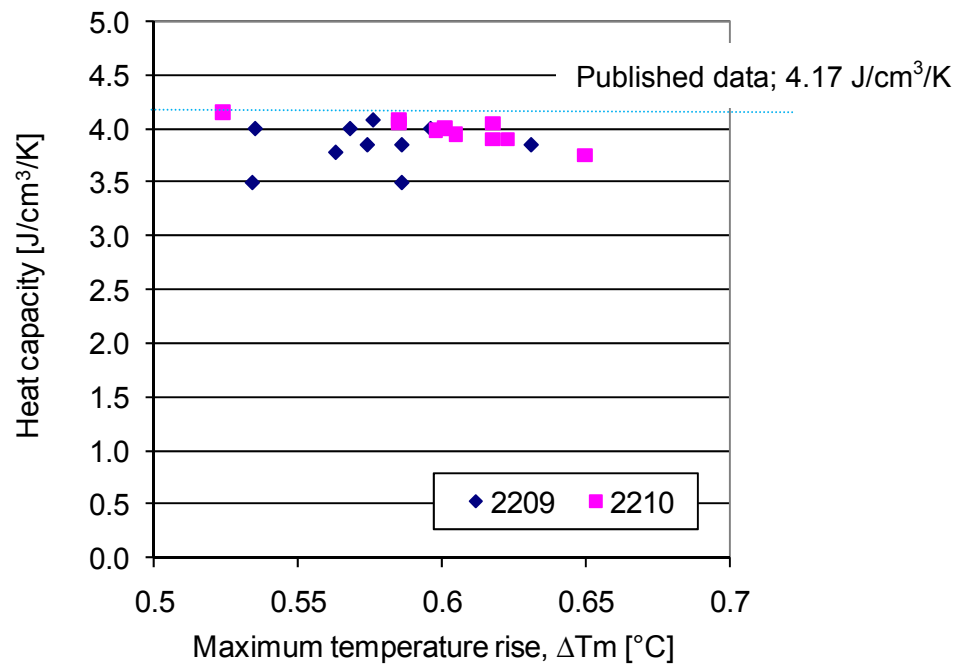
The thermal properties of water solidified with agar were inspected with the calibrated distances. 10 out of 13 sets of the measured results had sufficiently smooth series of dynamic data to analyse with solver (Figure 5.4). Published data of thermal conductivity and heat capacity are 0.61 W/m/K and 4,17 kJ/m³/K at 25 °C respectively (Holman, 2002). The differences of the recalculated thermal conductivities and heat capacity from the published data were respectively within $\pm 8.0\%$ and $\pm 8.0\%$ for sensor 2209 and $\pm 6.0\%$ and $\pm 5.0\%$ for sensor 2210. Though there must be a difficulty to obtain uniformed results with series of dynamic data, it could be said that the calibration tuned reasonably.

5.1.3 Error analysis

Uncertainty of the DPHP has been investigated. Kluitenberg et al. (1993) provide three error sources derived from the differences in conditions between experiments and the instantaneously heated infinite line source theory. The experiments use finite length line heater and the limited duration of heating process, while the theory is based on an infinite length cylindrical heater and instantaneous pulse heating. The investigation concludes that the overall error is within 1 % in comparison to other models. Kluitenberg et al. (1995) also finds that the error values caused by the first item and the second item are less than 2 % and less than 0.6 % respectively. On the other hand, Mori et al. (2003) mention that accuracy in manufacturing



1) Thermal conductivity



2) Heat capacity

Figure 5.4 Thermal properties of water after calibration

Chapter 5 Optimisation of Soil Thermal Properties for the GSHP

the sensors and the wire heater are equally essential for assumptions in the theory. Kluitenberg et al. (1995) find that the error caused by probe distance does not affect thermal conductivity. However, it is discovered that the measurement error of the maximum temperature rise, ΔT_m , has an impact on the experimental results.

Experimental uncertainty was calculated based on the British Standard (2004). Since the data analysis procedure included the use of Excel spreadsheet with solver, the investigation was conducted with the calibration data rather than calculating combined standard uncertainty from the applied formulas. Therefore, the statistical estimation, Type A evaluation, was conducted. The results are presented in Table 5.2. Bilskie et al. (1998) and Scheerlinck et al. (2008) report standard deviation of 5.9 % for glycerol

Table 5.2 Results of error analysis

Sensor			2209	2210
Average distance between two needles	d	mm	6.410	6.188
Average thermal conductivity of water ¹⁾	k_{ave}	W/m/K	0.641	0.617
Estimated standard deviation	s_k	W/m/K	0.044	0.026
Relative deviation	RD	%	6.930	4.180
Standard uncertainty of a mean ²⁾	$U_{(kmean)}$	%	2.200	1.300
Expanded uncertainty of a sample mean ³⁾	$U_{(kmean)}$	W/m/K	0.100	0.018
Relative expanded uncertainty	$U^*_{(kmean)}$	%	5.000	3.000

1) Data was analysed using obtained in calibration

2) Measuring conditions remained the same

3) Calculated with confidence of 95% (two standard deviations)

Chapter 5 Optimisation of Soil Thermal Properties for the GSHP

samples and 4.12 % for fruit samples respectively. These results are in the same range as the calculation results; 4.2 % for sensor 2209 and 6.9 % for sensor 2210. Furthermore, relative expanded uncertainty of a sample mean ($k = 2.26$, 95 % of confidence) was 5.0 % for sensor 2209 and 3.0 % for sensor 2210.

The accuracy of the HFM is provided by the International Organization for Standardization (1991); ± 3 %. Though it is not described clearly if this value is three deviations, it is possible that measurement at steady state makes reasonable accuracy.

5.2 Preparation of Experiments

Samples were collected and sieved to be less than either 2 mm (2 mm soil) or 14 mm (14 mm soil) to investigate the soil properties. This section describes methodologies of two fundamental measurements, particle size distribution in wet sieving method and optimum moisture content (OMC). Afterwards, sample preparation with various kinds of water content is explained to investigate the differences between the HFM and the DPHP.

5.2.1 Conditions of experiments

Soil sample was collected from the construction site at the School of the Built Environment, the University of Nottingham, 52°56'N 01°11'W. According to the Crown Copyright Geological Survey map, the soil surface consists of Bunter pebble beds and mottled sandstone (Edwards, 1966). In the geological map published by the British Geological Survey (1996), the soil is

Chapter 5 Optimisation of Soil Thermal Properties for the GSHP

categorised as Nottingham castle sandstone formation, which is a combination of sandstone, yellowish grey and pebbly. This feature was confirmed by classification tests.

The sample was oven-dried for more than 24 hours at 100 °C and sieved to control the maximum particle size.

5.2.2 Fundamental characteristics

Classification of the original soil was surveyed following the British Standard (1990). The tested categories were particle size distribution in wet sieving method and optimum moisture content, OMC. Soil characteristics are predictable from its particle distribution. Even though the mineralogy is similar among particles, soil samples with different size distribution create different behaviours. Moreover, a balance between different size categories determines the dominating characteristic. Wet sieving method is known as a more accurate method than dry sieving method to obtain particle size distribution. Soil samples need to be washed and oven-dried before machine sieving; therefore, this method requires more time for the treatment. However, this extra procedure increases the chance for accurate measurements by removing fine particles, which are adhered around larger particles. Hence, this method is preferable especially for samples containing certain amount of silt and clay, which are smaller than 63 μm . Referring to the British Standard, the recommended amount of dry soil was taken, such as 200 g for sample consisting of particles less than 6.3 mm. Subsequently, particles were divided into categories by operating an

Chapter 5 Optimisation of Soil Thermal Properties for the GSHP

electromagnetic sieve shaker (A059-12, Matest Srl, Treviolo, Italy, Figure 5.5) for 10 minutes at intensity of 50.

The OMC defines the largest density under the fixed compaction energy. Density is tightly connected to thermal properties and other behaviours of soil; therefore, investigating the OMC is an essential step to understand soil characteristics. Soil density is normally compared in dry density, in which the weight of air and water is not counted. Practically these substances occupy space and reduce dry density; however, water can take an interesting role against soil density. When water content becomes higher, clay loses a feature to be aggregated and friction between soil particles decreases. As a result, air voids can be removed more easily to generate



Figure 5.5 Electromagnetic sieve shaker

Chapter 5 Optimisation of Soil Thermal Properties for the GSHP

higher density (Barnes, 1995). Density increases until water content reaches the OMC and subsequently decreases, since water starts pushing soil particles away rather than contributing as a lubricant.

The same soil sample could have different OMC with dependence on the applied compaction energy (Barnes, 1995). Higher compaction energy leads to easier removal of air and moves particles to be packed more tightly. Therefore, the maximum density at the OMC could be larger with larger compaction energy. However, the effect of compaction energy has a peak as well and less effect is seen after soil contains water to a certain extent.

In order to find the OMC, the British Standard light compaction energy (standard compaction energy) was referred during a series of laboratory tests (British Standards Institution, 1990). Sample was divided into three layers and packed in one-litre mould. 2.5 kg of hammer was dropped 27 times for each layer in an automatic soils compactors (BS model SL130, Impact Test Equipment Ltd, Ayrshire, Scotland, Figure 5.6). The distance between the bottom of the hammer and the bottom of the mould was 0.3 m. When the average distance, 0.257 m, was considered, the standard compaction energy was 510.5 kJ/m³ quantified with an equation below.

$$energy = \frac{mhbng}{V} \quad \text{(Equation 5.3)}$$

energy Compaction energy J/m³

h Average height m



Figure 5.6 Automatic soil compactor

m	Weight of hammer	kg
b	Number of blows per layer	-
n	Number of layers	-
g	Gravity, 9.8	m/s^2
V	Volume	m^3

The other expression is a result without multiplying by gravity, $52.1 \text{ Mg}\cdot\text{m}/\text{m}^3$.

Water content was calculated from the weight difference before and after the oven dry process. After weighing soil samples in the litre mould, small amount of soil were taken into containers to obtain representative water content.

5.2.3 Sample making

Soil were collected from two different parts of the sampling site; sample Pd1 and Pd2. This enabled to examine the uniformity of characteristics regardless of the different sample locations. The fundamental tests were begun from particle size distribution and the OMC.

Two types of tray with different height were made for measurements with the HFM. The area was 280 mm X 280 mm and the height was 15 mm and 50 mm respectively. The walls were made of plywood, whose internal surfaces were varnished to create water-resistance. The bases were made of aluminium plates 5 mm and 2 mm thick respectively, in order to make the thermal resistance negligible. The maximum particle size was restricted in accordance to the tray height as mentioned in section 3.4.1. The same soil samples were prepared to be compared between the HFM and the DPHP; therefore, the maximum particle size for the 15 mm tray was restricted to be 2 mm.

When samples contain moisture, the trays are recommended to be covered with a water-proof sheet, such as cling film (Figure 5.7). Water molecules are fairly small; therefore, to block all moisture by the cling film cannot be expected. However, the use of cling film is applied to research in order to prevent from the shortest circuit of evaporation from samples (Schweizer, 1997). Since the HFM itself was not calibrated for the film, additional calibration was required. For the inspection, thermal conductivity of oven-dried soil was measured with and without cling film. The hot plate and



Figure 5.7 Soil sample covered with cling film

the cold plate were controlled to be 30 °C and 0 °C respectively for all the measurements. Material data and thickness of cling film are shown in Table 5.3. The relation can be expressed by the following theory (Holman, 2002).

$$\frac{k_{total}}{\Delta x_{total}} = \frac{1}{\left(\frac{\Delta x_{soil}}{k_{soil}} + \frac{\Delta x_{film}}{k_{film}} \right)} \quad \text{(Equation 5.4)}$$

k Thermal conductivity W/m/K

Δx Thickness m

, where subscript total, soil and film indicate the overall value and the values for layer of soil and cling film.

Table 5.3 Conditions for calibration with cling film

Thickness	Film ¹⁾	1.5E-05 m
	Soil	0.015 m
k ²⁾	Film	0.16 W/m/K

1) Thickness was measured with a micrometer

2) Polyvinyl chloride (Holman, 2002)

Chapter 5 Optimisation of Soil Thermal Properties for the GSHP

The measured conductivity of the wrapped soil was smaller than that of the soil without cling film, which must be due to the additional thermal resistance caused by cling film (Table 5.4). Subsequently, the thermal conductivity of the soil without cling film was estimated from Equation 5.4. The results were larger than the measured values for the wrapped soil samples. However, the measured values for the unwrapped soil samples were even larger. The thickness of cling film was so small that the influence was negligible in the estimation. A hypothesis is that air layer was trapped between the cling film and the soil sample and this was more influential than the enlarged overall thermal resistance by the cling film. The difference between the measurement and the estimation was within 3.6 %, which was larger than the accuracy of the HFM, ± 3 %. Hence, the average air layer, 0.036 mm, was considered to exist when the thermal conductivity of the soil sample without cling film was estimated throughout experiments.

Table 5.4 Comparison between estimated and measured thermal conductivity

	Sample 1	Sample 2	
Without film	0.2109	0.2191	W/m/K
With film	0.2035	0.2158	W/m/K
Estimated for without film	0.2036	0.2159	W/m/K
Difference between theoretical and measured value without film	3.5900	1.4800	%
Estimated air layer ¹⁾	0.0770	0.0310	mm

¹⁾ Referred air thermal conductivity; 0.02623 at 25 °C (Holman, 2002)

Chapter 5 Optimisation of Soil Thermal Properties for the GSHP

soil samples and the aluminium plate. Allinson (Appendix E) quantifies the thermal resistance of the air layer with the same soil sample, the HFM and an aluminium plate. Hence, the delivered value, $0.005 \text{ m}^2\text{K/W}$, was referred to estimate the soil thermal conductivity measured in the thicker tray with a 2 mm aluminium plate. For the shallower tray with a 5 mm aluminium plate, the estimated value, $0.013 \text{ m}^2\text{K/W}$, was used.

Samples with various kinds of water content were prepared. Tap water was mixed to completely dried and sieved soil by an industrial mixer. Each portion was weighed by a scale, which enables to measure up to two decimal places (Explorer Pro EP 4102, Ohaus, NJ, USA). Soil samples were compacted up to the standard compaction energy for measuring both with the HFM and the DPHP. Samples would not fit into the automatic soil compactor; therefore, they were compacted by dropping 6.215 kg of hammer from the fixed height, 0.25 m. The numbers of blows were calculated from the volume of each test sample to make the total compaction energy 510.5 kJ/m^3 . A test box for the DPHP has a 0.15 m depth and the sensors were ideally buried at mid depth. In order to make sure the location of sensors, a half amount of soil was firstly settled by 5 blows. After the sensors were laid, the rest half of soil was added on the top to be compacted up to the calculated number of blows.

5.3 Experimental Results – Effects of Water Content

The results from the two fundamental measurements identified the original soil. The HFM and the DPHP were compared in soil thermal conductivity with

Chapter 5 Optimisation of Soil Thermal Properties for the GSHP

different water content under the standard compaction energy. At last, the measured thermal conductivity was compared to the theoretical estimation based on Campbell's model.

5.3.1 Results of fundamental tests

Particle distribution of the original soil, sample Pd1 and Pd2, was measured. The samples were sieved to be less than 14 mm, which was the largest particle size used in the experiments. Figure 5.8 illustrated the results in a particle distribution chart. The ideal grading curve shows the mixture of different soil particles, which realises the largest packing ratio. The presented line was calculated for standard materials used for rammed earth, $n = 0.225$ in the following equation (Houben et al., 1994 and Barnes, 1995).

$$p = \left(\frac{d}{d_{max}} \right)^n \times 100 \quad \text{(Equation 5.5)}$$

p	Passing particle	%
d	Particle size	mm
d_{max}	Maximum particle size	mm
n	Factor, e.g. 0.5 for complete spheres	-

The two curves shaped differently from each other. However, the curves themselves looked similar in a range of smaller particles. It can be assumed that existence of larger particles were more influential on the results. Therefore, the line for sample Pd1 was recreated with one third of gravels. The line fit the original curve of sample Pd2. In fact, when both

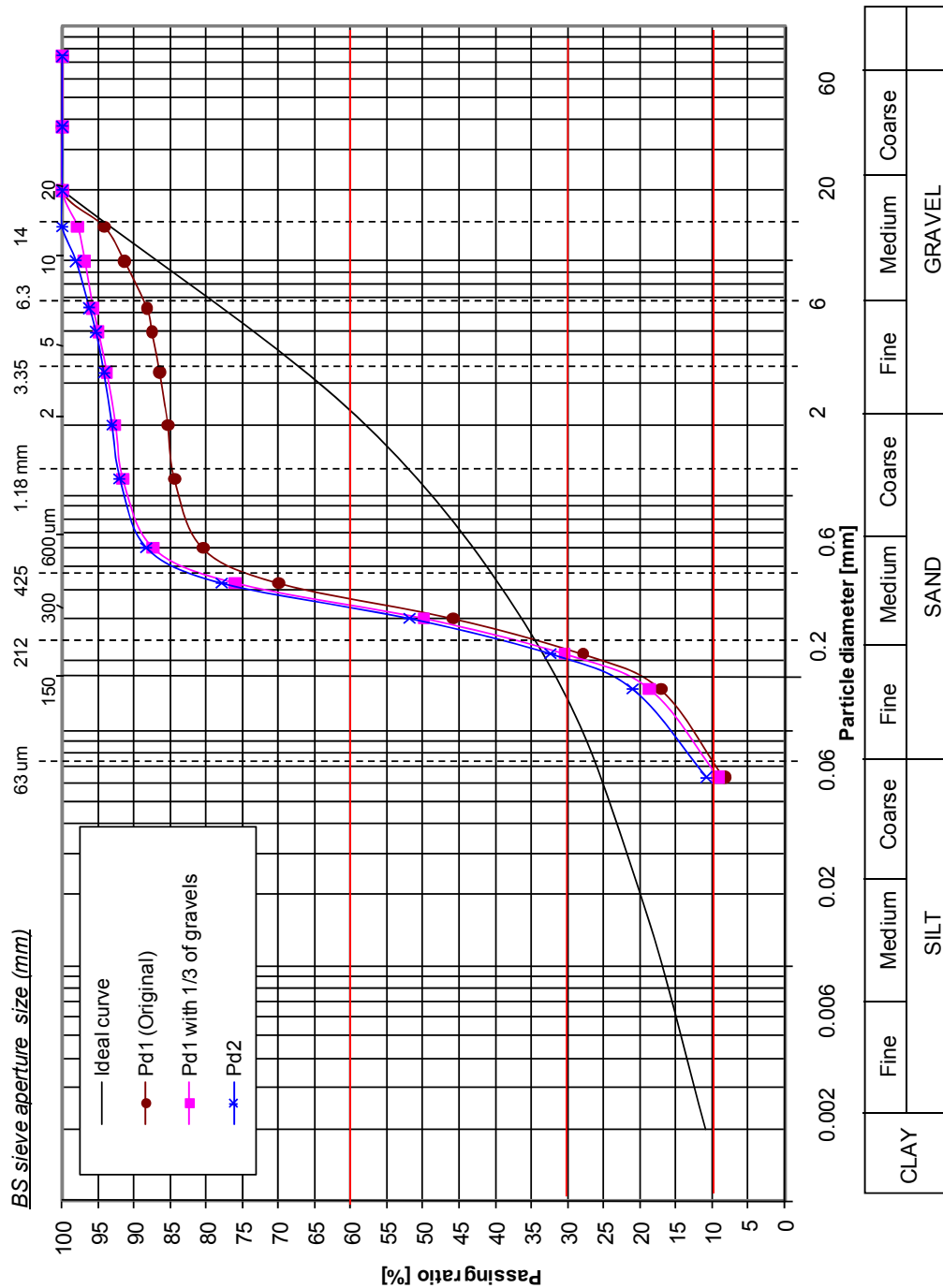


Figure 5.8 Particle distribution of the original soil

samples were sieved to be less than 2 mm, the two curves matched without adjustment (Figure 5.9). Therefore, it could be concluded that the base structure of the original soil was identified regardless of the different

Chapter 5 Optimisation of Soil Thermal Properties for the GSHP

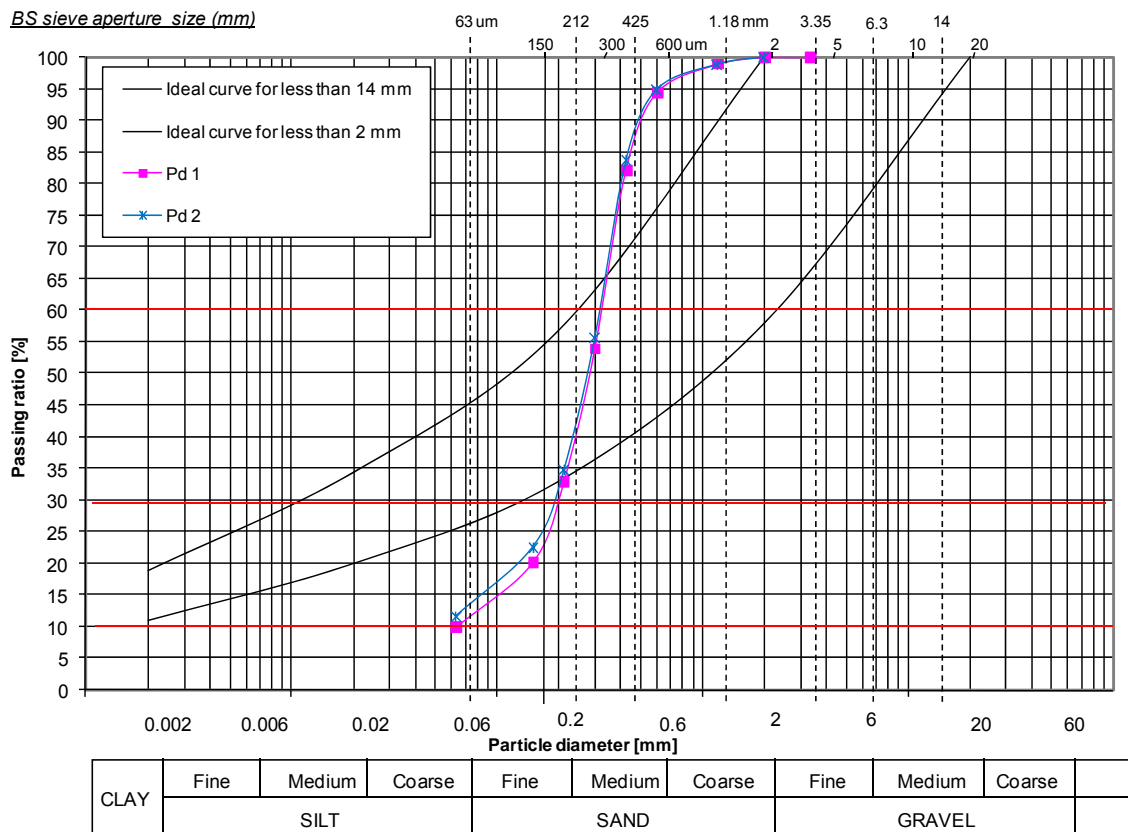


Figure 5.9 Particle distribution of the original soil less than 2 mm

sampling locations. The sharp rise in a range of sand indicates that the original soil was classified as sandy soil.

Compaction tests were conducted with a variety of water content. The derived dry density had a peak for each series of measurement as theories explained in section 5.2.2 (Figure 5.10). The OMC were discovered between 10.7 and 11 % by magnifying the graph and the largest dry density was approximately 1.9 Mg/m^3 . Once the density started dropping, thermal conductivity is also expected to drop due to less soil proportion. Even though air voids are replaced by water, its thermal conductivity, 0.6 W/m/K , is

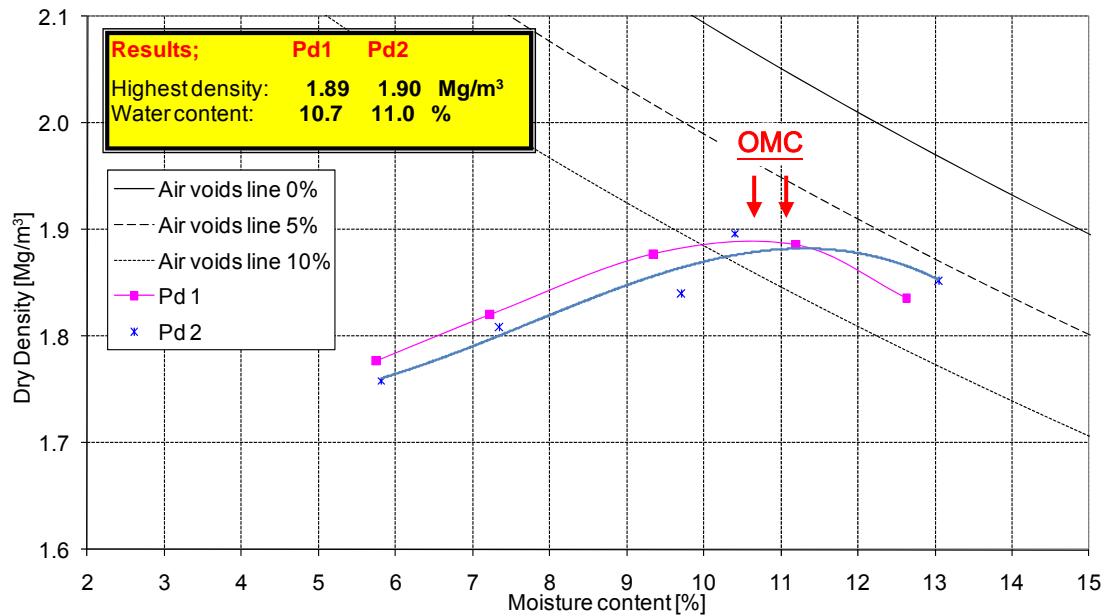


Figure 5.10 The OMC of the original soil

smaller than that of soil, e.g. sand stone, 3 W/m/K (Holman, 2002). Therefore, water content was chosen to be slightly less than the OMC for measuring the optimum thermal conductivity.

Though moisture content of natural soil frequently varies depending on soil structure, rainfall, solar gain and other environmental factors, Table 5.5 shows the collected data in December at the School of the Built Environment. Since the OMC shifts to larger moisture content with less compaction energy, the average moisture content, 11.6 %, should be less than the OMC with the sampled soil.

5.3.2 Results with the HFM

Four kinds of soil samples were investigated. Water was added to make

Table 5.5 Moisture content of natural soil

Sample		Pd1					
Container number		1	2	3	4	5	6
Mass of wet soil + container, m2	g	36.94	36.73	42.80	35.87	36.69	41.21
Mass of dry soil + container, m3	g	35.92	35.40	41.12	34.59	35.40	39.01
Mass of container, m1	g	24.03	25.22	23.28	24.03	25.22	23.28
Moisture content, $w=(m2-m3)/(m3-m1)*100$	%	8.58	13.06	9.42	12.12	12.67	13.99
Average moisture content	%						12.96

the least wet soil and more water was added every time measurements in one condition were finished. The results are presented in Figure 5.11. Thermal conductivity was plotted against degree of saturation, in order to compare water content among soil samples with different structural features. The results of sample Pd1 and Pd2 did not indicate different characteristics in relation of thermal conductivity against degree of saturation.

The higher degree of saturation became, the higher thermal conductivity was acquired. When water functioned as lubricant to pack soil particles more tightly, the dry density rose and consequently water replaced air in voids. In this series of experiments, both dry density and degree of saturation changed. The pure effect by the increase of degree of saturation is attempted in section 5.6.3. As de Vries's theory explains, the total thermal conductivity should be improved by reducing air portion and by increasing the impact of higher thermal conductivity that water has than that of air. Simultaneously, the effect of heat transfer through water evaporation

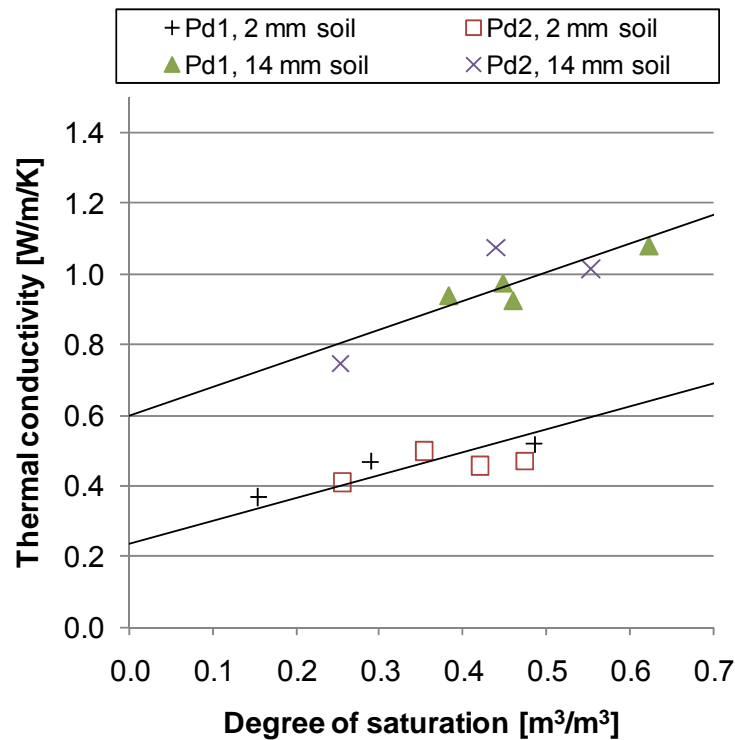


Figure 5.11 Thermal conductivity measured by the HFM

and condensation within air voids might be more significant. Hall et al. (2009) also illustrate that the added water provides thermal bridge between particles to reinforce the total heat transfer. Ewing et al. (2007) explain that the added water makes capillary bridge between particles after the surface sorption capacity of the particles is saturated. Furthermore, it is disclosed that capillary bridges can enhance thermal conductivity even at low water content, which is discussed in section 5.6.3.

There was a clear dependence on the maximum particle size. Samples consisting of particles of less than 14 mm (14 mm soil) showed higher thermal conductivity at the same degree of saturation. The plot of thermal

Chapter 5 Optimisation of Soil Thermal Properties for the GSHP

conductivity against dry density clearly indicated that density was a powerful factor in the enhancement of thermal conductivity (Figure 5.12). This tendency agrees with the results presented by Barnes (1995). There are several indications to achieve high density; however, a method to add large particles is attempted in section 5.4.

5.3.3 Results with the DPHP

Experiments were regularly conducted to observe the variation of thermal conductivity over days. The measurements sometimes took time until stable results were delivered among several experiments with the same samples. Thermal conductivity increased as degree of saturation and dry

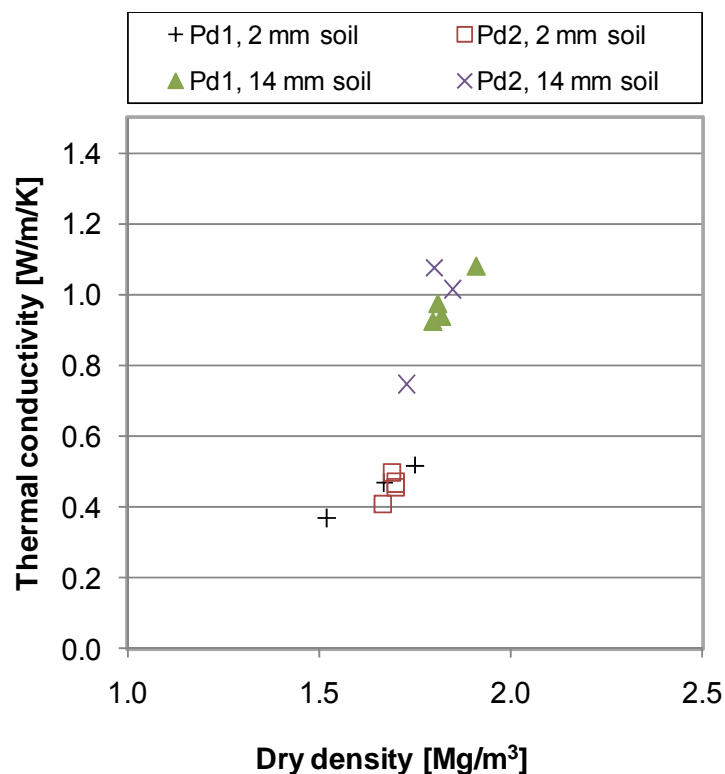


Figure 5.12 Thermal conductivity against dry density

Chapter 5 Optimisation of Soil Thermal Properties for the GSHP

density rose as the tendency with the HFM revealed (Figure 5.13 and Figure 5.14). The data from two samples, Pd1 and Pd2, matched well with the DPHP as well.

The results were derived by matching the prediction curve to the measured curve using a solver function. Degree of the agreement was returned in correlation coefficient. This parameter expresses the resemblance of shapes between two series of data as follow.

$$Correl(X,Y) = \frac{\sum (x - \bar{x})(y - \bar{y})}{\sqrt{\sum (x - \bar{x})^2 \sum (y - \bar{y})^2}} \quad (\text{Equation 5.6})$$

X, Y	Array of data	-
x, y	Data	-

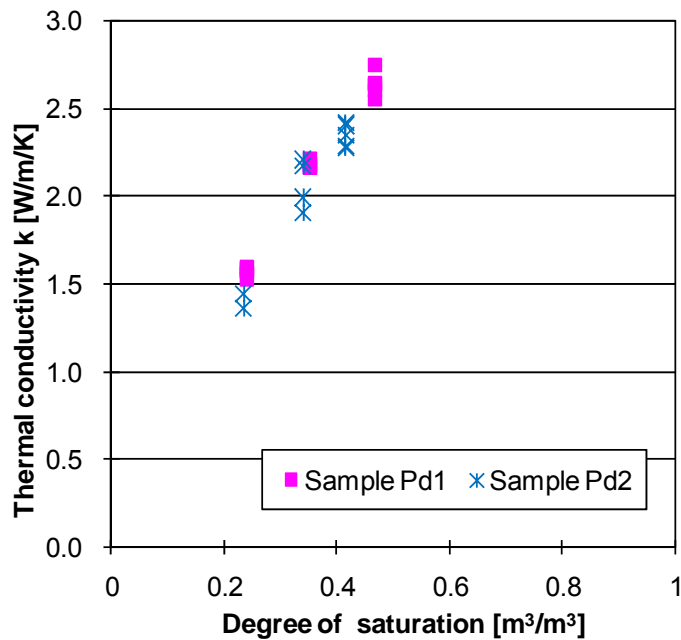


Figure 5.13 Thermal conductivity measurement with the DPHP

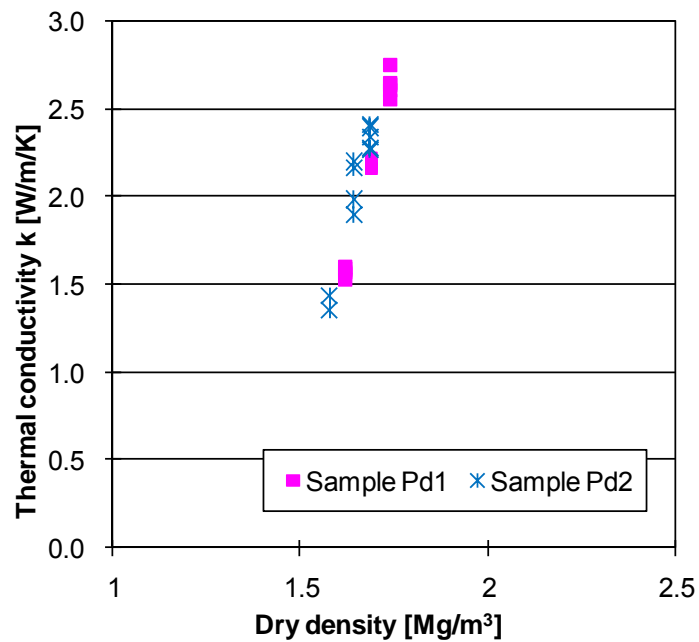


Figure 5.14 Thermal conductivity against dry density with the DPHP

\bar{x}, \bar{y}

Average of each array

-

The results for sample Pd1 and Pd2 were listed as well as the calibration data with sensor 2209 and 2210 in Table 5.6. Though the calibration data showed more successful fitting, it could be said that the agreement was within an acceptable range in the measurement of wet soil as well.

Verification of volumetric heat capacity was studied by comparing the derived data to theoretical data for sample Pd1 in Figure 5.15. The theoretical data of volumetric heat capacity was calculated based on Equation 2.8. The experimental data increased as degree of saturation increased at the same inclination as the theoretical results. The difference was within 6.9 %, which was smaller than that in the calibration with water; \pm

Table 5.6 Correlation coefficient in measurement with the DPHP

Correction coefficient, %				
Measurement	Calibration		Measurement of wet soil	
Sensor or sample	2209	2210	Pd1	Pd2
Minimum	99.4	99.5	97.0	97.8
Difference to 100 %	0.6	0.5	3.0	2.2
Maximum	100.0	100.0	98.5	98.7
Average	99.8	99.8	97.8	98.1

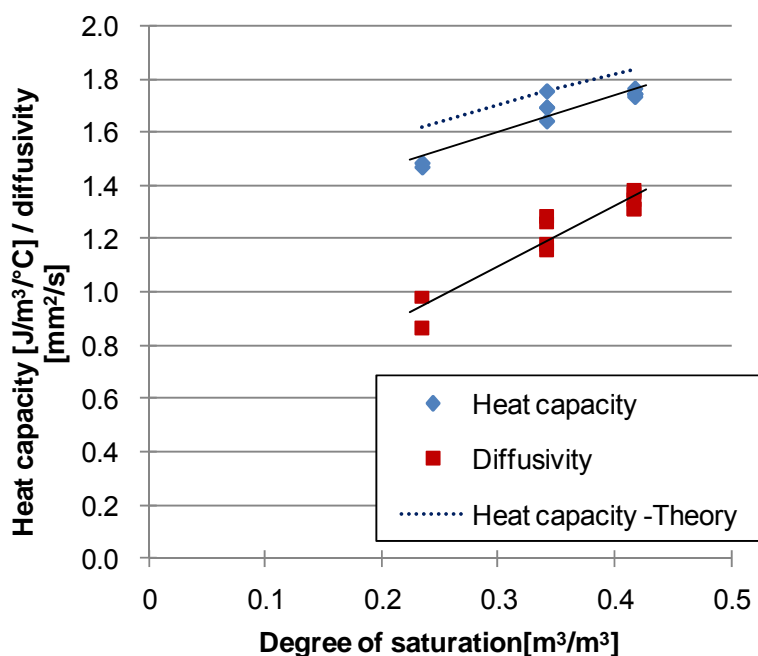


Figure 5.15 Derived heat capacity and diffusivity for sample Pd1

8.0 %, as presented in section 5.1.2. Similar plot was seen for case Pd2. Thus, the uncertainty of both thermal conductivity and volumetric heat capacity were quantified through the error analysis and the verification. Since the remaining factor, diffusivity, can be calculated from the two factors with Equation 2.7, the uncertainty was expected to be in a similar range.

Chapter 5 Optimisation of Soil Thermal Properties for the GSHP

5.3.4 Comparison between two methods

Two methods are compared in the measured thermal conductivity of 2 mm soil. The data from the DPHP was much bigger than that from the HFM in Figure 5.16. However, when the results with dry samples are added, the trendlines from each series of data seemed to meet at 0 degree of saturation. In fact, the difference with dry samples looks small in Figure 5.17. With regard to that the published thermal conductivity of dry sand is 0.2 W/m/K (Shokoku Sha, 2000), the series of data were within $\pm 9.5\%$ with the HFM and $\pm 4.8\%$ with the DPHP. The HFM is made for measuring building and insulating materials (P. A. Hilton Ltd., 1994); therefore, the calibration with water immobilised by agar would not be adequate. Conversely, the used

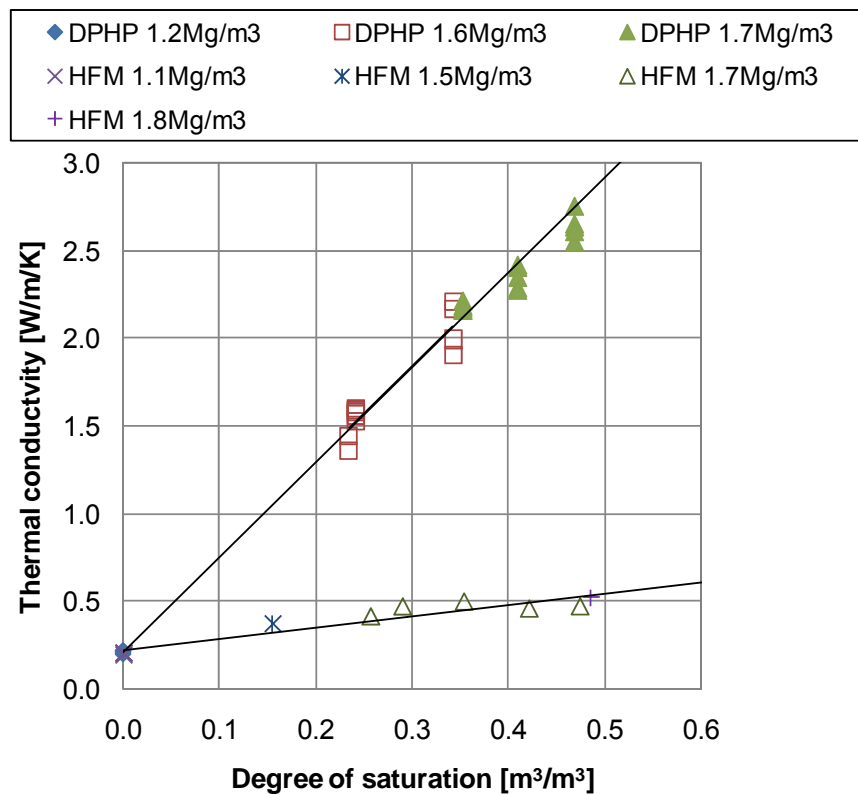


Figure 5.16 Comparison between the HFM and the DPHP

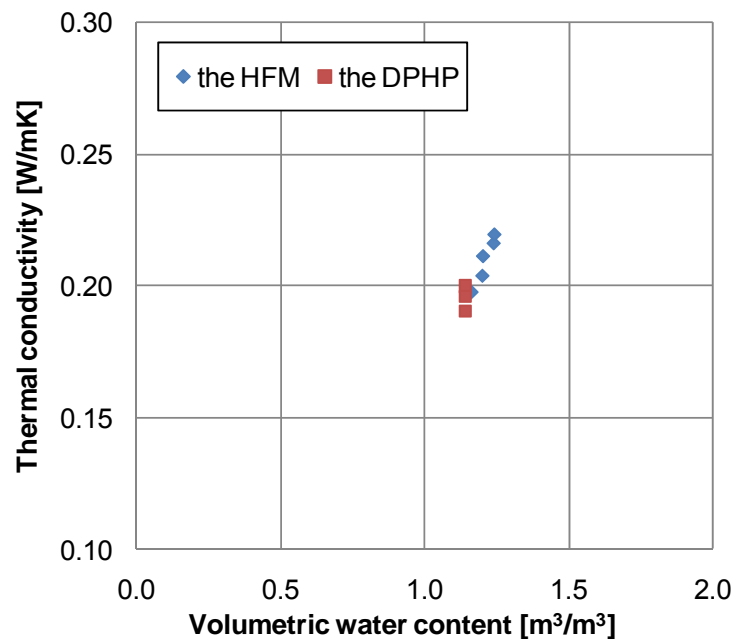


Figure 5.17 Comparison between the HFM and the DPHP with dry samples

DPHP sensors were suitable for the samples consisting of particles of a size no greater than 2 mm. Besides, the characteristics of aggregate vary with dependence on quarries; however, there was no supplier which could provide accurate thermal conductivity. Consequently, comparing the two methods with dry 2 mm sandy soil was one of the reasonable choices.

The reason of two different series of measured data must lie in the differences of measuring mechanisms. While thermal conductivity was measured instantly with the DPHP, the properties were quantified when thermal equilibrium was achieved with the HFM (Figure D.1). Since thermal energy kept inserted into samples, water migrated to create gradient (International Organization for Standardisation, 1996). Though the original

Chapter 5 Optimisation of Soil Thermal Properties for the GSHP

state was homogeneously mixed with water, moisture was vaporised near the hot plate and condensed near the cold plate. As a result, thermal conductivity was measured in a different water distribution from that of the original samples. Therefore, the HFM is usable as far as all the samples are compared under this condition.

The DPHP measures in a closer state to that of natural soil underground. This feature is preferable for optimising underground designs in terms of potential heat collection capacity using thermal conductivity of surrounding components. Since the uncertainty with confidence of 95 % was not particularly inferior to the uncertainty of the HFM, the DPHP was selected for further experimental investigation in this project.

5.3.5 Comparison with Campbell's theory

Both de Vries's and Campbell proposed a series of formulas to predict soil thermal conductivity as introduced in section 2.5.5. Since de Vries's theory requires specific parameters, which are difficult to measure, many researchers confirm their experimental results with Campbell's method. In order to compare with the experimental data with sample Pd1 and sample Pd2, theoretical values were calculated using Equation 2.17 to Equation 2.22 in Figure 5.18. Clay fraction was estimated to be 0.02 from the particle distribution curve in Figure 5.9. The volume fraction of quartz of the samples was extracted by seeking the minimum SSE between the experimental and the theoretical results, as Bristow (1998) conducts.

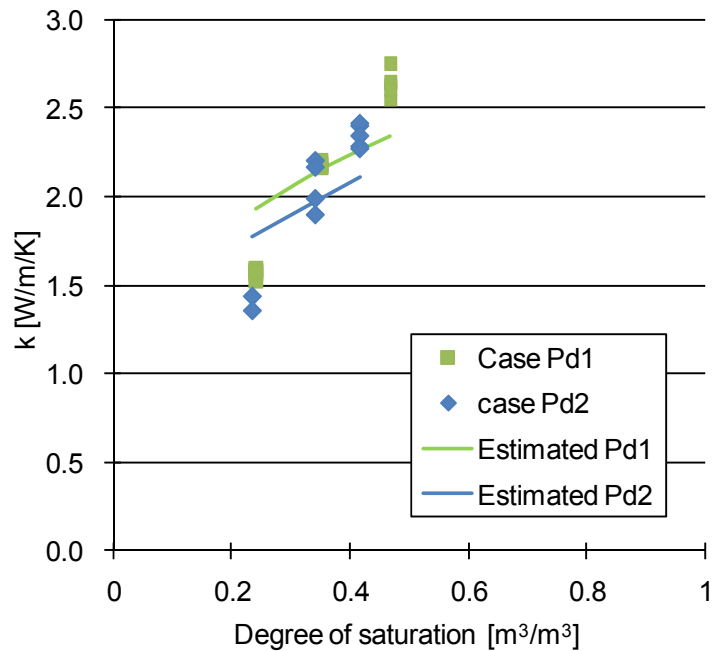


Figure 5.18 Comparison to Campbell’s prediction for sample Pd1 and Pd2

Solver disclosed that the SSE was the minimum, when quartz proportion to all solids was 0.66 for sample Pd1 and 0.61 for sample Pd2. A survey discloses that pebbles in Nottingham are mostly quartzite (Edwards, 1996), which also suggests considerable proportion of quartz in the original soil.

The experimental data was in a range of $\pm 23.2\%$ with sample Pd1 and $\pm 26.6\%$ with sample Pd2 from the theoretical results. It is common to see better match in other papers. The difference in the conditions was that these samples were prepared by water mixing, rather than water absorption as other research papers present. The differences of effects in between are discussed through the experiments with water spraying in section 5.6.3. The results are also compared with the theoretical values derived from Campbell’s theory.

5.4 Investigations for Higher Thermal Conductivity

Further investigation was conducted on the effects of high dry density achieved by soil samples containing large particles. As Figure 5.11 indicated, 14 mm soil had approximately double thermal conductivity of that of 2 mm soil. This section attempts to discover the reasons by analysing two soil samples with different particle distribution. Pore size distribution is inspected by x-ray micro scanning to compare between the original soil and a sample containing more large particles. Associations between the result and soil thermal conductivity are discussed.

5.4.1 Introduction of samples for the comparison

A sample consisting of more proportions of large particles was blended to compare with the original soil. The oven-dried original soil was sieved to granules of a size no less than 2 mm and added to the original sandy soil. The generated sample contained more large particles, such as medium to coarse sand and gravels (gravelly soil, Figure 5.19).

The ideal curves were plotted for 2 mm soil and 14 mm soil in Figure 5.19. The particle distribution indicated that the gravelly soil became closer to the ideal curve than two kinds of sandy soil with different maximum particle size. The sum of squared error (SSE) was calculated for each sample using Equation 2.10, so as to compare in between. The results confirm that the state of the gravelly soil was closer to the maximum packing, which might enlarge dry density and eventually thermal conductivity. The consequences are investigated in section 5.4.3.

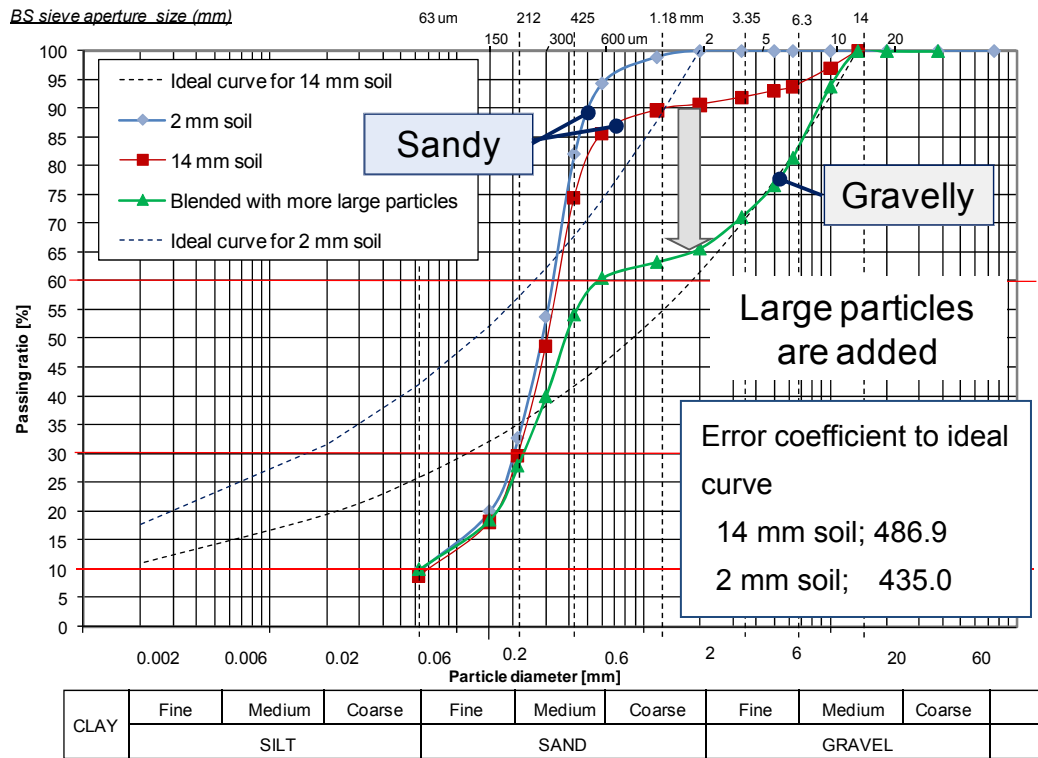


Figure 5.19 Blended sample with more large particles

5.4.2 Measurement of pore size distribution

Ideal curve is a convenient indication to increase contacts among particles by mixing various sizes of particles effectively (Houben et al., 1994). In order to confirm the achieved state, both samples were analysed with x-ray micro scanning (μ CT 40, Scanco Medical AG Ltd., Bassersdorf, Switzerland, Figure 5.20). This measuring tool scans samples and records the sliced images into a connected computer. The installed programme analyses the images to calculate pore size distribution and mean pore size.

The largest specimen holder was selected; however, the diameter was 35 mm. Therefore, both soil samples were sieved to be less than 10 mm, in

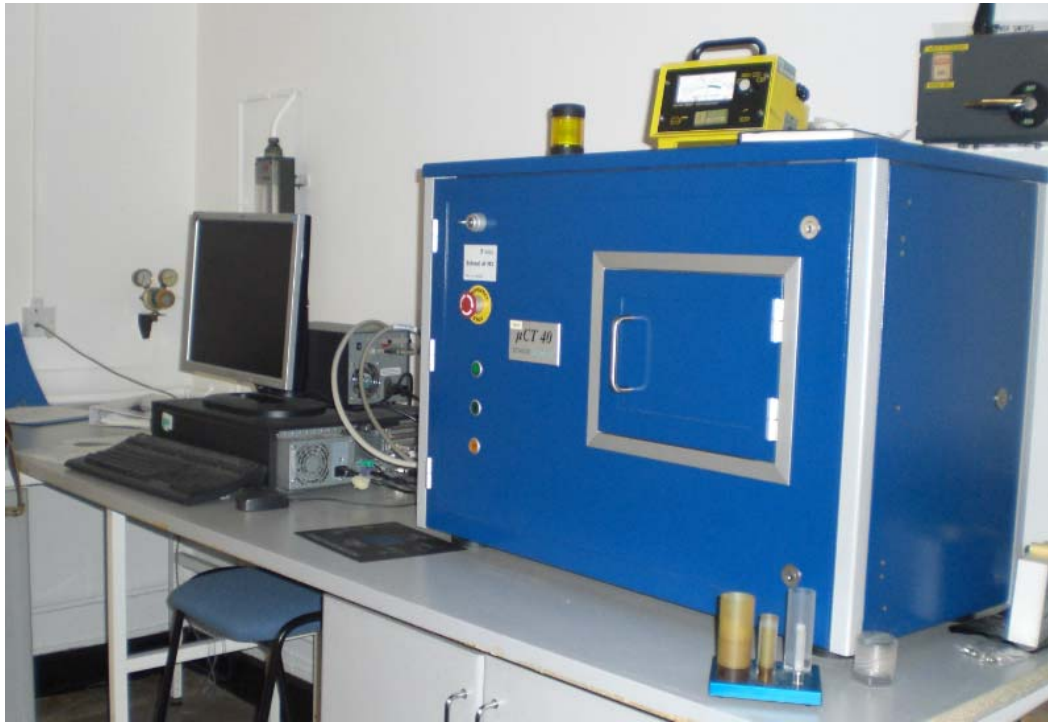


Figure 5.20 Setup of x-ray micro scanning

order to restrict the largest particle size to be less than a third of the diameter, 11.7 mm. This is for preventing too large particles from creating unplanned voids particularly near the internal wall of the holder. Each sample was attempted to be packed at the same bulk density as the measured value under the standard compaction energy (Figure 5.21). The target density was estimated by removing particles between 10 mm and 14 mm from the value for 14 mm soil. The prepared samples were packed to a 25 mm height in the holder. The samples were set to be scanned for approximately 140 slices at mid height. The minimum pixel was set as the lower limit for the x-ray scanner, 18 μm .

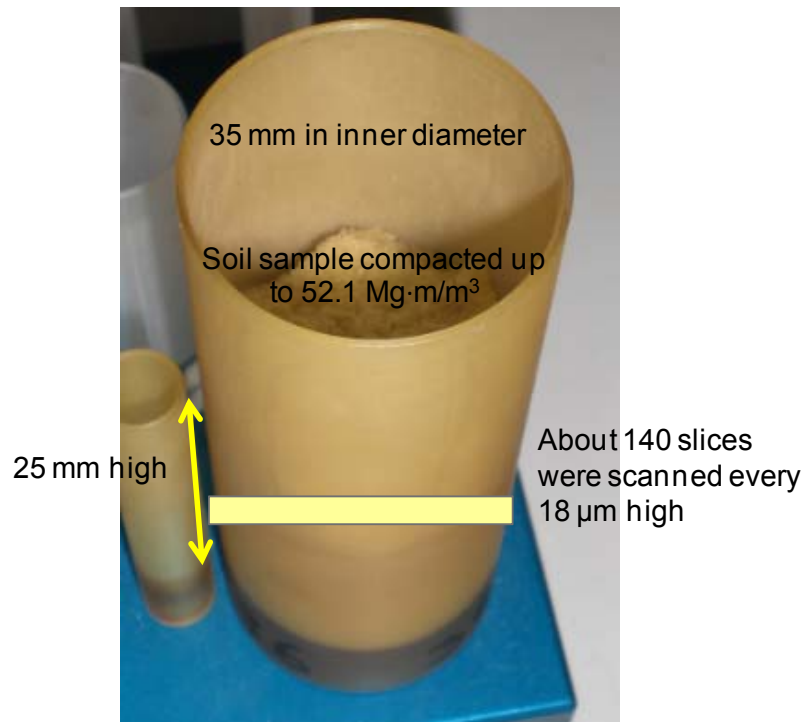
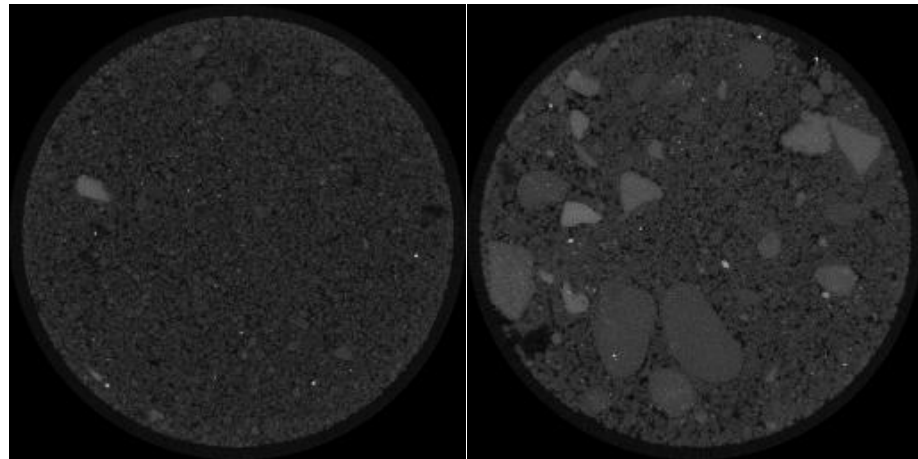


Figure 5.21 Preparation of specimen

The scanned images are displayed in Figure 5.22. It can be seen that the gravelly soil had more large particles than the sandy soil. Table 5.7 and Figure 5.23 present the results of the analysis. Density of the samples was similar to that for measurement with the HFM. The calculated pore size revealed that the gravelly soil had smaller mean pore size. This implied that the particles were packed efficiently and the mean distance between particles was closer than that of the sandy soil. In fact, the obtained porosity was smaller in the gravelly soil. Compared with the theoretical porosity, the minimum pixel of the x-ray scanner was not small enough to detect all pores; however, both measured and theoretical porosity indicated that the gravelly soil had smaller space between particles.



a) The sandy soil

b) The gravelly soil

Figure 5.22 Scanned images of the sandy and the gravelly soil

Table 5.7 Results of analysis

Soil sample		Sandy	Gravelly
Target density	Mg/m ³	1.840	1.985
Density	Mg/m ³	1.712	1.918
Achieved density in experiment	%	93.1	96.6
Mean pore size	mm	0.0645	0.0596
Standard deviation	mm	0.0290	0.0322
Mean porosity	%	13.85	6.79
Theoretical porosity ¹⁾	%	35.38	27.61
Undetected pores ²⁾	%	21.53	20.83

1) Calculated from a typical particle density of light-coloured sand, 2.65 Mg/m³ (Barnes, 1995)

2) Difference between measured and theoretical porosity

Smaller pore size encourages capillary action as the equation suggests (Hilpert, 2009).

$$\Delta p = \frac{2\gamma}{r} \cos \theta \quad \text{(Equation 5.7)}$$

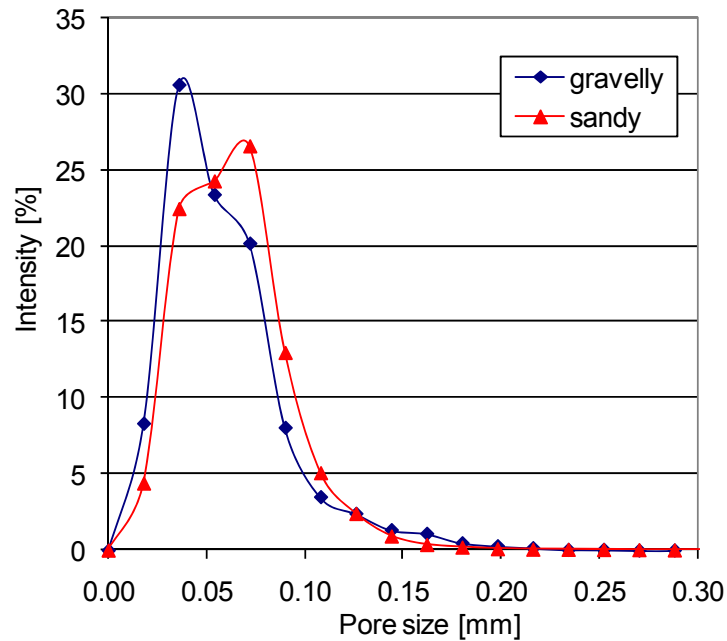


Figure 5.23 Pore size distribution

Δp	Capillary pressure	Pa
γ	Liquid-air surface tension	N/m
r	Radius of container	m
θ	Contact angle	°

The feature would be suitable to refill moisture by rainfall after the installation. Ismail et al. (2008) discover that finer pores can hold more water even if water source, such as water table, is not adjacent. Pereira et al. (2009) particularly focus on the presence of coarse aggregates in terms of the creation of pores. The large particles contribute to enlarge the path length of capillary pores and to increase their interconnectivity, which activates capillary suction effect.

5.4.3 Comparison in thermal conductivity

Thermal conductivity was measured with the DPHP. The results showed that the gravelly soil had higher thermal conductivity and larger dry density (Figure 5.24 and Figure 5.25). The improvement of thermal conductivity was not as large as it was seen between 2 mm soil and 14 mm soil. Alternatively, the effect of water presence was larger than the packing ratio under the same size restriction of the particles. Nevertheless, it was proved that the consequence of higher packing ratio in the gravelly soil was higher density and higher thermal conductivity. Therefore, more methods to enhance dry density were explored throughout further experiments.

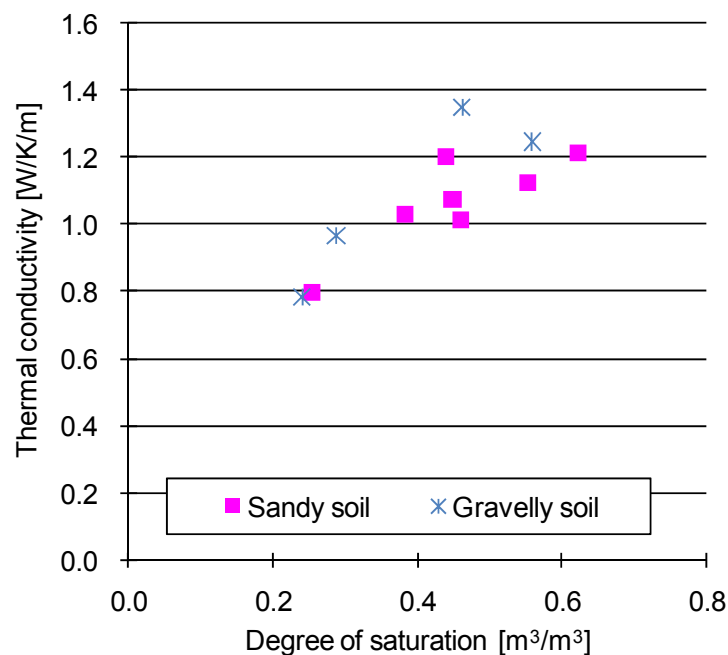


Figure 5.24 Comparison of thermal conductivity between the sandy and the gravelly soil

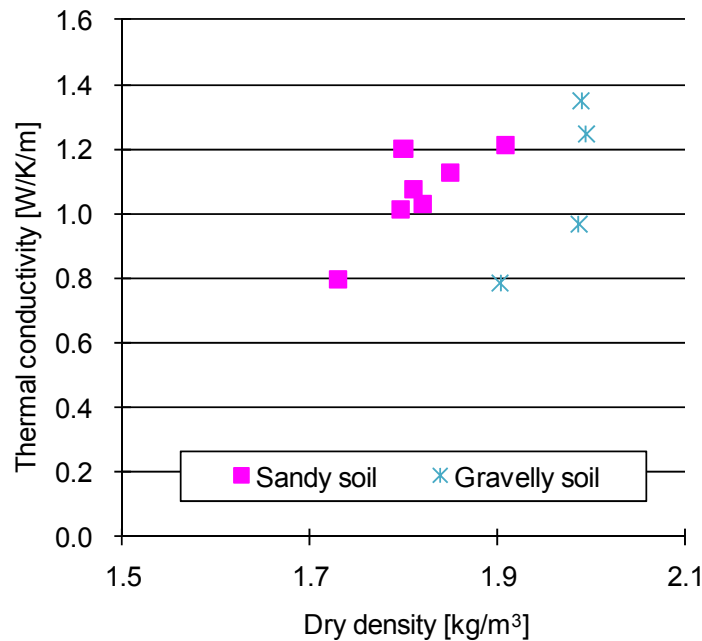


Figure 5.25 Comparison of thermal conductivity against dry density

5.5 Defining the Status of Natural Soil

It is essential to know a degree of enhancement compared with the original sub-soil. Though specifying the average state of natural soil is difficult, the specs are determined on the basis of references and assumptions.

The state of natural soil varies with dependence on environmental events, such as rain; however, typical bulk density, 1.5 Mg/m^3 , was referred (Campbell et al., [no date]). It could be imagined that sub-soil in natural environment is lightly compacted by a combination of weather and weight from soil above. However, it is difficult to find data to refer to; therefore, compaction energy to realise the typical bulk density in soil samples was investigated. The compaction test was attempted at the typical water content of sandy soil, $0.1 \text{ m}^3/\text{m}^3$ (Campbell et al., [no date]).

Chapter 5 Optimisation of Soil Thermal Properties for the GSHP

The result of compaction test displayed significant impact of compaction energy on density (Figure 5.26). Barnes (1995) explains that compaction enlarges density by removing air voids, though there is a limit in accordance to moisture content and soil strength. This phenomenon was seen in this experiment and density seemed to be saturated after 60 $\text{Mg}\cdot\text{m}/\text{m}^3$. The trendline disclosed that the required compaction energy for bulk density of 1.5 Mg/m^3 was 4.5 $\text{Mg}\cdot\text{m}/\text{m}^3$. Thus, the sample representing sub-soil was defined (natural soil). Consequently, thermal conductivity was measured with the DPHP. The average value was 1.18 $\text{W}/\text{m}/\text{K}$ (Figure 5.32 and Figure 5.33).

5.6 Investigation of Contributing Design Elements

The experiments in the section 5.4 highlighted the importance of high packing ratio and water content to enhance thermal conductivity. On the other hand, the compaction test in the previous section demonstrated the positive impact on dry

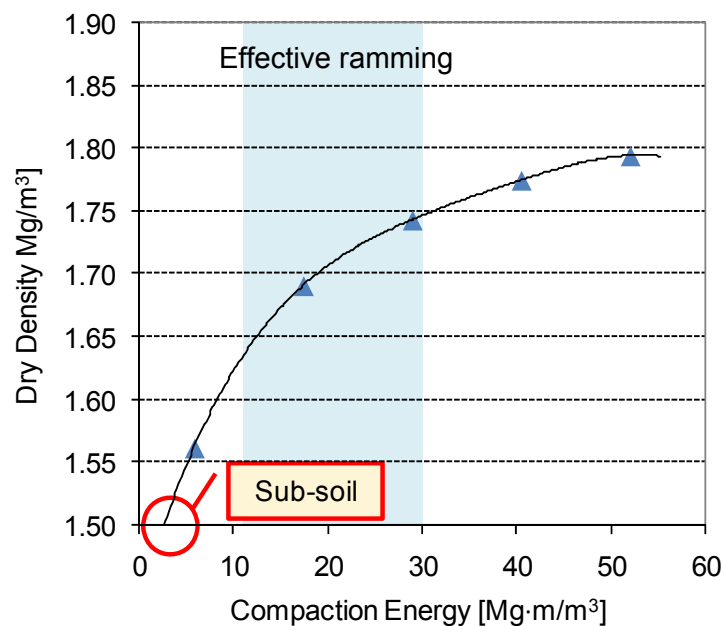


Figure 5.26 Relation between compaction energy and density

Chapter 5 Optimisation of Soil Thermal Properties for the GSHP

density. Hence, this section describes prepares for the thorough exploration of each parameter by creating two soil samples with the maximum packing ratio.

5.6.1 Effects of high dry density attained by compaction

This is a mechanical approach to increase soil density. Thermal conductivity of 2 mm soil was examined with different compaction energy. In addition to $4.5 \text{ Mg}\cdot\text{m}/\text{m}^3$ for natural soil and $52.1 \text{ Mg}\cdot\text{m}/\text{m}^3$ for the standard energy, one more kind of compaction energy was tested. The data of the compaction test in the previous section showed effective ramming area (Figure 5.26 and Table 5.8). When compaction is applied for practical systems, it is essence to recognise the most cost effective compaction energy. Therefore, $28.9 \text{ Mg}\cdot\text{m}/\text{m}^3$ was selected as the third test case for the comparison.

The importance of water content was clarified in the previous experiments;

Table 5.8 Results of compaction test at water content of $0.1 \text{ m}^3/\text{m}^3$

Total blow number	Compaction energy	Bulk density	Increase ratio of density ¹⁾
in blow	$\text{Mg}\cdot\text{m}/\text{m}^3$	Mg/m^3	%
7	4.50	1.50	
9	5.79	1.56	
27	17.36	1.69	8.3%
45	28.94	1.74	3.1%
63	40.51	1.77	1.8%
81	52.09	1.79	1.1%

1) Calculated only for a range where compaction energy was increased with the same interval

Chapter 5 Optimisation of Soil Thermal Properties for the GSHP

therefore, samples at the most effective water content, the OMC, was examined. To begin with, the OMC for each kind of compaction energy was investigated through the compaction test (Figure 5.27). The results displayed that larger compaction energy generated lower OMC and higher dry density at the OMC as Barnes (1995) summarises.

5.6.2 Effects of high dry density attained by packing ratio

Packing ratio is an essential indication for mechanical strength and the feature of water resistance as well as for thermal conductivity (Houben et al., 1994). Fuller originally found a desirable combination of particles to achieve the maximum packing ratio (Barnes, 1995). The following study

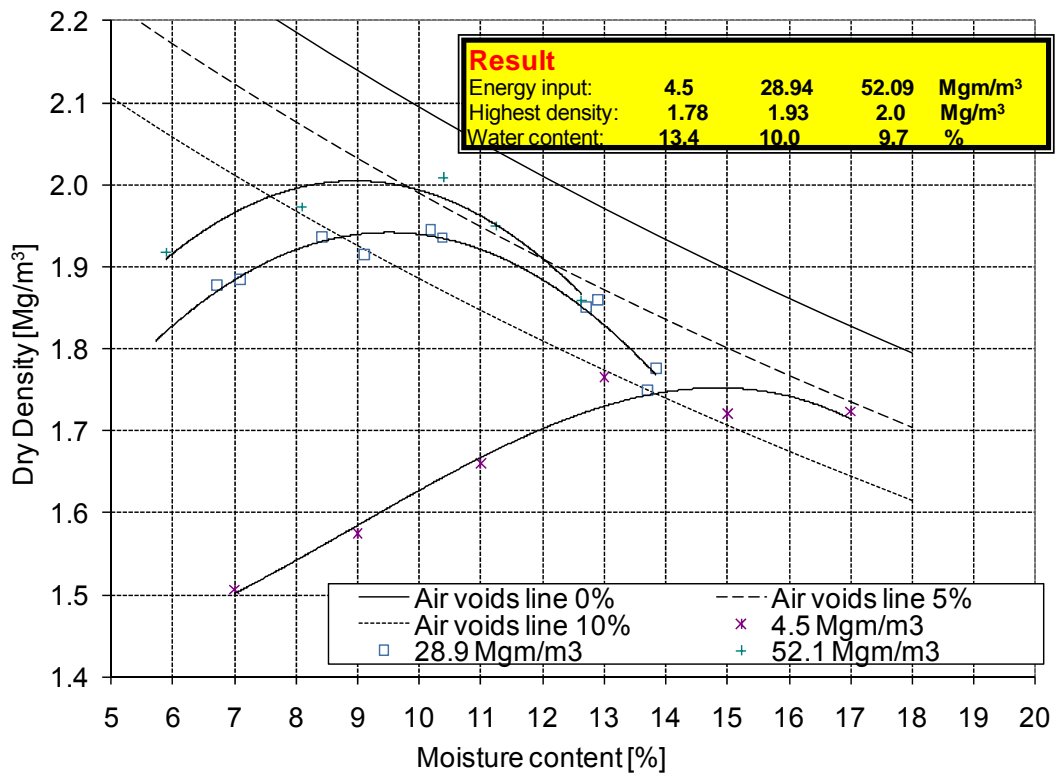


Figure 5.27 Investigation of the OMC

Chapter 5 Optimisation of Soil Thermal Properties for the GSHP

specifies that the ideal curve with $n = 0.225$ is suitable for rammed earth, while $n = 0.3$ and 0.5 for sandy soil and entirely spherical particles (Figure 5.28).

Soil samples at the maximum packing ratio were prepared following the ideal curves with $n = 0.255$ and with $n = 0.33$, so as to compare in between. The samples were required to be blended by adding larger sands, silt and clay. The oven-dried soil was sieved into different sizes and small particles adhered on the surface were washed away. Consequently, particles in each size category were carefully mixed to be shaped like the ideal curves

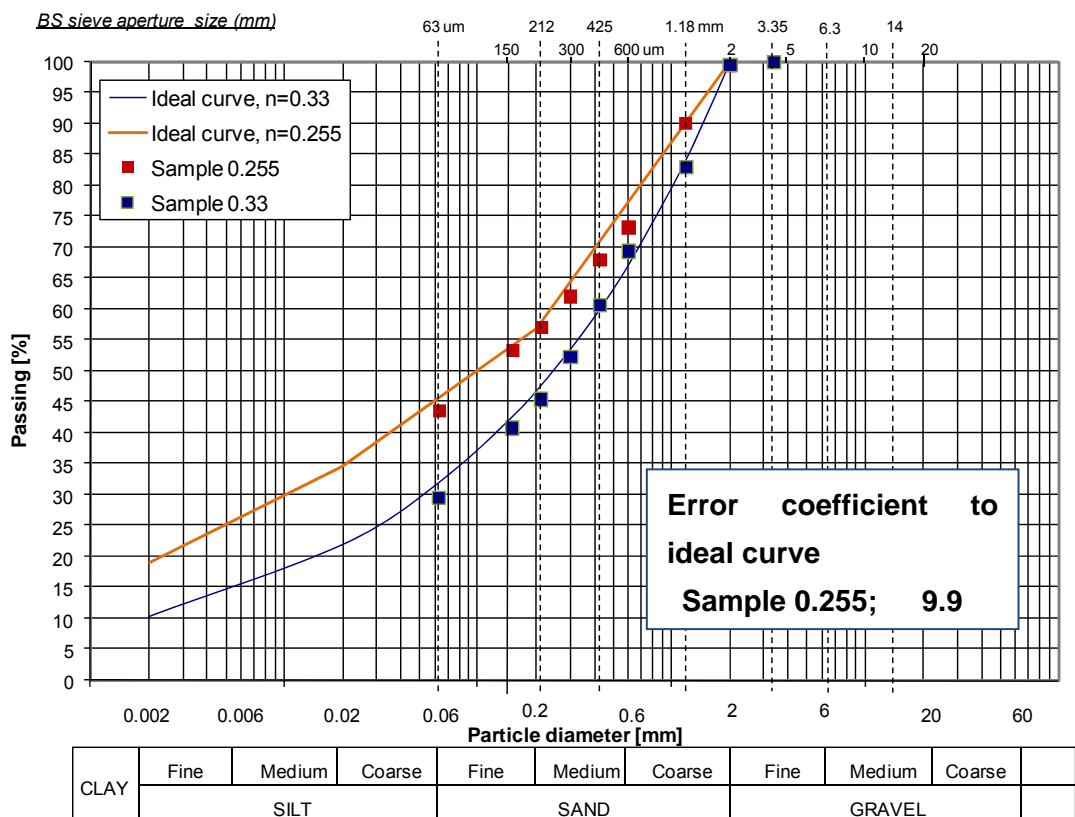


Figure 5.28 Ideal curves with different n factor

Chapter 5 Optimisation of Soil Thermal Properties for the GSHP

as presented in Figure 5.29 (Figure 5.28). The samples had smaller error coefficient than the sandy and gravelly soil in Figure 5.19.

Thermal conductivity at the OMC was planned to be measured to compare with that of the compacted samples in section 5.6.1. The compaction test revealed the OMC as plotted in Figure 5.30. Extra compaction on construction site was not assumed; hence, $4.5 \text{ Mg}\cdot\text{m}/\text{m}^3$ was applied as the condition.

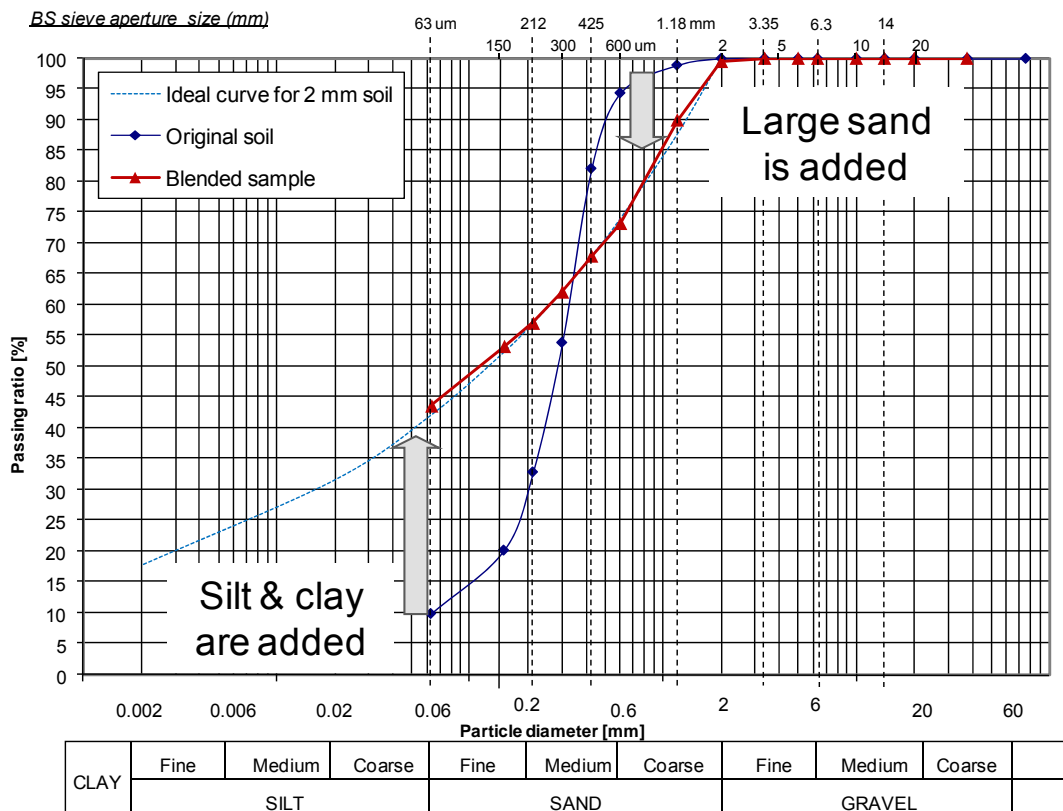


Figure 5.29 Blending for the maximum packing

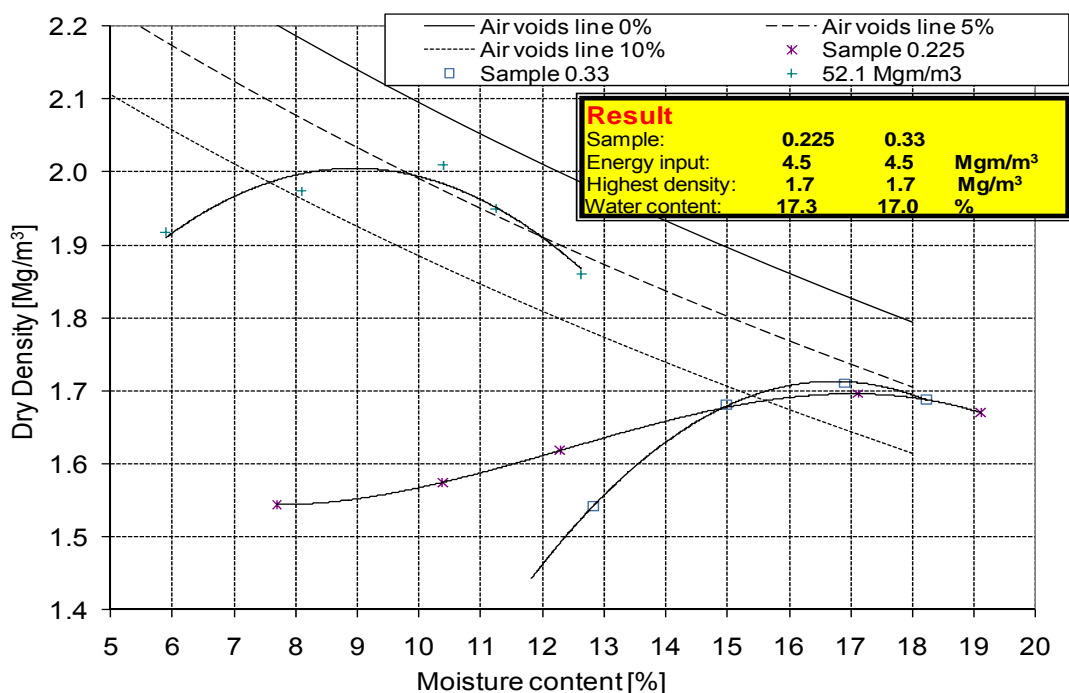


Figure 5.30 Compaction test of sample 0.225 and sample 0.33

5.6.3 Effects of water content added by suction

The analysis of the gravelly soil in section 5.4.2 implied that the small mean pore size could encourage capillary effect after installation. If this occurs, soil moisture content would be expected to rise after installation as well. When degree of saturation is less than 1.0, rainwater is theoretically capable of filling the air gaps further. Another question is if the increase of moisture content by absorbing water can be equivalent to that of water mixing. If this is possible, water content will be controllable even after the construction. This may reduce work for water mixing process on ground and may achieve high moisture content only by waiting for rainfall.

Soil sample was packed into a test box. 2 mm soil was prepared at water

Chapter 5 Optimisation of Soil Thermal Properties for the GSHP

content which provided the same degree of saturation as the compacted soil at $52.1 \text{ Mg}\cdot\text{m}/\text{m}^3$. Two kinds of samples were made with different compaction energy; $4.5 \text{ Mg}\cdot\text{m}/\text{m}^3$ and $28.9 \text{ Mg}\cdot\text{m}/\text{m}^3$ (sample 4.5 and sample 28.9 respectively). Thus, the increase of thermal conductivity by the increase of moisture content can be compared in the same conditions between water mixing and water absorption.

Tap water was weighed and sprayed from the top surface of the samples. A shallow concave curve was intentionally created on the top of samples, so as to guide water to be absorbed near the measuring point. The first measurement of thermal conductivity was started after all the water was seen to be absorbed into the soil. Data was regularly collected until the values indicated that the moisture distribution reached equilibrium. This state was judged from if the data measured for several days showed uniformity within a range of $\pm 2 \%$. When the agreed results were seen, the next lot of water was sprayed. Equal amount of water was sprayed until the total amount reached the required amount of water to generate degree of saturation of 0.7.

Though moisture content of the samples could not be measured during the series of spray tests, the measurement was conducted when degree of saturation reached 0.7 to finish the water spraying. Water content was inspected at different 9 points in the test box (Figure 5.31). The wet soil was taken into small containers to estimate the values from the weight difference between before and after oven drying. This method is known for

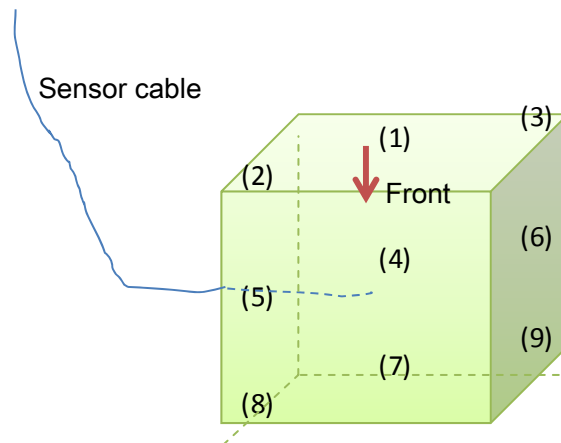


Figure 5.31 Sampling points for water content

the reliability in lab practice (British Standards Institution, 1990).

5.7 Results of Sensitive Analysis

Results of each investigation was presented and discussed respectively.

5.7.1 Enhancement of dry density attained by compaction

Thermal conductivity at the OMC under different compaction energy was compared with that of natural soil and the compacted original soil at the standard compaction energy (Figure 5.32 and Figure 5.33). On the whole, larger moisture content and density brought higher thermal conductivity. An interesting feature was that compaction energy affected dry density; however, the effect was not seen equivalently against degree of saturation. Furthermore, the measurement at the OMC showed similar thermal conductivity regardless of different compaction energy. Figure 5.34 demonstrates this tendency well. It seemed that there was a limit which 2 mm soil could achieve by mixing water to the OMC or compaction. Among

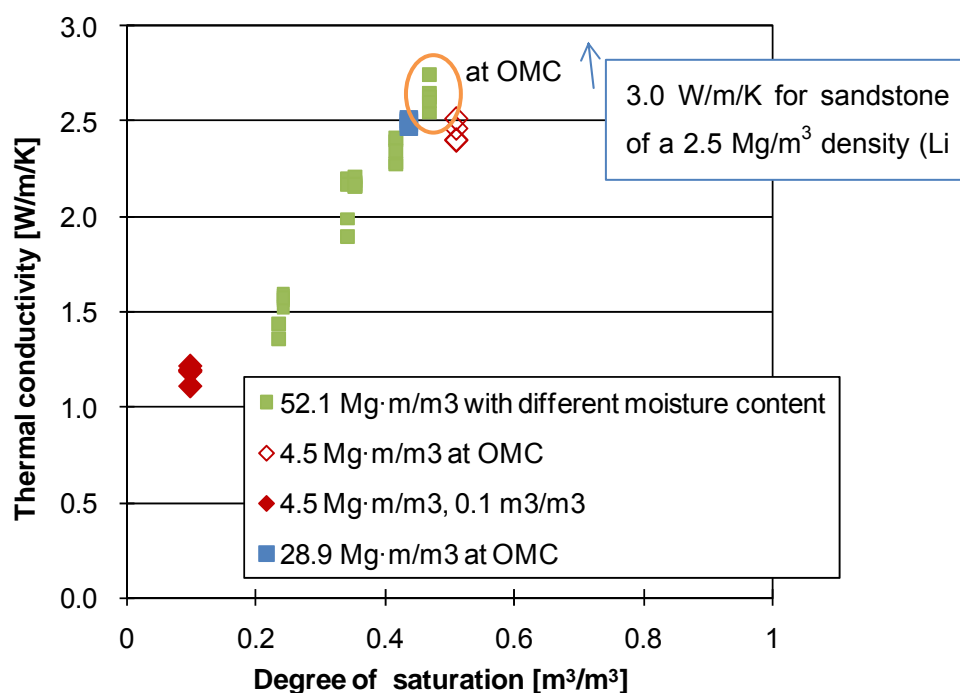


Figure 5.32 Comparison in thermal conductivity

these study cases, the samples at the OMC achieved the highest record, around 2.45 W/m/K. Regarding that thermal conductivity of sandstone is 3.0 W/m/K, this strategy must be one of the most effective options.

Figure 5.34 also shows the change of thermal conductivity with natural soil. When natural soil was compacted with the standard compaction energy, the thermal conductivity became higher than the original value. However, the improvement was approximately 30 %, while thermal conductivity was doubled by increasing the water content to the OMC but without extra compaction.

This investigation nailed that water content was more dominant factor on thermal conductivity than compaction energy. This finding provided a

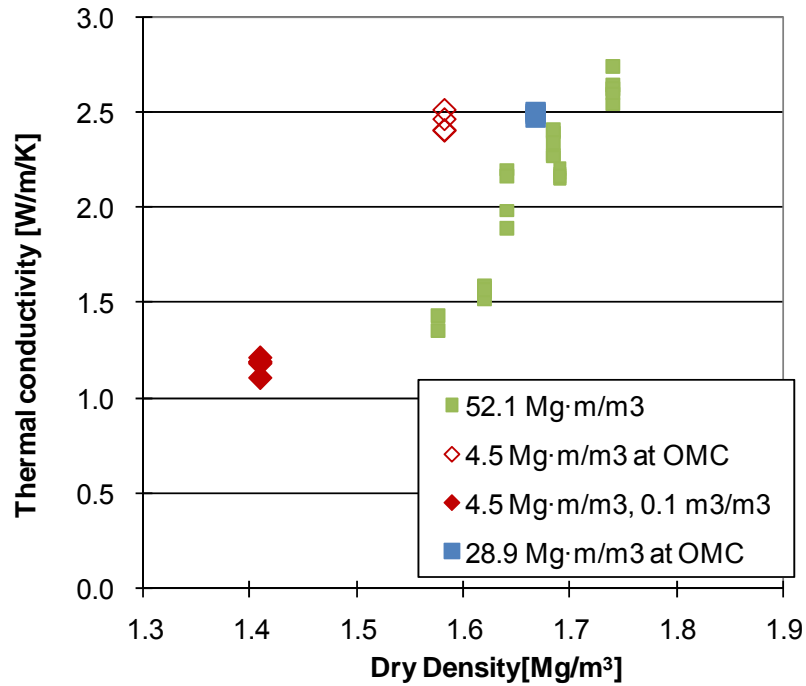


Figure 5.33 Thermal conductivity against density

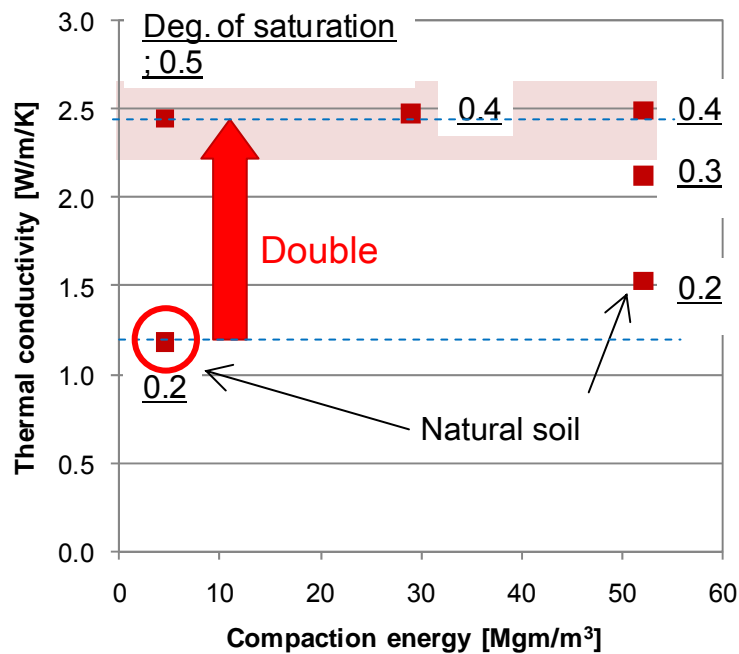


Figure 5.34 Effects of compaction energy on thermal conductivity

Chapter 5 Optimisation of Soil Thermal Properties for the GSHP

useful indication for practical construction. Mixing rainwater up to the OMC with the original soil might significantly enhance thermal conductivity without compacting on construction site. This will save labour and construction cost for bringing heavy machinery to the site.

It is of importance to estimate the impact of doubled soil conductivity on heat extraction in the underground system. This could be approximated from simulation results in section 4.5.3. When thermal conductivity increased from the original value, 1.7 W/m/K, to the double value, 3.4 W/m/K, the heat output was expected to rise by 5.8 %. This result was based on the calculation model included a rainwater collection tank but without water circulation inside. It is obvious that the impact could be different with different underground designs. Hence, various underground designs are compared through simulation analysis in Chapter 6. In addition, it is essential to estimate the annual effect, when higher thermal conductivity is maintained for a whole year. Hence, a yearly operation is simulated in Chapter 7.

Further experiment was attempted to make sure achievable thermal conductivity on construction sites. It was noticed that the condition for the OMC rarely goes beyond air void line 5 % as illustrated in Figure 5.27. Therefore, extra compaction energy was applied after natural soil reached the OMC. The extra compression on granular particles was expected to increase the contact area in between in comparison to that of point contact (Ewing et al., 2007).

Chapter 5 Optimisation of Soil Thermal Properties for the GSHP

The results displayed that the compaction after reaching the OMC raised both dry density and thermal conductivity (Figure 5.35). However, the improvement was saturated around compaction energy of 30 $\text{Mg}\cdot\text{m}/\text{m}^3$ and the maximum effect was approximately 5%. The achieved dry density was $1.74 \text{ Mg}/\text{m}^3$, which was on air void 5% line (Figure 5.27), which implied that removing all the air voids was impossible with a combination between water mixing and compaction. On the other hand, the achieved thermal conductivity was $2.64 \text{ W}/\text{m}/\text{K}$, which was as high as that of soil compacted with $52.1 \text{ Mg}\cdot\text{m}/\text{m}^3$ in Figure 5.32. Consequently, the compaction after water mixing up to the OMC was worthwhile if 5% of enhancement will pay off the additional labour and construction costs. This option is compared in heat transfer efficiency in section 5.8.

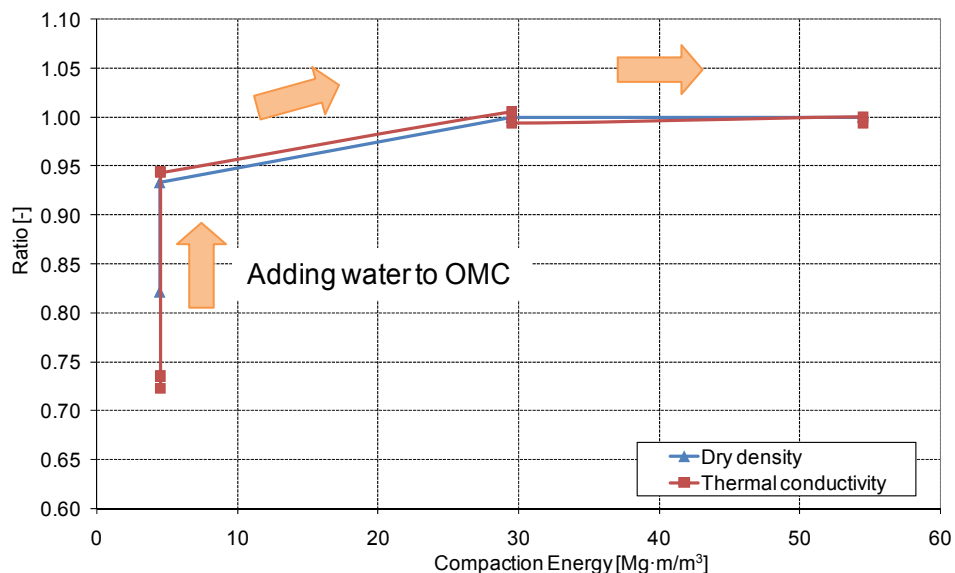


Figure 5.35 Effects of compaction energy after water mixing up to the OMC

Chapter 5 Optimisation of Soil Thermal Properties for the GSHP

5.7.2 Enhancement of dry density attained by packing ratio

When water was added to the oven-dried samples in an industrial mixer, the large proportions of silt and clay turned into lumps straightaway. This was because small voids were created in between and held water strongly (Barnes, 1995). As a result, extra compaction energy apart from 4.5 Mg·m/m³ was applied to achieve dry density at the OMC, 1.7 Mg/m³. The results are plotted at around 0.8 of degree of saturation and 2.5 W/m/K in Figure 5.36. Though the degree of saturation was much larger than that of the original soil, the achieved thermal conductivity was not particularly enhanced with the samples at the maximum packing ratio.

Extra compaction energy was applied until the volume stopped increasing with sample 0.225 (Figure 5.37). Both thermal conductivity and dry density

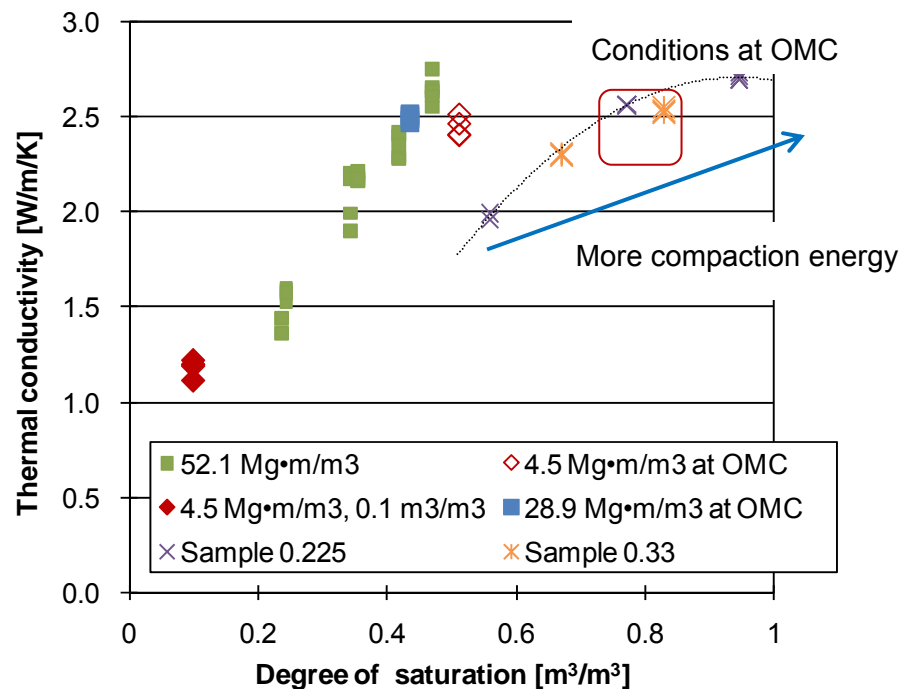


Figure 5.36 Effects of high packing ratio at the OMC

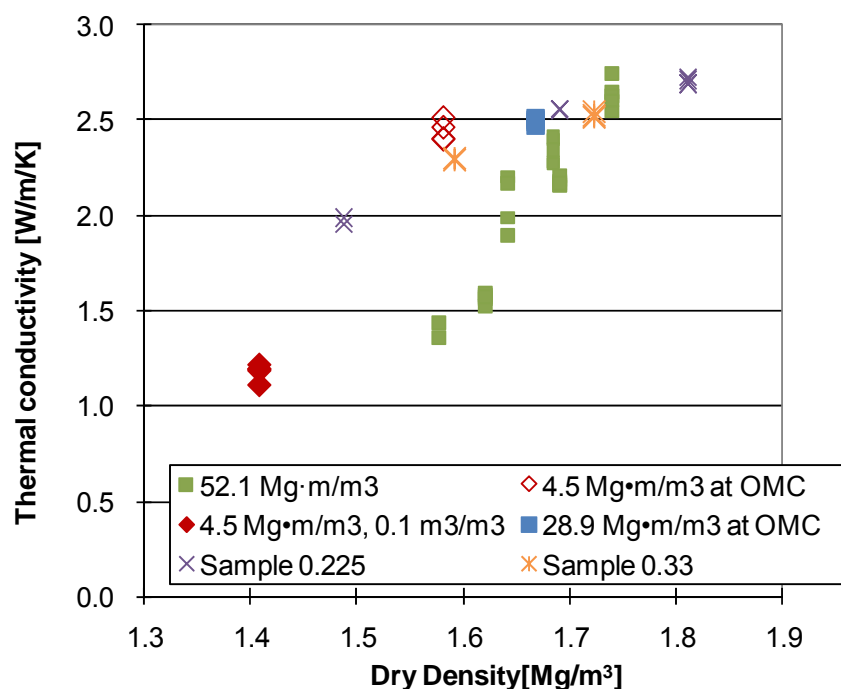


Figure 5.37 Effects of high packing ratio at the OMC against dry density

increased; however, these values seemed to be saturated as degree of saturation became closer to 1.0. It could be seen that even if degree of saturation was almost the highest due to the high packing ratio, obtainable thermal conductivity was not modified from that of non-compacted original soil at the OMC.

Sample 0.33 contained less silt and clay; however, aggregation was still seen instantly after adding water. This prevented from mixing soil particles uniformly; therefore, water needed to be added gradually while the sample was stirred and compacted as the process in compaction test. As a consequence, preparing the original soil at the OMC without compaction is easier and more practical, since the enhancement of thermal conductivity

Chapter 5 Optimisation of Soil Thermal Properties for the GSHP

was almost none. Even though compaction increased thermal conductivity; blending to fit the ideal curve was labour intensive. When compaction is applicable, compacting natural soil at the OMC will be more feasible to achieve similar thermal conductivity.

5.7.3 Contribution of additional water content

The investigation of sectional water content in sample 4.5 indicated inhomogeneous water suction in Table 5.9. Since there were larger cracks along the walls than the centre of the sample, water flowed near the walls or to the bottom rather than being absorbed at the centre. Moisture content was meant to be 26.5 % in the end; however, the average value was 24.54 %. The obtained thermal conductivity was for soil around the sensor; therefore, the correspondent moisture content ought to be the value at number 4, 19.24 %. Subsequently, the moisture content between the first

Table 5.9 Sectional moisture content in sample 4.5

Sampling number	Moisture content %	
1	23.64	
2	20.86	
3	22.61	
4	19.24	
5	18.82	
6	22.41	
7	32.87	Largest difference
8	30.13	14.05 %
9	30.29	0.43 -
		Average
		24.54 %

Chapter 5 Optimisation of Soil Thermal Properties for the GSHP

and the second to the last water addition was estimated proportionally to the water volume added each time.

The patterns of thermal conductivity are plotted in Figure 5.38. The more water was sprayed, the more both series of data increased. However, the values were lower than that of the compacted natural soil at the same degree of saturation. The trendlines indicated that both samples would end up with similar maximum thermal conductivity, approximately 2.5 W/m/K, when degree of saturation reaches 1.0. This value was equivalent to the maximum value that could be achieved during this experimental analysis. Hence, there is a possibility to achieve equally high thermal conductivity with water absorption. Nevertheless, filling all the air voids by capillary action

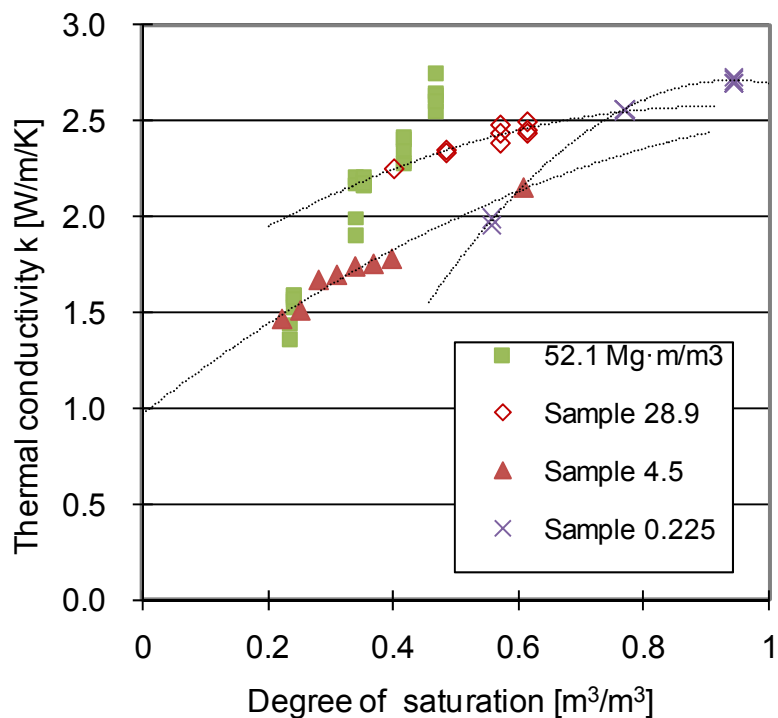


Figure 5.38 Change of thermal conductivity through water absorption

Chapter 5 Optimisation of Soil Thermal Properties for the GSHP

looked more difficult than water mixing and compression. The sectional water content showed that water content at the surface and bottom was larger than that of mid height. This indicated that air voids were likely to be replaced by water near the water-soil boundaries; however, the driving force for suction effect could drop as the distance from the boundaries became larger. In consequence, water mixing could secure more homogeneous water distribution.

The results were compared with the estimated values based on Campbell's theory in Figure 5.39. The estimated quartz proportion to all solids was 0.70 for sample 4.5 and 0.78 for sample 28.9. The difference between the experimental and the estimated data was in a range of $\pm 12.0\%$ with sample 4.5 and $\pm 0.5\%$ with sample 28.9. These values could indicate that

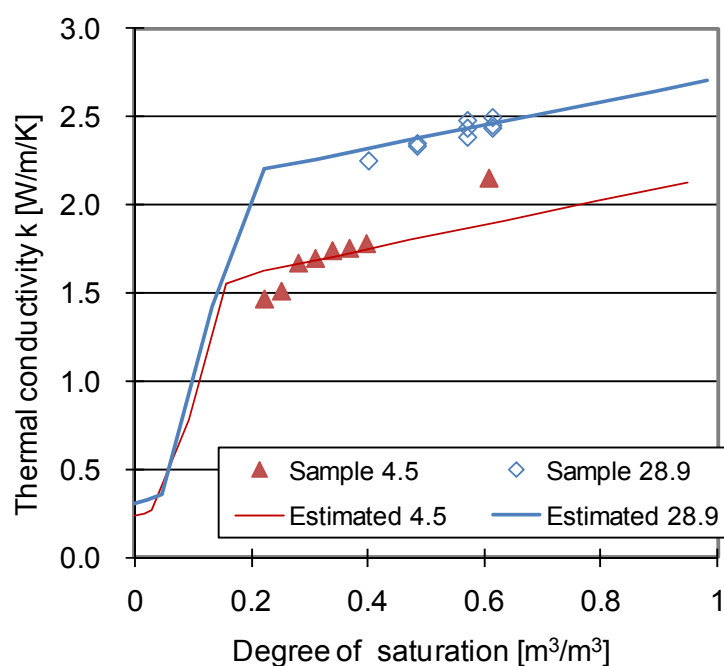


Figure 5.39 Comparison to theoretically estimated thermal conductivity

Chapter 5 Optimisation of Soil Thermal Properties for the GSHP

Campbell's theory estimated thermal conductivity more effectively, when water content varied due to water suction compared with due to water mixing. When thermal conductivity was predicted for a whole range of degree of saturation, a clear divergence could be seen around degree of saturation of 0.2 in the theory. This area was where the largest difference between the measured and the calculated results tended to be seen. Particularly, the values with samples made by water mixing were larger in comparison to the samples measured with water spraying. The former samples seemed to show more linear relation between thermal conductivity and degree of saturation as displayed in Figure 5.16. The effect of continuous water absorption is explained by a role shift of the added water from contributing to surface sorption to creating tighter particle contacts with capillary bridges (Ewing et al., 2007). Therefore, it is possible that relatively uniform water distribution by water mixing created capillary bridges from lower degree of saturation.

5.8 Evaluation in Heat Transfer Efficiency

There were several design options to reach the highest thermal conductivity among the study cases. Nevertheless, more essential factor than thermal conductivity in underground storage space is thermal effusivity, which is a square root of the ratio of thermal conductivity and heat capacity (Verma et al., 1990). The large value indicates both large storage capacity and efficient heat transfer. Some advantageous strategies for soil modification were compared in Table 5.10. All the soil modifications managed to increase thermal effusivity from the original state. Regarding that blending to the maximum packing ratio

Chapter 5 Optimisation of Soil Thermal Properties for the GSHP

Table 5.10 Comparison in thermal effusivity

		Water	Air	Natural soil	Natural soil at OMC	Sample 0.33 at OMC	
Compaction energy	Mg·m/m ³			4.5	originally 4.5 and extra 30	4.5	
Thermal conductivity	W/m/K	0.61	0.03	1.20	2.64	2.50	
Density ²⁾	kg/m ³	996.50	1.20	1,543.00	1,740.00	1,780.00	2,013.00
Specific heat	kJ/kg/K	4.18	1.01	1.11	0.99	1.15	1.12
Thermal eiffusivity ³⁾	Ws ^{0.5} /m ² /K	2,543.00	0.00	2,064.00	4,532.00	5,125.00	5,625.00
	-			1.00	2.20	2.48	2.73

1) Data for water and air was at 25 °C (Holman, 2002)

2) Bulk density for soil

3) $\beta_{eff} = (k/\rho Cp)^{0.5}$, $Ws^{0.5}/m^2/K$

was too labour intensive, preparing for the OMC was more recommended option. Since extra compaction did not create advantage, mixing water to natural soil for the OMC was the best strategy.

5.9 Conclusions

Preparation to measure soil thermal properties with the DPHP was conducted, including calibrations and error analysis. The sensors were calibrated in association with heater resistance, probe distance and the presence of air layers. The relative expanded uncertainty of a sample mean with confidence of 95 % after two kinds of calibration was 5.0 % and 3.0 % for each sensor.

The characteristics of the original soil samples were investigated by seeking particle distribution and the OMC. Subsequently, the association between thermal conductivity and water content was clarified with the HFM and the DPHP. Though the tendency matched between the two methods, the delivered values

Chapter 5 Optimisation of Soil Thermal Properties for the GSHP

were different due to the different measuring mechanisms. Since the DPHP measures without regenerating moisture gradient within samples unlike the HFM, the results with the DPHP were used for the design optimisation of underground heat collection in the next chapter.

The effects of more proportion of large particles (gravelly soil) were explored. The analysis of the scanned images demonstrated that the gravelly soil had smaller porosity with smaller mean pore size than the original sandy soil. This result justified that blending to make the particle distribution closer to the ideal curve was one of the indications for dense packing. The measurements of thermal conductivity revealed that the large density derived from higher packing ratio contributed to enhance conductivity as well as larger water content did. Creating soil samples in the state of natural soil was tackled. Referring to the typical dry density and moisture content of sub-soil, the required compaction energy was quantified through a compaction test.

Samples with different compaction energy and packing ratio were compared with natural soil, in terms of thermal conductivity. It was disclosed that preparing soil samples at the OMC led to the highest level of thermal conductivity that the original soil could achieve. In addition, water mixing was more efficient method for enhancing thermal conductivity than spraying water after packing soil particles. As a result, the soil at the OMC without extra compaction was the most feasible and advantageous to enhance heat transfer.

The next chapter intends to explore underground heat collection structure with

Chapter 5 Optimisation of Soil Thermal Properties for the GSHP

the soil modification through simulation analysis. The use of carbon fibres is particularly investigated.

Chapter 6 Design Optimisation of Underground Structure with Modified Soil

Introduction

It was beneficial to find a simple strategy to enhance soil thermal effusivity in the previous chapter. Therefore, the next process is to specify the underground designs to maximise the effects. Since the use of convective heat transfer within a rainwater collection tank was effective in Chapter 4, other design possibilities are discussed. Essential features to increase the effect of convective heat transfer are summarised according to the past research results. As a result, a design idea is suggested in combination with obliged facilities, septic tanks.

Twenty designs of the underground heat collection structure are examined through a simulation analysis with FLUENT. The standard model is set with horizontal slinky coils, which exchange heat with underground soil without a rainwater collection tank. The calculation is conducted mainly in two dimensions and the calculation is simplified to steady state. Ten study cases are created with different depth of heat exchanger and thermal conductivity of the modified soil space. Other four cases are for identifying the effects of solar gain. Moreover, design optimisation of thermal pillars containing carbon fibres is inspected by studying different length, the number of sub-roots, thermal conductivity and diameter. Consequently, the effects of thermal pillars and simple soil modification are compared in between.

6.1 Design Potentials with Convective Heat Transfer

It is commonly understood that convective heat transfer is more efficient than conductive heat transfer. Many studies have attempted to apply this effect into the designs of the GSHP. In order to develop financially reasonable methods, some try to combine with a complimentary water source, rainwater, as introduced in section 2.2.3. It is of essence to make sure convection occurs in the systems as discussed in section 4.3.2. However, adding an extra pump for circulation is not an economic option, since the small energy density of ground heat source has a difficulty to create sufficient cost performance. Hence, it is crucial to design regular water circulation with neither extra gadgets nor extra energy consumption, such as a simple rainwater retaining trick suggested in section 4.3.2.

It is known that the presence of underground water or water table is advantageous in underground heat collection. Even if the flow rate is low, heat transfer could be improved (Gehlin et al., 2003). However, Lim et al. (2007) find that the natural convection generated by groundwater effects below 3 m deep. Ismail et al. (2008) mention that the depth of groundwater table in sandy or gravelly sand can be considerably deeper than 1 to 3 m. Therefore, it can be difficult to create a positive impact using the targeted shallow heat collection system in a combination with groundwater. In addition, Hellström ([no data]) adds that the effects of groundwater movement is valid only at high temperatures, such as in solar heating systems.

Some research oppose to the positive results introduced above. The British Standard (1998) concludes that the effect is negligible unless the flow rate is

Chapter 6 Design Optimisation of Underground Structure with Modified Soil

high. Computer simulation also supports that the influence is insignificant for normal cases, even if groundwater is assumed to move homogeneously (Eskilson, 1987). The other negative side could be that groundwater movement reduces thermal resistance by 10 % and contributes to lose the stored energy (Hellström, [no date]). A strategic prevention is advisable for sandy soil, since the velocity is normally 0.15 to 15 m/day (Harter, 2003). This is beyond 0.05 m/day, which the heat loss becomes non-negligible.

The presence of groundwater could improve efficiency; however, this advantage should be only bonus for the shallow heat collection systems and should not be expected as a part of design capacity. Therefore, it is better to concentrate on designing for creating and retaining ideal water content. Even if heat collection space is not under water table, water may transmit to raise water content. Therefore, design methods which do not refuse this potential advantage ought to be considered.

One of the good practices to retain moisture in sub-soil is a use of septic tanks. For instance, the UK government has obliged rural areas and newly developed housings to install individual drainage systems to prevent potential floods by run-off water or storm water (Building Control Section Planning & Transport Angus Council, [no date]). The purpose is known as Sustainable Urban Drainage Systems (SUDS) and the details are ruled by the Building Regulations Part H3 2002 edition and the Planning Policy Guidance Note 25. Septic tanks are normally buried underground to collect run-off water and release it to greater depth gradually. If a tank with holes at the base is chosen, it is advantageous to install the heat exchanger under the tank. As the collected rainwater is fed into

the soil regularly, moisture content is maintained higher than that in the ordinary state.

6.2 Simulation Models

Heat collection capacity was compared among various kinds of underground structure in FLUENT. Though the second attempt was for examining the effect of solar gain, the rest was design optimisation to extract the criteria for efficient operation.

6.2.1 Standard model

Sensitivity analysis was conducted based on a standard model. The two dimensional model consisted of air, a slinky coil, modified soil space and sub-soil (Figure 6.1). The duration for the calculation was reduced by applying symmetric boundaries in the centre of the slinky coil. The calculation area was limited up to 2 m high from the ground level in air, up to 7 m wide in horizontal distance from the centre of the slinky coil and up to 12 m deep underground.

The loops of the slinky coil were assumed to be horizontally laid, 9 loops per meter with the loops overlapping every 0.11 m. The two dimensional model was supposed to express cross sectional view; therefore, small rectangular represented a slinky coil. The total heat exchange area per meter of installation was 1.09 m. Since the commercialised slinky coil has a 0.019 m diameter, 8 rectangular of 0.02 m high and 0.05 m wide were laid at intervals of 0.075 m. Thus, the total heat exchange area was within 1 m horizontally, which was a diameter of the slinky loop.

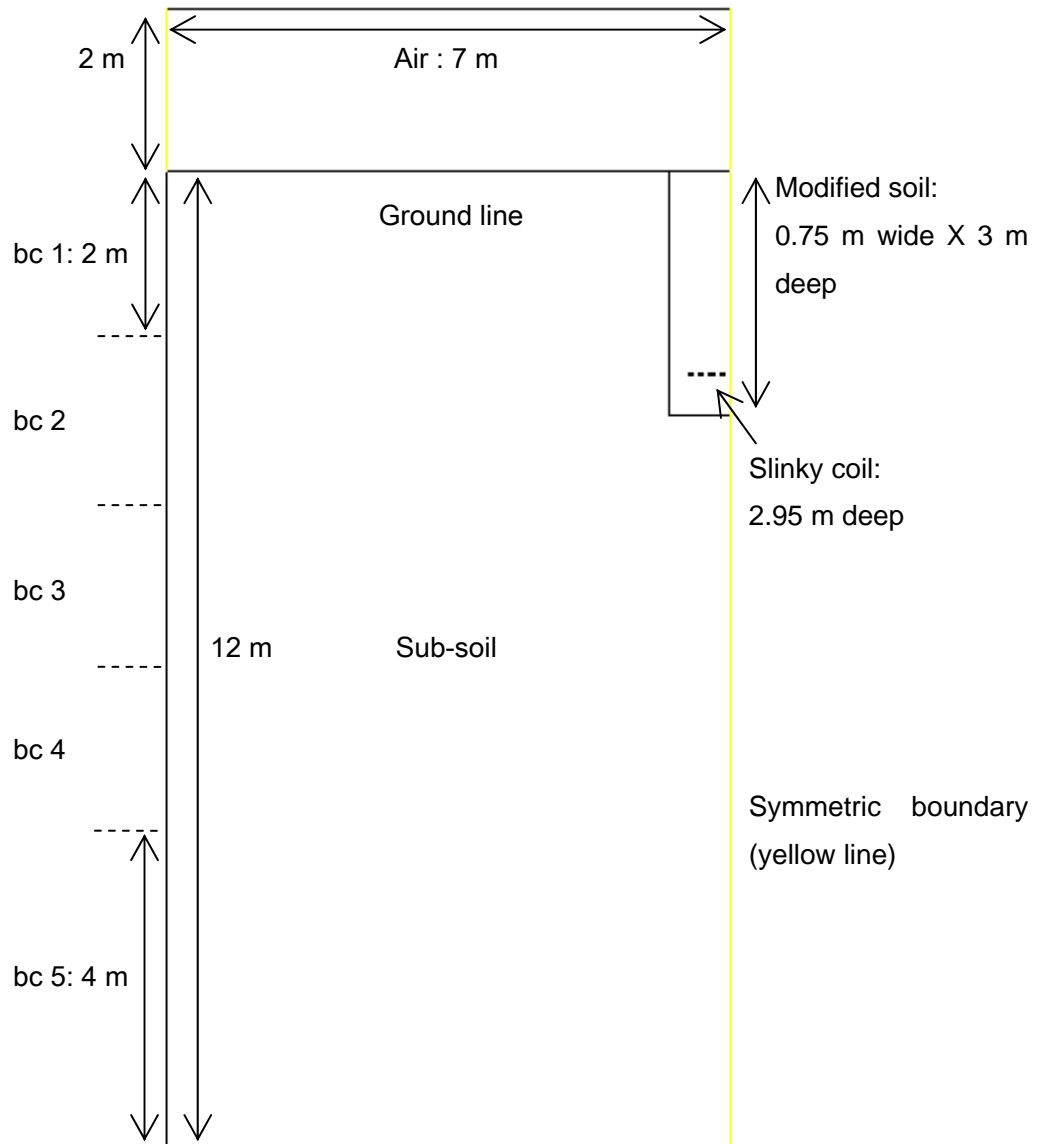


Figure 6.1 Simulation model in FLUENT

The measured thermal conductivity were applied for sub-soil and modified soil; 1.2 W/m/K and 2.5 W/m/K respectively. The same values were used for air and grass as those for the first design analysis listed in Table 4.6. Sensitivity analysis was studied for winter in Nottingham; therefore, the set temperatures were the same as the values in Table 4.7. Heat collection capacity was defined, when the average surface temperature on the heat exchanger reached 273.15 K.

Chapter 6 Design Optimisation of Underground Structure with Modified Soil

6.2.2 Effects of different depth of heat exchanger

The first parameter was the depth where the heat exchanger is placed. As underground temperature gradient varies depending on depth, collectable thermal energy would vary. Since shallower construction costs less, investigating the impact is of essence. Thermal conductivity of the modified soil space was set as either that of sub-soil or the modified soil to compare with the same study models listed in Table 6.1.

6.2.3 Effects of solar gain

Solar gain could be more influential on the shallow heat collection systems than borehole systems. When low ambient temperature in winter encourages excessive heat loss from the stored thermal energy underground, inserting insulation layer in between would be required. On the contrary, if solar gain provides extra thermal energy into the storage space, leaving highly conductive space near the ground surface would be a better operation tactic.

The extra heat gain from solar energy was set on the ground line. Dedeczek et al. (2006) find that the average temperature under 0.02 m of grass is

Table 6.1 Study cases with different depth of heat exchanger

Case	Depth m	
Lh-1	2.95	Standard
Lh-2	2.50	
Lh-3	2.00	
Lh-4	1.00	

Chapter 6 Design Optimisation of Underground Structure with Modified Soil

1.1 °C higher than ambient temperature as a result of three years measurement. The average ambient temperature during daytime in December was 5.59 °C between 2001 and 2005 in Nottingham. Therefore, the input temperature was 6.68 °C. As a consequence, air was not included in the calculation. Heat extract was calculated with different depth of heat exchanger as they were set in section 6.2.2, case Ldy-1 to Ldy-4.

6.2.4 Effects of modified soil

Soil thermal conductivity for the modified soil space was compared between sub-soil, the modified soil at the OMC and the modified soil at the OMC and extra compaction. As measured in Chapter 5, the value of the third condition was 2.64 W/m/K. Each study case was named case kmod-1, kmod-2 and kmod-3 respectively. Heat capacity and density are not reflected in two dimensional calculations in FLUENT; therefore, only the effect of thermal conductivity was evaluated. The depth of heat exchanger was selected after discussing the results in the previous analysis.

6.2.5 Effects of length of thermal pillars

An idea of thermal pillars was examined after this section. This intends to explore a more economic and efficient enhancement than mixing quartz. The pillars were assumed to be created by the deep injection technique which was introduced in section 2.4.3. A tube was inserted through a drilled hole and a mixture of highly conductive grout and substances, such as carbon fibres, was planned to be injected. Stainless steel was selected as a material for the tube, since the leaching of polluting ions was necessitated to be avoided as explained in section 2.4.2.

Chapter 6 Design Optimisation of Underground Structure with Modified Soil

In calculation models, a thermal pillar was attached to a part of the heat exchanger as illustrated in Figure 6.2. Since the setting was symmetric, the pillar was in effect calculated as if a vertical plate with endless length. Essential parameters were extracted in the two dimensional models with different length, sub-roots, thermal conductivity and diameter of thermal pillars. Consequently, the effect on the overall heat extraction was calculated in a three dimensional model with the best design case (section 6.2.9).

A company which provides the deep injection, Uretek, drills holes of a 0.15 m diameter; therefore, a diameter of stainless tube was set as 0.2 m in the calculation models. 1.4 % of high grade carbon fibres with thermal conductivity of 540 W/m/K was assumed to be efficiently mixed with the most conductive commercialised grout, Mix 111 with 2.42 W/m/K (Silvain et

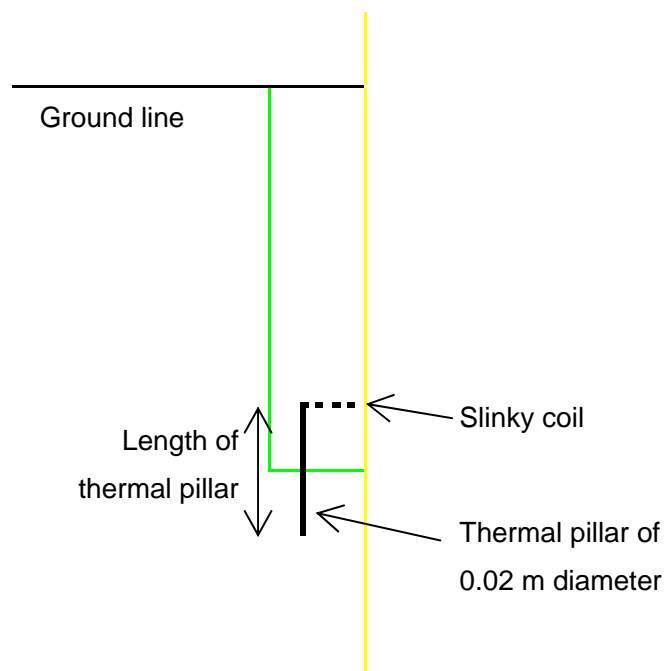


Figure 6.2 Thermal pillar in simulation model

al., 2008). Referring to the experimental results delivered by Fukai et al. (2000, section 2.4.3), 70 volume% of the added carbon fibres seem to contribute to improve the total thermal conductivity. Hence, a value 7.8 W/m/K was approximated, while the value for the tube, 15 W/m/K, was referred to the database summarised by Holman (2002). The depth of heat exchanger and thermal conductivity in the modified soil space were selected after examining the previous analysis. Solar gain was not considered; therefore, air above the ground level was concluded into the model. Studied cases with a length of 0 m, 1.0 m, 1.5 m and 2.0 m were named as case Lh-2 and Ltp-1 to Ltp-3 respectively.

6.2.6 Effects of sub-roots added to thermal pillars

The pillars would encourage heat transfer only for little space; therefore, creating conductive extension from the pillars was examined. It was ideal that root shaped extension was connected to the pillars themselves and was spread into voids underground as reported in section 2.4.3. Simultaneously, the construction cost was required to be low. Therefore, the injection of highly conductive grout through the holes of stainless steel tubes was proposed (Figure 6.3). Though the number and the length of each sub-root entirely depend on the distribution of underground voids around the pillar, this must be one of the methods that would cost the minimum.

The effect of sub-roots was compared among three kinds of simulation cases built on case Ltp-2 with 1.5 m of thermal pillars. Length of roots was set as 0.2 m on each side, while the number of sub-roots differed (Figure 6.4

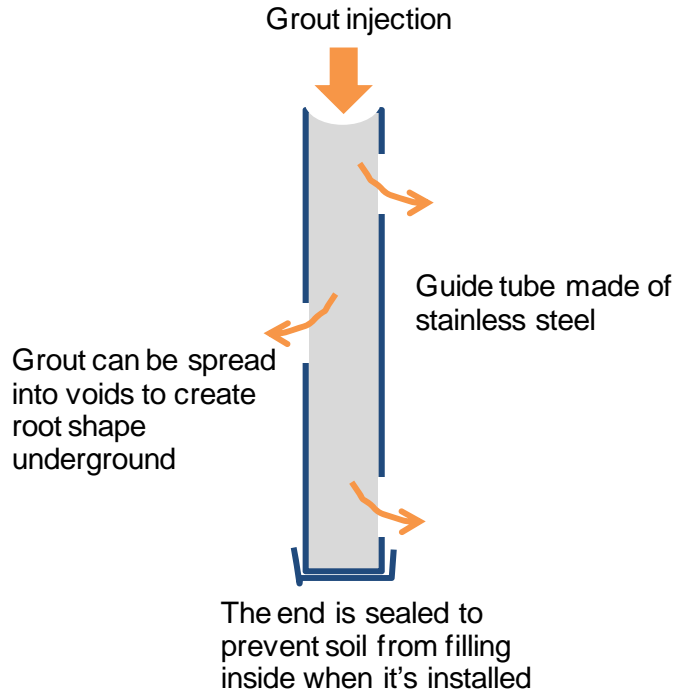


Figure 6.3 Image of grout injection to create sub-roots added to thermal pillars

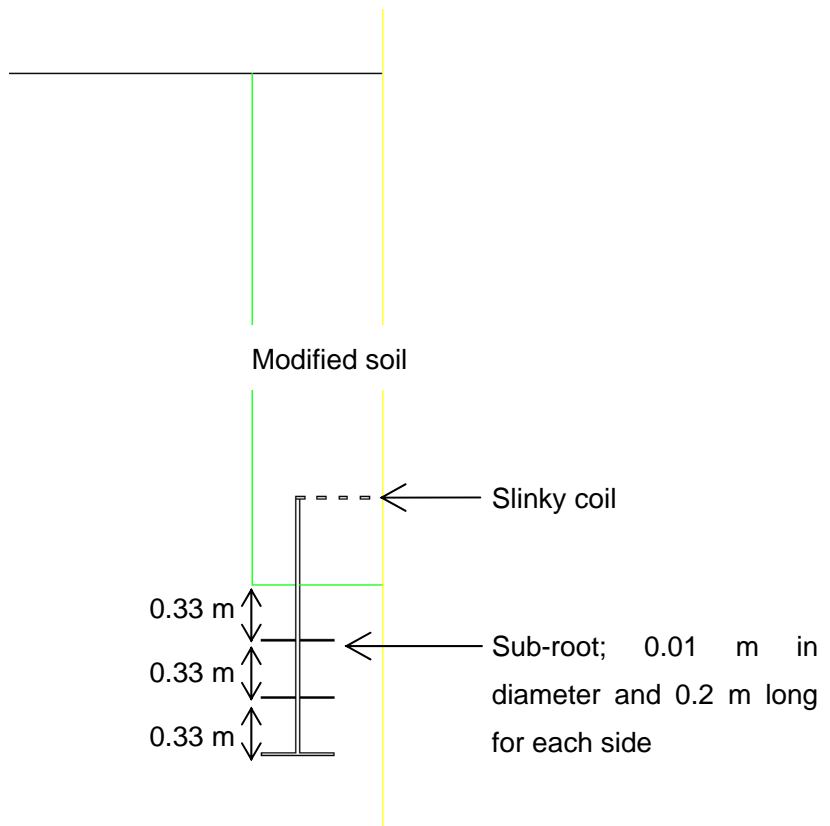


Figure 6.4 Calculation model with sub-roots, case Nsr-3

and Table 6.2). Thickness of sub-roots was set as 0.01 m.

6.2.7 Effects of thermal conductivity of thermal pillars

Different thermal conductivity of thermal pillars was studied as listed in Table 6.3. The base model was selected in accordance to the results of the previous analysis.

Table 6.2 Study cases with different number of sub-roots

Case	Number of sub-roots pair	Position
Standard	0	
Nsr-1	1	Only bottom
Nsr-2	2	Bottom and 0.5 m from bottom
Nsr-3	3	1/3 and 2/3 of pillar length and bottom

Table 6.3 Study cases with different thermal conductivity of thermal pillars

Case	Thermal conductivity of pillar W/m/K	Equivalent ratio of carbon fibre ¹⁾ volume%
Standard	7.8	1.4
ktp-0	2.4	0.0
ktp-0.7	5.1	0.7
ktp-1	13.2	2.9
ktp-2	18.5	4.3
ktp-3	29.3	7.2
ktp-4	45.4	11.4

1) 70 volume% of added carbon fibres were assumed to contribute to the total thermal conductivity (section 2.4.3).

Chapter 6 Design Optimisation of Underground Structure with Modified Soil

6.2.8 Effects of diameter of thermal pillars

Different diameter of thermal pillars was inspected; 0.03 m in case Ttp-1 and 0.04 m in case Ttp-2.

6.2.9 Effects of thermal pillars in three dimensional calculation

More realistic comparison between with and without thermal pillars was conducted in three dimensional calculation models. A model without and with pillars are displayed in Figure 6.5 and Figure 6.6 respectively. Pillars were assumed to be attached to the outer edges of the slinky coil on alternating sides at intervals of 0.25 m. Therefore, sliced space with a 0.25 m width was calculated. Pillars with many sub-roots were simplified into stainless steel pipes with rectangular cross section and rectangular

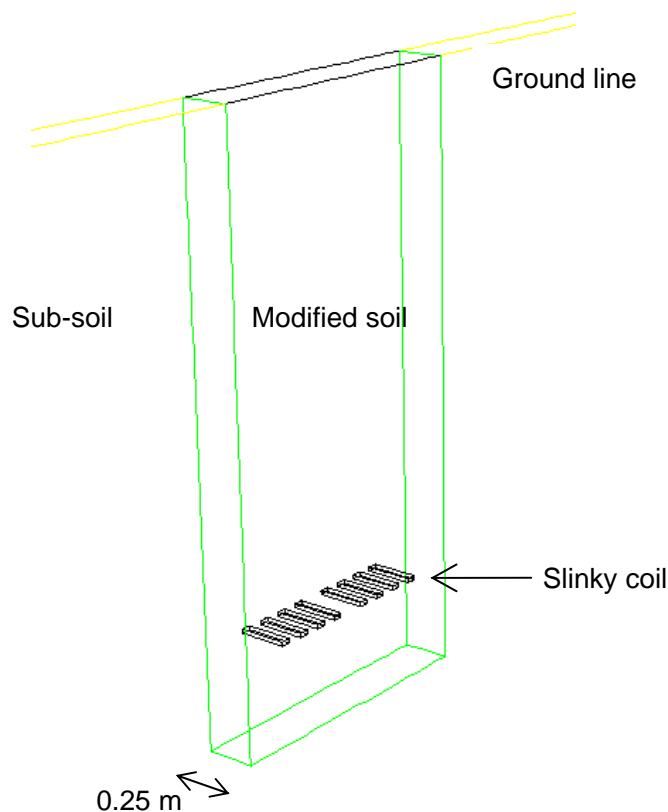


Figure 6.5 Calculation model without thermal pillars

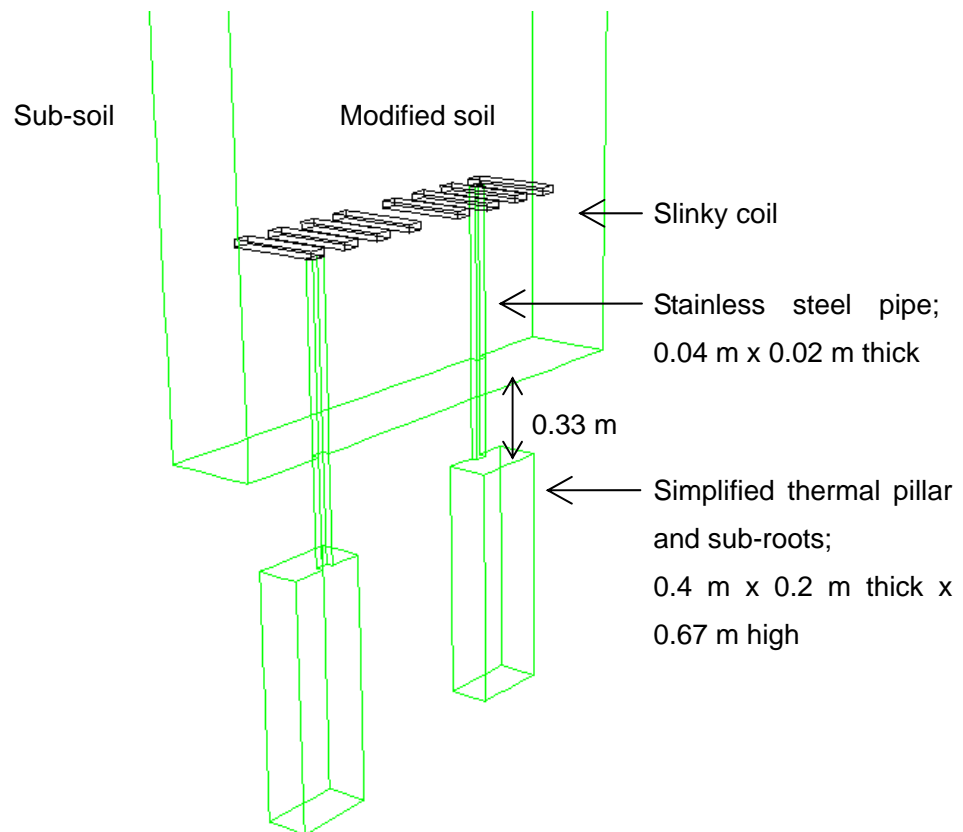


Figure 6.6 Calculation model with thermal pillars

sub-roots, which was filled with highly conductive grout and connected to the pipes. The geometry was assumed to be stretched radially. Since symmetric boundary area was set in the centre of each thermal pillar, a half volume of the pipes and the conductive space was modelled.

6.2.10 Effects of modified soil space

The last parameter for the sensitivity analysis was width or depth of the modified soil space. Study cases are listed in Table 6.4.

Table 6.4 Study cases with different depth and width of modified soil space

Case	Modified soil space	
	Depth m	Width m
Standard I	0.0	0.0
Standard II	3.0	1.5
Dmod-1	3.5	1.5
Dmod-2	4.0	1.5
Wmod-1	3.0	2.0
Wmod-2	3.0	2.5

6.3 Results of Sensitivity Analysis

Results for each sensitivity analysis and discussion are presented below.

6.3.1 Different depth of heat exchanger

Results are presented in Table 6.5 and Figure 6.7. Since the ambient temperature was lower than the underground temperature, heat flux was small with shallower location of slinky coil. However, study cases with the modified soil, whose thermal conductivity was 2.5 W/m/K, showed a little more efficient heat collection with a 2.5 m depth than that with a 2.95 m depth. This indicated that a slinky coil with conductive soil of a certain thickness both above and below it was also effective. Though the advantage was only 0.5 %, a 2.5 m depth was used as a base for the rest of sensitivity analysis.

6.3.2 Solar gain

Results indicated a significant impact of solar gain on heat flux (Table 6.6).

Table 6.5 Simulation results with different depth of a slinky coil

Thermal conductivity of modified soil space	Case		Lh-1	Lh-2	Lh-3	Lh-4
1.2 W/m/K (sub-soil)	Depth of slinky coil	m	2.95	2.50	2.00	1.00
	Heat flux ¹⁾	W/m ²	-17.50	-16.80	-16.07	-14.00
	Total flux ²⁾	W/m long	19.60	18.80	18.00	15.70
	Ratio of improvement ³⁾	W/m	-1.70	-1.60	-2.30	
2.5 W/m/K (modified soil)	Depth of slinky coil	m	2.95	2.50	2.00	1.00
	Heat flux ¹⁾	W/m ²	-19.80	-19.90	-19.22	-17.00
	Total flux ²⁾	W/m long	22.20	22.30	21.50	19.00
	Ratio of improvement ³⁾	W/m	0.20	-1.50	-2.50	

1) The maximum heat extract, in which the average temperature on the heat exchanger surface reached 0 °C

2) For every meter of installation

3) Improvement of total flux per increase in depth of slinky coil

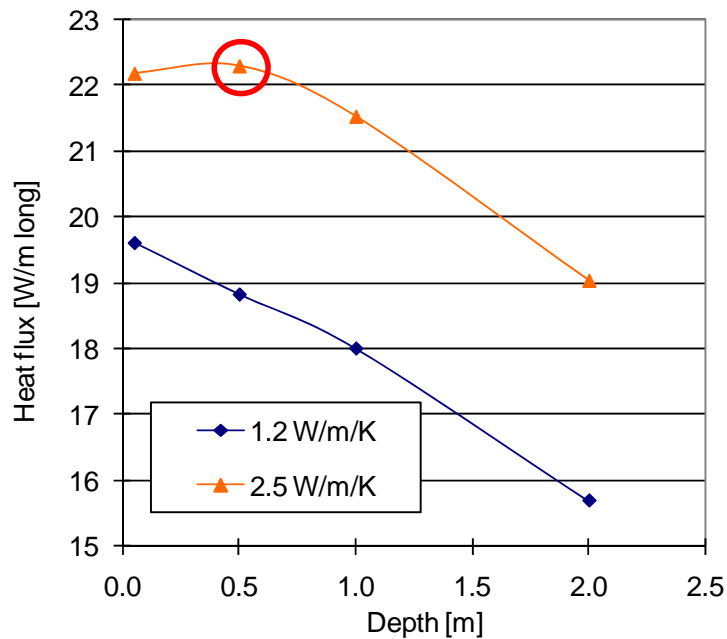


Figure 6.7 Heat flux with diferent depth of a slinky coil

The shallower the location of slinky coil was, the larger the total heat flux became. When the results of case Lh-1 to Lh-4 were combined to estimate daily heat flux, designs with shallower depth was more advantageous. This

Table 6.6 Simulation results with solar gain

Case		Ldy-1	Ldy-2	Ldy-3	Ldy-4
Depth of slinky coil	m	2.95	2.50	2.00	1.00
Heat flux ¹⁾	W/m ²	-24.30	-26.84	-29.40	-40.20
Total flux ²⁾	W/m long	27.20	30.10	32.90	45.00
Ratio of improvement ³⁾	W/m	6.40	5.70	12.10	
Daily heat flux ⁴⁾	Wh/m long	286.69	311.11	333.51	429.87
Ratio of improvement ³⁾	W/m	54.30	44.80	96.40	

1) The maximum heat extract, in which the average temperature on the heat exchanger

2) For every meter of installation

3) Improvement of total flux per increase in depth of slinky coil

4) Calculated from results of case Lh-1 to Lh-4 with 2.5 W/m/K and average night time in December, 2.5 h, from weather data between 2001 and 2005 in Nottingham during working hour, 8am to 7pm.

was because daytime was longer than night time during the working hour, 8 am to 7 pm. When movable insulation was applied during night, the effect would be even more increased. These results demonstrated that the heat flux near the ground surface during daytime required less effort to be enhanced. Therefore, the design analysis was continued for enhancing heat collection from greater depth without solar gain.

6.3.3 Thermal conductivity of modified soil space

Results showed that high thermal conductivity of the modified soil space enhanced heat flux (Table 6.7). Heat flux in case kmod-2 was increased by 18 % compared to case kmod-1 due to approximately double thermal conductivity. Regarding that 3.82 times larger thermal conductivity was required for the similar enhancement in cases with a rainwater collection tank in section 4.7.3, the impact of thermal conductivity in the modified soil space was larger in cases with horizontal slinky coil. This could imply that the enhancement of soil thermal conductivity was more effective when heat

Chapter 6 Design Optimisation of Underground Structure with Modified Soil

Table 6.7 Simulation results with different thermal conductivity of the modified soil space

Case ¹⁾		kmod-1	kmod-2	kmod-3
Thermal conductivity of modified soil space	W/m/K	1.20	2.50	2.64
Heat flux ²⁾	W/m ²	-16.80	-19.90	-20.10
Total flux ³⁾	W/m long	18.80	22.30	22.50
Ratio of improvement ⁴⁾	W/(W/mK)		2.70	1.60

1) kmod-1 and kmod-2 were the same as case Lh-2 with 1.2 W/m/K and 2.5 W/m/K respectively

2) The maximum heat extract, in which the average temperature on heat exchanger

3) For every meter of installation

4) Improvement of total flux per increase in thermal conductivity of the soil modified

was collected without the contribution of thermal energy in rainwater. This was discussed more in section 7.1.2.

Ratio of improvement did not drop significantly within the examined variation of thermal conductivity of the modified soil space. However, the enhancement of the total flux by extra compaction from case kmod-2 to kmod-3 dropped to 1 %. Therefore, thermal conductivity in case kmod-2 was chosen for the rest of analysis.

6.3.4 Length of thermal pillars

Longer pillars collected more thermal energy; however, the effect was 1.5 % between no pillars and 2.5 m long (Table 6.8). Ratio of improvement dropped after a 1.5 m long; therefore, the following analysis was conducted on the basis of case Ltp-2.

Table 6.8 Simulation results with different length of thermal pillars

Case		Lh-2	Ltp-1	Ltp-2	Ltp-3
Length of thermal pillars	m	0.00	1.00	1.50	2.50
Heat flux ¹⁾	W/m ²	-19.90	-20.04	-20.10	-20.20
Total flux ²⁾	W/m long	22.30	22.40	22.50	22.60
Ratio of improvement ³⁾	W/m		0.15	0.14	0.11

1) The maximum heat extract, in which the average temperature on the heat exchanger surface

2) For every meter of installation

3) Improvement of total flux per increase in length of thermal pillars

6.3.5 Sub-roots of thermal pillars

More sets of sub-roots contributed to heat collection; however, the effect was 1 % between 0 set and 3 sets (Table 6.9). Ratio of improvement indicated that the increase in root number became effective after two sets of sub-roots; therefore, the rest of analysis was conducted with the most effective design, three sets, as set in case Nsr-3.

6.3.6 Thermal conductivity of thermal pillars

The increase in heat collection capacity could be seen as thermal conductivity of thermal pillars rose (Table 6.10). However, the effect was approximately 6 % even if the conductivity became 18.8 times as large as that in case ktp-0. Furthermore, ratio of improvement indicated that the effect would be gradually saturated after 45 W/m/K as displayed in Figure 6.8. If this design parameter had significant advantage, convection heat transfer as Sanken Setsubi Kogyo Co., Ltd (section 2.2.3) or heat pipes could have been a beneficial design strategy. Effective thermal conductivity of heat pipes could be 10,000 to 100,000 W/m/K (Thyrum et al., 2001). However, the remarkably high conductivity would not be worthwhile in this

Table 6.9 Simulation results with different number of sub-roots

Case		Ltp-2	Nsr-1	Nsr-2	Nsr-3
Number of sub-roots	pair	0.00	1.00	2.00	3.00
Heat flux ¹⁾	W/m ²	-20.10	-20.10	-20.20	-20.30
Total flux ²⁾	W/m long	22.50	22.50	22.60	22.70
Ratio of improvement ³⁾	W/pair of sub-roots		0.00	0.11	0.11

1) The maximum heat extract, in which the average temperature on the heat exchanger surface

2) For every meter of installation

3) Improvement of total flux per increase in pair of sub-roots

Table 6.10 Simulation results with different thermal conductivity of thermal pillars

Case		ktp-0	ktp-0.7	Nsr-3	ktp-1	ktp-2	ktp-3	ktp-4
Thermal conductivity of thermal pillars	W/m/K	2.42	5.10	7.80	13.20	18.50	29.30	45.40
Heat flux ¹⁾	W/m ²	-20.10	-20.20	-20.30	-20.50	-20.70	-21.05	-21.30
Total flux ²⁾	W/m long	22.50	22.60	22.70	23.00	23.20	23.60	23.90
Ratio of improvement ³⁾	W/(W/m/K)		0.04	0.04	0.04	0.04	0.04	0.02

1) The maximum heat extract, in which the average temperature on the heat exchanger surface reached 0 °C

2) For every meter of installation

3) Improvement of total flux per increase in thermal conductivity of thermal pillars

design. As Gan et al. (2007) experienced, the rest of components, i.e. sub-soil, had far too large thermal resistance to improve the overall conductivity. This result was not reflected to the rest of analysis, and so conductivity of 7.8 W/m/K was continued to be used.

6.3.7 Diameter of thermal pillars

Little effect could be seen between a 0.02 m and 0.03 m diameter in Table 6.11. When the diameter was 0.04 m, 1 % of extra heat collection was expected. Considering that Uretek choses a 0.15 m diameter for practical applications, economical benefit for larger diameter ought to be evaluated.

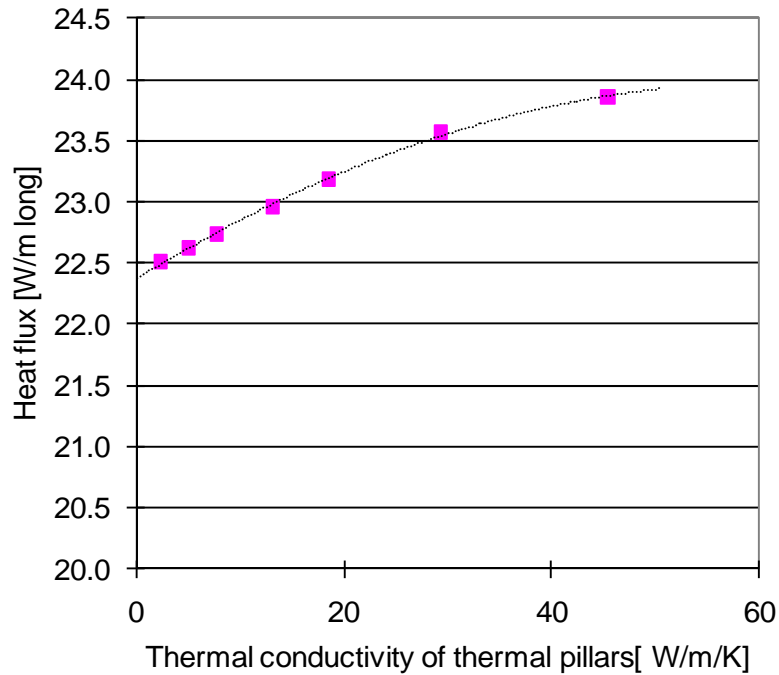


Figure 6.8 Effect of thermal conductivity of thermal pillars

Table 6.11 Simulation results with different diameter of thermal conductivity

Case		Nsr-2	Ttp-1	Ttp-2
Diameter of thermal pillars	m	0.02	0.03	0.04
Heat flux ¹⁾	W/m ²	-20.30	-20.31	-20.50
Total flux ²⁾	W/m long	22.70	22.70	23.00
Ratio of improvement ³⁾	W/m		0.86	21.54

1) The maximum heat extract, in which the average temperature on the heat exchanger surface reached 0 °C

2) For every meter of installation

3) Improvement of total flux per increase in diameter of thermal pillars

For the final analysis with thermal pillars, a 0.04 m diameter was used.

6.3.8 Thermal pillars in three dimensional calculation

Thermal pillars with sub-roots improved heat collection by up to 3 % in two

Chapter 6 Design Optimisation of Underground Structure with Modified Soil

dimensional calculation, while 2 % in three dimension (Table 6.12). Though the effective space of sub-roots was interpreted optimistically, thermal pillars were modelled more practically in three dimension. Therefore, the result was understood to be closer to the real effect. Nevertheless, Figure 6.9 displays that the injection of highly conductive grout with this design affects on small underground space. As a consequence, this attempt could not result in an attractive design idea.

6.3.9 Modified soil space

Both wider and deeper modification extracted more thermal energy (Table 6.13). Ratio of improvement suggested that the effect would eventually reach a point beyond which there was no further improvement. The effect against the volume of excavation suggested that deeper modification could be more cost effective (Figure 6.10). This must have been because more heat transfer with higher underground temperature was effective. Though the estimated heat flux was the same between case Dmod-2 and Wmod-2, the required excavation was less by 25 % with case Dmod-2.

It was difficult to generate positive impact with thermal pillars. When the modified soil space was extended by 1.0 m in case Dmod-2, approximately

Table 6.12 Comparison between with and without thermal pillars

Dimension		Two	Three
Heat flux in W/m ²	Without pillars	-19.9	-20.4
	With pillars	-20.5	-20.8
Improvement, %		3.0	2.0

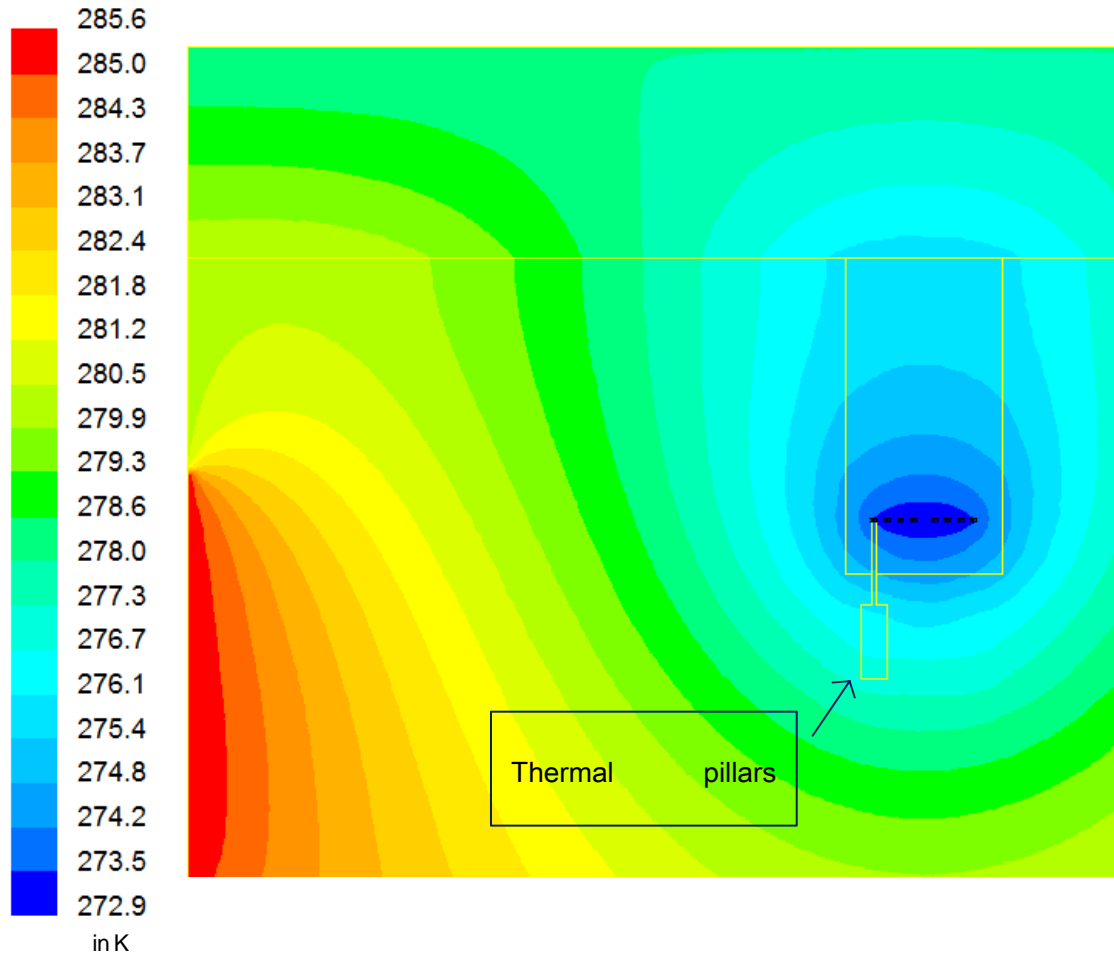


Figure 6.9 Temperature contour in three dimensional model with thermal pillars

Table 6.13 Simulation results with different width and depth of modified soil space

Case		kmod-1	Lh-2	Dmod-1	Dmod-2	Wmod-1	Wmod-2
Modified soil space	Depth m	0.0	3.0	3.5	4.0	3.0	3.0
	Width m	0.0	1.5	1.5	1.5	2.0	2.5
Heat flux ¹⁾	W/m ²	-16.8	-19.9	-20.5	-20.8	-20.4	-20.8
Total flux ²⁾	W/m long	18.8	22.3	23.0	23.3	22.9	23.3
Ratio of improvement ³⁾	Depth W/m		1.2	1.4	0.6		
	Width W/m		2.3			2.0	1.8

1) The maximum heat extract, in which the average temperature on the heat exchanger surface

2) For every meter of installation

3) Improvement of total flux against case kmod-1 per increase in depth or width of modified soil

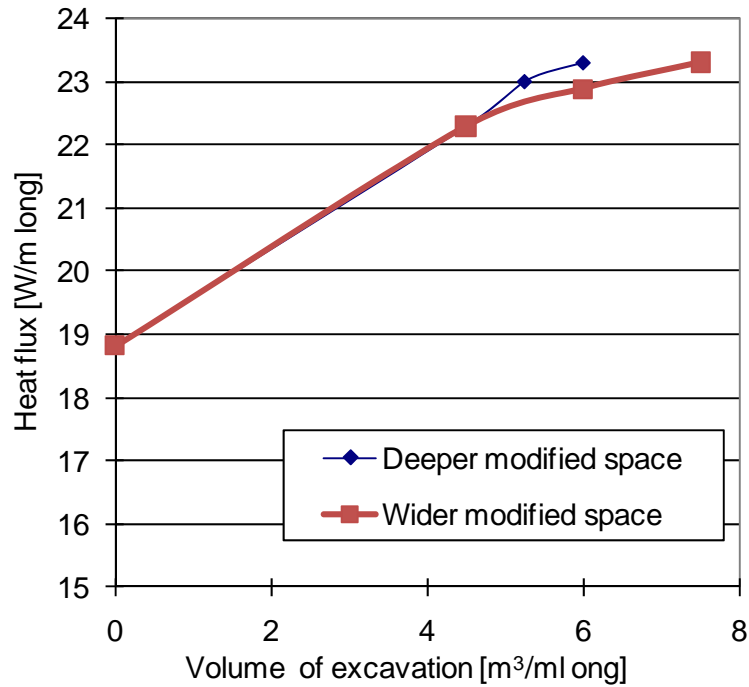


Figure 6.10 Comparison against volume of excavation

4.5 % of extra heat extract was expected in comparison to case Lh-2. If underground structure was modified to the same depth, the extension of soil modification was more effective strategy than thermal pillars with sub-roots. Though the grout injection was proposed to economically take advantage for larger scale modification, the extended soil modification had better technical benefit. The cost performance is studied in the section 7.1.

6.3.10 Summary of underground design analysis

The results from each sensitivity analysis are summarised in Table 6.14. The most significant design parameter was thermal conductivity in the modified soil space. This underlined the benefit of soil modification in underground heat collection. Although the best effect of thermal pillars was 3 % in two-dimensional simulation, three-dimensional calculation indicated an effect of up to 2 % even with rectangular sub-roots. Conversely, the

Table 6.14 Summary in effects of design parameters

Item		Accumulated improvement in %	Comment
Slinky coil at 2.5 m deep	(A)	0.5	better than 2.95 m deep
Thermal conductivity of modified soil at the OMC	(B)	18.5	better than sub-soil
With thermal pillars ¹⁾	1.5 m long	(C) 19.6	1 % better than (B)
	With three pairs of sub-roots	(D) 20.8	1 % better than (C)
	With 5% of carbon fibres	(E) 1.0	better than no carbon fibres
	Double diameter	(F) 22.0	1 % better than (D)
Extra 1 m deep modification	(G)	23.8	4.5 % better than (B)

1) The results were calculated in two dimension. Three dimensional calculation revealed less effect.

extension of the modified soil space demonstrated a clear effect, for instance, 4.5 % increase by extra 1 m deep modification. It is normally said that excavation cost has too much impact on the construction cost to make the payback period within a reasonable range. Therefore, cost performance was examined in the next chapter.

6.4 Conclusions

The advantage of conductive heat transfer has been shown in past research. However, the active intake into designs seemed to be limited in practice except combining with water storage tanks, i.e. septic tanks. Hence, the design strategy with a rainwater collection tank examined in Chapter 4 was one of the possible options.

Design optimisation was conducted to enhance the conductive heat transfer by

Chapter 6 Design Optimisation of Underground Structure with Modified Soil

soil modification in FLUENT. Though positive impact was expected from the thermal pillars created by injecting highly conductive grout, the partial enhancement of underground thermal conductivity did not demonstrate remarkable outcome. Conversely, extra soil modification at greater depth was more effective.

Chapter 7 Economic Analysis of Soil Modification for an Insulated Office Building

Introduction

A variety of experimental and numerical design optimisation was conducted until the previous chapter. However, modified systems are required to be economically viable as well as thermally efficient. Therefore, this chapter attempts to finalise the optimisation of underground heat collection system with economic evaluations.

The previous chapter ascertained that soil modification for a larger depth was more effective than applying carbon fibres as thermal pillars. As the last step, the most practical system design is sought out of six options. The variation is set to examine the effects of a rainwater collection tank, soil modification and depth of soil modification. As a consequence, the best design is selected in order to compete with the existing design to increase heat collection efficiency with reasonable extra costs.

Benefits of the best modified design are studied in a comparison with the existing design. Annual operation with each underground design is predicted in FLUENT. Firstly, monthly heating and cooling demands for an insulated office building are estimated for a year. Secondly, detailed operation conditions are defined to predict collectable ground heat source for each design case. These are thermal conductivity of natural soil in each month, installation depth of horizontal slinky coil, thermal resistance at the heat exchanger of the heat pump,

back-up energy suppliers and electricity consumption at a pump. As a result, monthly heat collection capacities are obtained to calculate the annual electricity consumption and economic benefit.

The last section seeks electricity price and initial costs to improve the positive impact of the modified design. Moreover, a further modification to achieve constantly high water content in soil is proposed with an economic aspect.

7.1 Comparison in a Variety of Underground Design for Heating

The thorough design analysis was concluded by comparing design strategies under the same conditions. Two main design categories were the use of conductive heat transfer with a buried rainwater collection tank and soil modification underground. It is ideal to improve the energy efficiency of buildings by modifying insulation and operation conditions before installing the GSHP. Therefore, six design combinations were compared to the existing design for heating an insulated office building.

7.1.1 Study cases

Study cases are listed in Table 7.1. The variations were created with or without soil modification around the rainwater collection tank and by the depth of the slinky coil and soil modification. Heat collection capacity was compared in FLUENT. Input data was selected based on the simulation analysis in Chapter 3 and the soil thermal conductivity obtained through the lab experiments in Chapter 4 (Table 7.2).

The cases with a rainwater tank were recalculated for more precise

Table 7.1 Study cases

Case	Rainwater tank	Horizontal slinky coil		
	-	Soil modification	Depth of coil m	Depth of modification m
A	0		1.5	0
B	0		2.5	3
C	0		2.5	4
D	1	Without	2.5	3
E	1	Without	2.5	4
F	1	With	2.5	3
G	1	With	2.5	4

Table 7.2 Input data

Item		
Tank size	m	1.5 in width and 5.33 in depth (vertical column)
Thermal conductivity of concrete bed ¹⁾	W/m/K	0.9
Thermal conductivity of sub-soil ²⁾	W/m/K	1.2
Thermal conductivity of modified soil ²⁾	W/m/K	2.5
Thickness of concrete bed	m	0.3
Thickness of modified soil	m	1.7
Thermal conductivity of tank ³⁾	W/m/K	0.5

1) Standard cement

2) Referring to soil thermal conductivity obtained by the experiments in Chapter 5

3) Polyethylene

comparison. The centre line in the two dimensional model was set as an axisymmetric boundary, in order to calculate the radial space. Since cases without rain inflow were also required as a part of the comparison, the slinky coil was modelled with gaps between the units of heat exchange loops as used after section 4.4.2. Heat capacity was determined when the average temperature on the heat exchanger surface reached 0 °C.

Chapter 7 Economic Analysis of Soil Modification for an Insulated Office Building

The required size of components was estimated for a heating system in the insulated seven story office building in Nottingham as introduced in section 3.1.5. Therefore, the climatic conditions in Nottingham were also referred, including rainwater flow rate. The initial cost for heat collection system was also estimated from the size requirements to contrast different designs.

The unit cost was calculated referring to published data (Langdon, 2006) and other supportive sources (Table 7.3). The costs for a water proof membrane to retain moisture above the base of the modified soil space and

Table 7.3 Cost estimation

Case		Dec 1	Dec 2	Jul 1	Jul 2
Operation month ¹⁾		Dec		Jul	
Modified soil	-	Y	N	Y	N
Depth of modified soil	m	3	0	3	0
Depth of heat exchanger	m	2.5	1.5	2.5	1.5
Without solar gain (i.e. Night)	Heat flux	W/m ²	-22.5	-17.5	
	Total heat collection ²⁾	kW/m	0.025	0.020	
With solar gain	Heat flux	W/m ²	-30.0	-25.0	25.8
	Total heat collection ²⁾	kW/m	0.034	0.028	0.029
Average capacity ³⁾	kWh/h	0.032	0.026	0.029	0.022
Required width ⁴⁾	m	9.6	8.5		
Required length of installation ⁵⁾	for heating	m	341	414	
	for cooling	m			627
	Design length ⁶⁾	m	239	269	829
Required area	m ²	2,295	2,295		
Unit cost ⁷⁾	Total cost	£/m-installation	33.60	9.08	
Total cost	£	8,018	2,439		

1) The hardest condition occurs when soil is relatively dry, such as in Jan for heating and Aug for cooling. However, the heat collection system was designed on the basis of a month with the hottest day and the coldest day

2) Heat exchange area is 1.12 m²/m-installation

3) Average duration without solar gain, 2.5 h/day, was calculated from the weather data between 2001 and 2005. The daytime is the rest, 8.5 h/day.

4) Distance less than the surface Temperature in Dec, 7.2 °C, was referred.

5) Required length was calculated based on average daily heat collection.

6) 70 % of required length for heating operation was selected for the modified system, while the required length was calculated to make the installation area for the existing design the same as the one for the modified system.

7) Refer to Table 7.3

for mixing rainwater were considered.

The heat capacity of cases with a rainwater collection tank was calculated with or without rainwater inflow. In accordance to the weather data collected in Nottingham between 2001 and 2005, the average duration for rainfall was 0.6 hour out of 11 working hours. Therefore, the average hourly capacity was derived by dividing the total daily capacity by 11 hours. As discussed in section 6.3.2, solar gain affected heat capacity. As the occurrence of rainfall and solar gain could not be associated, the effect of solar gain was disregarded. However, the effect was included for cases with the horizontal slinky coil. As introduced in section 6.3.2, the average hourly capacity was figured with reference to the average hours of daylight, 8.5 hours.

7.1.2 Evaluation of underground heat collection system

Heat flux for each case was listed in Table 7.4. It was revealed that the impact of rain inflow was much larger than that of solar gain. Therefore, disregarding solar gain for cases with a rainwater collection tank might not have been critical. Beside, the effect of soil modification was more significant when there was no rain inflow. The improvement was 1 % with rain flow, while 16 % without rain flow. Furthermore, the improvement ratio with a slinky coil was even more dramatic. When the ratio of the modified soil space per heat exchanger area in simulation was calculated for the same installation space, cases with a rainwater collection tank was $174.9 \text{ m}^3 / 11.8 \text{ m}^2 = 14.8 \text{ m}^3/\text{m}^2$. Considering that the value with a slinky coil was $24.8 \text{ m}^3 / 6.2 \text{ m}^2 = 4.0 \text{ m}^3/\text{m}^2$, the ratio was 3.7 times larger with a

Table 7.4 Heat flux with different combination of system components

kW/tank or m-installation for slinky coil					
Case	Cases with tank		Cases with slinky coil ¹⁾		
Soil modification	Without	With	Without	3 m deep	4 m deep
Rainfall	With	1.575	1.593		
	Without	0.135	0.156		
	Difference, % ²⁾	1,067	921		
	Average ³⁾	0.210	0.230		
Solar gain	With			0.023	0.031
	Without			0.017	0.022
	Difference, % ²⁾			35	41
	Average ⁴⁾			0.022	0.029

- 1) Depth of coil was 1.5 m without soil modification, while 2.5 m with modification
- 2) Between with and without rainfall / solar gain
- 3) (Total daily heat capacity) / (office hours; 11 hours). Duration for rainfall was 0.6 h/day.
- 4) (Total daily heat capacity) / (office hours; 11 hours). Duration for solar gain was 8.5 h/day.

rainwater collection tank. This indicated that the soil modification affected more significantly in cases with a slinky coil.

The temperature contour of two cases with soil modification and either with a rainwater collection tank, case MR, or with horizontal slinky coil, case MS, is displayed in Figure 7.1. The heat capacity of these cases is highlighted by blue in Table 7.4. Since the same temperature range was set, it could be seen that the temperature gradient in case MR was more significant. However, the operation in case MS reduced underground temperature more, which signified that more ground heat source was collected. This explained why more notable enhancement by the soil modification was seen in case MS.

The heat capacity in case MR was 1.59 kW, while that in case MS was 0.022

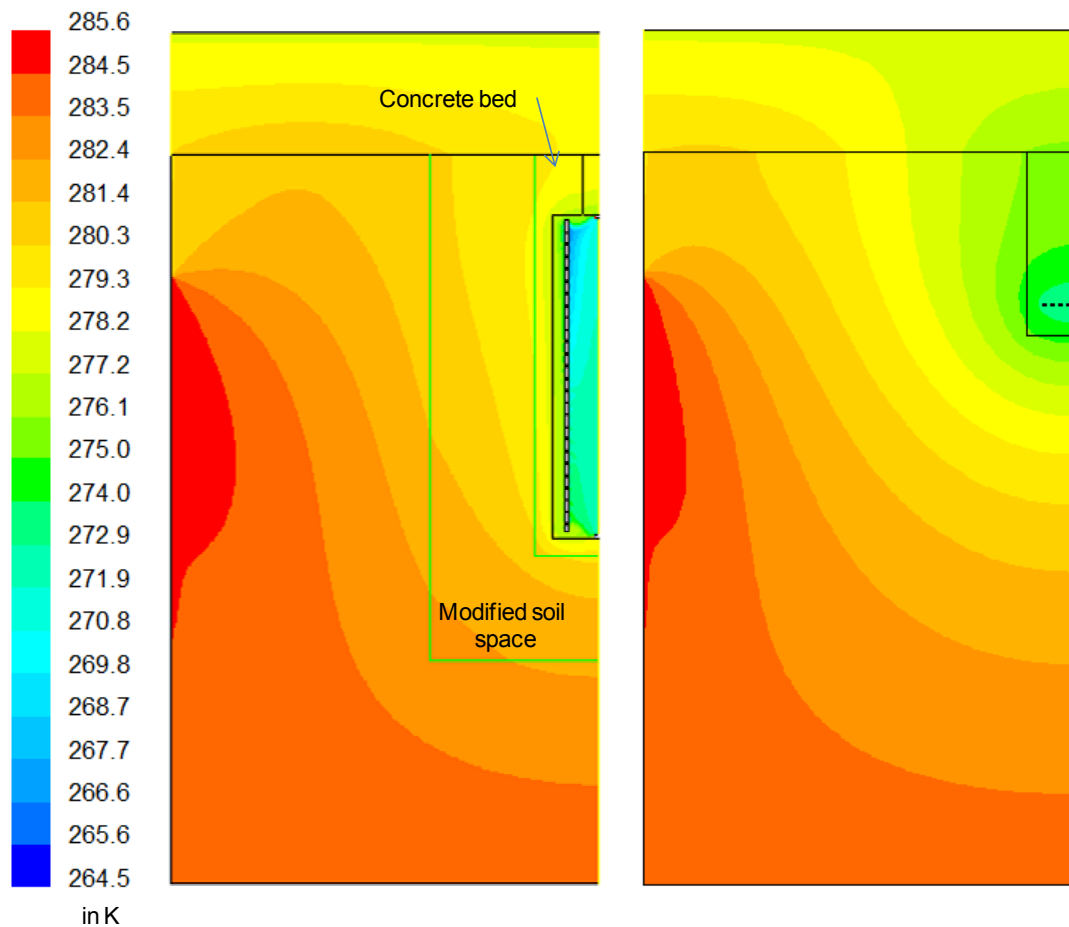


Figure 7.1 Comparison between case MR (left) and case MS (right)

kW for the same installation area; 5.5 m X 5.5 m. It could be hypothesised that the reason why case MR had approximately 72.4 times more active heat transfer with less temperature gradient outside of the tank was the contribution of thermal energy in rainwater. The average rainwater temperature in case MR was 273.1 K. With regard to the rainwater flow rate and the temperature difference from the inlet temperature, 279.3 K, extractable thermal energy in rainwater was approximately 0.72 kW. This demonstrated that 45.3 % of energy was collected from rainwater itself. Respecting that the heat capacity in case MR without rain inflow was 9.8 % of that with rain inflow, the rest 44.9 % was presumably the contribution by

conductive heat transfer. Thus, the use of thermal energy and the convective heat transfer by rainwater was suggested to be effective.

The estimated initial cost for underground heat collection structure without piping and the required installation area are compared in Table 7.5. Though the existing design required the largest installation area, the initial cost was notably smaller than the other cases due to the shallow excavation and no extra investment, such as that for soil modification. The most economically competitive strategy among the modified design cases was case B, while the cases with 4 m of soil modification could reduce the required area. Though the cases with rainwater inflow collected thermal energy efficiently, the average heat capacity was not equally large due to the short duration for rainfall. As a consequence, the daily capacity in case MR could be collected by approximately 7.9 m installation of case MS. As the required installation length for a rainwater tank was 5.5 m, the advantage

Table 7.5 Comparison in required design specs

Case	Components	Soil modification	Required amount		Initial cost		Required area ²⁾	
					£	Ratio, -	m ²	Ratio, %
A	Horizontal slinky coil at 1.5 m deep	Without	498.9	m	4,529	0.0	3,795	0.0
B	Horizontal slinky coil	3 m deep	374.4	m	12,582	1.8	3,639	-4.1
C	Horizontal slinky coil	4 m deep	368.6	m	19,044	3.2	3,612	-4.8
D	Rainwater tank	Without	1.0	-	18,133	3.0	3,582	-5.6
	Horizontal slinky coil	3 m deep	367.1	m				
E	Rainwater tank	Without	1.0	-	24,468	4.4	3,555	-6.3
	Horizontal slinky coil	4 m deep	361.4	m				
F	Rainwater tank	With	1.0	-	20,372	3.5	3,573	-5.8
	Horizontal slinky coil	3 m deep	366.4	m				
G	Rainwater tank	With	1.0	-	26,695	4.9	3,546	-6.5
	Horizontal slinky coil	4 m deep	360.7	m				

1) Depth of the slinky coil with soil modification was 2.5 m

2) Compared without solar gain

was small. On the other hand, the initial cost of case MR was 30.4 times as expensive as that of case MS; therefore, the use of rainwater collection tank seemed not practical. The two ratios were related to each other as plotted in Figure 7.2. Since the extra cost for the soil modification was large, case B was selected to compare with case A through an annual operation analysis in this chapter.

7.2 Estimation of Yearly Demands

The analysis of annual operation was conducted for a seven story insulated office building located in Nottingham as introduced in section 3.1.5. Hourly loads on the basis of the measured climatic data were summarised as a representative load for each month.

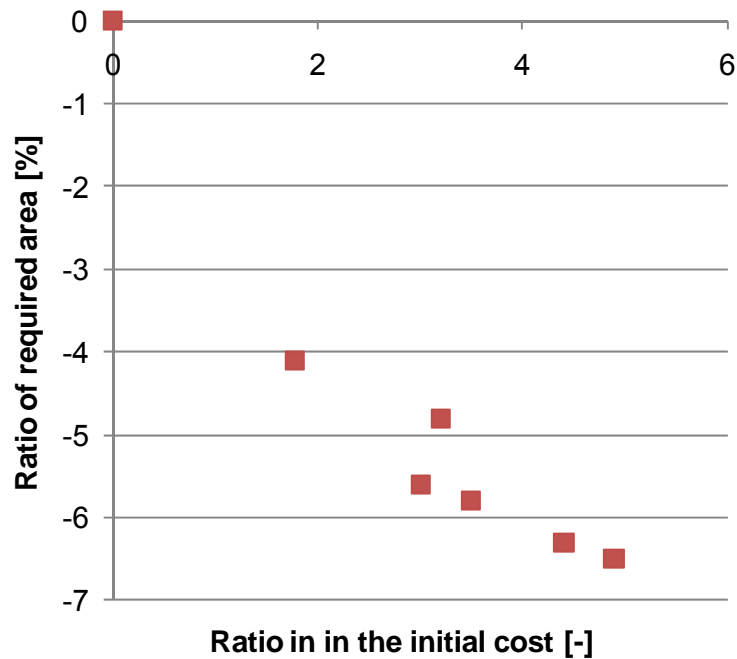


Figure 7.2 Relation between ratio of the initial cost and ratio of required installation area

7.2.1 Methodology

The design loads obtained in section 3.1.5 were only for two sets of extreme environmental conditions, winter and summer. Therefore, a relation between loads and environmental conditions needed to be acquired to estimate for other months. Calculation for the design demands presented in section 3.1.3 indicated that dominant environmental parameters were solar radiation and ambient temperature. Though solar radiation cannot express the change of demands at nights, ambient temperature continuously varies being influenced by a degree of solar radiation. For that reason, ambient temperature was chosen to be the main parameter to calculate hourly demands. As solar radiation varies with solar altitude, monthly ambient temperature and representative solar altitude for each month were correlated.

Heating and cooling loads were calculated for different ambient temperatures with the same method as introduced in section 3.1.3, so as to predict loads for the rest of ambient temperature range (Table 7.6). The increase of cooling load against the change of ambient temperature was larger than that of heating load. As a result, cooling load had a possibility to exceed the cooling capacity of the selected heat pump, 24.9 kW, when ambient temperature rises higher than 27.6 °C.

7.2.2 Calculation of heating and cooling demand

The obtained trendlines by plotting loads against ambient temperature were applied to the hourly ambient temperature to calculate hourly loads. The weather data recorded in 2002 was selected, as the yearly data had less

Table 7.6 Estimation of the change of load against ambient temperature

Operation		Heating ¹⁾			Ventilation ²⁾		Cooling		
Outside temp	°C	-3.3	0.0	3.0	20.0	23.3	27.3	28.0	30.0
Conduction	kW	15.7	11.8	10.3			-0.8	2.8	5.4
Solar gain	kW	0.0	0.0	0.0			8.0	7.1	10.5
Infiltration and ventilation	kW	19.9	17.1	14.5			-2.0	0.4	1.4
Internal heat gain	kW	-17.7	-17.7	-17.7			17.7	17.7	17.7
Cooling load	kW	0.0	0.0	0.0	0.0	0.0	22.8	28.0	35.0
Heating load	kW	18.0	11.2	7.2	0.0	0.0	0.0	0.0	0.0

1) From the trendline, the real heating load occurred below ambient temperature of 7.1 °C

2) The design ambient temperature was lower than the target indoor temperature; therefore, the total cooling demand had cooling effect below 27.3 °C.

missing data than other years. Monthly loads and the average precipitation are shown in Figure 7.3. It could be seen that heating and cooling load would occur for about 6 months and for two months respectively.

Both heating and air-conditioning loads were expected for the office building. Heat pumps can technically deal with both operation modes at the same time. However, none of the months required this operation mode for this case study, and so modes were assumed to be transferred by reversing the direction of the working fluid flow between evaporator and condenser. This process will be accomplished only by changing a valve.

7.3 Conditions for Annual Operation

Annual operation was estimated by calculating representative state for each month in FLUENT, though heating and cooling loads were approximated hourly. The calculation was conducted at steady-state, which was assumed to demonstrate under the average thermal environments. Real systems would be operated under changing conditions, contrasting to equilibrium state. However,

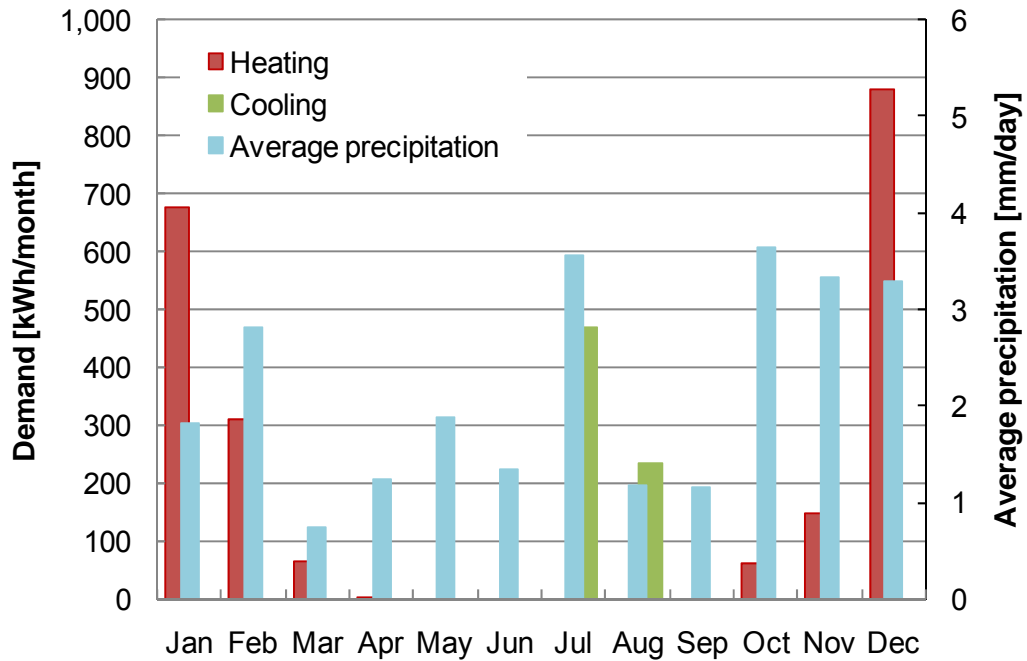


Figure 7.3 Monthly heating and cooling load

this project attempted the quicker assessment before moving to dynamic calculation for a year, which required abundant time and computational capacity. Considerations for annual operation analysis were introduced as follows.

7.3.1 Estimation of soil thermal conductivity

Thermal conductivity of sub-soil for each month was required for the simulation. As studied in Chapter 4, soil thermal conductivity largely depends on its water content. However, data was measured only in December as stated in section 5.3.1. Therefore, a field work was referred to estimate water content in soil and eventually representative thermal conductivity.

Zreda et al. (2008, Figure A.5) collect rainfall data and moisture content in sub-soil at 30 cm deep. The location is the San Pedro River Valley in

Arizona, USA. The sampling point is a riverside and the soil consists of gravel, sand and clay (Scarborough, [no date]), which are the same characteristics as soil has in the School of the Built Environment in Nottingham (section 5.3.1). Therefore, a relation between rainfall and moisture content was acquired from the field data (Figure F.1). Water content is a consequence of continuous occurrence among rainwater absorption, evaporation, transference and storage; therefore, defining simple interaction is difficult. However, the data was used as an indication to estimate soil moisture content in Nottingham.

The average daily rainfall for each month in Nottingham was calculated from the weather data. Subsequently, a relation between moisture content and thermal conductivity of natural soil was derived from the experimental data presented in section 5.7.3 (Table 7.7). Soil was prepared with $4.5 \text{ Mg}\cdot\text{m}/\text{m}^3$ of compaction energy to acquire $1.5 \text{ Mg}/\text{m}^3$ of bulk density; however, the achieved data was $1.54 \text{ Mg}/\text{m}^3$. Hence, thermal conductivity of soil at $1.5 \text{ Mg}/\text{m}^3$ of bulk density measured in section 5.7.1 was used to estimate a trend (Figure 7.4). As a result, estimated moisture content for December, 11.2 %, was close to the measured value in section 5.3.1, 11.6 %.

7.3.2 Other environmental conditions

Input data for air boundary at 2 m high from the ground line and for boundary on grass with solar gain are listed in Table 7.8. Soil temperature gradient was calculated with Equation 3.9.

Table 7.7 Estimated thermal conductivity of sub-soil for each month

Month	Average precipitation in Nottingham ¹⁾	Estimated moisture content	Estimated soil thermal conductivity
	mm/day	%	W/m/K
Jan	1.8	8.2	1.24
Feb	2.8	10.2	1.35
Mar	0.7	6.1	1.13
Apr	1.3	7.1	1.18
May	1.9	8.4	1.25
Jun	1.3	7.3	1.19
Jul	3.5	11.7	1.43
Aug	1.2	7.0	1.18
Sep	1.1	6.9	1.17
Oct	3.6	11.9	1.44
Nov	3.3	11.3	1.40
Dec	3.3	11.2	1.40

1) Data recorded at the School of the Built Environment

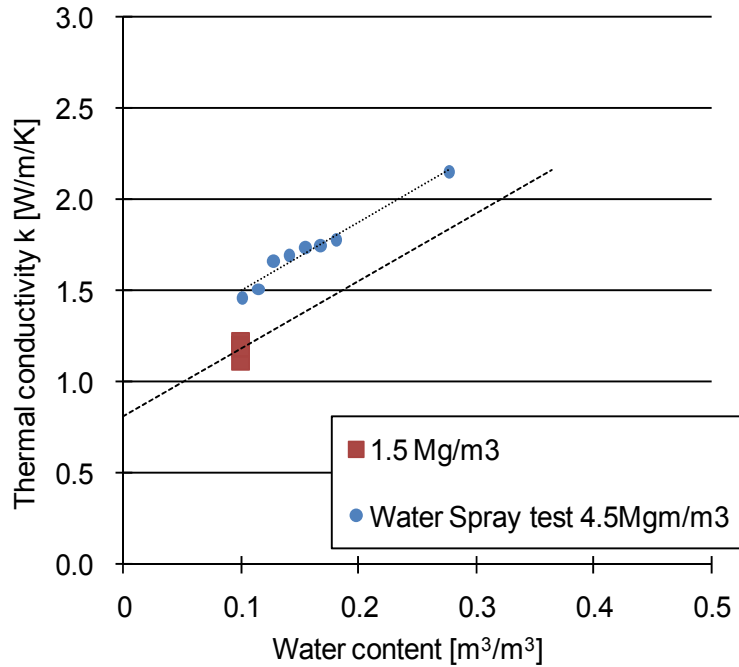


Figure 7.4 Trendline derived from experiments for soil at 1.5 Mg/m³

Table 7.8 Input data for each month

°C

Month	Ambient temperature	Temperature under 2cm of grass ¹⁾	Ambient temperature at night ²⁾
Jan	7.0	8.1	6.3
Feb	8.1	9.2	6.6
Mar	9.9	11.0	7.7
Apr	12.9	14.0	
May	14.4	15.5	
Jun	18.4	19.5	
Jul	20.1	21.2	
Aug	21.1	22.2	
Sep	17.4	18.5	13.6
Oct	11.3	12.4	10.1
Nov	8.8	9.9	7.6
Dec	5.9	7.0	5.2

1) 1.1 °C larger than ambient temperature as introduced in section 6.2.3.

2) No operation at night between Apr and Aug

7.3.3 Calculation for designing

Design length of slinky coil was determined by calculating required length between in winter and in summer (Table 7.9). Air-conditioning capacity required more than double installation length of slinky coil. Hourly loads for a year suggested that duration for cooling operation was considerably shorter than that for heating (Figure 7.5). In addition, the obtained hourly heating loads surpassed 70 % of design heating capacity for only 2.4 % of operation time in a year. Therefore, the installation length of slinky coil was determined on the basis of 70 % of heating requirement. Since operation with modified soil was more efficient, required length was smaller by 17.6 % to achieve design heating demand than the existing design. Though the efficient heat collection necessitated wider distance from the next coil to avoid thermal interference; the total installation area was smaller by 7.2 %. Nevertheless, the construction cost 2.3 times more than the existing design

Table 7.9 Designing heat exchanger

Case		Dec 1	Dec 2	Jul 1	Jul 2	
Operation month ¹⁾		Dec		Jul		
Modified soil	-	Y	N	Y	N	
Depth of modified soil	m	3	0	3	0	
Depth of heat exchanger	m	2.5	1.5	2.5	1.5	
Without solar gain (i.e. Night)	Heat flux	W/m ²	-22.5	-17.5		
	Total heat collection ²⁾	kW/m	0.025	0.020		
With solar gain	Heat flux	W/m ²	-30.0	-25.0	25.8	19.5
	Total heat collection ²⁾	kW/m	0.034	0.028	0.029	0.022
Average capacity ³⁾	kWh/h	0.032	0.026	0.029	0.022	
Required width ⁴⁾	m	9.6	8.5			
Required length of installation ⁵⁾	for heating	m	341	414		
	for cooling	m			627	829
	Design length ⁶⁾	m	239	269		
Required area	m ²	2,295	2,295			
Unit cost ⁷⁾	Total cost	£/m-installation	33.60	9.08		
Total cost	£	8,018	2,439			

1) The hardest condition occurs when soil is relatively dry, such as in Jan for heating and Aug for cooling.

However, the heat collection system was designed on the basis of a month with the hottest day and the coldest day.

2) Heat exchange area is 1.12 m²/m-installation

3) Average duration without solar gain, 2.5 h/day, was calculated from the weather data between 2001 and 2005. The daytime is the rest, 8.5 h/day.

4) Distance less than the surface Temperature in Dec, 7.2 °C, was referred.

5) Required length was calculated based on average daily heat collection.

6) 70 % of required length for heating operation was selected for the modified system, while the required length was calculated to make the installation area for the existing design the same as the one for the modified system.

7) Refer to Table 5.17

for the same installation area.

7.3.4 Thermal resistance at heat exchanger

Slinky coil was made of polyethylene with a 1.4 mm thickness. Liquid thermal media, ethylene glycol, flowed within the tube; hence convection heat transfer could reduce thermal resistance on the internal surface. However, the overall temperature drop between soil and the media was

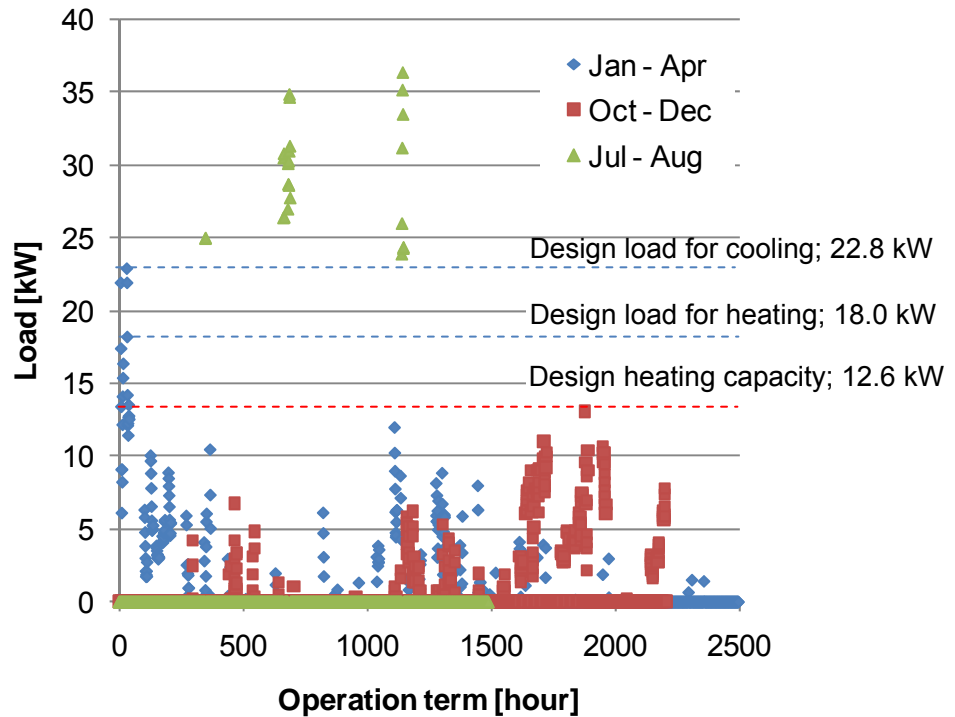


Figure 7.5 Estimated loads in a year

approximated. Table 7.10 and Figure 7.6 present the conditions of the tube. The state of the liquid thermal media was calculated as listed in Table 7.11. Subsequently, temperature drop was calculated with the following theoretical formulas (Holman, 2002, Table 7.12). The formula to obtain Nusselt number is suitable for $2,300 \leq Re \leq 5 \times 10^6$; therefore, Equation 7.2 was applicable for both heating and cooling conditions.

$$f = \frac{1}{(1.82 \log_{10} Re - 1.64)^2} \quad (\text{Equation 7.1})$$

$$Nu = \frac{(f/8)(Re-1000)Pr}{1 + 12.7\sqrt{f/8}(Pr^{2/3}-1)} \quad (\text{Equation 7.2})$$

$$h = Nu \cdot \frac{k_{brine}}{d_{in}} \quad (\text{Equation 7.3})$$

$$R = \frac{1}{h_i A_i} + \frac{d_d}{k_{polyethylene} A_m} \quad (\text{Equation 7.4})$$

Table 7.10 Conditions of heat exchange tube

Operation			Heating	Cooling
Specific heat capacity	$C_{p_{brine}}^{1)}$	J/kg/K	3,800	3,850
Viscosity	μ	Pa·s	0.0035	0.0014
Conductivity	k_{brine}	W/K/m	0.5	0.52
	$k_{polyethylene}$	W/K/m	0.47	0.47
Density	ρ	kg/m ³	1,035	1,028
Tube	$d_o^{2)}$	m	0.02667	
	d_{in}	m	0.02093	
	d_d	m	0.00287	
Area	A_i	m ²	0.066	
	A_m	m ²	0.075	

1) Ethylene glycol 20% for freezing point of -8 °C

2) Outer diameter; therefore, $d_o = 2r_o$

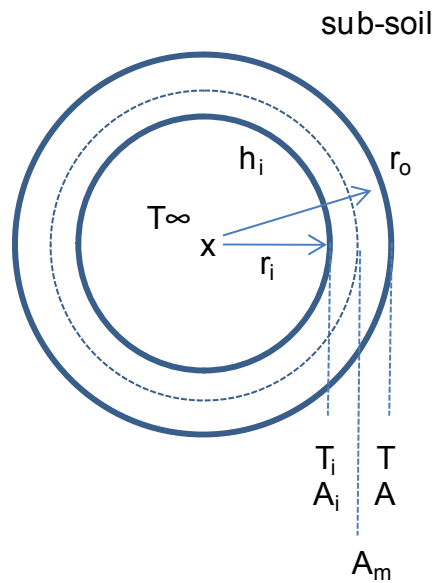


Figure 7.6 Conditions around tube

$$Q = \frac{T - T_\infty}{R} \quad \text{(Equation 7.5)}$$

f Friction factor for smooth pipes -

Nu Nusselt number -

Table 7.11 State of liquid thermal media

Operation		Heating	Cooling
Heat source	kW	10.80	17.90
Brine temperature difference at heat exchanger	°C	3.00	5.00
Flow per row ¹⁾	m ³ /h	1.10	1.08
Prandtl number	Pr	26.60	10.37
Reynolds number	Re	5,500	13,656

1) The heat exchanger consists of 3 coils, which makes a coil 89.6 m for the existing design and 79.5 m for the modified design.

Table 7.12 Estimated temperature drop

Design			Existing		Modified	
Operation			Heating	Cooling	Heating	Cooling
Design load ¹⁾		kW/m-heat exchanger	2.19	3.64	2.47	4.10
Nusselt number	Nu	-	71.37	122.78	71.37	122.78
Heat transfer coefficient	h_i	W/m ² /K	1,705	3,050	1,705	3,050
Total thermal resistance	R	K/W	0.09	0.09	0.09	0.09
Temperature drop between the centre of brine and outer surface of slinky	dT	°C	0.20	0.32	0.22	0.36
Required temperature at the outer tube ²⁾	T_{req}	°C	0.20	24.68	0.22	24.64

1) Length of heat exchanger in 1 m of installation was 18.28 m.

2) In order to achieve design brine temperature, 0 °C for heating and 25 °C for cooling respectively

h Heat transfer coefficient W/m²/K

R Total thermal resistance K/W

Q Heat flow W

The delivered temperature drops needed to be taken into consideration to determine the target average outer surface temperature in simulation.

Thus, the thermal media temperatures were secured to be the same as the

design values, 0 °C for heating and 25 °C for cooling.

7.3.5 Backup energy suppliers

The installation length of the heat exchanger was designed based on climatic conditions in the hottest and the coldest month in section 7.2.2. However, heat collection capacity could be remarkably influenced by soil thermal conductivity as section 6.3.3 demonstrated. In fact, lower soil thermal conductivity than that in the coldest month was estimated while heating load was still large in January (Table 7.7). Therefore, the heating system was required to prepare backup heating suppliers. In order to satisfy all the demands in the operation analysis, electric boilers with the COP of 1.0 were chosen (Argo Controls, 2008). The same phenomenon occurred in August for cooling; hence, electric chillers with the COP of 2.23 were referred (ANON., [no date]).

7.3.6 Consideration of pump electricity consumption

The heat exchanger in both modified and existing design was assumed to consist of 3 heat exchange coils, which were split at a header pipe placed after a heat pump and combined at another header pipe before returning to the heat pump to complete the circuit. Since the required length per coil for the modified design was shorter, electricity consumption on a pump to circulate ethylene glycol was less than that of the existing design. Hence, the extra electricity consumption was estimated to be added to the total electricity consumption in the existing design. As operation term for heating was longer than that for air conditioning in this case study, the value was estimated for heating. Pressure drop and pumping power were calculated

with the following equations (Holman, 2002).

$$\Delta p = f \left(\frac{L}{din} \right) \frac{\rho u_{ave}^2}{2} \quad \text{(Equation 7.6)}$$

$$P = \frac{m \cdot \Delta p}{\rho} \quad \text{(Equation 7.7)}$$

Δp	Pressure drop	kg/m/s ²
L	Length of pipe	m
ρ	Density	kg/m ³
u_{ave}	Average velocity	m/s
P	Pump power	W/m-installation
m	Mass flow rate	kg/s

The result was considered in analysis (Table 7.13).

7.3.7 Other assumptions for analysis

Two conditions were assumed for the year-round analysis. Soil thermal conductivity was set as the same value in the existing design, though the design did not include a water proof membrane to deliberately retain moisture around the heat exchanger. In reality, moisture content could be unstable without the membrane or the water-holding characteristic of soil components. Hence, the use of representative thermal conductivity for the shallow sandy soil layer could overestimate heat collection capacity.

The operational COP of heat pump with an inverter controlled compressor could be increased at low loads. As reliable data was not available, this characteristic was not taken into consideration in the analysis. When this

Table 7.13 Estimation of extra electricity consumption at a pump in the existing design

Friction factor for smooth pipes	f	0.038
Length for calculation	L	1 m
Pipe diameter	d_{in}	0.021 m
Density of ethylene glycol	ρ	1,035 kg/m ³
Average velocity	u_{ave}	0.89 m/s
Pressure drop	Δp	732 kg/m/s ²
Pump power	P	0.22 W/m
Pump efficiency ¹⁾		0.45
Motor efficiency ²⁾		0.70
Electric consumption	Modified soil	56.48 W/coil
	Existing soil	63.62 W/coil
	Difference	7.14 W/coil

1) Refer to the smallest pump with head of 10 m for flow rate of 20 m³/h (European Commission, 2003 a).

2) Refer to the smallest pump with power of 1 HP (Power Efficiency Corporation, [no date]).

effect was interpreted into the calculation, operation with the modified design could have been expected to have higher operational COP than that with the existing design.

7.4 Estimation of the Annual Operation

Heat collection capacity was estimated for each month. The effects of the modified design were inspected by comparing to the predicted operation in the existing design in terms of electricity consumption and CO₂ emission.

7.4.1 Monthly heat collection

Results reported that the modified design could extract more ground source energy than the existing design (Table 7.14). It was noticed that capacity in

Table 7.14 Estimation of heat collection capacity

kW						
Design Solar gain	Existing design			Modified design		
	Heating		Cooling	Heating		Cooling
	with	without	with	with	without	with
Jan	6.9	3.9		7.9	4.6	
Feb	8.5	3.9		8.9	4.6	
Mar	8.1	3.3		9.1	3.9	
Apr	10.3			11.2		
May						
Jun						
Jul			5.9			6.9
Aug			4.1			5.3
Sep						
Oct	12.0	6.8		12.0	7.6	
Nov	9.6	6.0		10.0	6.7	
Dec	7.5	5.3		8.0	6.0	

Oct with solar gain was nearly the same between two design cases. Since soil thermal conductivity for the month was the highest, solar energy could have been collected with the heat exchanger even at shallow location effectively without soil modification. Figure 7.7 demonstrates that soil modification was more effective when soil thermal conductivity was lower. This indicated that soil modification could be more beneficial when the original soil drains water quickly, such as sandy soil. As a result, the effect of high thermal conductivity was up to 29.2 % and 13 % on average, which explained that soil modification was expected to successfully enhance the heat extraction.

7.4.2 Year-round electricity consumption

Collectable heat source was converted into energy supply capacity from the

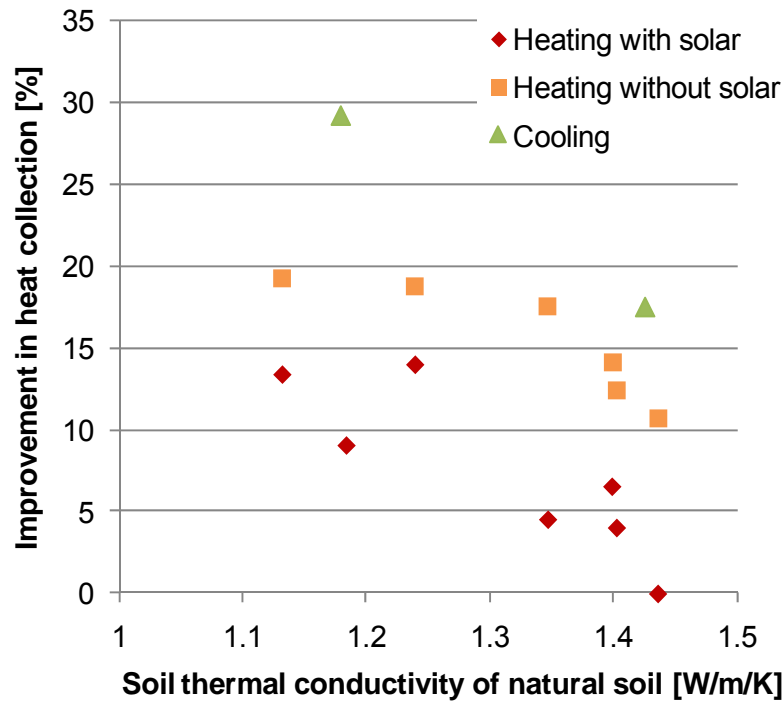


Figure 7.7 Effect of soil modification against soil thermal conductivity

heat pump. When the capacity was larger than hourly load, the outlet temperature at the heat pump was assumed to rise in heating and to conversely drop in cooling. This temperature change raises the COP as Figure A.3 displays. In the opposite case, back up energy suppliers were assumed to be operated at lower COP than that of the heat pump as introduced in section 7.3.5. As a consequence, advantages of the modified design were evaluated in annual energy consumption.

Results showed that the modified design reduced the total electricity consumption (Table 7.15). When the system consisted of only electric boilers and electric air-conditioners, the total consumption would be 2,381 kWh/year. This was approximately 2.1 times as large as the value in the existing design, which was a clear benefit of the GSHP in energy saving.

Table 7.15 Comparison of annual electricity consumption

kWh								
Design	Existing				Modified			
Item	For heating	Electric boiler	For cooling	Electric air conditioner	For heating	Electric boiler	For cooling	Electric air conditioner
Jan	218.5	97.7			226.0	76.2		
Feb	114.6	0.0			114.4	0.0		
Mar	22.7	0.0			22.6	0.0		
Apr	1.5	0.0			1.5	0.0		
May								
Jun								
Jul			25.7	155.9			30.2	146.6
Aug			9.0	86.4			11.6	80.9
Sep								
Oct	21.3	0.0			21.3	0.0		
Nov	52.3	0.0			52.2	0.0		
Dec	326.8	7.0			328.1	0.6		
Sum	757.7	104.7	34.6	242.3	766.2	76.8	41.7	227.5
Pump	3.2		0.2					
Total	1,142.7				1,112.2			

However, the saved electricity with the modified design was 30.5 kWh/year, which was approximately 2.7 % of the total consumption in the existing design. Though the average heat collection increased by 13.0 %, the energy saving benefit was disappointingly lower. The first reason was that the design capacity was constantly larger than loads for most of heating operation in a year as displayed in Figure 7.5. Though the modified design had extra heat supply capacity by 12.7 % on average, the advantage was taken only in January and December by operating backup boilers at less efficiency.

The larger capacity of the modified design should have raised the operational COP of heat pump and should have been still beneficial. However, the COP improvement against the outlet heat source temperature

was small for the referred heat pump. With this characteristic, heating COP would be enhanced by only 1.2 % even if the outlet temperature rose up by 13 % of the design temperature difference. This 1 tenth reduction of efficiency was critical in justifying the modified design. Therefore, it was of essence to combine heat pumps with which the COP rises against the outlet heat source temperature as close as possible to the directly proportional rate.

7.4.3 Economic and ecological feasibility

The modified design was assessed in payback period and CO₂ emission from the obtained annual electricity consumption. The approved document Part L2 (2000) sets a standard rate to estimate electricity bill, 5.0 p/kWh. Therefore, the total saved energy bill was disappointing 1.5 £/year, which made payback period incredibly large.

$$\begin{aligned} (\text{SimplePaybackPeriod}) &= \frac{(\text{AdditionalCost})}{(\text{AnnualSaving}) \times (\text{ElectricityCost})} \\ &= \frac{£5,578}{30.50 \text{ kWh/year} \times 5.000 \text{ p/kWh} \div 100.0} \\ &= 3,654 \text{ years} \end{aligned}$$

Considering it is said that the lifetime of the slinky coil could be about 50 years (LitchfieldGeothermal, [no date]), this design case was far from a feasible option.

The reduced CO₂ emission was proportional to the electric consumption; therefore, the existing design also decreased 52 % of emission compared to

the conventional heating and cooling system consisting of electric boilers and electric air-conditioners. Comparing the modified design to the existing design, the reduction was 2.7 %. Since the approved document Part L2 (2000) also defines a standard ratio between CO₂ emission and electricity consumption, 0.422 kg/kWh, the prevented emission was approximately 12.9 kg/year.

7.5 Conditions for Practical Use of Soil Modification

Soil modification successfully enhanced underground heat transfer. Nevertheless, the assessment of annual performance of the modified design did not designate reasonable feasibility. Hence, this section aims to explore useful cases in which the technical advantage generates practical payback period.

7.5.1 Prospects in electricity prices

Payback period was calculated following the approved document; however, electricity prices have risen since the document was issued in 2000. Hence, prospective payback period was predicted with growing electricity prices in Table 7.16. Electricity prices have possibly become 2.9 times larger since 2000; however, the payback period was still far from practical value. In order to reduce the value to within the lifetime of the slinky coil, electricity prices ought to go up to 365.5 £/kWh. The expected unit cost might not come true soon; therefore, feasibility by a growth in electricity prices was unlikely.

7.5.2 Prospects in the initial costs

The other parameter which principally influenced on the payback period was

Table 7.16 Prediction of payback period with growing electricity prices

Source		Approved document Part L2	Jersey Electricity ²⁾	EdF ³⁾	Future	Future	Future
Time		Apr 2000	2007	Apr 2009			
Unit cost	p/kWh	5.0	7.4	14.3	30.0	60.0	365.5
Annual saving	£	1.5	2.2	4.4	9.2	18.3	111.6
Simple payback period	years	3,654.6	2,480.3	1,278.7	609.1	304.6	50.0

1) The saved electricity consumption; 30.5 kWh/year

2) (Jersey Electricity, [no date])

3) (SSH Associates, [no date])

the initial cost. Table 7.17 demonstrates an effect of construction price for 1 m installation. Sample calculation with the original unit price is displayed below.

$$\begin{aligned}
 (\text{SimplePaybackPeriod}) &= \frac{\left\{ (\text{InstallationCost}_{\text{modified}}) \times (\text{InstallationDistance}_{\text{modified}}) \right\} - \left\{ (\text{InstallationCost}_{\text{existing}}) \times (\text{InstallationDistance}_{\text{existing}}) \right\}}{(\text{AnnualSaving}) \times (\text{ElectricityCost})} \\
 &= \frac{33.60 \text{ £/m} \times 238.6 \text{ m} - 9.08 \text{ £/m} \times 268.8 \text{ m}}{30.50 \text{ kWh/year} \times 14.30 \text{ p/kWh} \div 100.0} \\
 &= 1,279 \text{ years}
 \end{aligned}$$

When the unit cost went below 11.14 £/m, payback period could be predicted to be less than 50 years. Table 7.18 intends to propose design options to diminish the construction cost to obtain a reasonable payback period. Since modifying soil for 3 m could not provide solutions, locating the slinky coil at a 1.5 depth was considered. It was expected that a water proof membrane laid below the slinky coil could retain moisture content. As a consequence, cases with the membrane and with or without modified soil for 1.5 m deep were within the feasible cost and with payback period of less

Table 7.17 Prediction of payback period with different construction cost

Case		Original for modified design	Cases with different initial cost				
						Case S-1	Payback 0 year
Unit price	£/m	33.60	25.00	20.00	11.14	10.52	10.22
Difference of investment cost ²⁾	£/system	5,578.0	3,525.2	2,332.2	218.1	70.4	-
Simple payback period ³⁾	years	1,278.7	808.1	534.6	50.0	16.1	-

- 1) The saved electricity consumption; 30.5 kWh/year
 2) Compared to the existing design
 3) Based on electricity unit price for 2009, 14.3 p/kWh

Table 7.18 Design suggestions to reduce payback period

Case		Existing	Suggested	Suggested
			S-1	S-2
			with membrane and modified soil	with membrane
1) Materials				
	Slinky coil ²⁾	£	2.35	2.35
	Membrane	£	0.57	0.57
	Area ³⁾	m ²	1.00	1.00
	Sum	£	2.35	2.92
2) Construction				
	Digging ⁴⁾	£	4.53	4.53
	Depth	m	1.50	1.50
	Mixing ⁵⁾	£	0.87	
	Time	hr	0.03	
	Filling ⁶⁾	£	2.20	2.20
	Volume	m ³	1.50	1.50
	Sum	£	6.73	6.73
	3) Total cost	£	9.08	9.65

- 1) (Langdon, 2006). Data was compared for 1 m-installation.
 2) Made of high density polyethylene with density of 960 kg/m³ (Holman, 2002), 604.6 £/ton (Kavanaugh et al., 1
 3) Only for base area
 4) Including labour, plant and machine hire
 5) Including plant and fuel
 6) Including labour and plant

than 16.1 years. When soil modification is not applied, it would take time until rain is absorbed equally around the slinky coil to enhance soil thermal conductivity.

One of the strategies to enhance conductive heat transfer was mixing highly conductive materials, such as quartz. Quartz is contained in natural soil; therefore, the procurement cost could be lower than that of carbon fibres. Nevertheless, less than 50 years of payback period is crucial, and so practically applicable amount ought to be estimated. The result indicated that mixing 3.8 volume% of quartz could be possible (Table 7.19). The method would be random mixing; therefore, estimated effective quartz content was 70 % of 3.8 volume%, 2.7 % (see section 2.4.3). With regard to quartz sand with the lowest published data of thermal conductivity, 6.21 W/m/K, the total thermal conductivity could be approximately 2.57 W/m/K after the soil reaches the OMC (Equation 2.1). This was lower than that of soil at OMC with compaction, 2.64 W/m/K, as measured in section 5.7.1. A

Table 7.19 Estimation of practically feasible quartz mixture

Available budget for quartz soil ¹⁾	1.49 £/m-installation
	0.99 £/m ³ ²⁾
Unit price for soil ³⁾	13.5 £/m ³
Quartz content ⁴⁾	78.1 vol%
Affordable quartz soil	0.074 m ³ /m-installation
	4.9 vol%
Genuine content of quartz	3.8 vol%

1) Difference between price for case S-2 and price which made payback period within 50 years, 11.14 £/m in Table 7.17.

2) For a 1.5 depth

3) The total volume for soil modification was 357.9 m³; therefore, price for under £1,000 of reasonable quality topsoil was referred. (Langdon, 2006)

4) Refer to commercialised quartz soil, which contained 83 weight% quartz. (Bucbricks, 2007 and Holman, 2002)

parametric analysis for the soil with the slinky coil buried at a 2.5 m depth demonstrated 1 % gain of the total heat collection in section 6.3.3. Therefore, it was presumed that the effect would be less than that of this case. This impact did not encourage considering the practical use; therefore, improving the consistency of soil thermal conductivity around the heat exchanger would be more feasible modification strategy.

7.5.3 Design proposal to retain soil moisture content

It would be economic to allow the ground surface to be remained in the conventional condition, such as being covered with grass or being exposed to the sunshine. Though solar gain is welcome for recovering stored heat during heating operation seasons, water evaporation from the soil surface would decrease soil thermal conductivity underground. Rainfall is expected to naturally top-up the lost moisture; however, applying a function to assure effective moisture recovery would be more desirable. Therefore, combining a design of soakaways is proposed to be investigated.

Soakaways are normally vertical holes to collect run-off water and release it to greater depth underground. The design typically consists of an invert, top cover, tube structure with holes in the vertical wall, solid base and backfill with coarse sand or gravel around the structure (Pavingexpert, 2003). Run-off water is guided into the underground structure through the invert and distributed into the surrounding soil through the holes in the wall. Small soil particles should not contaminate the remained water within the soakway; therefore, a layer of coarse particles are prepared between sub-soil and the holes.

To avoid water evaporation on the internal surface of the wall, the tube should be filled with water all the time. Nevertheless, holding large volume of water in the middle of heat transfer area could be costly due to the reinforcement or could disturb the high conductive heat transfer as discussed in section 4.3.2. Hence, installing a number of small soakaways would be a suitable design solution for this case.

The small tube is buried above the slinky coil to distribute water in the modified soil space in the proposed design idea (Figure 7.8). Small construction cost is one of the essential criteria. To eliminate the solid bed and the tube wall with thick reinforcement, packing the internal tube space with gravels can be considered. Nonetheless, a drawback needs to be noted in this strategy. The water within the tube will stay still most of the time; therefore, convective heat transfer would not be expected unlike designs with a rainwater tank examined in Chapter 4. Thermal conductivity

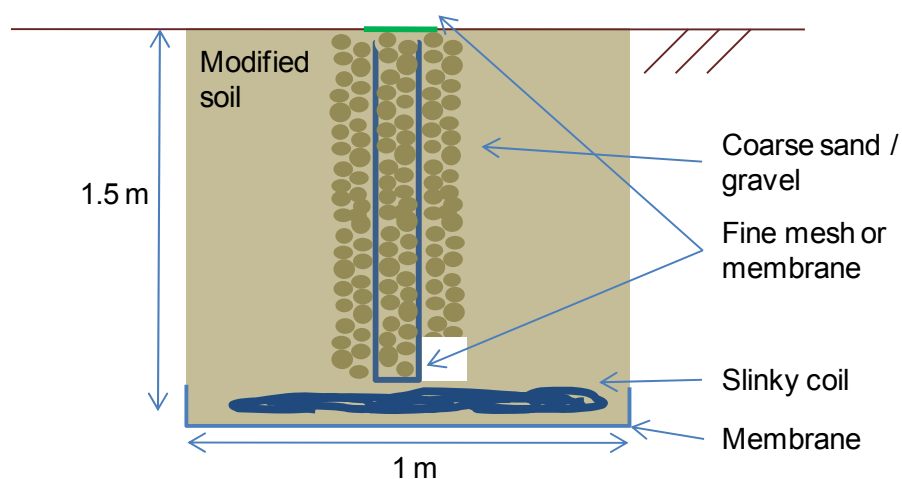


Figure 7.8 Design proposal to apply soakaways to modified underground structure

of water itself, 0.6 W/m/K, would be dominant over the total conductivity within the tube, even though the packed gravels have a larger value.

The structure could be composed from light and commercialised materials, such as flexible mesh to cover the underground tube space and to distribute rainwater to the surrounding soil. Thickness of the coarse sand or gravel outside of the mesh ought to be small, so as to minimise the disturbance by the lower thermal conductivity than that of the modified soil.

Required volume of soakaways can be calculated for a case study, which is case S-1 with soil modification and a membrane applied to the existing design as discussed previously. The average rainfall in Nottingham, UK was 1.12 mm/hour between 2001 and 2005. Regarding the system required to install slinky coil for area of 269 m X 1 m wide, the required total soakaway volume is 0.1 m³ according to Equation 7.8 (Pavingexpert, 2003).

$$\text{Required volume [m}^3\text{]} = \text{Area [m}^2\text{]} \times (\text{Rainfall [mm/hr]} / 3,000)$$

(Equation 7.8)

When each soakaway has a column shape of a 0.05 m diameter and 1.5 m deep with 50 % of packed gravels inside, the required number is approximately 67.9 for the whole system. When these soakaways are buried every 4 m for 269 m, the total will be 67.2. When the site is obliged to construct soakaways, this design strategy can fulfil the requirement.

The economic estimation is the most critical aspect to judge if this strategy

can be feasible. Unit costs for setting the membrane and the gravels for 0.1 m thick are referred to published database (Lngdon, 2006). Each value includes its labour, material and plant cost; 3.32 £/m² for a membrane and 18.35 £/m³ for gravels respectively. When a soakaway is installed every 4 m, the cost would be approximately 0.23 £/m. When only membrane above the slinky coil and soakaways are added to the existing design, the total unit cost would be around 9.31 £/m, which leads to its payback period of less than 1 year. Thus, this combination would ensure the consistent moisture content and high thermal conductivity around the slinky coil within reasonable investment costs.

7.6 Conclusions

Six design combinations with soil modification were compared to the existing design in terms of heat collection capacity. The required size of components and the required installation area were estimated for heating an insulated office building in Nottingham. Though the effects of convective heat transfer and thermal energy in rainwater were confirmed, the initial cost was remarkably larger than that of the existing design. As a consequence, it was found that a case with the horizontal slinky coil and 3 m of soil modification was the most competitive among the six

Annual operation is compared between the modified design and the existing design, so as to judge if the cost performance of the modification is feasible. Both design cases were applied to a heating and air-conditioning system for an insulated office building. Annual demands were firstly approximated based on the climatic data measured in Nottingham, UK.

Simulation for each month showed that the existing design decreased 52 % of CO₂ emission compared to the conventional heating and cooling system consisting of electric boilers and electric air-conditioners. Besides, the modified design could collect more ground source energy by 13 % on average. However, the saved electricity consumption was 30.5 kWh/year, which was equivalent to 2.7 % of the total consumption in the existing design. The main reason was a small increase of the operational COP of the selected heat pump against the enhanced heat collection. Therefore, it was critical to assess the COP curve, in order to create practical benefits.

The calculated payback period was too large to consider practical. Therefore, an idea of laying a water proof membrane below the heat exchanger to retain soil moisture content for higher thermal conductivity was assessed. A sensitivity analysis suggested that this strategy could make payback period less than 16.1 years with or without soil modification for 1.5 m. As a consequence, it was concluded that focusing on increasing the reliability of heat collection performance was a feasible approach due to already reasonable initial cost of the existing design.

The next chapter summarises the outcomes of this thesis and suggests future works to make the modification proposal ready for practical use.

Chapter 8 Conclusions and Future Works

Introduction

This research sought to address the problem of slow uptake of ground source heat pumps (GSHP) in the commercial and small industrial sectors. The main barriers of the GSHP were unpredictable operational performance, modest efficiency which requires large installation space and discouraging economic feasibility. Therefore, design solutions were investigated for horizontal slinky coil systems, which have less impact of construction costs than borehole systems. The findings of this project are briefly reviewed in this chapter. Subsequently, further works to accomplish the investigations are highlighted.

8.1 Conclusions

A thorough sensitivity analysis with computational fluid dynamics (CFD) was a constructive first step to narrow down essential design parameters. The results revealed that significantly more heat was collected when rainwater flowed into an underground rainwater collection tank compared with study cases without flow. In addition, deeper rainwater collection tanks and higher thermal conductivity in grout and soil surrounding the slinky coil brought more efficient heat collection.

Measurements with dual probe heat pulse method (DPHP) showed that soil samples at the optimum moisture content (OMC) achieved high thermal conductivity. It was also found that extra compaction at construction sites would provide the highest thermal conductivity among the study cases and

blending soil particles to attain the maximum packing ratio increased thermal effusivity remarkably. Nevertheless, it was concluded that mixing rainwater to the OMC delivers the largest effusivity with the most effortless and economic method.

Design investigation with the CFD disclosed that a combination between soil modification and thermal pillars consisting of highly conductive grout and graphite raises little underground conductive heat transfer. Alternatively, extending the depth of the soil modification space could increase collectable thermal energy more effectively.

The outcome of simulation analysis among different design combinations clarified that design cases with a rainwater collection tank were more efficient. However, designs focusing on conductive heat transfer had more economic feasibility. The subsequent comparison with the CFD unveiled that the modified design with soil modification and no rainwater collection tank could collect more ground heat source than the existing design. However, the yearly electricity saving was too little to replace the existing design on the current market situation. It seemed that improvements would be potentially seen when the COP inclination against a rise in the outlet heating source temperature is close to the proportional rate. Nevertheless, it was suggested that laying a water proof membrane below the slinky coil would bring consistently high soil thermal effusivity within a reasonable payback period.

The investigation revealed that the existing design itself provides remarkable economic benefits with reasonable construction costs. However, the proposed

modification with the membrane would add more reliable performance by maintaining higher heat transfer efficiency with feasible extra investment costs.

8.2 Suggestions for Future Works

The investigation highlighted the criteria to make effective use of the proposed modification strategy. Further researches are advised to cover the weak characteristics and to find the best conditions for practical use. This section describes the suggestions in three steps.

The annual operation analysis demonstrated the technical advantages of soil modification, though the economic feasibility was unconvincing. Therefore, searching beneficial applications would expand a chance of the effective use of the findings. When the strategy is used for the GSHP, it is of essence to investigate the heat pump market for advantageous COP characteristics, in which the increase is large against the rise in the outlet heat source temperature. Once system applications are determined, simulation analysis with precise input data ought to be considered to raise the accuracy. Particularly, underground data, such as yearly soil temperature gradient and soil thermal conductivity, is vital. Hence, conducting yearly field measurement would be ideal. Furthermore, building more precise simulation models would be ideal, for instance, models with reasonable validation results and more realistic modelling of the slinky coil.

An effective strategy to refill water must be required in practice. The design ideas and the cost estimation for rainwater feeders inspired from soakaways

seemed fine for the first consideration as proposed in section 6.4.3. Therefore, it would be worthwhile to examine the concrete design criteria for effective use. Firstly, the necessity of the feeders needs to be questioned. If a drop in soil moisture content is seen over the operation of the modified design, whether this design improves the situation or not must be evaluated, for instance, through experiments. When the positive effects are confirmed, the detailed design should be optimised. One of the most sensitive parameters is the thickness of the outer gravels and the diameter of the feeders. As mentioned in section 6.4.3, too thick steady water and too thick gravel layer might lessen the overall heat transfer. Finally, the distance between the feeders must have the optimum value, which brings the best cost performance.

More case studies with different climatic and operational conditions would clarify the criteria for feasible projects. This would be useful to judge if the project is worthwhile to consider designing, construction and operation. When the project is approved to be potentially successful, design optimisation ought to be finalised with dynamic simulation for annual operation. It would be sensible to progressively confirm the performance through field tests or operation in small scale systems. Once the facilities start the operation, analysing the operational data to update the understanding of the modification is vital.

References

- Al-Huthaili, Salim Saif (2004) *Experimental and theoretical investigation of ground source heat pump systems at the Marmont Centre and the David Wilson Millennium Eco-House*. Ph. D. thesis, University of Nottingham.
- Al Khaleej Coat Metal L.L.C ([no date]) *Honeycomb Insulated Steel Door* [on line]. Al Khaleej Coat Metal L.L.C. Available at URL: <
http://www.al-khaleejcoating.com/Door%20division/Honeycomb_Insulated_Steel_Door.html > [Accessed 20th July 2009]
- Allan, Marita L. (2000) Materials characterization of superplasticized cement-sand grout. *Cement and Research*, 30, 937-942.
- American Institute of Aeronautics and Astronautics (1998) AIAA G-077-1998. *Guide for the Verification and Validation of Computational Fluid Dynamics Simulations*. Reston: American Institute of Aeronautics and Astronautics.
- American Society of Heating, Refrigerating and Air-Conditioning Engineers ([no date]) 1118-TRP. *Methods for Determining Soil and Rock Formation Thermal Properties from Filed Tests*. (s.l.): (s.n.).
- Anderson, Bruce and Wells, Malcolm (1996) *Passive Solar Energy – The Homeowner’s Guide to Natural Heating and Cooling*. Massachusetts: Brickhouse Pub. Co..
- Angel Plastics ([no date]) *Technical Guide Gutter and Downpipe Systems* [on line]. Angel Plastics. Available at URL: <
http://www.angelplastics.co.uk/installation_guttering_technical.asp > [Accessed 20th July 2009]

- ANON ([no date]) *Rapid Unico Air Conditioning Range* [on line]. Available at URL: <
http://www.discountedheating.co.uk/shop/acatalog/Rapid_Unico__Air_Conditioning_Range.html > [Accessed 10th April 2009]
- Ansari, F. A., Mokhtar, A. S., Abbas, K. A. and Adam, N. M. (2005) A Simple Approach for Building Cooling Load Estimation. *American Journal of Environmental Science*, 1(3), 209-212.
- Arens, Edward, Xu, Tengfang, Miura, Katsuhiko, Hui, Zhang, Fountain, Marc and Bauman, Fred (1998) A study of occupant cooling by personally controlled air movement. *Energy and Buildings*, 27, 45-59.
- Argo Controls (2008) *"AT" Series Electric Boilers Rev. 10*. New York: Argo Controls.
- Ashrae (2007) *2007 ASHRAE handbook; heating, ventilating, and air-conditioning applications*. Atlanta: American Society of Heating, Refrigerating and Air-conditioning Engineers.
- Baltik Engineering (2005) *How to Get Started on a ComfortAir Project Quickly*. (s.l.): (s.n.).
- Barbier, Enrico (2002) Geothermal energy technology and current status: an overview. *Renewable and Sustainable Energy Reviews*, 6, 3-65.
- Barnes, G. E. (1995) *SOIL MECHANICS Principles and Practice*. Malaysia: Macmillan Press Ltd.
- Bilskie, J. R., Horton, R. and Bristow, K. L. (1998) Test of dual-probe heat-pulse method for determining thermal properties of porous materials. *Soil Science*, 163(5), 346–355.
- Blanuša, Peter, Čurčija, Dragan and Goss, William P. (1999) *Therm Heat*

Transfer Analysis of Simulation Round Robin 1998-99. Amherst: Building Energy Research Laboratory.

Brandrup, J., Immergut, E. H. And Grulke, E. A. (1999) *Polymer handbook (4th Edition)*. New York: Wiley.

Bristow, K. L., Bilski, J. R., Kluitenberg, G. J. and Horton, R. (1995) Comparison of techniques for extracting soil thermal properties from dual-probe heat-pulse data. *Soil Science*, 160, 1-7.

Bristow, Keith L. (1998) Measurement of thermal properties and water content of saturated sandy soil using dual-probe heat-pulse probes. *Agricultural and Forest Meteorology*, 89, 75-84.

Bristow, Keith L., Kluitenberg, Gerard J., Goding, Chris J. and Fitzgerald, Terry S. (2001) A small multi-needle probe for measuring soil thermal properties, water content and electrical conductivity. *Computers and Electronics in Agriculture*, 31, 265-280.

Bristow, K.L., Kluitenberg, G.J., Horton, R. (1994) Measurement of soil thermal properties with a dual-probe heat-pulse technique. *Soil Science Society of America Journal*, 58, 1288-1294.

Bristow, Keith L. (1998) Measurement of thermal properties and water content of unsaturated sandy soil using dual-probe heat-pulse probes. *Agricultural and Forest Meteorology*, 89, 75-84.

British geological survey (1996) *Nottingham England and Wales Sheet 126 Solid and Drift Geology*. 1:50 000. Keyworth, Nottingham: British Geological Survey.

British Standards Institution (1990) BS 1377-2:1990. *Methods of test for Soils for civil engineering purposes Part 2; Classification tests*. Offices and shops.

British Standards Institution (1998) BS 13370:1998. *Thermal performance of*

buildings – Heat transfer via the ground – Calculation methods. Offices and shops.

British Standards Institution (2004) PD 6461-4:2004. *General metrology – Part 4: Practical guide to measurement uncertainty*. Offices and shops.

Bucbricks (2007) *Technical Specifications*. [on line]. Bucbricks Co. Ltd. Available at URL: < <http://www.bucbricks.com/technical.html> > [Created 2007. Accessed 26 October 2008]

Building Control Section Planning & Transport Angus Council ([no date]) *Septic tanks and soakaways to houses and the building regulations*. Forfar: Angus Council.

Busby, Jon (2005) *Site conditions: Initial considerations before installing a ground source heat pump*. Keyworth: British Geological Survey.

Campbell, Gaylon S. and Bristow, Keith, L. ([no date]) *Underground Power Cable Installations: Soil Thermal Resistivity*. Armidale: ICT International.

Campbell, Gaylon S. and Norman, John M. (1998) *An Introduction to Environmental Biophysics*. New York: Springer.

Campbell, G.S., Calissendorff, C. And Williams, J.H. (1991) Probe for measuring soil specific heat using a heat-pulse method. *Soil Science Society of America Journal*, 55, 291–293.

Campbell, G.S. (1985) *Soil Physics with BASIC-Transport Models for Soil-Plant Systems*. Elsevier: New York.

Chang, C. W., Han, Wei-Qiang and Zettl, A. (2005) Thermal conductivity of B-C-N and BN nanotubes. *Journal of Vacuum Science & Technology B*, 23(5), 1883-1886.

Chong, Chiew Shan Anthony (2006) *Experimental and Numerical Study of a*

- Rainwater Ground-Source Heat Pump*. Ph. D. thesis, University of Nottingham.
- Choongho, Yu, Saha, Sanjoy, Zhou, Jianhua and Shi, Li (2006) Thermal contact resistance and thermal conductivity of a carbon nanofibre. *Journal of Heat Transfer*, 128, 234-239.
- Dedecek, P., Safanda, J., Kresl, M. and Cermak, V. (2006) Ground Surface Temperature Monitoring under Different Types of Surfaces – the Three Year Results. *Geophysical Research Abstracts*, 8, 07795.
- de Vries, D.A. (1963) Thermal properties of soils. *In: W.R., van Wijk, ed.: Physics of plant environment*. Amsterdam: North-Holland Publ. Co. p. 210–235.
- Demirboğa, Ramazan and Gül, Rüstem (2003) The effects of expanded perlite aggregate, silica fume and fly ash on the thermal conductivity of lightweight concrete. *Cement and Concrete Research*, 33, 723-727.
- Department of Energy & Climate Change and Energy Trust (2009) *Low Carbon Buildings Programme (LCBP) Phase 1* [on line]. Department of Energy & Climate Change and Energy Trust. Available at URL: <
<http://www.lowcarbonbuildings.org.uk/> > [Revised 2009. Accessed 5th December 2009]
- Department for Environment, Food and Rural Affairs (2006) *The United Kingdom's Report on Demonstrable Progress under the Kyoto Protocol*. London: Department for Environment, Food and Rural Affairs.
- Department of the Environment, Transport and the Regions (1999) *Government Response to the Third Annual Report of The Government's Panel On Sustainable Development*. London: Department of the Environment, Transport and the Regions

- de Vries, D.A. (1963) Thermal properties of soils. *In: Van Wijk, ed. W.R.: Physics of plant environment*. Amsterdam : North-Holland Publ. Co. pp. 210-235.
- Doherty, P.S., Al-Huthaili, S., Riffat, S.B. and Abodahob, N. (2004) Ground source heat pump – description and preliminary results of the Eco House system. *Applied Thermal Engineering*, 24, 2627-2641.
- Down, P. G. (1969) *Heating and Cooling Load Calculations*. London: Pergamon Press Ltd.
- Durham, William B. (1999) Methane Hydrate: A Surprising Compound. *Science & Technology*, March, 20-25.
- East 30 Sensors (2007) *Specific Heat Sensor User's Manual*. Washington: East 30 Sensors.
- Edwards, K. C. (1966) *Nottingham and Its Region*. Nottingham: Derry and Sons Limited.
- Energy white paper Our energy future – creating a low carbon economy, (Cmnd. 5761, 2003)
- envireau (2006) *Water-Fast Facts* [on line]. envireau. Available at URL: < http://www.envireau.co.uk/water_facts.htm > [Revised March 2006. Accessed 5th December 2006]
- Eskilson, P. (1987) *Thermal analysis of heat extraction borehole*, Thesis, Lund Institute of Technology.
- European Commission (2003 a) *European Guide to Pump Efficiency for Single Stage Centrifugal Pumps*. Varese: European Commission, JRC.
- European Commission (2003 b) *World energy, technology and climate policy outlook*. Luxembourg: Office for Official Publications of the European Communities.

- Ewing, R. P. and Horton, R. (2007) Thermal conductivity of a cubic lattice of spheres with capillary bridges. *Journal of Physics D: Applied Physics*; 40(16). 4959-4965.
- Fanchi, John R. (2004) *Energy - technology and directions for the future*. London: Elsevier Academic Press.
- Fluent Inc. (2001) *Database Materials in Fluent 6.1.18*. (s.l): (s.n.).
- Fontana, A.J., Varith, J., Ikediala, J., Reyes, J. and Wacker, B. (1999) *Thermal properties of selected foods using a dual needle heat-pulse sensor*. An ASAE Meeting Presentation. Paper No. 996063, 1-10. U.S.A: ASAE.
- Forsen, Martin, Nowak, Thomas and Ransquin, Johan (2008) *European Heat Pump Statistics Outlook 2008*. Belgium: The European Heat Pump Association.
- Fukai, Jun, Kanou, Matoko, Kodama, Yoshikazu and Miyatake, Osamu (2000) Thermal conductivity enhancement of energy storage media using carbon fibers. *Energy Conversion & Management*, 41, 1543-1556.
- Gan, Guohui, Riffat, Saffa B. And Chong, C. S. A. (2007) A novel rainwater-ground source heat pump – Measurement and simulation. *Applied Thermal Engineering*, 27, 430-441.
- Gehlin, Signhild. (1998) *Thermal response test – In situ measurements of thermal properties in hard rock*. Licentiate thesis, Lulea University of Technology.
- Gehlin, S. E. A. and Hellstoröm, G. (2003) Influence on thermal response test by groundwater flow in vertical fractures in hard rock. *Renewable Energy*, 28, 2221-2238.
- Geo-Heat Center ([no date]) *Where are Geothermal Resources Located?* [online]. Geo-Heat Center. Available at URL: < <http://geoheat.oit.edu/colres.htm> > [Revised December 2008. Accessed 3rd August 2008]

- Gibert, Benoit and Mainprice, David (2009) Effect of crystal preferred orientations on the thermal diffusivity of quartz polycrystalline aggregates at high temperature. *Technophysics*, 465, 150-163.
- Hall, Matthew and Allinson, David (2009) Assessing the effects of soil grading on the moisture content-dependent thermal conductivity of stabilised rammed earth materials. *Applied Thermal Engineering*, 29 (4), 740-747.
- Harter, Thomas (2003) *Reference: Basic Concepts of Groundwater Hydrology*. Publication 8083 - FWQP Reference Sheet 11.1. Oakland: Division of Agriculture and Natural Resources, University of California.
- Helling, B., Reinecke, S. A. and Reinecke, A. J. (1999) Effects of the Fungicide Copper Oxychloride on the Growth and Reproduction of *Eisenia fetida* (Oligochaeta). *Ecotoxicology and Environmental Safety*, 46, 108-116.
- Hellström, Goran ([no date]) *Thermal performance of borehole heat exchangers*. [on line]. The Richard Stockton College of New Jersey. Available at URL: <
http://intraweb.stockton.edu/eyos/energy_studies/content/docs/proceedings/HELLS.pdf > [Accessed 6 July 2007]
- Hevacomp Ltd (2006) *DMAT – Access to materials database v22.00*. (s.l.): (s.n.).
- Hilpert, Markus (2009) Effects of dynamic contact angle on liquid infiltration into inclined capillary tubes: (Semi)-analytical solutions. *Journal of Colloid and Interface Science*, 337, 138-144.
- Holman, J. P. (2002) *Heat transfer*. New York: McGraw-Hill.
- Houben, Hugo and Guillard, Hubert (1994) *Earth Construction: A comprehensive Guide*. Rugby: Practical Action Publishing.
- Houghton, J. T., Ding, Y., Griggs, D. J., Noguer, M., van der Linden, P. J., Dal, X. , Maskell, K. And Johnson, S. A. (2001) *Climate Change 2001: The Scientific*

Basis. Cambridge: Cambridge University Press.

IEA Heat Pump Centre (2004) *How heat pumps achieve energy savings and CO₂ emissions reduction – an introduction* [on line]. IEA Heat Pump Centre. Available at URL: < <http://www.heatpumpcentre.org/> > [Revised 1st March 2004. Accessed 6th November 2006]

IEA Heat Pump Centre (2005) *News Letters Volume 23. No.4*. Boras: IEA Heat Pump Centre.

International Organization for Standardization (1991) ISO 8301:1991(E). *Thermal insulation – Determination of steady-state thermal resistance and related properties – Heat flow meter apparatus*. Geneva: International Organization for Standardization.

International Organization for Standardization (1996) ISO 10051:1996(E). *Thermal insulation – Moisture effects on heat transfer – Determination of thermal transmissivity of a moist material*. Geneva: International Organization for Standardization.

Ismail, A. I. M. and El-shamy, A.M. (2008) Engineering behaviour of soil materials on the corrosion of mild steel. *Applied Clay Science*, 42 (3-4), 356-362.

Japan Meteorological Agency (2006) *Search Engine for past climatic data* [on line]. Japan Meteorological Agency. Available at URL: < http://www.data.jma.go.jp/obd/stats/etrn/index.php?prec_no=&prec_ch=&block_no=&block_ch=&year=&month=&day=&view= > [Revised 2006. Accessed 2006]

Jersey Electricity ([no date]) *A guide to The Energy Efficiency Home*. St Helier: Jersey Electricity.

Kavanaugh, Steve, Gilbreath, Christopher and Kilpatrick, Joseph (1995) *Cost Containment for Ground-source Heat Pumps*. Alabama: Alabama

Universities-TVA Research Consortium (AUTRC).

Klargester ([no date]) *Sealed cresspool for effective containment of domestic sewage*. Aylesbury: Klargester Environmental Limited.

KIKO Network (2006) *Creating a Vision – Cutting Emissions 30% by 2020 A reduction Scenario and Policy Proposals for Japan’s Residential and Commercial Sectors*. Tokyo: KIKO Network.

Kluitenberg, G. J., Bristow, K. L., Das, B. S. (1995) Error analysis of heat pulse method for measuring soil heat capacity, diffusivity and conductivity. *Soil Soil Science Society of America Journal*, 59, 719-726.

Kluitenberg, G. J., Ham, J. M. and Bristow, K. L. (1993) Error analysis of the heat pulse method for measuring soil volumetric heat capacity. *Soil Science Society of America Journal*, 57, 1444-1451.

Kluitenberg, G. J. ([no date]) *5.2 Heat Capacity and Specific Heat (Draft for “Soil Heat”)*

Kreith, Frank and Goswami, D. Yogi (2005) *The CRC handbook of mechanical engineering*. Boca Raton: CRC Press.

Kusuda, T. And Archenbach, P.R. (1965) *Earth temperature and thermal diffusivity at selected stations in the United States*, ASHRAE Transactions 71 (Part 1). (s.l.): American Society of Heating, Refrigerating and Air-conditioning Engineers.

Langdon, D. (2006) *SPON’S – Civil Engineering and Highway Works Price Book*. Abingdon: Taylor & Francis.

Leech, Andrew (2006) *Why are ground source heat pumps being left behind?* [on line]. 4ecotips.com. Available at URL: <

http://www.4ecotips.com/eco/article_show.php?aid=700&id=257 > [Created 9th

May 2006. Accessed 31st May 2008]

Lienhard IV, John H. and Lienhard V, John H. (2006) *A heat transfer textbook third edition*. Massachusetts: Phlogiston Press.

Lim, Kyoungbin, Lee, Sanghoon and Lee, Changhee (2007) An experimental study on the thermal performance of ground heat exchanger. *Experimental Thermal and Fluid Science*, 31(8), 985-990.

Lipiec, J., Usowicz, B. And Ferrero, A. (2007) Impact of soil compaction and wetness on thermal properties of sloping vineyard soil. *International Journal of Heat and Mass Transfer*, 50, 3837-3847.

LitchfieldGeothermal ([no date]) Frequently Asked Questions (FAQ) [on line]. LitchfieldGeothermal.com. Available at URL: <

http://www.litchfieldgeothermal.com/frequently_asked_questions.htm >

[Accessed 25th April 2009]

Li, Xiao-Yan, Xie, Zhong-Kui and Yan, Xiang-Ku (2003) Runoff characteristics of artificial catchment materials for rainwater harvesting in the semiarid regions of China. *Agricultural Water Management*, 65, 211-224.

Li, Xinguo, Zhao, Jun and Zhou, Qian (2005) Inner heat source model with heat and moisture transfer in soil around the underground heat exchanger. *Applied Thermal Engineering*, 25, 1565-1577.

Lund, J., Sanner, B., Rybach, L., Curtis, R. and Hellström, G. (2004) Geothermal (Ground-source) Heat Pumps A World Overview. *GHC Bulletin*, September 2004. 26, 1.

Lu, Sen, Ren, Tusheng, Gong, Yuanshi and Horton, Robert (2007) An Improved Model for Predicting Soil Thermal Conductivity from Water Content at Room Temperature. *Soil Science Society of America Journal*, 71(1), 8-14.

- Majumdar, Pradip (2005) *Computational methods for heat and mass transfer*. London: Taylor & Francis.
- M. Conde Engineering (2002) *Thermophysical Properties of Brines – Models*. Zurich: M. CONDE ENGINEERING.
- Michaels, Joelle (2002) *Commercial Buildings Energy Consumption Survey – commercial energy uses and costs* [on line]. Energy Information Administration. Available at URL: < <http://www.eia.doe.gov/emeu/cbecs/> > [Created 15 August 2002. Accessed 5th October 2007]
- Moghadas, J., Muller-Steinhagen, H., Jamialahmadi, M. and Sharif, A. (2004) Theoretical and experimental study of particle movement and deposition in porous media during water injection. *Journal of Petroleum Science and Engineering*, 43, 163-181.
- Mori, Y., Hopmans, J. W., Mortensen, A. P. and Kluitenberg, G. J. (2003) Multi-Functional Heat Pulse Probe for the Simultaneous Measurement of Soil Water Content, Solute Concentration, and Heat Transport Parameters. *Vadose Zone Journal*, 2, 561-571.
- Nagano, Katsunori (2006) *Development of Ground Source Heat Pump Systems in Japan* [on line]. IEA Heat Pump Centre. Available at URL: < http://www.heatpumpcentre.org/Workshops/Workshop_Tokyo_May_2006/Sum_GSHP_Nagano.pdf > [Created May 2006. Accessed 31st May 2008]
- Nahar, N.M., Sharma, P. and Purohit, M.M. (2003) Performance of different passive techniques for cooling of buildings in arid regions. *Building and Environment*, 38, 109-116.
- Nayak, J. K., Spivastava, A., Singh, U. and Sodha, M. (1982) The relative performance of different approaches to the passive cooling of roofs. *Building and*

Environment, 17(2), 145-161.

Nidal, H., Abu-Hamdeh. and Randall, C. Reeder. (2000) Soil Thermal Conductivity: Effects of Density, Moisture, Salt Concentration, and Organic Matter. *Soil Science Society of America Journal*, 64, 1285-1290.

Noborio, Kosuke, McInnes, K.J. and Heilman, J.L. (2002) On measuring soil thermal properties with a dual-probe heat-pulse technique. *Journal of Japan Society of Soil Physics*, 90, 3-9.

Ochsner, Tyson E., Horton Robert and Ren Tusheng (2003) Use of the Dual-Probe Heat-Pulse Technique to Monitor Soil Water Content in the Vadose Zone. *Vadose Zone Journal*, 2, 572-579.

Office of Geothermal Technologies (1999) *Geothermal Heat Pumps for Medium and Large Buildings*. Washington DC: Office of Geothermal Technologies.

Office of the Deputy Prime Minister (2000) *The Building Regulations 2000 – Conservation of fuel and power – Approved document L2B 2006 edition*. London: NBS.

Office of Water Services (2006) *Facts and figures – May 2006*. Birmingham: Office of Water Services.

Onmura, S., Matsumoto, S. and Hokoi, S. (2001) Study on evaporative cooling effect of roof lawn gardens. *Energy and Buildings*, 33, 653-666.

P. A. Hilton Ltd. (1994) *Experimental Operating and Maintenance Manual*. Hampshire: P. A. Hilton Ltd..

Pavingexpert (2003) *Soakaway design and construction* [on line]. pavingexpert. Available at URL: < <http://www.pavingexpert.com/drain08.html> > [Revised 2009. Accessed 18th June 2009]

Pedersen, Per, Henrik (2003) *Evaluation of the possibilities of substituting potent*

- greenhouse gases (HFCs, PFCs and SF6) – Environmental Project No. 771.*
København: The Danish Environmental Protection Agency.
- Pereira, Cristiana, Gonilho, Castro-Comes, João and Pereira de Oliveira, Luis (2009) Influence of natural coarse aggregate size, mineralogy and water content on the permeability of structural concrete. *Construction and Building Materials*, 23, 602-608.
- Pilkington Building Products ([no date]) *Pilkington Architectural Product Guide*. Toledo: Pilkington Building Products.
- Power Efficiency Corporation ([no date]) *White Paper – Motor Efficiency Controllers*. Las Vegas: Power Efficiency Corporation.
- Purdue University School of Civil Engineering (2002) *The Purdue TDR Method for Water Content and Density of Soil*. (s.l.): (s.n.).
- Ramirez, Isaias, Jayaram, Shesha and Cherney, Edward A. (2009) *Thermal Conductivity of Silicone Rubber Nanocomposites*. In proceedings of a conference, '2009 Electrostatics Joint Conference', Boston, 16-18 June, 2009.
- Rees, S. W., Adjali, M. H., Zhou, Z. And Davies, M. (2000) Ground heat transfer effects on the thermal performance of earth-contact structures. *Renewable and Sustainable Energy Reviews*, 4, 213-265.
- Runsheng, Tang, Etzion, Y. and Erell, E. (2003) Experimental studies on a novel roof pond configuration for the cooling of buildings. *Renewable Energy*, 28, 1513-1522.
- Sahu, S. K., Pradhan, K. C. and Sarangi, D. (2004) *Soil Pollution in Orissa*. Orissa Review. September – 2004. 13-15. Bhubaneswar: Information & Public Relations Department, Government of Orissa.
- Sanken Setsubi Kogyo Co., Ltd. (2005) *Radial-well*. (s.l.): (s.n.).

- Sanyo (2006) *Release of CO₂ heat pump “Eco cute”* [on line]. Sanyo. Available at URL: < <http://www.sanyo.co.jp/koho/hypertext4/0609news-j/0913-1.html> > [Created 13th November 2006. Accessed 3rd December 2006]
- Scarborough, Robert ([no date]) *The Geologic Origin of the Sonoran Desert* [on line]. Arizona-Sonora Desert Museum. Available at URL: < http://www.desertmuseum.org/books/nhsd_geologic_origin.php > [Accessed 15th Jun 2009]
- Scheerlinck, Nico, Berhane, Nahor, H., Moles, Carmen, G. And Banga, Julio, R. (2008) Optimal dynamic heat generation profiles for simultaneous estimation of thermal food properties using a hotwire probe: Computation. *Journal of Food Engineering*, 84, 297–306.
- Schweizer, Michael (1997) *Methods in Biotechnology*. London: Taylor & Francis.
- Shokoku Sya, 2000. *Encyclopaedia of design methods of passive architecture for the use of renewable energy*. Tokyo: Shokoku Sya.
- Silvain, Jean-François and Heintz, Jean-Marc (2008) *Drain thermique composite cuivre-carbone* [on line]. Seeds. Available at URL: < <http://seedsresearch.eu/download/2008/08-04-11/4-CuC.pdf> > [Created 11th April 2008. Accessed 15th July 2009]
- Singh, A. K., Chaudhary, D. R. and Jaipur (1991) Parallel wire method for the determination of thermal conductivity and diffusivity of soils. *Soil Technology*, 4, 191-194.
- Smith, Marvin (2006) *Shallow heat exchanger performance and Cost-Reduction potential*. In proceedings of a special conference, ‘2006 Technical Conference and Expo’, U.S.A., 11-12 October, 2006.
- Sodha, M. S., Govind, Bansal, P. K. and Kaushik, S. C. (1980) Reduction of heat

flux by a flowing water layer over an insulated roof. *Building and Environment*, 15, 133-140.

SSH Associates ([no date]) *Domestic Electricity Prices* [on line]. SSH Associate. Available at URL: < <http://sshassociates.co.uk/DomesticElectricityPrices.aspx> > [Accessed 15th April 2009]

Tao, William K. Y. (2001) *Mechanical and electrical systems in buildings*. Upper Saddle River: Prentice Hall.

The Scottish Government (2009) *Community Renewable Energy Toolkit* [on line]. The Scottish Government. Available at URL: < <http://www.scotland.gov.uk/Publications/2009/03/20155542/3> > [Revised 20th March 2009. Accessed 4th June 2008]

Tiwari, G.N., Upadhyay, M. and Rai, S.N. (1994) A comparison of passive cooling techniques. *Building and Environment*, 29(1), 21-31.

Thyrum, G. and Cruse, E. (2001) *Heat pipe simulation: a simplified technique for modelling heat pipe assisted heat sinks* [on line]. Advanced Packaging, Available at URL: < http://ap.pennnet.com/articles/print_toc.cfm?p=36&v=10&i=12 > [Created December 2001. Accessed 29th July 2009]

United Nations (1998) *Kyoto protocol to the united nations framework convention on climate change*. (s.l.): (s.n.).

Uretek USA (2004) *The URETEK deep injection process (UDI) for roadways and building structures*. (s.l.): (s.n.).

U. S. Department of Energy (1999) *Geothermal technologies Vol.4 Issue 4*. Washington, DC: U. S. Department of Energy.

Verma, L. S, Shrotriya, A. K., Singh, U. and Chaudhary, D. R. (1990) Heat storage coefficient – an important thermophysical parameter and its experimental determination, *Journal of Physics D: Applied Physics*, 23. 1405–1410.

Viessmann Limited (2004) *Technical Series – Heat pumps*. Telford: Viessmann Limited.

Water Features On-line ([no date]) *3P Column Tank 500 Litre* [on line]. Water Features On-line. Available at URL: <
http://www.oak-barrel.com/plastic_water_butts/3p_column_tank.htm >
[Accessed 20th May 2009]

Weber, Susanne (2006) *Cushman & wakefield European survey: German employees have the most spacious offices* [on line]. Cushmans & wakefield. Available at URL: <
<http://www.cushwake.com/cwglobal/jsp/newsDetail.jsp?Language=EN&repld=c5900013p&Country=DE> > [Created 12 July 2006. Accessed 6th October 2007]

Wiegand, Manfred, Groenenboom, Aad and Klaassen, Fred (2009) *Crisis or not, renewable is hot – To reap the rewards, governments and companies should act now*. (s.l.): Price Waterhouse Coopers.

Zeneral heat pump Co. Ltd. (2006) *Electric catalogue Ver. 1.19* [CD-ROM]. Aichi: Zeneral heat pump company.

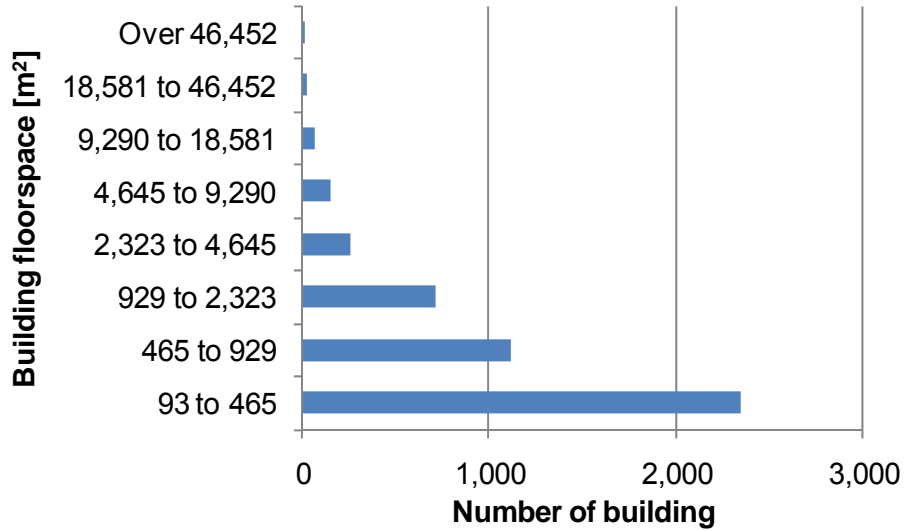
Zeneral Heat Pump Co. Ltd. (2005) *Product list of heat pumps and the specs*. (s.l.): (s.n.).

Zreda, Marek, Desilets, Darin, Ferre, T. P. A. and Scott, Russel L. (2008) *Measuring soil moisture content non-invasively at intermediate spatial scale*

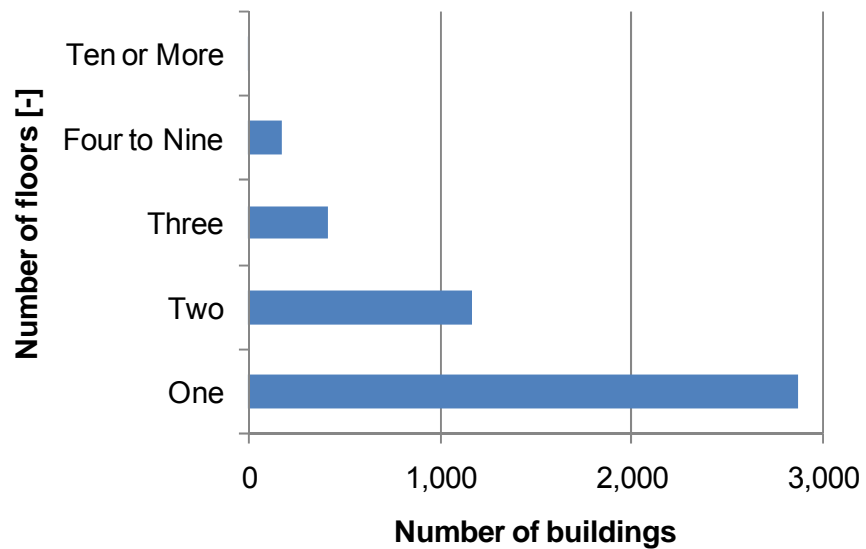
using cosmic-ray neutrons. Geophysical Research Letters. Vol. 35. L21402.

(s.l.): American Geophysical Union.

Appendix A Background Data for Building a Model System for the Simulation Analysis



(1) Number of office buildings categorised by building size



(2) Number of office buildings categorised by floor number

Figure A.1 Statistics of office buildings in the USA (Michaels, 2002)

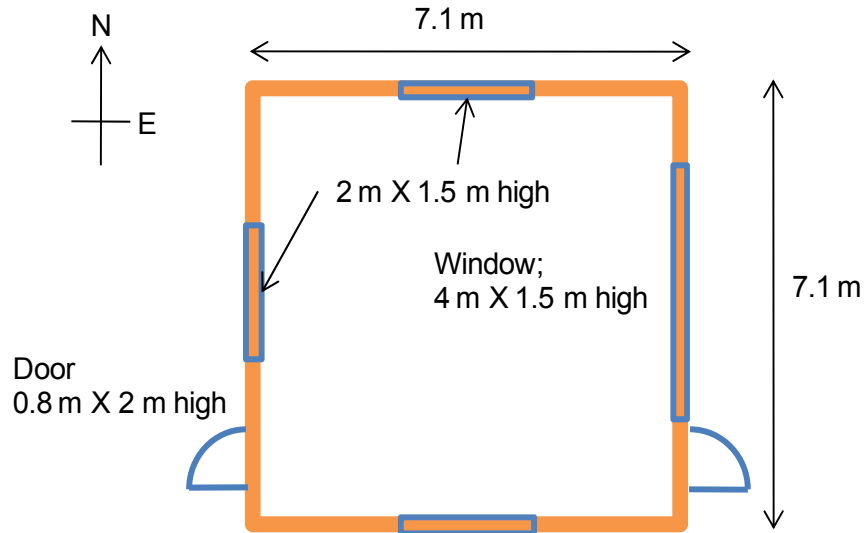


Figure A.2 Plan of the model office building

Table A.1 Materials and conditions of the building model (Baltil Engineering, 2005)

Component	Season	Structure
Roof	Summer	1) the suspended ceiling without loft fan, 1/2 inch Gypsum or Plaster Board, 2) Sand and Gravel or Stone Aggr, a thickness of 4 inches, 3) Still Air, Horizontal Position, Heat Flow Down for the inside air film, 4) 7.5 MPH Wind, Heat Flow in Any Direction for the outside air film under, 5) In Roof Air Space, Horizontal, Heat Flow Down
	Winter	the same until 2), 3) Still Air, Horizontal Position, Heat Flow Up for the inside air film, 4) 15 MPH Wind, Heat Flow in Any Direction for the outside air film, 5) In Roof Air Space, Horizontal, Heat Flow Up no insulation + 100mm common brick
Wall	Summer	1) Still Air, Vertical Position, Heat Flow Horizontal, 2) 7.5 MPH Wind, Heat Flow in Any Direction for the outside air film
	Winter	the same as above apart from 15 MPH wind for the outside air
Floor	Winter	1) covered With Carpet and Rubber Pad , 2) 6 inch Concrete Floor, Concrete Block, Sand and Gravel Aggregate, 3) Still Air, Vertical Position, Heat Flow Horizontal for the inside air film Ground temp in winter;4.74 °C no insulation + 35mm plywood
Door	Summer	1) Still Air, Vertical Position, Heat Flow Horizontal, 2) 7.5 MPH Wind, Heat Flow in Any Direction for the outside air film
	Winter	the same as above apart from 15 MPH wind for the outside air

Table A.2 Indoor conditions of the building model

Components	Condition	
Light	On after 9am for 11 hours until 8pm	
	Classification of lights; 0.55 (recessed lights, not vented, air \geq 0.5ft ² /min/ft ² , diffusers below / through ceiling)	
	Illumination for general office ¹⁾	30 lm/ft ²
	65W fluorescent light ¹⁾	21.5 W/m ²
	Total installed watts	2.2 kW/100m ²
Occupancy	Start working at 9am for 11 hours	
	Very light work ²⁾	4 people
	Light work ²⁾	4 people
	Medium Ventilation Rate	
Electric equipments	Office with computer and other equipments ³⁾	80 W/m ²
		8.0 kW/100m ²
Air infiltration ratio	Summer for 29 °C and tight building	0.3
	Winter for -1.1 °C and tight building	0.6
Glass ⁴⁾	6 mmsingle grey tint	
	Solar heat gain	0.57
	Shading coefficient	0.66

1) (Down, 1969)

2) European standard (Weber, 2006)

3) (ASHRAE, 2007)

4) (Pilkington Building Products, [no date])

*) Other standards (Baltik Engineering, 2005)

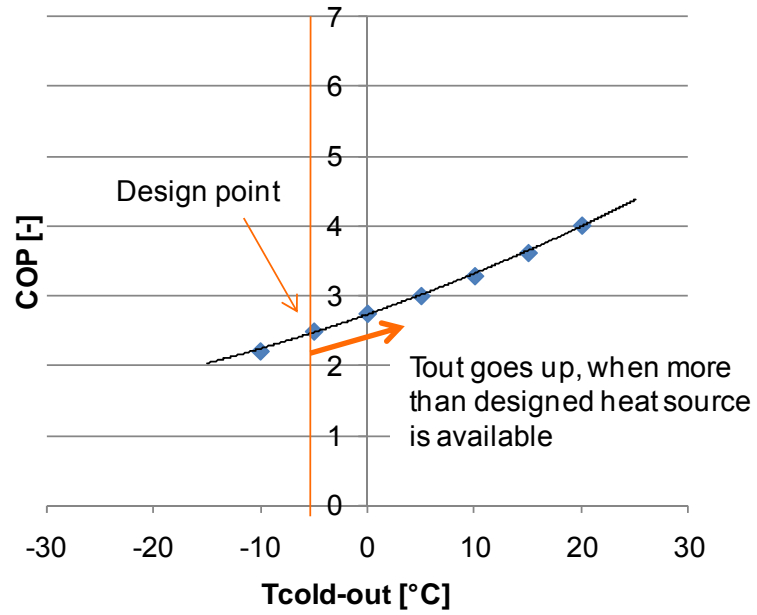
Table A.3 Temperatures settings to calculate design demands

		Heating	Cooling
Outdoor temperature ¹⁾	°C	-3.33	23.3
Target indoor condition ²⁾	°C	20.00	27.3 ³⁾
	RH%		50.0

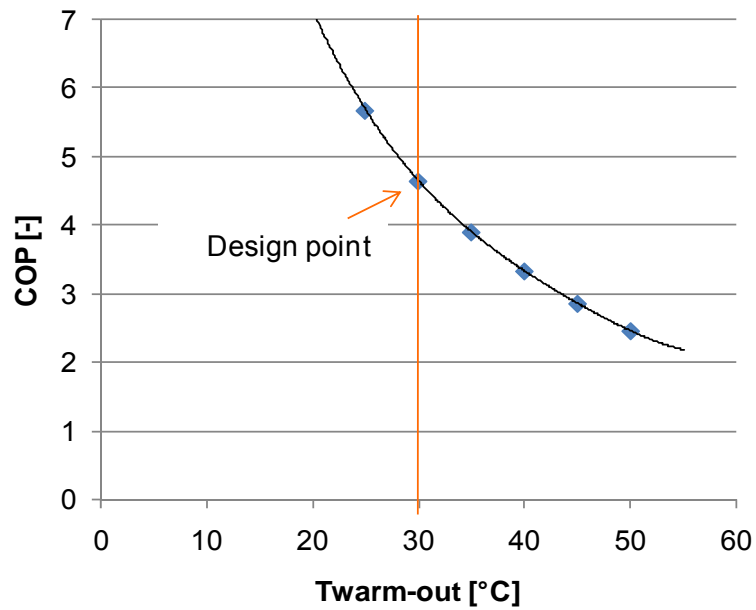
1) Referred to the database in ComfortAir software

2) Target value for heating is recommended by American ministry (Down, 1969)

3) The neutral acceptable temperature when air velocity is 0.7-0.8 m/s and occupants are seated and relaxed (Arend et al., 1998). Cooling load was handled with ventilation until 27.3 °C.



(1) For heating operation (Twarm-out is 45 °C)



(2) For cooling operation (Tcold-out is 7 °C)

Figure A.3 The COP characteristics of the selected heat pump (Zeneral Heat Pump Co. Ltd., 2005)

Table A.4 Properties of 20 % ethylene glycol solution (M. Conde Engineering, 2002)

Correspond operation	Temperature °C	Density kg/m ³	Heat capacity kJ/kg/K	Thermal conductivity W/m/K	Viscosity Pa·s
Heating	0	1,035	3.80	0.50	0.0035
Cooling	30	1,028	3.85	0.52	0.0014

1) Properties were calculated with developed mathematical models for each operation temperature.

Table A.5 Examples to improve U-values in the building model

Component	Season	Structure
Roof	Summer	140 mm mineral wool insulation 1) the suspended ceiling without loft fan, 1/2 inch Gypsum or Plaster Board, 2) Sand and Gravel or Stone Aggregate, a thickness of 4 inches, 3) Still Air, Horizontal Position, Heat Flow Down for the inside air film, 4) 7.5 MPH Wind, Heat Flow in Any Direction for the outside air film under, 5) In Roof Air Space, Horizontal, Heat Flow Down
	Winter	the same until 2), 3) Still Air, Horizontal Position, Heat Flow Up for the inside air film, 4) 15 MPH Wind, Heat Flow in Any Direction for the outside air film, 5) In Roof Air Space, Horizontal, Heat Flow Up
Wall	Summer	110 mm mineral wool insulation + 100mm common brick 1) Still Air, Vertical Position, Heat Flow Horizontal, 2) 7.5 MPH Wind, Heat Flow in Any Direction for the outside air film
	Winter	the same as above apart from 15 MPH wind for the outside air
Floor	Winter	150 mm mineral wool insulation 1) covered With Carpet and Rubber Pad , 2) 6 inch Concrete Floor, Concrete Block, Sand and Gravel Aggregate, 3) Still Air, Vertical Position, Heat Flow Horizontal for the inside air film Ground temp in winter:4.74 °C
	1)	44.5 mm polyurethane foam insulation + 1.2 mm steel plate
Door	Summer	1) Still Air, Vertical Position, Heat Flow Horizontal, 2) 7.5 MPH Wind, Heat Flow in Any Direction for the outside air film
	Winter	the same as above apart from 15 MPH wind for the outside air

1) (Al Khaleej Coat Metal L.L.C, [no date])

Table A.6 Indoor conditions of the insulated building model

Components	Condition	
Light	On after 9am for 11 hours until 8pm	
	Classification of lights; 0.55 (recessed lights, not vented, air \geq 0.5ft ² /min/ft ² , diffusers below / through ceiling)	
	Illumination for general office	15.0 lm/ft ²
	65W fluorescent light	5.4 W/m ²
	Total installed watts	4.0 kW/735m ²
Occupancy	Start working at 9am for 11 hours	
	Very light work ¹⁾	26 people
	Light work	0 people
	Medium Ventilation Rate	
Electric equipments	Office with computer and other equipments	25.0 W/m ²
		18.4 kW/735m ²
Air infiltration ratio	Summer for 29 °C and tight building	0.3
	Winter for -1.1 °C and tight building	0.6
Glass ²⁾	6 mm double grey tint	
	Solar heat gain	0.4
	Shading coefficient	0.52

1) Refer to German average in office area per worker (Weber, 2006)

2) (Pilkington Building Products, [no date])

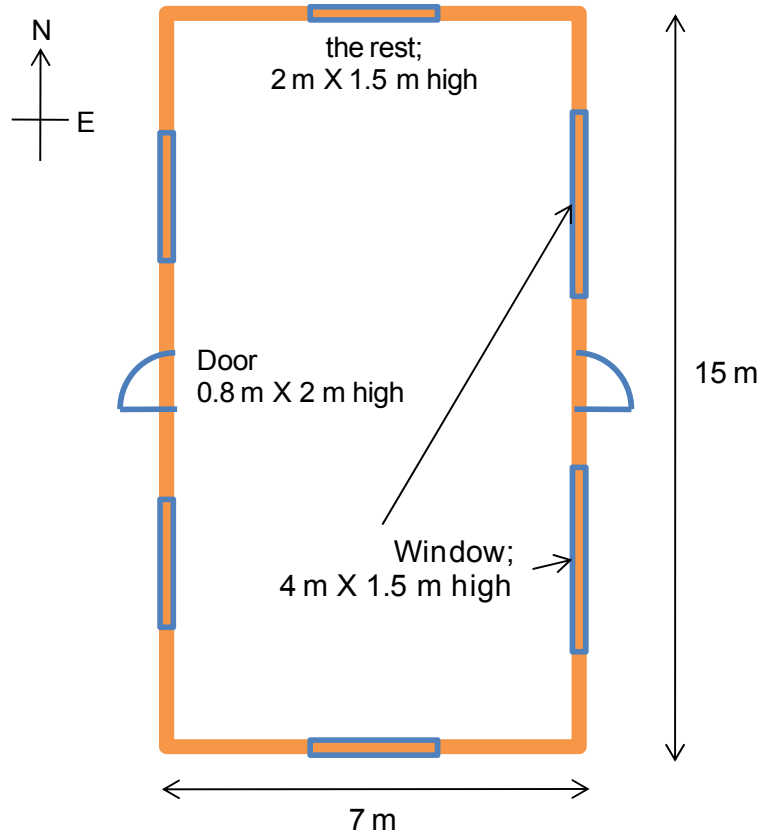


Figure A.4 Plan of the insulated office building (Ansari et al., 2005)

Table A.7 Comparison in ratio of window area

Building		Non-insulated	Insulated
Number of story	story	4.0	7.0
Number of window	small -	12.0	28.0
	large -	4.0	14.0
Total window area ¹⁾	m ²	60.0	168.0
Total wall area	m ²	394.0	1,232.0
Ratio of window area	%	15.2	13.6

1) Small window; 2 m x 1.5 m high, large window; 4 m x 1.5 m high

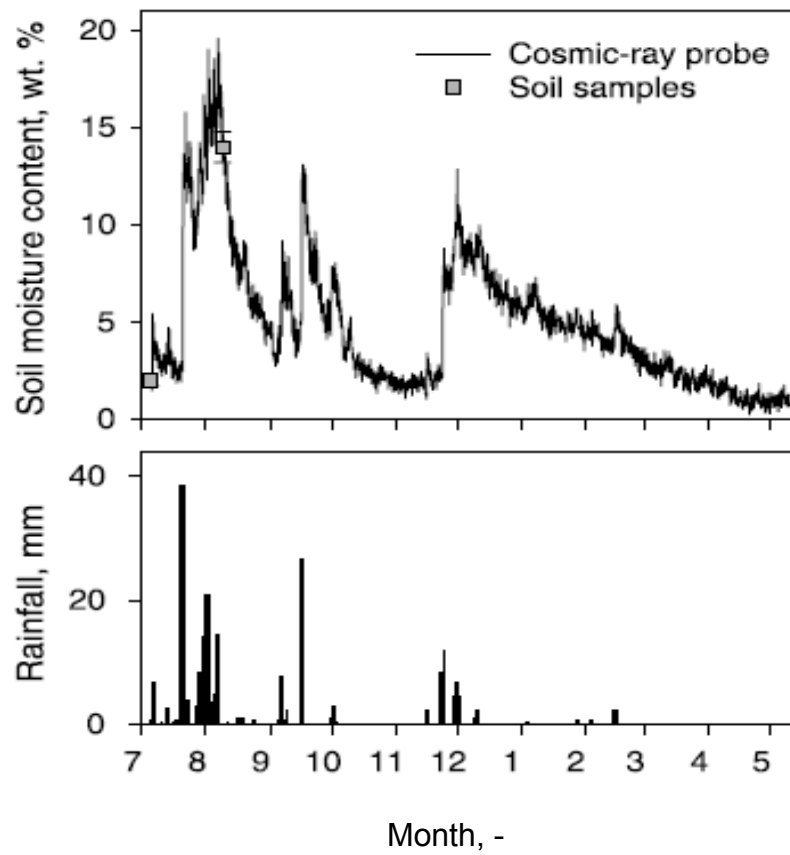


Figure A.5 Field data of soil moisture content and precipitation (Zreda et al., 2008)

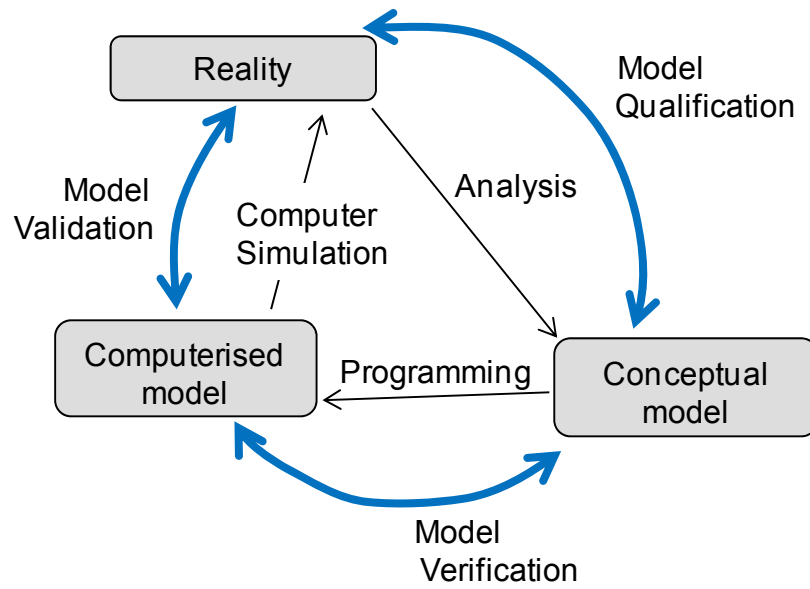


Figure A.6 Phases of modelling and simulation (American Institute of Aeronautics and Astronautics, 1998)

Appendix B Programme to Control a Data Collection

Process of the DPHP

Here is a programme built for the sensor 2209.

```
'CR1000 Series Datalogger
'date: February 18, 2008
'program to read East 30 Sensors dual needle specific heat sensor
'C1 controls interface board heating, Diff Ch1 reads thermocouple
'Diff Ch2 reads voltage drop over pickoff resistor
'wiring:      purple (thermocouple HI): 1 HI
'             red (thermocouple LOW): 1L
'             black (heater HI): HI on interface board
'             blue (reference resistor HI): 2H
'             gray (reference resistor LOW): 2L AND gnd on interface board
'             user supplied jumper (GND): connect GND on datalogger to
GND on interface board
'             user supplied jumper 2 (C1): connect C1 on datalogger to
control on interface board
'             user supplied power cable (12V): connect +12 V supply to
interface board
'             user supplied power cable (GND): connect power supply gnd to
interface board gnd

'program output:
'first sample column: time (s) begins with zero at begining of 90 s loop
'second sample column: deltaT (C)
'third sample column: Q (J/m) - average the Q values for first 8 seconds for Q in
calculations

Public Tpanel, Tinitial, time, Tneedle, deltaT, Vref, power, Q

const Rref = 1.032 'INPUT VALUE OF REFERENCE RESISTOR HERE -
No.2209
```

Appendix B Programme to Control a Data Collection Process of the DPHP

const Rheater = 1270.0

DataTable (Table1,1,-1)

Sample (1,time,FP2)

Sample (1,deltaT,FP2)

Sample (1,Q,FP2)

EndTable

BeginProg

Scan (1,Sec,0,0)

If Time (0,60,Min) Then 'measure thermal properties every 60 minutes

time = 0 'reset timer

PanelTemp (Tpanel,_60Hz)

TCDiff

(Tinitial,1,mV25,1,TypeE,Tpanel,True ,0,_60Hz,1.0,0)'measure initial temperature

endif

If time<90 then

If time <8 Then

portset(1,1)'turn on heater for first 8 seconds

Else

portset(1,0)'turn off heater

EndIf

PanelTemp (Tpanel,_60Hz)

TCDiff

(Tneedle,1,mV25,1,TypeE,Tpanel,True ,0,_60Hz,1.0,0)'measure needle T while heating and cooling

deltaT = Tneedle-Tinitial'calculate T rise in needle

VoltDiff

(Vref,1,mV5000,2,True ,0,_60Hz,.001,0)'measure V drop over reference resistor
power = (Vref/Rref)^2*Rheater'calculate power
dissipation in needle (W/m)

Q = power * 8 '(J/m)

CallTable Table1'output time, deltaT, and power every time through loop

Appendix B Programme to Control a Data Collection Process of the DPHP

```
        time = time+1
    Endif
NextScan
EndProg
```

Appendix C Programme to Define Heater Resistance

(East 30 Sensors, 2007)

Here is a programme provided by the DPHP sensor supplier, East 30 Sensors, to calibrate with the thermal resistance of the sensors.

```
;  
{CR10X or CR1000 type}  
;Program to find resistance of reference resistor  
;Flag 1 starts program  
;Input Channel 1s.e. supply voltage  
;                2s.e. reference voltage
```

*Table 1 Program

01: 1 Execution Interval (seconds)

1: If Flag/Port (P91)

1: 21 Do if Flag 1 is Low

2: 0 Go to end of Program Table

2: Z=F (P30)

1: 37.1 F

2: 0 Exponent of 10

3: 2 Z Loc [R_probe]

;this is the resistance of YOUR heater (black to green)

3: Beginning of Loop (P87)

1: 0 Delay

2: 20 Loop Count

4: Volt (SE) (P1)

1: 1 Repts

Appendix C Programme to Define Heater Resistance

2: 5 2500 mV Slow Range
3: 1 SE Channel
4: 3 Loc [V_supply]
5: .001 Mult
6: 0 Offset

5: Volt (SE) (P1)

1: 1 Repts
2: 4 250 mV Slow Range
3: 2 SE Channel
4: 5 Loc [V_ref]
5: .001 Mult
6: 0 Offset

6: End (P95)

7: Z=X/Y (P38)

1: 3 X Loc [V_supply]
2: 2 Y Loc [R_probe]
3: 4 Z Loc [current]

Appendix D Information in Association with Measurements of Thermal Properties

Table D.1 Results of calibration to obtain unique heater resistance (P. A. Hilton Ltd., 1994)

Sensor	Reference resistance Ω	Heater resistance $\Omega/0.03m$
2209	1.032	38.1
2210	1.035	38.0

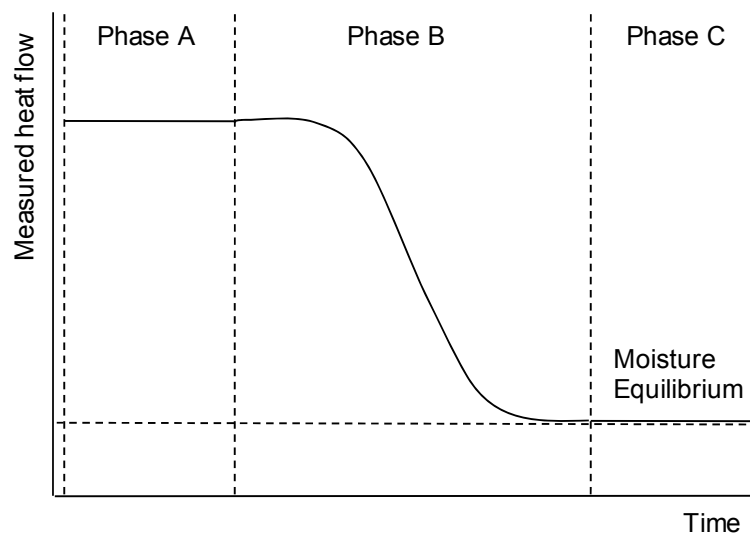


Figure D.1 Thermal transmission in the HFM (International Organization for Standardisation, 1996)

Appendix E Investigation of Thermal Resistance Caused by Aluminium Plate

The investigation was conducted by Dr. David Allinson with the same soil sample, the HFM and an aluminium plate as follows.

E.1 Sample Making

The soil sampled at the School of the Build Environment was sieved to make 2 mm soil. The soil was mixed with water until the water content reached 6 %. Two kinds of soil samples were prepared to understand the difference of thermal resistance between with and without the 2 mm aluminium plate. The wet soil was compacted into size 0.3 m X 0.3 m X 0.44 m high by dropping a 6.215 kg hammer from a 0.5 m high. Since 88 blows were applied, the compaction energy was 596.1 kJ/m³. Sample A was made by packing and oven-drying the wet sample in a tray with the aluminium base. The wet soil was also packed in a tray with which the base could be disassembled after oven-drying to make sample B.

E.2 Measurement of Thermal Conductivity

The measured values were 0.81 W/m/K for sample A and 0.85 W/m/K for sample B. The fact that sample A had smaller thermal conductivity made sense due to the extra resistance by the aluminium plate and possible air layer. The thermal resistance created by measuring on the aluminium plate was 0.005 m²K/W in accordance to Equation 5.4 with x_{al} / k_{al} instead of x_{film} / k_{film} . When the

Appendix E Investigation of Thermal Resistance Caused by Aluminium Plate

theoretical resistance of aluminium plate itself was calculated from the thickness and standard thermal conductivity of aluminium, 211 W/m/K (Holman, 2002), the value was 0.0000095 m²K/W. This difference revealed that the aluminium plate was likely to create air layer between itself and the sample. Since the impact was significant, the overall thermal resistance with the use of aluminium plate ought to be taken into consideration for estimating soil thermal conductivity.

E.3 Conclusion

Comparison of the measured thermal conductivity between with and without an aluminium base nailed that the effect of air layer between soil sample and the plate was not negligible. Hence, the delivered thermal resistance, 0.005 m²K/W, was used to estimate thermal conductivity of soil itself from the measured overall thermal conductivity.

Appendix F Processed Field Data between Soil Moisture Content and Rainfall

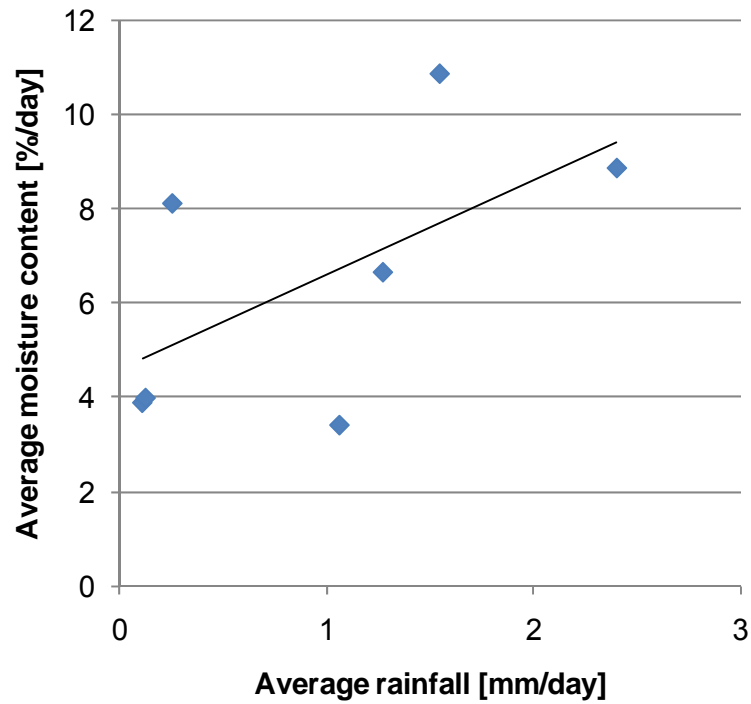


Figure F.1 Relation between soil moisture content and rainfall in San Pedro River Valley (Zreda et al., 2008)

Publications

- 1.** Hiromi Mori, David Allinson, Matthew Hall, Guohui Gan and Saffa Riffat, 2008. *Enhancement of Sub-soil Thermal Conductivity for Geothermal Heat Pump Systems with Rainwater Collection. Proceedings of International Conference on Sustainable Energy Technologies; Seoul, Korea, 24-27 August, 2008.* Seoul: Korea Institute of Ecological Architecture and Environment
- 2.** Hiromi Mori, David Allinson, Matthew Hall, Guohui Gan and Saffa Riffat, 2008. *Feasibility Study of Modifying Soil Thermal Conductivity for Ground Source Heat Pump Systems. Proceedings of International Conference on Sustainable Energy Technologies; Aachen, Germany, 31 August-3 September, 2009.* Aachen: University Duisburg-Essen